Stable Isotope Systematics of Coalbed Methane

by

Martin Niemann
Diplom Geowissenschaftler, Universität Hannover, 2002

A Dissertation Submitted in Partial Fulfillment of the
Requirements for the Degree of

DOCTOR OF PHILOSOPHY

in the School of Earth and Ocean Sciences

© Martin Niemann, 2006
University of Victoria

All rights reserved. This dissertation may not be reproduced in whole or in part, by photocopying or other means, without the permission of the author.

Stable Isotope Systematics of Coalbed Methane

by

Martin Niemann
Diplom Geowissenschaftler, Universität Hannover, 2002

Supervisory Committee

Dr. Michael Whiticar, (School of Earth and Ocean Sciences)
Supervisor

Dr. Kevin Telmer, (School of Earth and Ocean Sciences)
Departmental Member

Dr. Stephen Johnston, (School of Earth and Ocean Sciences)
Departmental Member

Dr. Eileen van der Flier–Keller, (Department of Geography)
Outside Member

Dr. Barry Ryan, (Geological Survey of British Columbia, Victoria)
Additional Member

Dr. Martin Fowler (Geological Survey of Canada, Calgary)
External Examiner

Supervisory Committee

Dr. Michael Whiticar (School of Earth and Ocean Sciences)
Supervisor

Dr. Kevin Telmer (School of Earth and Ocean Sciences)
Departmental Member

Dr. Stephen Johnston (School of Earth and Ocean Sciences)
Departmental Member

Dr. Eileen van der Flier–Keller (Department of Geography)
Outside Member

Dr. Barry Ryan (Geological Survey of British Columbia, Victoria)
Additional Member

Dr. Martin Fowler (Geological Survey of Canada, Calgary)
External Examiner

Abstract

Coalbed methane (CBM) is a growing resource for "clean" natural gas and is becoming of great interest for academic research. Despite much research already be done, geochemical investigations, especially with focus on the stable carbon and hydrogen isotope composition of CBM, are rare.

For this study, over 1,000 CBM samples were analyzed. The samples were collected during 10 different sample campaigns from seven different coal bearing basins worldwide. Seven sample sets were collected during desorption experiments following drilling of exploration wells and three sample sets were collected from CBM producing wells. The considered coals range in maturity from sub bituminous A (min. 0.57%R_O) to anthracite (max. 4.55%R_O), cover a wide range of different maceral compositions and were accessed in depths between 10m and 1312m beneath surface. Samples cover a production time of up to 6312 hours and a desorption time of up to 2773 hours.

The geochemical analyzes were carried out using GC–IRMS. Analyzes include gas composition (methane, ethane, propane, *n*–butane, *i*–butane and carbon dioxide) and

the proportions of the different gas species, as well as stable carbon isotope ratios for all gas species and stable hydrogen isotope ratios for methane.

The analyzed averaged and normalized gas composition of the considered samples reveals average proportions for methane between 44.3% and 98.7%, for ethane between 0% and 9.98%, for propane between 0% and 1.15%, for *n*–butane between 0% and 1.09%, for *i*–butane between 0% and 0.003% and for carbon dioxide between 1.34% and 53.9%. The gas composition does not show conclusive trends with increasing production/desorption time. Methane stable carbon isotope ratios vary with production/desorption time. Samples from production scenarios show a general depletion in ^{13}C for methane with increasing production time and isotope shifts between -1.6% and -35.8‰. Samples from desorption experiment scenarios show mostly enrichment in ^{13}C for methane with increasing desorption time and isotope shifts of up to -43.4‰, but also ^{12}C enrichment was observed in some sample sets with isotope shifts of up to +32.1‰. Overall, the magnitudes of the observed isotope shifts vary considerably between different sample sets, but also within samples from the same source.

The stable carbon isotope composition of methane does not display the expected composition of methane generated from coal. This indicates the influence of secondary processes. The secondary processes mixing, adsorption, desorption and diffusion/migration cannot be separated and considered individually, because they overlap and have identical directions for compositional and isotope alteration. The significant alteration of the considered gases generated from coal has therefore to be considered as a combined effect of the mentioned secondary processes. Because of multiple complicating factors it was not possible to delineate the presence of primary and secondary microbial gas, but due to the geologic context and the retentive ability of coal the presence of these gases is reasonable to assume. Indications were found in samples for the presence of gases generated from a Kerogen Type II shale in CBM gases. The unaltered molecular and isotope composition of CBM gases is unknown. This parameter cannot be estimated, because during the physical history of a coal seam, the coal probably had experienced the loss of gas accompanied by molecular and isotope effects of unknown extent and magnitude. Based on the current knowledge and the data available from this and other studies, a classification of CBM is unreasonable and more work is

required for the establishment of a stable isotope systematic for CBM, including the separate experimental evaluation of molecular and isotope effects of adsorption, desorption and diffusion/migration of gases in coal.

Table of Contents

Supervisory Committee ..... *ii*
Abstract ..... *iii*
Table of Contents ..... *vi*
List of Tables ..... *xii*
List of Figures ..... *xvi*
List of Abbreviations and Symbols ..... *xxvii*
Acknowledgements ..... *xxx*

1. Introduction *1*

2. Background *4*
2.1 Coal and Coal Formation 4
2.1.1 Coal Macerals 4
2.1.2 Vitrinite Reflectance 7
2.1.3 Coal Types 8
2.1.4 Peatification 8
2.1.5 Coalification 9
2.2 Gas Generation from Coal 10
2.2.1 Biogenesis 10
2.2.2 Thermogenesis 12
2.3 Sorption and Desorption 13
2.4 Gas Content Measurement 17
2.5 Stable Isotope Geochemistry 20
2.5.1 Carbon 24
2.5.2 Hydrogen 33
2.5.3 Secondary Processes 35
2.5.3a Mixing 36
2.5.3b Oxidation 36

2.5.3c Adsorption/Desorption..... 37
2.5.3d Diffusion..... 39

3. Methods..... 45
3.1 Sampling..... 45
3.1.1 Production Sampling..... 45
3.1.2 Desorption Experiment Sampling..... 46
3.2 Gas Chromatography–Isotope Ratio Mass Spectrometry (GC–IRMS) 47
3.3 Measurement..... 49

4. Samples..... 53
4.1 Sample Description..... 53
4.2 Production Samples..... 54
4.2.1 Sample Set P1..... 54
4.2.2 Sample Set P2..... 55
4.2.3 Sample Set P3..... 55
4.3 Desorption Experiment Samples..... 56
4.3.1 Sample Set D1..... 56
4.3.2 Sample Set D2..... 57
4.3.3 Sample Set D3..... 57
4.3.4 Sample Set D4..... 58
4.3.5 Sample Set D5..... 59
4.3.6 Sample Set D6..... 60
4.3.7 Sample Set D7..... 61

5. Results..... 62
5.1 Sample Set P1..... 64
5.2 Sample Set P2..... 65
5.3 Sample Set P3..... 67
5.4 Sample Set D1..... 69

5.5 Sample Set D2 71
5.6 Sample Set D3 73
5.7 Sample Set D4 75
5.8 Sample Set D5 78
5.9 Sample Set D6 79
5.10 Sample Set D7 83

6. Discussion 101
6.1 Coal–Gas Relationships 101
6.1.1 Influence of Maturity on Isotope Ratios 102
6.1.2 Influence of Maceral Composition on Isotope Ratios 104
6.1.2a Vitrinite 105
6.1.2b Liptinite 108
6.1.2c Inertinite 109
6.1.3 Influence of Depth on Isotope Ratios 110
6.2 Gas Classification 113
6.2.1 Gas Origin: Primary Effects 114
6.2.1a Composition 114
6.2.1b $\delta^{13}C$ (CH_4) Estimation 119
6.2.1c Comparison: Calculated vs. Measured Carbon Isotope Ratios 121
6.2.1d Gas Classification Approach 124
6.2.2 Secondary Alteration Effects 133
6.2.2a Mixture of Coal Gas with Microbial Gas 133
6.2.2b Mixture of CBM Gas with Kerogen Type II Gas 141
6.2.2c Mixture of CBM Gas A with CBM Gas B 157
6.2.2d Microbial Oxidation of Methane 158
6.2.2e Adsorption and Desorption 161
6.2.2f Diffusion/Migration 167
6.3 Production vs. Desorption Experiment 172
6.3.1 CBM Samples from Production Scenarios 174

6.3.2 CBM Samples from Desorption Experiment Samples..... 177
6.3.3 Systematic of CBM Production from Producing Wells..... 182
6.4 Sample Set P3..... 189
6.4.1 Compositional Aspects..... 189
6.4.2 Isotope Aspects..... 190
6.4.3 Modelation of CBM Production for Sample Set P3..... 191

7. Synthesis..... 196
7.1 Coal–Gas Relationships..... 196
7.2 Primary Effects..... 197
7.3 Secondary Effects..... 200
7.4 Production vs. Desorption Experiment..... 206
7.5 Effect of CBM Production..... 213

8. Conclusions..... 215

9. References..... 219

Appendix A *Datasheet Sample Set P1*..... ***232***
Appendix B *Datasheet Sample Set P2*..... ***233***
Appendix C *Datasheet Sample Set P3*..... ***234***
Appendix D *Datasheet Sample Set D1*..... ***240***
Appendix E *Datasheet Sample Set D2*..... ***242***
Appendix F *Datasheet Sample Set D3*..... ***244***
Appendix G *Datasheet Sample Set D4*..... ***252***
Appendix H *Datasheet Sample Set D5*..... ***260***
Appendix I *Datasheet Sample Set D6*..... ***261***
Appendix J *Datasheet Sample Set D7*..... ***265***

Appendix K *Estimated $\delta^{13}C$ values for methane, ethane and propane, based on maturities of coals considered for all ten sample sets. Calculations are performed by using maturity–$\delta^{13}C$ relationships by Berner and Faber (1996)*..... **267**

Appendix L *Calculated differences between measured and estimated $\delta^{13}C$ ratios for methane. Estimated $\delta^{13}C$ values for methane are based on maturities of coals considered for all ten sample sets. Calculations are performed by using maturity–$\delta^{13}C$ relationships by Berner and Faber (1996)*..... **269**

Appendix M *Calculated differences between measured and estimated $\delta^{13}C$ ratios for ethane. Estimated $\delta^{13}C$ values for ethane are based on maturities of coals considered for all ten sample sets. Calculations are performed by using maturity–$\delta^{13}C$ relationships by Berner and Faber (1996)*..... **271**

Appendix N *Calculated differences between measured and estimated $\delta^{13}C$ ratios for propane. Estimated $\delta^{13}C$ values for propane are based on maturities of coals considered for all ten sample sets. Calculations are performed by using maturity–$\delta^{13}C$ relationships by Berner and Faber (1996)*..... **272**

Appendix O *Extrapolated $\delta^{13}C$ values for methane and calculated proportions of thermogenic and microbial gas in sample sets D6 and D7*..... **273**

Appendix P *Calculated $\delta^{13}C$ values for methane and calculated proportions of thermogenic and microbial gas in sample sets D6 and D7*..... **274**

Appendix Q *Comparison of calculated fractions for thermogenic gas generated from a Kerogen Type III source rock and microbial based on the approaches by Chung et al. (1988) and Berner and Faber (1996) for sample sets D6 and D7*..... **276**

Appendix R *Calculated differences for the estimated $\delta^{13}C$ ratios for methane based on the approaches by Chung et al. (1988) and Berner and Faber (1996) for sample sets D6 and D7*..... **277**

Appendix S *Comparison between calculated and measured $\delta^{13}C$ values for ethane and propane from sample set D7*..... **278**

Appendix T *Comparison between measured $\delta^{13}C$ ratios for methane with calculated $\delta^{13}C$ ratios for methane expected to be generated from a Kerogen Type II and Kerogen Type III source rock. Calculations are conducted by applying maturity–$\delta^{13}C$ relationships by Berner and Faber (1996)*..... **279**

Appendix U *Comparison between measured $\delta^{13}C$ ratios for ethane with calculated $\delta^{13}C$ ratios for ethane expected to be generated from a Kerogen Type II and Kerogen Type III source rock. Calculations are conducted by applying maturity–$\delta^{13}C$ relationships by Berner and Faber (1996)*..... **280**

Appendix V *Comparison between measured $\delta^{13}C$ ratios for propane with calculated $\delta^{13}C$ ratios for propane expected to be generated from a Kerogen Type II and Kerogen Type III source rock. Calculations are conducted by applying maturity–$\delta^{13}C$ relationships by Berner and Faber (1996)*..... **281**

Appendix W *Comparison of proportions of Kerogen Type II derived gas (methane, ethane and propane) for sample sets D6 and D7. Fractions are calculated by applying maturity–$\delta^{13}C$ relationships by Berner and Faber (1996) with a consequent comparison with measured $\delta^{13}C$ ratios for methane, ethane and propane (see text for details)*..... **282**

Appendix X *Maturities, amounts of liptinite and average proportions for higher gaseous hydrocarbons (ethane, propane, n–butane and i–butane) from sample sets D6 and D7*..... **283**

Appendix Y *Weighted $\delta^{13}C$ values for methane, ethane and propane. See text for details about calculation of t_{WGH} values*..... **284**

List of Tables

Table 3.1: GC–IRMS set–up used for measurement of gas composition, proportions and $\delta^{13}C$–ratios of the different gas species..... **52**

Table 3.2: GC–IRMS set–up used for measurement of δD–ratios of methane..... **52**

Table 4.1: General information about coals under investigation and general information about type and duration of used sample methods. Ø = average; Vit = Vitrinite; Iner. = Inertinite; Lipt. = Liptinite; HV Bit.A = high volatile bituminous A; HV Bit.B = high volatile bituminous B; HV Bit.C = high volatile bituminous C; MV Bit. = medium volatile bituminous; LV Bit. = low volatile bituminous; Sub Bit.A = sub bituminous A. **53**

Table 4.2: Rank, maturity, maceral content and depth for the different considered coals of production sample set P1, as well as maximal considered duration of production time for the different wells. Vit. = Vitrinite; Inert. = Inertinite; Lipt. = Liptinite..... **54**

Table 4.3: Rank, maturity, maceral content and depth for the different considered coals from production sample set P2, as well as maximal considered duration of production time for the different wells. Vit. = Vitrinite; Inert. = Inertinite; Lipt. = Liptinite; HV Bit.A = high volatile bituminous A; MV Bit = medium volatile bituminous..... **55**

Table 4.4: Rank, maturity, maceral content and depth for the different considered coals from production sample set P3, as well as maximal considered duration of production time for the different wells. Vit. = Vitrinite; Inert. = Inertinite; Lipt. = Liptinite; HV Bit.C = high volatile bituminous C; Sub Bit.A = sub bituminous A..... **56**

Table 4.5: Rank, maturity, maceral content and depth for the different considered coals from desorption experiment sample set D1, as well as maximal considered duration of desorption time for the different canisters. Vit. = Vitrinite; Inert. = Inertinite; Lipt. = Liptinite..... **56**

Table 4.6: Rank, maturity, maceral content and depth for the different considered coals from desorption experiment sample set D2, as well as maximal considered duration of desorption time for the different canisters. Vit. = Vitrinite; Inert. = Inertinite; Lipt. = Liptinite..... **57**

Table 4.7: Rank, maturity, maceral content and depth for the different considered coals from desorption experiment sample set D3, as well as maximal considered duration of desorption time for the different canisters. Vit. = Vitrinite; Inert. = Inertinite; Lipt. = Liptinite; HV Bit.C = high volatile bituminous C; Sub Bit.A = sub bituminous A..... **58**

Table 4.8: Rank, maturity, maceral content and depth for the different considered coals from desorption experiment sample set D4, as well as maximal considered duration of desorption time for the different canisters Vit. = Vitrinite; Inert. = Inertinite; Lipt. = Liptinite; HV Bit.C = high volatile bituminous C; Sub Bit.A = sub bituminous A..... **59**

Table 4.9: Rank, maturity, maceral content and depth for the different considered coals from desorption experiment sample set D5, as well as maximal considered duration of desorption time for the different canisters. Vit. = Vitrinite; Inert. = Inertinite; Lipt. = Liptinite; HV Bit.C = high volatile bituminous C; Sub Bit.A = sub bituminous A..... **60**

Table 4.10: Rank, maturity, maceral content and depth for the different considered coals from desorption experiment sample set D6, as well as maximal considered duration of desorption time for the different canisters. Vit. = Vitrinite; Inert. = Inertinite; Lipt. = Liptinite; MV Bit = medium volatile bituminous; LV Bit = low volatile bituminous..... **60**

Table 4.11: Rank, maturity, maceral content and depth for the different considered coals from desorption experiment sample set D7, as well as maximal considered duration of desorption time for the different canisters. Vit. = Vitrinite; Inert. = Inertinite; Lipt. = Liptinite; HV Bit.B = high volatile bituminous B; HV Bit.C = high volatile bituminous C; Sub Bit.A = sub bituminous A..... **61**

Table 5.1: Gas composition of samples collected from all ten sample sets. Samples from different wells and canisters per sample set are averaged and presented per sample set. Proportions are normalized on the basis of proportions of methane, ethane, propane, *n*–butane, *i*–butane and carbon dioxide. norm. = normalized..... **63**

Table 5.2: Compositional and isotope results for sample set P1. Results are represented per well with minimum and maximum values for proportions and $\delta^{13}C$ and δD respectively. Proportions are normalized on the basis of proportions of methane, ethane, propane, *n*–butane, *i*–butane and carbon dioxide. Ethane, propane, *n*–butane and *i*–butane are combined under the term C_{2+} (higher hydrocarbons). Legend for symbols used for the characterization of observed trends is given above..... **64**

Table 5.3: Compositional and isotope results for sample set P2. Results are represented per well with minimum and maximum values for proportions and $\delta^{13}C$ and δD respectively. Proportions are normalized on the basis of proportions of methane, ethane, propane, *n*–butane, *i*–butane and carbon dioxide. Ethane, propane, *n*–butane and *i*–butane are combined under the term C_{2+} (higher hydrocarbons). Legend for symbols used for the characterization of observed trends is given above..... **66**

Table 5.4: Compositional and isotope results for sample set P3. Results are represented per well with minimum and maximum values for proportions and $\delta^{13}C$ and δD respectively. Proportions are normalized on the basis of proportions of methane, ethane, propane, *n*–butane, *i*–butane and carbon dioxide. Ethane, propane, *n*–butane and *i*–butane are combined under the term C_{2+} (higher hydrocarbons). Legend for symbols used for the characterization of observed trends is given above..... **68**

Table 5.5: Compositional and isotope results for sample set D1. Results are represented per canister with minimum and maximum values for proportions and $\delta^{13}C$ and δD respectively. Proportions are normalized on the basis of proportions of methane, ethane, propane, *n*–butane, *i*–butane and carbon dioxide. Ethane, propane, *n*–butane and *i*–butane are combined under the term C_{2+} (higher hydrocarbons). Legend for symbols used for the characterization of observed trends is given above..... **69**

Table 5.6: Compositional and isotope results for sample set D2. Results are represented per canister with minimum and maximum values for proportions and $\delta^{13}C$ and δD respectively. Proportions are normalized on the basis of proportions of methane, ethane, propane, *n*–butane, *i*–butane and carbon dioxide. Ethane, propane, *n*–butane and *i*–butane are combined under the term C_{2+} (higher hydrocarbons). Legend for symbols used for the characterization of observed trends is given above..... **71**

Table 5.7: Compositional and isotope results for sample set D3. Results are represented per canister with minimum and maximum values for proportions and $\delta^{13}C$ and δD respectively. Proportions are normalized on the basis of proportions of methane, ethane, propane, *n*–butane, *i*–butane and carbon dioxide. Ethane, propane, *n*–butane and *i*–butane are combined under the term C_{2+} (higher hydrocarbons). Legend for symbols used for the characterization of observed trends is given above..... **74**

Table 5.8: Compositional and isotope results for sample set D4. Results are represented per canister with minimum and maximum values for proportions and $\delta^{13}C$ and δD respectively. Proportions are normalized on the basis of proportions of methane, ethane, propane, *n*–butane, *i*–butane and carbon dioxide. Ethane, propane, *n*–butane and *i*–butane are combined under the term C_{2+} (higher hydrocarbons). Legend for symbols used for the characterization of observed trends is given above..... **76**

Table 5.9: Compositional and isotope results for sample set D. Results are represented per canister with minimum and maximum values for proportions and $\delta^{13}C$ and δD respectively. Proportions are normalized on the basis of proportions of methane, ethane, propane, *n*–butane, *i*–butane and carbon dioxide. Ethane, propane, *n*–butane and *i*–butane are combined under the term C_{2+} (higher hydrocarbons). Legend for symbols used for the characterization of observed trends is given above..... **78**

Table 5.10: Compositional and isotope results for sample set D6. Results are represented per canister with minimum and maximum values for proportions and $\delta^{13}C$ and δD respectively. Proportions are normalized on the basis of proportions of methane, ethane, propane, *n*–butane, *i*–butane and carbon dioxide. Ethane, propane, *n*–butane and *i*–butane are combined under the term C_{2+} (higher hydrocarbons). Legend for symbols used for the characterization of observed trends is given above..... **80**

Table 5.11: Compositional and isotope results for sample set D7. Results are represented per canister with minimum and maximum values for proportions and $\delta^{13}C$ and δD respectively. Proportions are normalized on the basis of proportions of methane, ethane, propane, *n*–butane, *i*–butane and carbon dioxide. Ethane, propane, *n*–butane and *i*–butane are combined under the term C_{2+} (higher hydrocarbons). Legend for symbols used for the characterization of observed trends is given above..... **83**

Table 6.1: Stable carbon and hydrogen isotope ratios of macerals vitrinite, liptinite and inertinite. Values from Schwarzkopf (1984)..... **104**

Table 6.2: Minimum and maximum amounts of the macerals vitrinite, liptinite and inertinite in coals considered in this study..... **105**

Table 6.3: Proportions of methane (CH_4), higher hydrocarbons (C_{2+}) and carbon dioxide (CO_2) in gases encountered in coal gases. Data from Jüntgen and Karweil (1966a) represent selected bituminous coals of Germany. Data from Rice (1993) represent gases from CBM basins worldwide. For Rice (1993): C_{2+} maximum from Upper Carboniferous of Germany; CO_2 maximum from Upper Carboniferous of Poland..... **114**

Table 6.4: Average maturities of coals considered for the different sample sets in relation to average gas composition and average amounts of liptinite in the considered coals. Proportions are normalized on the basis of proportions of methane, ethane, propane, *n*–butane, *i*–butane and carbon dioxide. Ethane, propane, *n*–butane and *i*–butane are combined under the term C_{2+} (higher hydrocarbons). norm. = normalized..... **116**

Table 6.5: Calibration limits for the relationships between maturity and the stable carbon isotope ratios of methane, ethane and propane by Berner and Faber (1996)..... **119**

Table 6.6: Estimated $\delta^{13}C$ values for methane, ethane and propane, based on maturities of coals considered for all ten sample sets. Calculations were performed by using maturity–$\delta^{13}C$ relationships by Berner and Faber (1996). Maturities below 0.6%R_O and above 2.5%R_O are not included, because the applied maturity–$\delta^{13}C$ relationships by Berner and Faber (1996) are not calibrated for these maturity ranges..... **120**

Table 6.7: Calculated carbon isotope ratios for methane, ethane and propane derived from a Kerogen Type III source rock. Calculations are performed by applying the lowest and highest maturities encountered in coals from this study to $\delta^{13}C$–%R_O relationships for methane, ethane and propane by Berner and Faber (1996)..... **121**

List of Figures

Figure 2.1: van Krevelen diagram showing atomic oxygen/carbon ratios versus atomic hydrogen/carbon ratios of different plant materials and main coal macerals. Waxes, cuticles, spores and cutinites comprise the maceral group liptinite (modified from Tissot and Welte, 1978)..... **5**

Figure 2.2: Different coal ranks ranging from peat to meta–anthracite in relation to coal parameters maturity, volatile matter content, carbon content, bed moisture and calorific value (modified from Rice, 1993)..... **6**

Figure 2.3: Relative proportions of gases formed as a function of temperature from sapropelic and humic coal (modified from Hunt, 1991)..... **12**

Figure 2.4: Diagram shows variations in gas volumes adsorbed onto coal with pressure. Gas volumes adsorbed onto coal increases with increasing pressure, regardless of water content. Increasing water content has the effect of decreasing gas volumes adsorbed onto the coal. This trend continues until equilibrium moisture is reached; see text for details (modified from Joubert et al., 1974)..... **15**

Figure 2.5: Possible transport mechanisms of gases in coal. A: Flow of fluids and gases in the cleat network of a coal. B: Desorption of gases from cleat surfaces. C: Molecular diffusion of gas molecules from internal desorption sites through the coal matrix towards cleat surfaces (modified from McLennan et al., 1995)..... **17**

Figure 2.6: Principle set–up of equipment used for volumetric determination of gases in coal (canister method). See text for details..... **18**

Figure 2.7: Schematic gas desorption diagram (canister method) showing time versus gas volume. Total gas volume consists of three separate volumes: lost gas, measured gas, residual gas. See text for description (modified from McLennan et al., 1995)..... **19**

Figure 2.8: Energy level diagram for hydrogen. ZPE = zero–point–energy. See text for description (from O'Neill, 1986)..... **22**

Figure 2.9: Rayleigh distillation curves showing $\delta^{13}C$ ratio of kerogen and its variation with progressing generation and loss of gas. Initial $\delta^{13}C$ ratio of the kerogen in this example is -25‰. With decreasing fraction of kerogen remaining for the conversion to gas, the kerogen becomes relatively ^{13}C enriched, due to the loss of relatively ^{12}C enriched gases. Right side diagram shows section indicated on left side diagram in expanded scale. Curves are calculated using different fractionation factors. See text for equations and details (from Whiticar, 1996a)..... **24**

Figure 2.10: Bernard Diagram showing $\delta^{13}C$ ratios for methane versus gas wetness (ratio of proportions of methane over ethane and propane) and distinct areas for gases of thermogenic and microbial origin. A and B represent mixing lines between gases, based on two endmembers. See text for description (modified from Whiticar, 1999)..... **27**

Figure 2.11: Idealized natural gas plot showing 1/carbon number for methane, ethane, propane and butane versus corresponding $\delta^{13}C$–ratios. Black dots indicate measured samples and stippled red line represents extrapolation for the determination of $\delta^{13}C$–ratio of kerogen and $\delta^{13}C$ of pure thermogenic methane. Difference between extrapolated $\delta^{13}C$–ratio for pure thermogenic methane and actual measured $\delta^{13}C$–ratio for methane indicates input of microbial methane. In the shown example, the $\delta^{13}C$–ratio of pure thermogenic methane is -40‰ and the extrapolated $\delta^{13}C$–ratio of the kerogen is -20‰. See text for details (modified from Chung et al., 1988)..... **28**

Figure 2.12: Graphic presentation of relationships between the maturity (vitrinite reflectance) of a source rock with the stable carbon isotope composition ($\delta^{13}C$) of methane, ethane and propane generated from this type of source rock. Left hand diagram shows relationships for a Kerogen Type II source rock and the right hand diagram for a Kerogen Type III source rock. See text for equations and details (modified from Berner and Faber, 1996)..... **31**

Figure 2.13: Cross–plot of δD– and $\delta^{13}C$–ratios of methane. Based on the isotope composition of methane, different possible origins can be determined and are shown in the diagram with distinct areas. See text for details (modified from Whiticar, 1996b)..... **34**

Figure 2.14: Stable carbon and hydrogen isotope composition of different main coal maceral groups and sapropelic coal (modified from Schwarzkopf, 1984)..... **35**

Figure 2.15: Diffusion plot showing $\delta^{13}C$ ratio for methane versus ratio of proportions of methane over ethane. Samples plotting in a straight line indicate presence and alteration due to mixing, whereas samples plotting in a logarithmic curve indicate alteration due to the process of diffusion. See text for details (from Colombo et al., 1970 and Prinzhofer and Pernaton, 1997)..... **44**

Figure 3.1: Schematic illustration of the Gas Chromatograph–Isotope Ratio Mass Spectrometer (GC–IRMS), including its main components. C = carbon; H = hydrogen. A represents the point where gases are trapped in liquid nitrogen, if the measurement requires it..... **48**

Figure 3.2: Example of a calibration curve for methane to allow proportion measurements with the use of a GC–IRMS. The proportions of methane in different dilutions of a standard gas with known methane proportions are shown on the y–axis (actual data are shown in insert). The resulting peak areas, relative to known proportions of methane, are shown on the x–axis (actual data are shown in insert). A linear relationship exists between these two parameters and the corresponding mathematical equation to describe this relationship is shown. By applying this equation, relative proportions of methane in CBM samples can be calculated by determining the peak areas of the correlating peaks. Calibration curves were measured for methane, ethane, propane and butane. Calibration curves are subject to changes when different sample loops, flow rates and columns are applied for the measurements..... **50**

Figure 5.1: Proportions of methane for samples from production sample sets P1, P2 and P3 presented versus production time. First available sample is set to 0 hours. Proportions are normalized on the basis of proportions of methane, ethane, propane, *n*–butane, *i*–butane and carbon dioxide. For discussion of data see text. Note the different scales.... **87**

Figure 5.2: Proportions of higher hydrocarbons (ethane, propane, *n*–butane and *i*–butane) for samples from production sample sets P1, P2 and P3 presented versus production time. First available sample is set to 0 hours. Proportions are normalized on the basis of proportions of methane, ethane, propane, *n*–butane, *i*–butane and carbon dioxide. For discussion of data see text. Note the different scales..... **88**

Figure 5.3: Proportions of carbon dioxide for samples from production sample sets P1, P2 and P3 presented versus production time. First available sample is set to 0 hours. Proportions are normalized on the basis of proportions of methane, ethane, propane, *n*–butane, *i*–butane and carbon dioxide. For discussion of data see text. Note the different scales..... **89**

Figure 5.4: $\delta^{13}C$ ratios for methane from samples of production sample sets P1, P2 and P3 presented versus production time. First available sample is set to 0 hours. For discussion of data see text. Note the different scales..... **90**

Figure 5.5: δD ratios for methane from samples of production sample sets P1, P2 and P3 presented versus production time. First available sample is set to 0 hours. For discussion of data see text. Note the different scales..... **91**

Figure 5.6: $\delta^{13}C$ ratios for carbon dioxide from samples of production sample sets P1, P2 and P3 presented versus production time. First available sample is set to 0 hours. For discussion of data see text. Note the different scales..... **92**

Figure 5.7: $\delta^{13}C$ ratios for ethane from samples of production sample sets P3 presented versus production time. First available sample is set to 0 hours. Results for samples from production scenarios P1 and P2 are not available. For discussion of data see text..... **93**

Figure 5.8: Proportions of methane for samples from desorption experiment sample sets D1, D2, D3, D4, D5, D6 and D7 presented versus desorption time. Proportions are normalized on the basis of proportions of methane, ethane, propane, *n*–butane, *i*–butane and carbon dioxide. For discussion of data see text. Note the different scales.... **94**

Figure 5.9: Proportions of higher hydrocarbons (ethane, propane, *n*–butane and *i*–butane) for samples from desorption experiment sample sets D1, D2, D3, D4, D6 and D7 presented versus desorption time. No results are available for desorption experiment sample set D5. Proportions are normalized on the basis of proportions of methane, ethane, propane, *n*–butane, *i*–butane and carbon dioxide. For discussion of data see text. Note the different scales..... **95**

Figure 5.10: Proportions of carbon dioxide for samples from desorption experiment sample sets D1, D2, D3, D4, D5 and D7 presented versus desorption time. No results are available for desorption experiment sample set D6. Proportions are normalized on the basis of proportions of methane, ethane, propane, *n*–butane, *i*–butane and carbon dioxide. For discussion of data see text. Note the different scales..... **96**

Figure 5.11: $\delta^{13}C$ ratios for methane from samples of desorption experiment sample sets D1, D2, D3, D4, D5, D6 and D7 presented versus desorption time. For discussion of data see text. Note the different scales..... **97**

Figure 5.12: δD ratios for methane from samples of desorption experiment sample sets D1, D2, D3, D4, D5, D6 and D7 presented versus desorption time. For discussion of data see text. Note the different scales..... **98**

Figure 5.13: $\delta^{13}C$ ratios for carbon dioxide from samples of desorption experiment sample sets D1, D2, D3, D4, D5, D6 and D7 presented versus desorption time. For discussion of data see text. Note the different scales..... **99**

Figure 5.14: $\delta^{13}C$ ratios for ethane from samples of desorption experiment sample sets D2, D3, D6 and D7 presented versus desorption time. Results for desorption experiment sample sets D1, D4 and D5 are not available. For discussion of data see text. Note the different scales..... **100**

Figure 6.1: $\delta^{13}C$–ratios (t_{START}, t_{END} and t_{WGH}) for methane from production and desorption experiment samples presented versus maturity (vitrinite reflectance) of the corresponding coals. t_{START} represents the first sample available per well or canister respectively, t_{END} represents the last sample available per well, or canister respectively. For calculation of value t_{WGH} see text. No results are available for sample sets P1 and D1..... **102**

Figure 6.2: δD–ratios (t_{START}, t_{END} and t_{WGH}) for methane from production and desorption experiment samples presented versus maturity (vitrinite reflectance) of the corresponding coals. t_{START} represents the first sample available per well or canister respectively, t_{END} represents the last sample available per well, or canister respectively. For calculation of value t_{WGH} see text. No results are available for sample sets P1 and D1. Note the different scales..... **103**

Figure 6.3: $\delta^{13}C$–ratios (t_{START}, t_{END} and t_{WGH}) for methane from production and desorption experiment samples presented versus amount of vitrinite in the corresponding coals. t_{START} represents the first sample available per well or canister respectively, t_{END} represents the last sample available per well, or canister respectively. For calculation of value t_{WGH} see text. No results are available for sample sets P1, P2, D1 and D2..... **106**

Figure 6.4: δD–ratios (t_{START}, t_{END} and t_{WGH}) for methane from production and desorption experiment samples presented versus amount of vitrinite in the corresponding coals. t_{START} represents the first sample available per well or canister respectively, t_{END} represents the last sample available per well, or canister respectively. For calculation of value t_{WGH} see text. No results are available for sample sets P1, P2, D1 and D2. Note the differences in scale..... **107**

Figure 6.5: $\delta^{13}C$–ratios (t_{START}, t_{END} and t_{WGH}) for methane from production and desorption experiment samples presented versus amount of liptinite in the corresponding coals. t_{START} represents the first sample available per well or canister respectively, t_{END} represents the last sample available per well, or canister respectively. For calculation of value t_{WGH} see text. No results are available for sample sets P1, P2, D1 and D2..... **108**

Figure 6.6: δD–ratios (t_{START}, t_{END} and t_{WGH}) for methane from production and desorption experiment samples presented versus amount of liptinite in the corresponding coals. t_{START} represents the first sample available per well or canister respectively, t_{END} represents the last sample available per well, or canister respectively. For calculation of value t_{WGH} see text. No results are available for sample sets P1, P2, D1 and D2. Note the differences in scale..... **109**

Figure 6.7: $\delta^{13}C$–ratios (t_{START}, t_{END} and t_{WGH}) for methane from production and desorption experiment samples presented versus amount of inertinite in the corresponding coals. t_{START} represents the first sample available per well or canister respectively, t_{END} represents the last sample available per well, or canister respectively. For calculation of value t_{WGH} see text. No results are available for sample sets P1, P2, D1 and D2..... **110**

Figure 6.8: δD–ratios (t_{START}, t_{END} and t_{WGH}) for methane from production and desorption experiment samples presented versus amount of inertinite in the corresponding coals. t_{START} represents the first sample available per well or canister respectively, t_{END} represents the last sample available per well, or canister respectively. For calculation of value t_{WGH} see text. No results are available for sample sets P1, P2, D1 and D2. Note the differences in scale..... **111**

Figure 6.9: $\delta^{13}C$–ratios (t_{START}, t_{END} and t_{WGH}) for methane from production and desorption experiment samples presented versus depth of the corresponding coals. t_{START} represents the first sample available per well or canister respectively, t_{END} represents the last sample available per well, or canister respectively. For calculation of value t_{WGH} see text. No results are available for sample sets P1 and D6..... **112**

Figure 6.10: δD–ratios (t_{START}, t_{END} and t_{WGH}) for methane from production and desorption experiment samples presented versus depth of the corresponding coals. t_{START} represents the first sample available per well or canister respectively, t_{END} represents the last sample available per well, or canister respectively. For calculation of value t_{WGH} see text. No results are available for sample sets P1 and D6. Note the differences in scale..... **113**

Figure 6.11: Methane proportions versus maturity (%R_O) of the corresponding coals for production sample sets P2 and P3 and for desorption experiment sample sets D2, D3, D4, D5, D6 and D7. No data are available for sample sets P1 and D1. Shown are averaged proportions and maturities per well, respectively canister. Proportions are normalized on the basis of methane, ethane, propane, *n*–butane, *i*–butane and carbon dioxide proportions..... **117**

Figure 6.12: Proportions of carbon dioxide versus maturity (%R_O) of the corresponding coals for production sample sets P2 and P3 and for desorption experiment sample sets D2, D3, D4, D5 and D7. No data are available for sample sets P1, D1 and D6. Shown are averaged proportions and maturities per well, respectively canister. Proportions are normalized on the basis of proportions of methane, ethane, propane, *n*–butane, *i*–butane and carbon dioxide..... **117**

Figure 6.13: Proportions of higher hydrocarbons (ethane, propane, *n*–butane and *i*–butane) versus maturity (%R_O) of the corresponding coals for production sample sets P2 and P3 and for desorption experiment sample sets D2, D3, D4, D5, D6 and D7. No data are available for sample sets P1 and D1. Shown are averaged proportions and maturities per well, respectively canister. Proportions are normalized on the basis of proportions of methane, ethane, propane, *n*–butane, *i*–butane and carbon dioxide..... **118**

Figure 6.14: Proportions of higher hydrocarbons (C_{2+}; ethane, propane, *n*–butane and *i*–butane) presented versus proportions of liptinite in the corresponding coals. Proportions are normalized on the basis of proportions of methane, ethane, propane, *n*–butane, *i*–butane and carbon dioxide. No results are available for sample sets P1, P2, D1 and D2..... **118**

Figure 6.15: Graphic presentation of relationships between the maturity (vitrinite reflectance) of a Kerogen Type III source rock with the stable carbon isotope composition ($\delta^{13}C$) of methane, ethane and propane generated from this type of source rock. See text for equations and details (modified from Berner and Faber, 1996)..... **120**

Figure 6.16: $\delta^{13}C$–ratios (t_{START}, t_{END} and t_{WGH}) for methane from production and desorption experiment samples presented versus maturity (vitrinite reflectance) of the corresponding coals. t_{START} represents the first sample available per well or canister respectively, t_{END} represents the last sample available per well, or canister respectively. For calculation of value t_{WGH} see text. Also shown is line representing relationship between maturity of a Kerogen Type III source rock and $\delta^{13}C$–ratio for methane expected to be generated from this type of source rock (after Berner and Faber, 1996). No results are available for sample sets P1 and D1 ..... **122**

Figure 6.17: $\delta^{13}C$–ratios (t_{START}, t_{END} and t_{WGH}) for ethane from production and desorption experiment samples presented versus maturity (vitrinite reflectance) of the corresponding coals. t_{START} represents the first sample available per well or canister respectively, t_{END} represents the last sample available per well, or canister respectively. For calculation of value t_{WGH} see text. Also shown is graph representing relationship between maturity of a Kerogen Type III source rock and $\delta^{13}C$–ratio for ethane expected to be generated from this type of source rock (after Berner and Faber, 1996). No results are available for sample sets P1, P2, D1, D4 and D5 ..... **123**

Figure 6.18: $\delta^{13}C$–ratios (t_{START}, t_{END} and t_{WGH}) for propane from samples of desorption experiments D6 and D7 presented versus maturity (vitrinite reflectance) of the corresponding coals. t_{START} represents the first sample available per well or canister respectively, t_{END} represents the last sample available per well, or canister respectively. For calculation of value t_{WGH} see text. Also shown is graph representing relationship between maturity of a Kerogen Type III source rock and $\delta^{13}C$–ratio for propane expected to be generated from this type of source rock (after Berner and Faber, 1996). No results are available for sample sets P1, P2, P3, D1, D2, D3, D4 and D5 ..... **124**

Figure 6.19: Bernard Diagram indicating areas where natural gases associated with coal are expected to plot (methyl–type fermentation and Kerogen Type III areas). For discussion of diagram see text (modified from Whiticar, 1996a and 1999) **125**

Figure 6.20: Bernard Diagram showing samples from production sample sets P1, P2 and P3. Diagram is modified from Whiticar (1999). For explanations of different areas see Figure 6.19. Note the different scales **126**

Figure 6.21: Bernard Diagram showing samples from desorption experiment sample sets D1, D2, D3, D4, D5, D6 and D7. Diagram is modified from Whiticar (1999). For explanations of different areas see Figure 6.19. Note the different scales **128**

Figure 6.22: $\delta^{13}C$–δD (methane) Diagram indicating areas where natural gases associated with coal are expected to plot (methyl–type fermentation and humic kerogen areas). For discussion of diagram see text (modified from Whiticar, 1996a and 1999) **129**

Figure 6.23: $\delta^{13}C$–δD (methane) Diagram showing samples from production sample sets P1, P2 and P3. Diagram is modified from Whiticar (1999). For explanations of different areas see Figure 6.22 ..... **130**

Figure 6.24: $\delta^{13}C$–δD (methane) Diagram showing samples from desorption experiment sample sets D1, D2, D3, D4, D5, D6 and D7. Diagram is modified from Whiticar (1999). For explanations of different areas see Figure 6.22 ..... **132**

Figure 6.25: Natural gas plots for samples from desorption experiment sample sets D6 and D7. See text for discussion. Diagram is modified after Chung et al., 1988 ..... **133**

Figure 6.26: Calculated fractions of thermogenic and microbial gas in sample sets D6 and D7. Calculations are based on natural gas plots and are performed following description by Chung et al. (1988). Calculations of proportions of thermogenic and microbial gas are performed by applying a mass–balance equation (see text for equation). See text for discussion..... **135**

Figure 6.27: Calculated fractions of thermogenic and microbial gas in CBM samples. A shows sample sets P2, D3, D4 and D5. B shows sample sets D6 and D7. Calculations are based on a comparison between measured $\delta^{13}C$ ratios for methane with $\delta^{13}C$–$\%R_O$ relationship for methane from Berner and Faber (1996). Calculations of proportions of thermogenic and microbial gas are performed by applying a mass–balance equation (see text for equation). See text for discussion..... **137**

Figure 6.28: Comparison of calculated fractions for thermogenic gas generated from a Kerogen Type III source rock based on the approaches by Chung et al. (1988) and Berner and Faber (1996) for sample sets D6 and D7. See text for description of both approaches..... **138**

Figure 6.29: $\delta^{13}C$–ratios (t_{START}, t_{END} and t_{WGH}) for methane from samples of desorption experiment sample sets D6 and D7 presented versus maturity (vitrinite reflectance) of the corresponding coals. t_{START} represents the first sample available per canister, t_{END} represents the last sample available per canister. For calculation of value t_{WGH} see text. Also shown are $\delta^{13}C$–maturity relationships for methane generated from a Kerogen Type II and Kerogen Type III source rock from Berner and Faber (1996). For equations see text..... **142**

Figure 6.30: $\delta^{13}C$–ratios (t_{START}, t_{END} and t_{WGH}) for ethane from samples of desorption experiment sample sets D6 and D7 presented versus maturity (vitrinite reflectance) of the corresponding coals. t_{START} represents the first sample available per canister, t_{END} represents the last sample available per canister. For calculation of value t_{WGH} see text. Also shown are $\delta^{13}C$–maturity relationships for ethane generated from a Kerogen Type II and Kerogen Type III source rock from Berner and Faber (1996). For equations see text..... **143**

Figure 6.31: $\delta^{13}C$–ratios (t_{START}, t_{END} and t_{WGH}) for propane from samples of desorption experiment sample sets D6 and D7 presented versus maturity (vitrinite reflectance) of the corresponding coals. t_{START} represents the first sample available per canister, t_{END} represents the last sample available per canister. For calculation of value t_{WGH} see text. Also shown are $\delta^{13}C$–maturity relationships for propane generated from a Kerogen Type II and Kerogen Type III source rock from Berner and Faber (1996). For equations see text..... **144**

Figure 6.32: Calculated fractions of methane generated from a Kerogen Type III and Kerogen Type II source rock in sample sets D6 and D7. Calculations are based on $\delta^{13}C$–$\%R_O$ relationships for methane by Berner and Faber (1996). Calculations of proportions of thermogenic and microbial gas are performed by applying a mass–balance equation (see text for equation). See text for discussion..... **145**

Figure 6.33: Calculated fractions of ethane generated from a Kerogen Type III and Kerogen Type II source rock in sample sets D6 and D7. Calculations are based on $\delta^{13}C$–$\%R_O$ relationships for ethane by Berner and Faber (1996). Calculations of proportions of thermogenic and microbial gas are performed by applying a mass–balance equation (see text for equation). See text for discussion..... **146**

Figure 6.34: Calculated fractions of propane generated from a Kerogen Type III and Kerogen Type II source rock in sample sets D6 and D7. Calculations are based on $\delta^{13}C$–$\%R_O$ relationships for propane by Berner and Faber (1996). Calculations of proportions of thermogenic and microbial gas are performed by applying a mass–balance equation (see text for equation). See text for discussion..... **147**

Figure 6.35: $\delta^{13}C$–ratios (t_{START}, t_{END} and t_{WGH}) for methane from samples of desorption experiment sample set D7 presented versus depth of the corresponding coals. t_{START} represents the first sample available per canister, t_{END} represents the last sample available per canister. For calculation of value t_{WGH} see text. For discussion see text.... **153**

Figure 6.36: $\delta^{13}C$–ratios (t_{START}, t_{END} and t_{WGH}) for ethane from samples of desorption experiment sample set D7 presented versus depth of the corresponding coals. t_{START} represents the first sample available per canister, t_{END} represents the last sample available per canister. For calculation of value t_{WGH} see text. For discussion see text.... **154**

Figure 6.37: $\delta^{13}C$–ratios (t_{START}, t_{END} and t_{WGH}) for propane from samples of desorption experiment sample set D7 presented versus depth of the corresponding coals. t_{START} represents the first sample available per canister, t_{END} represents the last sample available per canister. For calculation of value t_{WGH} see text. For discussion see text.... **155**

Figure 6.38: Idealized and schematic model for mixture of methane generated from a Kerogen Type III and methane from a Kerogen Type III source rock from samples of sample set D7. CH_4 = methane; + = medium; ++ = strong; +++ = very strong Stippled red line does not represent an actual mixing line, but illustrates the changes for the $\delta^{13}C$ ratio for methane. See text for discussion..... **156**

Figure 6.39: $\delta^{13}C$ methane–$\delta^{13}C$ ethane plot showing expected isotope trends for methane and ethane due to processes of admixture of bacterial methane, mixture of different thermogenic gases and microbial methane oxidation. Shown are results from production and desorption experiment sample sets P3, D2, D3, D6 and D7, together with vitrinite reflectance values of the corresponding coals. No results for the other sample sets are available. Black line indicates unaltered gases (methane and ethane) with increasing maturity (modified from Berner and Faber, 1996)..... **160**

Figure 6.40: Idealized diagram showing effect of temperature and pressure on the sorption capacity of coal during burial and uplift. See text for discussion..... **162**

Figure 6.41: Diffusion plot showing $\delta^{13}C$ ratio for methane versus ratio of proportions of methane over ethane for samples of production sample sets P1, P2 and P3. See text for details (diagram from Colombo et al., 1970 and Prinzhofer and Pernaton, 1997)..... **169**

Figure 6.42: Diffusion plot showing $\delta^{13}C$ ratio for methane versus ratio of proportions of methane over ethane for samples of desorption experiment sample sets D1, D2, D3, D4, D6 and D7. See text for details. No results are available for sample set D5 (diagram from Colombo et al., 1970 and Prinzhofer and Pernaton, 1997)..... **171**

Figure 6.43: Cross–plot of $\delta^{13}C$ methane versus proportions of methane for samples of production sample sets P1, P2 and P3. Proportions are normalized on the basis of proportions of methane, ethane, propane, *n*–butane, *i*–butane and carbon dioxide. See text for discussion..... **174**

Figure 6.44: Cross–plot of $\delta^{13}C$ ethane versus proportions of ethane for samples of production sample set P3. Proportions are normalized on the basis of proportions of methane, ethane, propane, *n*–butane, *i*–butane and carbon dioxide. No results are available for sample sets P1 and P2. See text for discussion..... **175**

Figure 6.45: Cross–plot of $\delta^{13}C$ carbon dioxide versus proportions of carbon dioxide for samples of production sample sets P1, P2 and P3. Proportions are normalized on the basis of proportions of methane, ethane, propane, *n*–butane, *i*–butane and carbon dioxide. See text for discussion..... **176**

Figure 6.46: Cross–plot of $\delta^{13}C$ methane versus proportions of methane for samples of desorption experiment sample sets D1, D2, D3, D4, D5, D6 and D7. Proportions are normalized on the basis of proportions of methane, ethane, propane, *n*–butane, *i*–butane and carbon dioxide. See text for discussion..... **179**

Figure 6.47: Cross–plot of $\delta^{13}C$ ethane versus proportions of ethane for samples of desorption experiment sample sets D2, D3, D6 and D7. Proportions are normalized on the basis of proportions of methane, ethane, propane, *n*–butane, *i*–butane and carbon dioxide. No results are available for sample sets D1, D4 and D5. See text for discussion..... **180**

Figure 6.48: $\delta^{13}C$–ratios of carbon dioxide versus proportions of carbon dioxide for samples of desorption experiment sample sets D1, D2, D3, D4, D5 and D7. Proportions are normalized on the basis of proportions of methane, ethane, propane, *n*–butane, *i*–butane and carbon dioxide. No results are available for sample set D6. See text for discussion..... **181**

Figure 6.49: Idealized model of a coal seam showing the effect of water and gas production, as well as the influence of hydraulic fracturing on selected physical and chemical parameters. See text for discussions..... **184**

Figure 6.50: Idealized model for isotope and compositional development of methane during the production of CBM. Actual distances of Areas 1, 2 and 3 are not known and should differ strongly between different coal seams. Vol. = Volume. See text for discussion..... **186**

Figure 6.51: Proportions of methane, higher hydrocarbons (C_{2+}; ethane, propane, *n*–butane and *i*–butane) and carbon dioxide of samples from production sample set P3 presented versus production time. Proportions are normalized on the basis of proportions of methane, ethane, propane, *n*–butane, *i*–butane and carbon dioxide. Black line represents sample 15 (2424 hours). See text for discussion..... **190**

Figure 6.52: $\delta^{13}C$– and δD–ratios of methane and $\delta^{13}C$–ratios of carbon dioxide of samples from production sample set P3 presented versus production time. Black line represents sample 14 (2280 hours). See text for discussion..... **191**

Figure 6.53: Idealized model showing closing and opening of fracture systems in coal seams and lateral extension of fracture system as a result of the production of CBM from wells of production sample sets P3. See text for discussion..... **192**

Figure 6.54: Gas production volumes for the considered three wells of production sample set P3 between January 14th 2004 and January 8th 2005. Yellow area indicates time period between August 21st and August 29th 2004, where in samples from all three wells major compositional and isotope changes are observed. See text for discussion..... **194**

Figure 6.55: Conceptual and relative map for the set up of the three wells considered for production scenario P3. Location, exact distance between the wells and further details about these wells are confidential. Reported distances between the wells are several hundred meters..... **194**

Figure 7.1: Bernard Diagram showing samples from production sample sets P1, P2 and P3 and desorption experiment sample sets D1, D2, D3, D4, D5, D6 and D7. Diagram is modified from Whiticar (1999). For explanations of different areas see figure 6.16..... **199**

Figure 7.2: $\delta^{13}C$–δD (methane) Diagram showing samples from production sample sets P1, P2 and P3 and from desorption experiment sample sets D1, D2, D3, D4, D5, D6 and D7. Diagram is modified from Whiticar (1999). For explanations of different areas see figure 6.19..... **200**

Figure 7.3: Diffusion plot showing $\delta^{13}C$ ratio for methane versus proportion ratio of methane over ethane for samples of desorption experiment sample sets D1, D2, D3, D4, D6 and D7. See text for details. No results are available for sample set D5. Diffusion lines are exemplary only and do not resemble measured values. Mixing line 1 is taken from Prinzhofer and Pernaton (1997); Mixing line 2 is based on pure microbial methane and gas generated from a Kerogen type III source rock with a maturity of ca. 1.5%R_O. Mixing line 1: Endmembers are based on $\delta^{13}C$ values of -80‰ and -35‰ and C_2/C_1 • 1000 ratios of 0 and 300. Mixing line 2: Endmembers are based on $\delta^{13}C$ values of -60‰ and -26‰ and C_2/C_1 • 1000 ratios of 0 and 200 (diagram from Colombo et al., 1970 and Prinzhofer and Pernaton, 1997)..... **204**

Figure 7.4: Semi logarithmic diffusion plot showing $\delta^{13}C$ ratio for methane versus proportion ratio of methane over ethane for samples of desorption experiment sample sets D1, D2, D3, D4, D6 and D7. See text for details. No results are available for sample set D5. Diffusion lines are exemplary only and do not resemble measured values (diagram from Colombo et al., 1970 and Prinzhofer and Pernaton, 1997)..... **205**

Figure 7.5: Cross–plot of $\delta^{13}C$ methane versus proportion of methane for samples of production sample sets P1, P2 and P3. Concentrations are normalized on the basis of methane, ethane, propane, *n*–butane, *i*–butane and carbon dioxide concentrations. Isotope range for Kerogen Type III source rocks (coals) from Whiticar (1996a). See text for discussion..... **206**

Figure 7.6: Cross–plot of $\delta^{13}C$ carbon dioxide versus carbon dioxide proportions for samples of production sample sets P1, P2 and P3. Proportions are normalized on the basis of methane, ethane, propane, *n*–butane, *i*–butane and carbon dioxide proportions. See text for discussion..... **208**

Figure 7.7: Cross–plot of $\delta^{13}C$ carbon dioxide versus carbon dioxide proportions for samples of production sample sets P1, P2 and P3. Proportions are normalized on the basis of methane, ethane, propane, *n*–butane, *i*–butane and carbon dioxide proportions. Only proportions between 0% and 10% are shown. For the entire range see Figure 7.6. See text for discussion..... **208**

Figure 7.8: Cross–plot of $\delta^{13}C$ methane versus methane proportions for samples of desorption experiment sample sets D1, D2, D3, D4, D5, D6 and D7. Proportions are normalized on the basis of methane, ethane, propane, *n*–butane, *i*–butane and carbon dioxide proportions. See text for discussion..... **210**

Figure 7.9: $\delta^{13}C$–ratios of carbon dioxide versus carbon dioxide proportions for samples of desorption experiment sample sets D1, D2, D3, D4, D5 and D7. Proportions are normalized on the basis of methane, ethane, propane, *n*–butane, *i*–butane and carbon dioxide proportions. No results are available for sample set D6. Isotope ratio for coal is an average value. $\delta^{13}C$ ratios of coal range generally between -22‰ and -27‰ (Whiticar, 1996a). Isotope ratios of carbon dioxide approach a value of ca. -10‰ with increasing proportion of carbon dioxide. Based on the difference between -10‰ and the average isotope ratio of coal, the fractionation factor (α) is 14‰ or 1.014. See text for discussion..... **211**

Figure 7.10: Cross–plot of $\delta^{13}C$ ethane versus ethane proportions for samples of desorption experiment sample sets D2, D3, D6 and D7. Proportions are normalized on the basis of methane, ethane, propane, *n*–butane, *i*–butane and carbon dioxide proportions. No results are available for sample sets D1, D4 and D5. Isotope ratio for coal is an average value. $\delta^{13}C$ ratios of coal range generally between -22‰ and -27‰ (Whiticar, 1996a). Isotope ratios of ethane approach a value of ca. -28‰ with increasing proportion of ethane. Based on the difference between -28‰ and the average isotope ratio of coal, the fractionation factor (α) is -3‰ or 0.997.See text for discussion..... **212**

List of Abbreviations and Symbols

CBM	Coalbed methane
C_1	Methane
C_2	Ethane
C_3	Propane
n–C_4	normal–butane
i–C_4	iso–butane
C_{2+}	Higher hydrocarbons (ethane, propane, n–butane and i–butane)
^2H	Deuterium
$\%R_O$	Maturity; per cent vitrinite reflectance
[ ]	Concentration or proportion
Px	Production sample set x
Dx	Desorption experiment sample set x
GC–IRMS	Gas Chromatograph – Isotope Ratio Mass Spectrometer
PDB	PeeDee Belemnite: standard for stable carbon isotope ratios
SMOW	Standard Mean Ocean Water: standard for stable hydrogen isotope ratios
ZPE	Zero point energy
ν_0	Ground frequency
h	Planck's constant
α	Fractionation factor n
J	Diffusive flux
D	Diffusion coefficient
C	Volume
D_{eff}	Effective diffusion coefficient
C_{bulk}	Bulk volume concentration
TOC	Total organic carbon (wt.%)
$\delta^{13}C_{org}$	Stable carbon isotope ratio of organic carbon

$\delta^{13}C_{coal}$	Stable carbon isotope ratio of coal
$\delta^{13}C_{Plant}$	Stable carbon isotope ratio of plant material
$\delta^{13}C_{1(I)}$	Stable carbon isotope ratio of instantaneous methane
R_r; $\delta^{13}C_r$	Stable carbon isotope ratio of initial reactant pool
R_0; $\delta^{13}C_0$	Stable carbon isotope ratio of residual reactant pool
$\delta^{13}C_g$	Stable carbon isotope ratio of total cumulative gas already generated
f	Fraction
Ø	Average
Vit.	Vitrinite
Iner.; Inert.	Inertinite
Lipt.	Liptinite
n/a	Not available
Prod.	Production scenario
Des.	Desorption experiment scenario
HV–Bit.A	High volatile bituminous A coal
HV–Bit.B	High volatile bituminous B coal
HV–Bit.C	High volatile bituminous C coal
MV–Bit.	Medium volatile bituminous coal
LV–Bit.	Low volatile bituminous coal
Sub–Bit.A	Sub bituminous A coal
norm.	normalized
(2)	Sample number
(s.s.)	Several samples
t_{start}	$\delta^{13}C$ and δD value for methane available from the earliest sample per well or canister of each sample set
t_{end}	$\delta^{13}C$ and δD value for methane available from the latest sample per well or canister of each sample set

$t_{WEIGHTED}$; t_{WGH}	Individual $\delta^{13}C$ and δD values set into relation with the proportion of methane of corresponding samples, based on the following relationships: $t_{WEIGHTED}\ (\delta^{13}C) = (\delta^{13}C\ a \cdot [CH_4\ a]) + (\delta^{13}C\ b \cdot [CH_4\ b]) + ... + (\delta^{13}C\ n \cdot [CH_4\ n]) / \Sigma\ [CH_4\ a \rightarrow n]$ $t_{WEIGHTED}\ (\delta D) = (\delta D\ a \cdot [CH_4\ a]) + (\delta D\ b \cdot [CH_4\ b]) + ... + (\delta D\ n \cdot [CH_4\ n]) / \Sigma\ [CH_4\ a \rightarrow n]$
Σ	Sum
$\uparrow$	Increase in proportion/ increase in ^{13}C/ increase in D
$\downarrow$	Decrease in proportion/ increase in ^{12}C/ increase in ^{1}H
$\rightarrow$	No overall trend in relation to decrease or increase
$\cap$	Distinct maximum
F	Fluctuations
SF	Strong fluctuations
>>	Followed by
⌐	Until 100% are reached
Vol.%	Volume per cent
Can.	Canister
meas.	Measured
calc.	Calculated

Acknowledgements

I would like to thank my supervisor Michael Whiticar for not only giving me the opportunity to do my Ph.D. and to work with him, but also for the possibility to do it in Canada. My almost four years here in Victoria have been a tremendous experience and I feel lucky to have the chance to life and work in such a beautiful place. In this context I also want to thank Peter Gerling and Bernhard Cramer from the Federal Institute for Geosciences and Resources (BGR) in Hanover, Germany, who thought of me, when Michael was looking for a new Ph.D. student. Without them none of this would have happened.

A special thank you goes to Barry Ryan from the Geological Survey of British Columbia here in Victoria. Without his support, knowledge and connections the sample situation would by far not have been as good as it is and this thesis would not exist. He introduced me to many interesting people and I have learned so much during our discussions.

I want to thank my supervising committee Kevin Telmer, Stephen Johnston and Eileen van der Flier-Keller for correcting my thesis and I feel really sorry for the length of the thesis. I tried to keep it as short as possible, but was apparently not really successful in doing so. Special thanks go to Tony Lemay who stepped in as my external examiner.

Samples, knowledge and help were provided by several companies and especially from many people working for these companies. Both, companies and their people, wish to stay anonymous, but I want to thank them all for their uncomplicated and invaluable help and sample supply.

Paul Eby had to life with my presence in the lab for quite some time and was probably constantly concerned about the "health" of his mass spec., but I have managed to kill it only once. I want to thank him for all his great and invaluable help. Regardless what problem was occurring, related to hardware or my samples, he always found a solution and saved me from spending too many nights in the lab.

I want to thank the British Columbia Ministry for Energy and Mines for funding my work and agreeing on shifting the focus of the work from water to gas.

In the last years I have met so many new people and I call many of them friends now. For help and the good times I want to thank you all. I cannot mention all of you here, but I will do my best. I say sorry already to all the ones I forget. Thanks to Doc Martin, Steve, Mike, Mikhail, Ruben, Dave, Paul, Michael, Shawn, Genevieve, Kim, Rebecca, Torge, Evodia, Ulrich, Hildegard, the crew of the CCGS John P. Tully, Manfred, Erika, Ross, George, Sussi, Carrie, Leslie, Mae, Julie, Shannon, Hinrich, Kathleen and Rob.

And I do not want to forget all the help from family and friends over in good old Europe. I want to thank my mom Helga, Roland, Jutta, Dieter, my grandma Anna, Inge, Dieter, Jochen, Regina, Britta, Alex, Babs, Arne, Dirk, Olli, Schaetzle, Nicole, Kai, Imke, Matze and Cristina.

Last but not least I want to thank my wife Ulrike. Regardless of what crazy idea I came up with, she was always on my side and there for me. Her support in so many different ways was incredible and helped me to put this work together. I thank you for all you have done and I love you. And I promise that there are more crazy ideas.

There is a theory which states that if ever anyone discovers exactly what the Universe is for and why it is here, it will instantly disappear and will be replaced by something even more bizarre and inexplicable.

There is another theory which states that this has already happened.

Douglas Adams (1952–2001)
"The Restaurant at the End of the Universe"

1. Introduction

Increasing petroleum prices and environmental considerations are leading to the development of alternative energies, like solar energy, wind and water energy and fuel cells. The present development of fuel cells, especially in Europe, is encouraging, but it will take several more years for fuel cells, and even more time for the other alternative energies to be competitive on the energy market. Therefore, there is still a market for "clean" fossil fuel in the form of natural gas. Considering that the hydrogen source for fuel cells is methane, there will be also a market for natural gas in the future.

Coalbed methane (CBM) is a source for "clean" fossil fuel and is gaining strong attention. The production of CBM is not as extensive and expensive as offshore oil and gas production and coal seams are widespread all over the world, implying huge resources of methane. The presence of natural gases in coal seams has been known for centuries and was and still is the reason for many devastating catastrophes in the history of coal mining. At the end of the 19th and the beginning of the 20th century, gas emitting from coal became the focus of scientific research. The focus of this research was on the identification of the source and the amount and composition of these gases, as well as on how to handle these gases to prevent future mine explosions (e.g. Chamberlin, 1909). Coal itself was a huge focus of scientific research until the 1960's, because of its use for energy generation. The increasing demand for natural gas, especially methane, as a "clean" energy source brought coal and coal gases again into the focus of scientific research at the end of the 20th century.

This research focussed mainly on the use of CBM as an energy source, the production of CBM and the physical, chemical and geological parameters influencing the ability of coal to store gases (e.g. Bertard et al., 1970; Joubert et al., 1974; McCulloch & Diamond, 1976; Kim, 1977; Diamond & Levine, 1981; Rigby & Smith, 1981; Meissner, 1984; Creedy, 1988; Levine, 1993; Rice, 1993; Yee et al., 1993; Ryan & Dawson, 1994; Beamish & Crosdale, 1995; Bustin et al., 1995; McLennan et al., 1995; Diamond & Schatzel, 1998; Crosdale et al., 1998; Laubach et al., 1998; Kopp et al., 2000). The consideration of stable isotopes in CBM started with a study by Colombo et al. (1970) about carbon isotopes in methane from German coals. In their study the importance of

secondary processes, like adsorption, desorption and diffusion were emphasized. Currently, a strong emphasis is on the investigation of natural gases generated from coal during pyrolysis experiments (e.g. Gaschnitz et al., 2001; Cramer, 2004; Kotarba & Lewan, 2004). Results from these experiments deliver information about the generation of gas from coal and the composition of gases expected for coals of different ranks, both molecular and isotopic. The importance of effects as a result of secondary processes, as they are anticipated in a natural coal setting is not considered. Work by Colombo et al. (1970), Friedrich and Jüntgen (1972 and 1973), Smith et al. (1985), Gould et al. (1987) and Hosgörmez et al. (2002) considered CBM samples collected directly from the coal during desorption experiments. But for these studies the amount of samples were limited and represented only a short time period in the total duration of the desorption experiment or are actually mixtures of gases desorbing from the coal over a substantial amount of time. To my knowledge, no systematic study of stable carbon and hydrogen isotopes for CBM was undertaken, including the consideration of samples from desorption experiments and from producing wells, as well as samples coming from coals covering a wide range of different maturities and other coal petrological parameters like maceral content.

Secondary processes like adsorption, desorption and diffusion are anticipated to influence the molecular and isotope composition of CBM. The aim of this study was to identify the impact of these processes on the molecular and isotope composition of the different gas species contained in CBM. The origin of gases collected from coal was determined based on the molecular and isotope composition of analyzed CBM samples. The same parameters might lead to the identification of mixing processes between CBM and microbial gas, between CBM and gases generated from a different type of source rock and between CBM generated from different coals. Because of the availability of samples from both, desorption experiments and actual CBM production, a comparison of stable isotope systematics between both types of samples was conducted.

If the stable isotope systematic of CBM is understood and governed by quantifiable principles and processes, isotope studies of CBM might have the potential to replace the currently used canister desorption technique for the evaluation of the total gas content of a coal seam. Isotope ratios and isotope shifts for gas species in CBM might

allow the quantification of the amount of lost and residual gas. This would reduce the required time for the conventional canister approach substantially.

Besides the current attention CBM is gaining, more research has to be conducted to understand the implications of primary and especially secondary processes for coal and CBM, both molecular and isotopic. A better molecular and isotopic understanding of the coal system in terms of gas generation, loss, storage, release and finally production is needed for a more sophisticated evaluation and exploitation of this natural resource.

2. Background

2.1 Coal and Coal Formation

Organic matter in rocks can be differentiated into kerogen and bitumen. Kerogen is the organic constituent, which is defined as not soluble in organic or alkaline solvents. Bitumen is the soluble constituent (Perrodon, 1983). Kerogen is a macro–molecular complex composed of benzene rings and connected by heteroatomic (ketones, ester, ether, sulphide, disulfide) or aliphatic ($-(CH_2)_n-$) links; it may also contain lipids (Tissot and Welte, 1978; Perrodon, 1983). Kerogen occurring in sedimentary rocks can be differentiated into three different Types (I, II and III), in regard to chemical composition and depositional environment. Kerogen Type I and Type II have a very high potential for the generation of oil and gas, whereby the potential for Kerogen Type I is greater than for Type II; Kerogen Type III has only a moderate oil potential, but has, when buried to greater depths, a high gas potential (Tissot and Welte, 1978; Perrodon, 1983).

Coal is a sedimentary rock of biological and geological origin. Predominantly terrestrial organic matter (Kerogen Type III) is deposited in swamps or swamp–like environments and when subjected to time, pressure and temperature, this material is diagenetically altered into coal by the process of coalification. The type of organic matter and the intensity and duration of the coalification process determine the coal rank, its properties and finally the presence of gaseous and sometimes also liquid hydrocarbons in the coal.

2.1.1 Coal Macerals

Coal contains a wide variety of different plant tissues, which can, depending on the stage of preservation, be identified by the use of a microscope. These tissues can be related to certain parts of plants, such as wood, spores and cuticles. These particles, together with less certain identifiable particles, are termed macerals and are the petrographic components of coal (Taylor et al., 1998). Macerals, and consequently, the composition of coals vary according to the stage of coalification or their coal rank

respectively (van Krevelen, 1963). Macerals can be separated into three main groups: Liptinites, vitrinites and inertinites. Their separation is generally based on their appearance and reflectance, which depends on the coal rank, shape, structure and by their H/C and O/C atomic ratios (see Figure 2.1; Tissot and Welte, 1978).

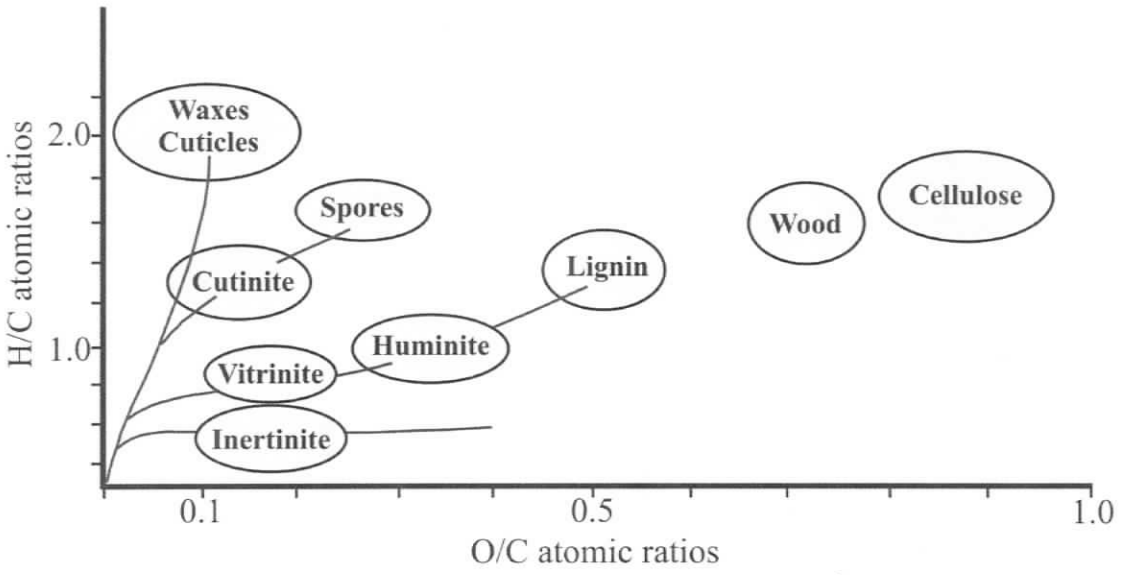


Figure 2.1: *van Krevelen diagram showing atomic oxygen/carbon ratios versus atomic hydrogen/carbon ratios of different plant materials and main coal macerals. Waxes, cuticles, spores and cutinites comprise the maceral group liptinite (modified from Tissot and Welte, 1978).*

The liptinite group (previously called 'exinite') shows the lowest reflection of all maceral groups and is identifiable under the microscope as former spores, cuticles and algae (Taylor et al., 1998). Liptinites are chemically resistant and enriched in hydrogen, based on the fact that a large fraction of liptinites derives from plant lipids (Taylor et al., 1998). The hydrogen–rich components make liptinite rich coals prone not only for the generation of gas, but also for oil generation (Schwarzkopf, 1984). Liptinites can be further separated according to the precursor material. Sporinites are composed of spores, cutinites of cuticles, resinites of remains of plant resins, and waxes and alginates of algal bodies.

Vitrinites are the most common macerals in coal and show a medium reflectance. These macerals are derived from lignin– and cellulose–rich woody substances (Teichmüller and Teichmüller, 1967). The vitrinites can be sub–divided into telinite with a visible cell structure of wood and bark and into structureless collinite and tello–vitrinite.

Inertinites show the highest reflectance of all maceral groups and are believed to form prior to the coalification process by the oxidation of the organic matter due to forest fires and/or atmospheric and bacterial action resulting in carbon enrichment and hydrogen depletion (Tissot and Welte, 1978; Taylor et al. 1998). The most important inertinites are fusinite and semi–fusinite, which still show the distinct cell structure of wood. Macerals of the liptinite and vitrinite groups, subjected to pre–coalification oxidation can also be transformed into inertinites. Figure 2.1 shows a van Krevelen diagram with selected plant materials and their relation to the above mentioned maceral groups. For a more vigorous treatment of coal petrology, refer to the publication by Taylor et al. (1998).

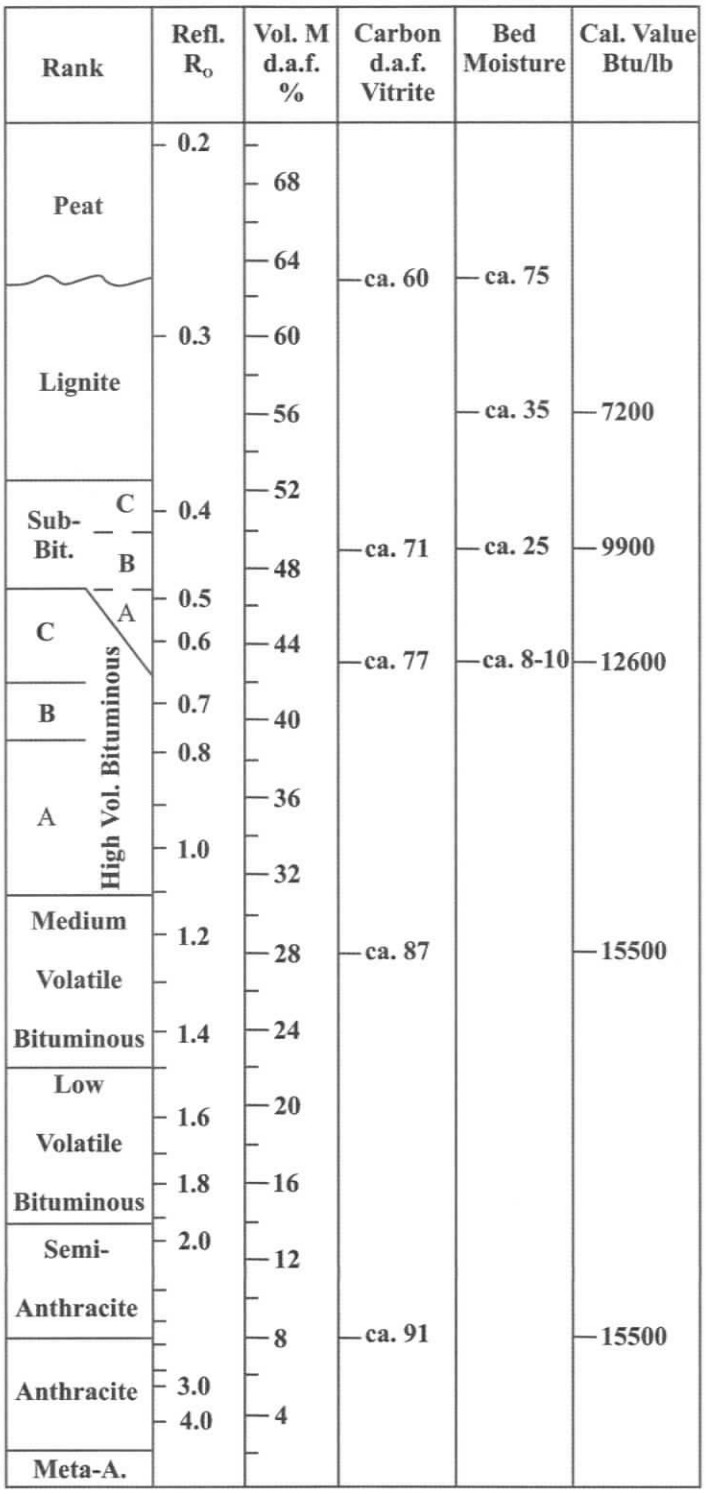


Figure 2.2: *Different coal ranks ranging from peat to meta–anthracite in relation to coal parameters maturity, volatile matter content, carbon content, bed moisture and calorific value (modified from Rice, 1993).*

2.1.2 Vitrinite Reflectance

Vitrinite reflectance is probably the most important and most used maturation index because it is only significantly affected by temperature and not by time (Tissot and Welte, 1978; Welte and Yalçin, 1988; Hunt, 1995). Vitrinite reflectance was developed as a tool for the evaluation of coal ranks and later became a tool for the determination of the maturity of organic matter in sediments and sedimentary rocks.

The reflectance of the maceral vitrinite ($\%R_O$) is measured as the amount of light, reflected from a polished surface of vitrinite compared to light reflected from a standard of known reflectance. The measurements are generally conducted under monochromatic green light with a wavelength of 546nm. To enhance the contrast of petrographic components, oil immersion objective lenses are used (Tissot and Welte, 1978). The reflectance is expressed in % and has a maximum value of 15% for graphite (Tissot and Welte, 1978; Hunt, 1995).

Vitrinite reflectance increases with increasing maturation because of chemical and physical changes of the vitrinite structure (Hunt, 1995). These changes include condensation, polymerization, aromatization, loss of functional groups, decreasing water content, density increase and porosity decrease (Tissot and Welte, 1978). The building blocks of vitrinite are clusters of condensed aromatic rings, which are stacked on top of each other, linked with hydroaromatic– and methylene–groups and fringed with methyl–, hydroxyl–, carboxyl– and other functional groups (Tissot and Welte, 1978; Hunt, 1995). Increasing maturation has the effect that the clusters become combined into larger condensed–aromatic rings, which eventually form sheets of condensed rings, assuming an orderly structure (Hunt, 1995). This preferred orientation and the increased size of the sheets are responsible for the increase in reflectivity (Welte and Yalçin, 1988; Hunt, 1995). The final product of this coalification process (see Chapter 2.1.5) is meta–anthracite, which is highly aromatic in structure and comparable to poorly ordered graphite (Tissot and Welte, 1978).

2.1.3 Coal Types

Coals are divided into sapropelic and humic coals. Sapropelic coals are formed from fine–grained organic mud, deposited in a reducing low–energy environment, such as lakes, ponds and lagoons (Teichmüller and Teichmüller, 1967; Taylor et al., 1998). Sapropelic coals do not undergo peatification (see Chapter 2.1.4), normally the first step of the coalification process (Tissot and Welte, 1978). The organic components of sapropelic coals consist of autochthonous algal remains and allochthonous degradation products from nearby peat swamps or spores from more distant plants (Tissot and Welte, 1978). Microscopically, sapropelic coals can be divided into cannel and boghead coals. Cannel coals are characterized by a higher concentration of spores, whereas boghead coals are characterized by a higher concentration of algal remains (van Krevelen, 1963). Humic coals are typically stratified and the autochthonous deposited organic matter that has undergone the process of peatification (Teichmüller and Teichmüller, 1967; Tissot and Welte, 1978). Kerogen Type I and II source rocks are comparable with sapropelic coals and Kerogen Type III source rocks are comparable with humic coals (Whiticar, 1996a).

2.1.4 Peatification

The process of peatification is divided into two steps: a primary oxidation phase at, and immediately below, the surface of the water and a secondary reduction phase in greater depth beneath the water table (Tissot and Welte, 1978). The oxidation starts immediately after the deposition of dead plant material and is accompanied by microbial and fungal activity, as well as mechanical breakage and compaction. Depending on the intensity of these processes, large parts of the plant structures disappear. Easily hydrolysable substances like cellulose (aliphatic structure) and lignin (aromatic structure) are decomposed first, which results in a relative enrichment in carbon and of the more inert substances like waxes and resins (Teichmüller and Teichmüller, 1967). The aerobic degradation of organic matter is accompanied by the generation of carbon dioxide and water (Levine, 1993). The aerobic oxidation of the organic matter consumes the oxygen

present, resulting in anaerobic conditions under which the second step of peatification takes place. Greater burial of the peat results in compaction, an accompanied decrease in porosity and the expulsion of interstitial water (Levine, 1993).

2.1.5 Coalification

Whereas the process of peatification involves biological activity, the process of coalification is restricted to physical and chemical changes due to the influence of temperature, pressure and time. Coalification follows peat formation and transforms peat into the different coal ranks; lignite (brown coal), sub–bituminous and bituminous coal and finally anthracite. The coal rank can be determined by the measurement of reflectance, contents of moisture, volatile matter, carbon and hydrogen and calorific value (Figure 2.2; Tissot and Welte, 1978). With increasing rank, reflectance, carbon content and calorific value increase, whereas water content and volatile matter content decrease. Coalification also results in an increase in density and an accompanied decrease in porosity. Chemical changes related to coalification are condensation, polymerisation and the loss of functional groups. Coalification also changes hydrogen and oxygen content relative to the carbon content, (Figure 2.1; van Krevelen, 1963). Waxes and cuticles are highly aliphatic and, therefore, hydrogen rich. Hydrogen loss for these substances is predominant during coalification. Lignin and cellulose are subjected to a dominant oxygen loss. During this process, lignin is transformed into huminite, the low–rank variety of vitrinite, and secondly into vitrinite. Inertinites, characterized by high initial carbon and low initial hydrogen and oxygen contents, show a predominant loss of oxygen during coalification.

The transition from peat to lignite involves an increase in aromaticity and specific gravity; the porosity is decreasing due to physical compaction, which also results in lower moisture content (Levine, 1993). The process of gelification (Tissot and Welte, 1978) generates water, carbon dioxide and methane, which are thought to be derived from the removal of methoxyl–, hydroxyl– and methyl–groups (Levine, 1993). Lignite experiences a volumetric shrinkage due to overburden pressure (Teichmüller and Teichmüller, 1967), which results in the formation of shrinkage cracks, the initial cleats (Laubach et al.,

1998). The transition from sub–bituminous to bituminous coal correlates with the end of diagenesis. At the rank of bituminous coal a rearrangement of the coal structure and composition occurs. The microscopic structure of coal develops a more dense and homogeneous character. The most significant change is the transformation of low–rank huminite into vitrinite (Levine, 1993). This vitrinitization results in a loss of macropores and a decrease in moisture content. Decarboxylation reactions are important at this stage because they result in the formation of carbon dioxide. With increasing rank (end of high volatile A bituminous coal) the hydrogen/carbon (H/C) ratio decreases significantly (Levine, 1993) due to the expulsion of low molecular weight hydrocarbons like methane (Rice, 1993). The changes in the coal ranks of anthracite and meta–anthracite are mainly related to a rearrangement of the coal structure, whereas the chemical changes are minor and primarily involve the loss of hydrogen (Levine, 1993), due to the loss of methane and water (Cooper and Murchison, 1969; Kopp et al, 2000). The aromatic carbon structure of the coal condenses to form a two–dimensional and, finally, a three–dimensional structure of aromatic layers (Levine, 1993).

2.2 Gas Generation from Coal

2.2.1 Biogenesis

Based on the generation pathway, natural gas, including coalbed methane, can be classified as microbial or thermogenic gas. Microbial generated gas accounts for ca. 20% of the worldwide gas reservoirs (Rice and Claypool, 1981; Rice, 1992, Whiticar, 1994). Microorganisms (methanogens), which feed on organic matter at shallow depths under anaerobic conditions and temperatures below ca. 90°C (Faber et al., 1992) are responsible for the formation of microbial methane,

Based on the substrate utilized by the methanogens, microbial methane can be generated by two principle pathways: carbon dioxide reduction and methyl–type fermentation (Whiticar et al., 1986; Schoell, 1988; Faber et al., 1992; Whiticar, 1994).

The carbon dioxide reduction pathway can be represented by the following chemical reaction (Whiticar, 1994):

$$CO_2 + 8\,H^+ + 8\,e^- \rightarrow CH_4 + 2\,H_2O \qquad (2.1)$$

The eight hydrogen atoms mentioned in Equation (2.1) are supplied by water present during the reaction (Faber et al., 1992). The formation of microbial methane by carbon dioxide reduction dominates in marine environments (Whiticar, 1996b).

The methyl–type fermentation pathway can be represented by the following chemical reaction (Whiticar, 1994):

$$*CH_3COOH \rightarrow *CH_4 + CO_2 \qquad (2.2)$$

The asterisk (*) indicates the intact transfer of the methyl–group from the acetate to the methane. This means that three hydrogen atoms are supplied from the methyl–group and one hydrogen atom from water present during the reaction (Whiticar et al., 1986; Faber et al., 1992). Recent studies, however, proposed that all four hydrogen atoms are supplied by the water present during the reaction (Waldron et al., 1999). This would have severe implications for the use of hydrogen isotope compositions of methane as a tool for the distinction between the two above mentioned microbial methane generation pathways (see Chapter 2.2.1). The methyl–type fermentation is the dominant methane generation pathway in shallow freshwater environments, whereas carbon dioxide reduction occurs at greater depths in these environments (Whiticar, 1996b). Higher gaseous hydrocarbons are generated only in trace amounts by either pathway and therefore microbial generated gas is dry (Schoell, 1980; Whiticar et al., 1986; Faber et al., 1992).

The primary microbial generation of methane occurs during diagenesis, regardless of the above mentioned generation pathways (Figure 2.3). With increasing depth and temperatures exceeding ca. 90°C, the generation of primary microbial gas is terminated and the stage of thermogenesis is reached. Secondary generation of microbial gas occurs when the coal is uplifted, so that physical, chemical and biological conditions allow the presence of methanogens and subsequent gas generation.

2.2.2 Thermogenesis

Increasing temperature and pressure, are factors influencing the transformation of organic matter. Time is not as significant as temperature and pressure, as the example of the Moscow Basin shows (Tissot and Welte, 1978). During geological history three main coal forming episodes are known for the Northern Hemisphere: the Carboniferous, the Cretaceous and the Tertiary. Generally, Carboniferous coals are bituminous, whereas Tertiary coals are lignite (brown coals). This difference is due to the increased influence of temperature, pressure and time on the Carboniferous coals. The coals of the Moscow Basin are Carboniferous in age, but due to a lack of sufficient burial and therefore low temperatures and pressures, they are lignites (Tissot and Welte, 1978). During diagenesis, the main gas generated, besides microbial methane, is carbon dioxide due to the elimination of oxygen from the organic matter (Figure 2.3; Hunt, 1991). At temperatures below 100°C the generation of carbon dioxide and microbial methane continues but is now accompanied by the liberation of water and small amounts of thermogenic methane (van Heek et al., 1971). The generation of carbon dioxide peaks at the transition from diagenesis to catagenesis (Figure 2.3; Whiticar, 1996a).

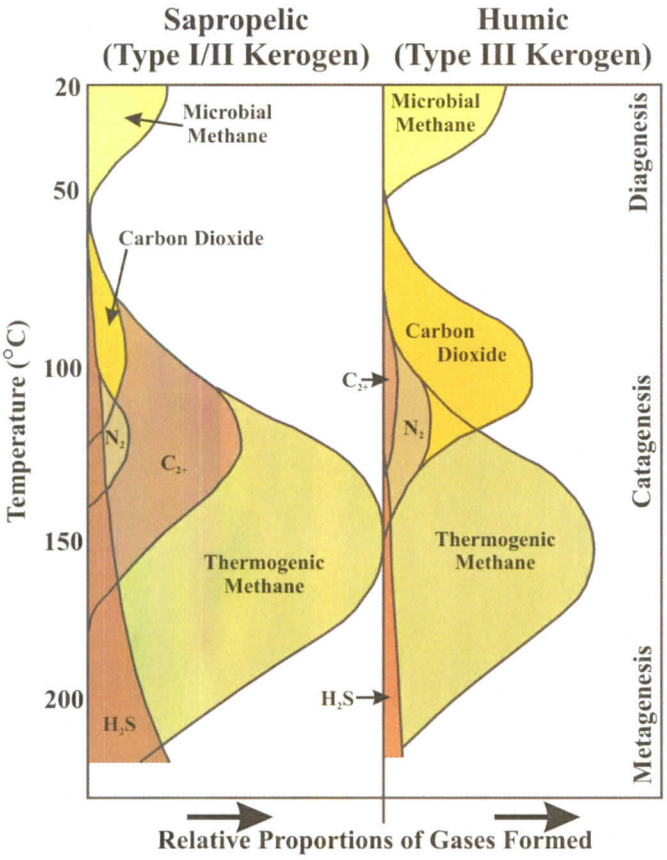


Figure 2.3: *Relative proportions of gases formed as a function of temperature from sapropelic and humic coal (modified from Hunt, 1991).*

Early catagenesis is marked by the onset for the generation of significant amounts of thermogenic methane (Figure 2.3). The onset of catagenesis occurs at lower

temperatures and lower maturation for sapropelic coals (Kerogen Types I and II), compared to humic coals (Kerogen Type III; Hunt, 1995). This difference can be explained with the different activation energies of the different kerogen. Kerogen Type I has activation energies mainly between 52kcal/mol and 53kcal/mol, whereas Kerogen Type III has values mainly between 56kcal/mol and 58kcal/mol (Whiticar, 1996a). The onset of the bulk generation of methane corresponds to a vitrinite reflectance value of 1.3% to 1.4%, temperatures of ca. 150°C and a rank of medium volatile bituminous coal (Tissot and Welte, 1978). The composition of the generated gas is mostly methane with small amounts of higher gaseous hydrocarbons (ethane, propane, butane).The relative amount of higher hydrocarbons being greater for sapropelic coals than for humic coals; gas generated from a humic coal can be considered as dry (Levine, 1993; Whiticar, 1996a). Exceptions include several Late Carboniferous coal fields in Germany with concentrations of higher gaseous hydrocarbons of up to 70% (Hunt, 1995). The generation of higher gaseous hydrocarbons takes place mainly during catagenesis (Figure 2.3). Liquid hydrocarbons are normally not present, or occur only in very small amounts in coals (Tissot and Welte, 1978; Hunt, 1995). Exceptions are very liptinite–rich coals (Levine, 1993) such as those of the Cooper Basin, Australia, where significant and economical amounts of gaseous and liquid hydrocarbons are derived from coals (Rigby and Smith, 1981; Hunt, 1991). The generation of liquid hydrocarbons takes place at vitrinite reflectance values of 0.7% to 1.0% (Tissot and Welte, 1978).

The generation of methane continues during metagenesis (Figure 2.3), but with decreasing amounts and at the transition to anthracite, only a carbon residue is left, lacking the possibility of further methane generation (Tissot and Welte, 1978; Levine, 1993).

2.3 Sorption and Desorption

A coal seam differs from a conventional source rock in the way that it is the source rock as well as the reservoir. In conventional gas reservoirs the gas is present as a free gas phase in the pore spaces of the reservoir rock (Yee et al., 1993). In coal however, the gas is proposed to be stored in four different ways (Crosdale et al., 1998):

1. Free gas phase compressed in the available pore spaces,
2. Condensed as a liquid or a solid phase,
3. Dissolved phase in the coal structure,
4. Adsorbed on the internal surfaces of the coal particles.

Adsorption is in most cases the most significant process of gas storage in coal (Yee et al., 1993).

Coal is a microporous solid with pores ranging from micrometer wide cracks (cleats) to pores, which are too small for molecules (like helium at room temperature) to pass through (Beamish and Crosdale, 1995). The highly porous character of coal provides a huge internal surface and, therefore, the ability to adsorb huge quantities of gas (Jüntgen and Karweil, 1966a, b; Beamish and Crosdale, 1995). The adsorption of gas in coals is dominated by physical, rather than chemical, adsorption; physical adsorption is characterized by the reversibility of the process, its non–specificness and the rapid sorption rate when the coal is subjected to changes in temperature and pressure (Crosdale et al., 1998). Physical sorption (= adsorption) occurs due to weak van–der Waals forces (weak intermolecular attraction) and electrostatic forces (Yee et al., 1993).

The sorption capacity of coal depends on external and internal parameters like surface area, pressure, temperature, coal rank, maceral composition, water content and mineral matter content (Rice, 1993; Yee et al., 1993; Crosdale et al., 1998). Increasing pressure results in an increased sorption (storage) capacity (Figure 2.4), which means that more gas can be adsorbed onto the surface of the coal particles; this trend continues until the saturation limit is reached (Meissner, 1984; Yee et al., 1993). The influence of pressure on the sorption capacity of a coal is important. This relationship provides the tool for the production of coalbed methane by pumping water out of a coal formation, thus lowering the hydrostatic pressure, resulting in the desorption of the gases (Rice, 1993; McLennan et al., 1995). Temperature has the inverse effect on the sorption capacity; an increase in temperature favours more gas in the free than in the adsorbed phase, resulting in a decrease of the coals sorption capacity (Meissner, 1984; Yee et al., 1993). The general trend related to increasing coal rank is an increase in sorption capacity due to increased pressure (McCulloch and Diamond, 1976; Creedy, 1988; Yee et al.,

1993). With increasing coalification, the pore structure changes (Crosdale et al., 1998). Pores can be subdivided into micropores (< 2nm), mesopores (50nm to 2nm) and macropores (> 50nm; Crosdale et al., 1998). The porosity in sub–bituminous coals is mainly due to the presence of macropores, in high–volatile bituminous coals due to the presence of meso– and micropores, and for coals with a carbon content of 85% to 91% due to the presence of micropores (Beamish and Crosdale, 1995). Large pores are not necessarily associated with a large pore surface, because the pore surface area depends on the pore size distribution. A higher surface area is associated with a larger proportion of micropores (Beamish and Crosdale, 1995), which underpins the general trend of increasing storage capacity with increasing coal rank (Rice, 1993). The presence of even small concentrations of liquid hydrocarbons or tar, especially in coals dominated by a micropore structure, can lead to a "plugging" of the pores and thus a significant decrease in sorption capacity (Levine, 1993; Rice, 1993). The removal of these substances, for example by thermal cracking, results in an increasing sorption capacity (Rice, 1993).

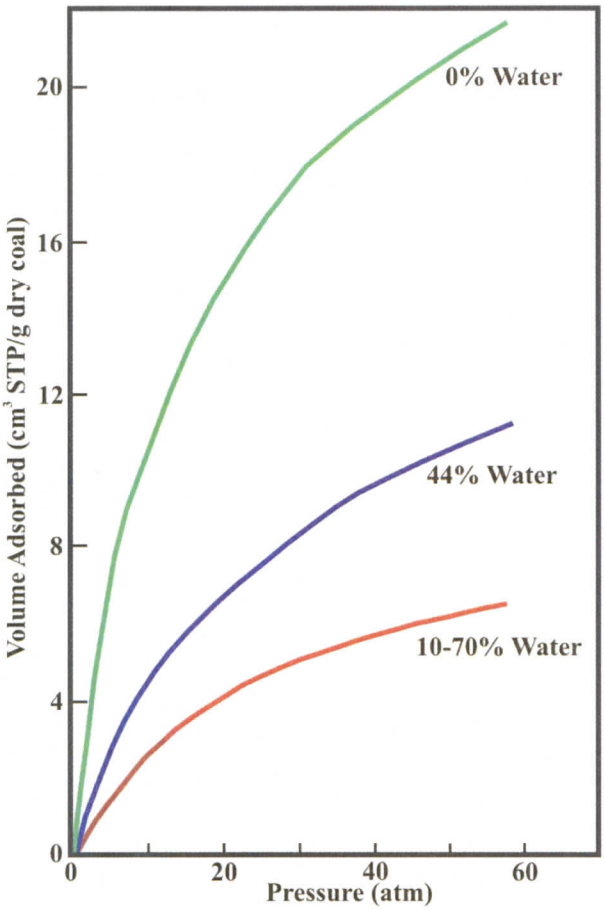


Figure 2.4: *Diagram shows variations in gas volumes adsorbed onto coal with pressure. Gas volumes adsorbed onto coal increases with increasing pressure, regardless of water content. Increasing water content has the effect of decreasing gas volumes adsorbed onto the coal. This trend continues until equilibrium moisture is reached; see text for details (modified from Joubert et al., 1974).*

It is mostly accepted that coals rich in vitrinite can adsorb more gas, especially methane, than inertinite–rich coals of the same rank (Beamish and Crosdale, 1995; Bustin et al., 1995; Crosdale et al., 1998). Beamish and Crosdale (1995) pointed out that the rank

dependent higher sorption capacity of vitrinite–rich coals relates to porosity and surface area. Inertinite–rich coals have a greater porosity (6.0% to 13.7%) and lower internal surface area in comparison to vitrinite–rich coals of the same rank, which have a lower porosity (0.8% to 5.3%) and a higher internal surface area (Beamish and Crosdale, 1995). Opposite trends have also been found, for example by Ettinger et al. (1966).

Physical adsorption on the pore surface results, if enough pore space is available, in several layers of molecules, depending on pressure and saturation; the adsorption of several layers requires high pressure, with the result that the adsorbed molecules are condensed into a bulk liquid (Crosdale et al., 1998). The initial monolayer is bound more strongly than the following layers and therefore more energy is required for the removal of the initial layer (Hunt, 1991). Friedrich and Jüntgen (1972) and Hunt (1991) also pointed out that higher hydrocarbons present in the coal would be adsorbed more strongly than methane. The presence of water molecules would decrease the sorption capacity of a coal (Figure 2.4), because water molecules would occupy sorption sites, which are then not available for hydrocarbon gases, especially methane (Yee et al., 1993). This reduction of sorption capacity continues until the water saturation level is reached; thereafter no further decrease occurs, even with increasing water content (Joubert et al., 1973). Mineral matter (inorganic constituents of coal) dilutes the concentration of organic matter and reduces the available space for adsorption, resulting in a decreased sorption capacity (Yee et al., 1993). Coals with a low mineral matter concentration have a higher sorption capacity than coals with a high mineral matter concentration. A decrease in the mineral matter concentration and the accompanied gas content increase are coupled by a linear relationship (Yee et al., 1993).

As mentioned above, the hydrostatic pressure in a coal seam must be lowered by pumping water out of the formation to produce the adsorbed gases. The transport of the gas in the coal takes place in three processes (Figure 2.5; McLennan et al., 1995; Crosdale et al., 1998):

1. Fluid flow,
2. Desorption,
3. Molecular diffusion.

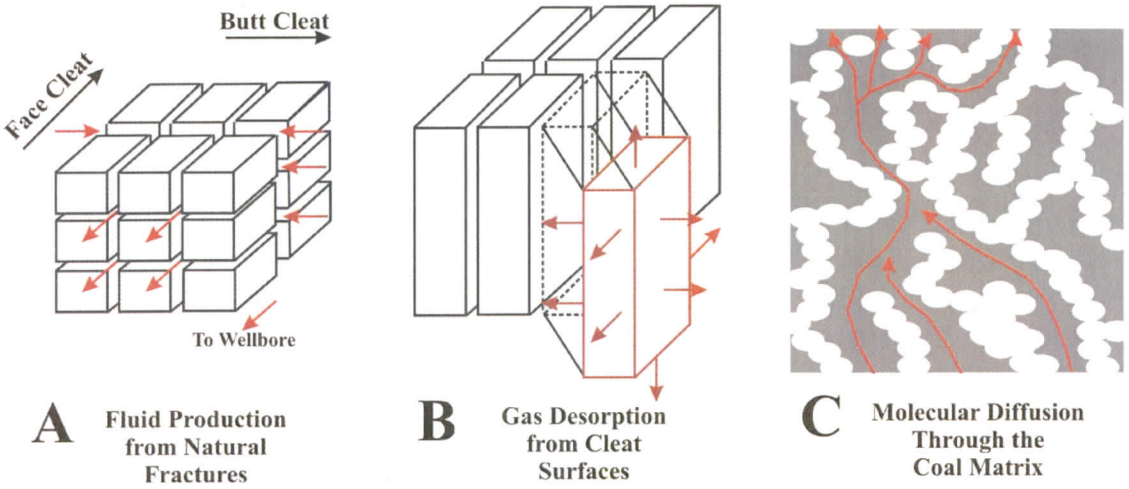


Figure 2.5: *Possible transport mechanisms of gases in coal. A: Flow of fluids and gases in the cleat network of a coal. B: Desorption of gases from cleat surfaces. C: Molecular diffusion of gas molecules from internal desorption sites through the coal matrix towards cleat surfaces (modified from McLennan et al., 1995).*

Fluid flow (Darcy flow) can occur in sufficiently large pores and in the cleat network of the coal due to decreased pressure (McLennan et al., 1995). Decreasing pressure due to water removal creates a pressure gradient in the coal seam, resulting in the desorption of gas (Yee et al., 1993). Differences in concentration result in the diffusion of gas through the coal matrix and cleat network (McLennan et al., 1995; Crosdale et al., 1998). It is assumed that movement of gas through the matrix, especially through a micropore matrix is minor and that the main transport happens along microfissures and cleats in the coal (Sevenster, 1959; Airy, 1968; McLennan et al., 1995). Without diffusive flow, desorbing gas will not reach the microfissure and cleat network, meaning that even a high porosity coal will not produce gas when the diffusivity is low.

2.4 Gas Content Measurement

The measurement of the total gas content of a coal seam is important for the evaluation of a coal basin, in terms of gas producibility and economical aspects. These measurements can be carried out in two different ways, using the direct or the indirect method. The indirect method uses sorption isotherms, which allow a determination of the gas sorption capacity of the coal. This method provides information about the maximum volume of gas, which can be adsorbed by the coal under laboratory conditions, but not

about the volume that is actually adsorbed by coal in the subsurface (Yee et al., 1993; McLennan, 1995; Diamond and Schatzel, 1998). For the direct method, coal cores or cuttings recovered during drilling are used, providing the opportunity to measure the actual volume and type of gas adsorbed onto the coal (Yee et al., 1993; McLennan, 1995; Diamond and Schatzel, 1998). From this point forward only the direct method is considered. For a review of the indirect method the reader is referred to the work of Kim (1977), Yee et al. (1993), McLennan et al. (1995) and Diamond and Schatzel (1998).

The direct method was first described by Bertard et al.(1970). For this method a fresh coal sample recovered during drilling is sealed into a canister at atmospheric pressure (Figure 2.6). Due to the reduced pressure in comparison to the subsurface conditions the adsorbed gas begins to desorb and is collected in the headspace of the canister. At measured time intervals (time intervals are chosen so that a huge pressure build–up in the canister can be avoided) the gas is released and measured volumetrically. After release of desorbed gas, the canister is resealed and more gas is allowed to desorb. The volume is measured by the use of a manometer.

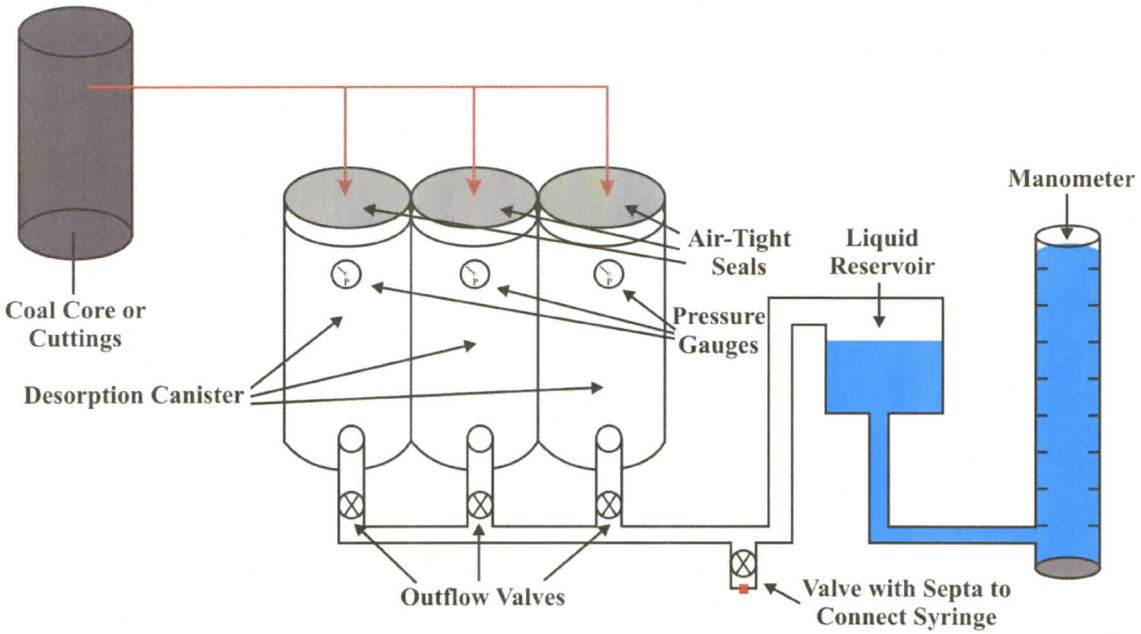


Figure 2.6: *Principle set–up of equipment used for volumetric determination of gases in coal (canister method). See text for details.*

Initial desorption from coal is significantly higher than desorption occurring after several days have elapsed (Figure 2.7). Therefore shorter sample and measurement intervals are required during the initial desorption phase. Frequent measurements of the desorbed gas volume during the initial desorption phase are also necessary for the lost gas estimation (see below). Desorption data are presented in a desorption diagram (Figure 2.7)

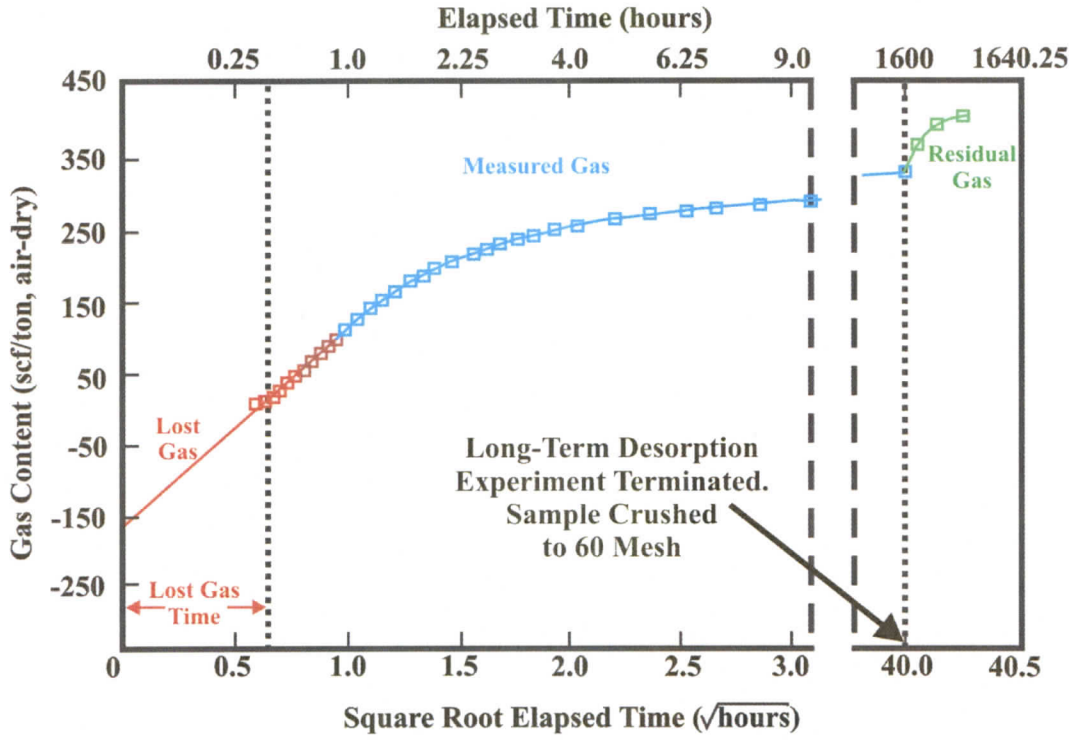


Figure 2.7: *Schematic gas desorption diagram (canister method) showing time versus gas volume. Total gas volume consists of three separate volumes: lost gas, measured gas, residual gas. See text for description (modified from McLennan et al., 1995).*

The total gas volume desorbed from a coal can be divided into three separate volumes: the lost gas volume, the measured gas volume and the residual gas volume (Ryan and Dawson, 1994; Yee et al., 1993; McLennan et al., 1995). The measured gas volume is represented by the volumes measured during the desorption experiment in the canister (Figure 2.7). When the gas volume falls below a limit of typically $0.1 cm^3$ to $1 cm^3$ per measurement the desorption experiment can be terminated (McLennan et al., 1995). The portion of gas remaining adsorbed onto the coal at the end of the desorption experiment is termed residual gas (Yee et al., 1993; McLennan et al., 1995). The residual

gas can be released and measured by grinding the coal to a fine powder and collecting the released gas (Figure 2.7).

A significant uncertainty for total desorbed gas is the contribution from the lost gas component. The lost gas is the portion of gas, which is desorbed and lost from the time the coal first experiences a reduced pressure until the coal (core or cuttings) is placed and sealed into a canister (Ryan and Dawson, 1994; Yee et al., 1993; McLennan, 1995; Diamond and Schatzel, 1998). For an economic estimation of the total amount of gas stored in a coal seam the lost gas component is extremely important and has to be estimated and included in the calculations. Frequent volumetrical measurements during the initial desorption process results in a high density of datapoints in the desorption diagram (Figure 2.7; red datapoints); when these data (cumulative gas content) are plotted versus square root of time the datapoints plot on a straight line (Ryan and Dawson, 1994). The lost gas volume can now be estimated by extrapolation back to time zero (Figure 2.7), which represents theoretically the time at which the coal was first subjected to a decreased pressure, resulting in desorption (Ryan and Dawson, 1994; McLennan et al., 1995). If the data points not plot on a straight line, the lost gas estimation is not likely to be precise (Ryan and Dawson, 1994). In general, the lost gas estimation is important, but even slight mistakes can lead to enormous errors in the calculation of the total gas content.

2.5 Isotope Geochemistry

Starting with Stahl (1973), stable isotopes were used for the delineation of different source materials and their maturity, as well as for the delineation of different generation pathways. Isotopic analysis allows the differentiation between thermogenic and microbial generated gases, the correlation of hydrocarbons with their sources (Kerogen Type I, II or III) and the estimation of the source rocks maturity.

Isotope ratios are generally presented in the δ–notation:

$$\delta R_X\ (‰) = \{[(R_A/R_B\ \text{sample})/(R_A/R_B\ \text{standard})] - 1\} \cdot 10^3 \qquad (2.3)$$

where R_X and R_A/R_B are the isotope ratios ($^{13}C/^{12}C$, $^{2}H/^{1}H$) relative to the PDB (PeeDee Belemnite) and SMOW (Standard Mean Ocean Water) standards.

Generally, isotope fractionation is caused by two types of reactions, kinetic isotope effects and equilibrium isotope effects. For the generation, migration, storage and destruction of hydrocarbons, kinetic isotope effects are most important and are described briefly below. For a detailed description of equilibrium isotope reactions the reader is referred for example to the work of Criss (1999) and Hoefs (2004).

Kinetic isotope effects are associated with unidirectional reactions or processes like evaporation, condensation, dissociation reactions, biologically induced reactions and diffusion (Hoefs, 2004). Kinetic isotope effects are mostly related to the bond strength or the energy of the same molecules containing different isotopes as described by quantum mechanics. Among the components to describe the energy of a molecule, translational, rotational and vibrational energies are important, with vibrational energy being the most important for the process of isotope fractionation. As stated in quantum theory, the energy of a molecule is restricted to certain discrete energy levels, which depend on mass. Even at absolute zero the molecule will have a ground frequency (ν_0) with the amount of $\frac{1}{2}h\nu_0$, where h is Planck's constant. This energy level, the so–called zero–point–energy (ZPE) depends on several factors, such as electron arrangement, nuclear charge and the atomic arrangement in the molecule. These factors are identical for the same element. But because energy depends inversely on the masses of the involved atoms, the zero–point–energy will be different for different isotopes of the same atom and molecules containing different isotopes. Therefore, the energy level (based on vibrational energy) for a given quantum number will be lower for a bond involving the heavier isotope of an element (Figure 2.8). Therefore molecules with identical chemical formulas that contain different isotope species have different zero–point–energies; molecules containing the heavier isotope have a lower zero–point–energy than molecules containing the lighter isotope (Figure 2.8). Bonds involving heavier isotopes are stronger and require more energy to break, whereas bonds involving lighter isotopes are weaker and break more easily and therefore participate more readily in chemical reactions. If reactions do not reach completion, kinetic isotope effects occur.

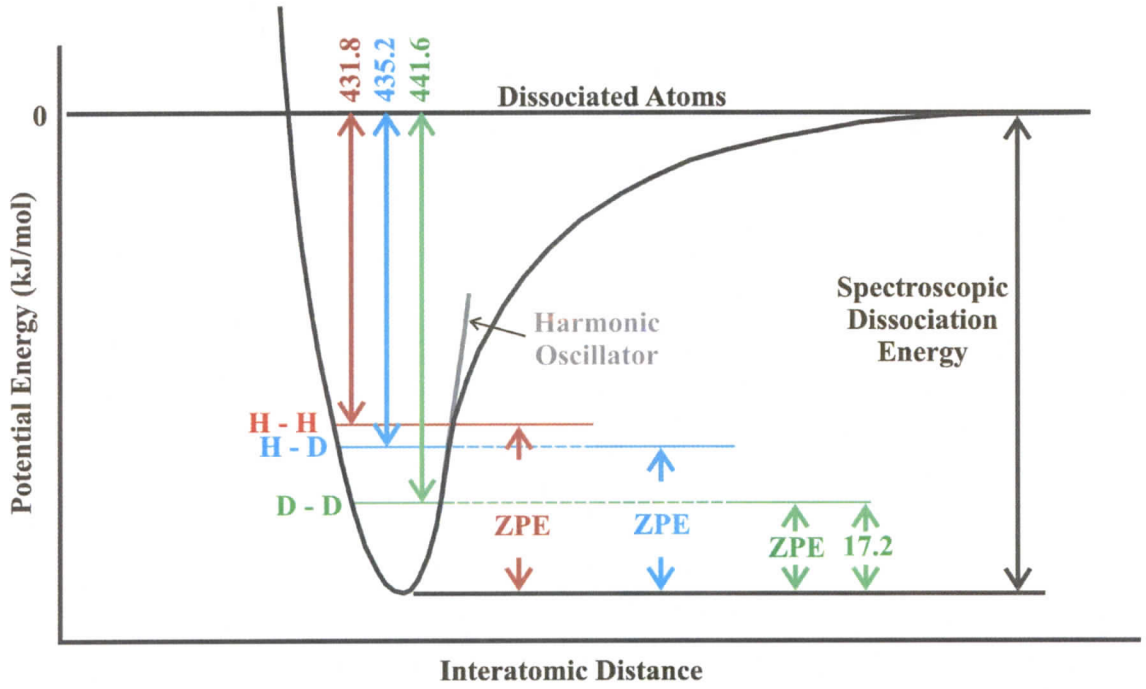


Figure 2.8: *Energy level diagram for hydrogen. ZPE = zero–point–energy. See text for description (from O'Neill, 1986).*

In an evaporation–condensation process the lighter isotopes are enriched in the vapour phase and the heavier isotopes in the liquid phase (Hoefs, 2004).In general the lighter isotopes concentrate in the less dense phase, whereas the heavy isotopes concentrate in the denser phase (Lindemann, 1919). This may be normally the chemical compound in which it is most strongly bonded. Kinetic isotope effects, which discriminate against an isotope species, can be described by Rayleigh (1896) distillation relationships (e.g. Whiticar, 1994; Berner and Faber, 1996; Whiticar, 1996a). By using these relationships, the isotope ratio of the reactant pool (for example coal or kerogen), as well as the isotope ratio of the generated or released products (for example generated hydrocarbons), can be estimated. When assuming a closed–system the isotope ratio of the remaining reactant pool can be estimated with the following equation (Whiticar, 1996a):

$$R_r/R_0 = f^{(1/\alpha-1)} \qquad (2.4)$$

where R_r is the isotope ratio of the initial reactant pool (for example $^{13}C/^{12}C$ of initial coal), R_0 is the isotope ratio of the residual reactant pool (for example $^{13}C/^{12}C$ of

remaining coal) at a specified point in the reaction and removal, f is the fraction of the residual reactant pool (1 to 0) and α is the fractionation factor. The fractionation factor is defined as (Whiticar 1996a):

$$\alpha = R_A/R_B \tag{2.5}$$

where R_A and R_B are isotope ratios of two phases A and B (for example coal and generated hydrocarbons). A fractionation factor bigger than 1 describes discrimination against the heavy isotope, whereas a fractionation factor smaller than 1 describes discrimination against the light isotope. When converted to the δ–notation for carbon isotopes, Equation 2.4 becomes (Whiticar, 1996a):

$$\delta^{13}C_r = \{(\delta^{13}C_0 + 1000) \cdot f^{(1/\alpha c - 1)}\} - 1000 \tag{2.6}$$

For the generation of hydrocarbons from coal the fractionation factor for this conversion is α_c = 1.003 (Berner, 1989; Berner et al., 1992; Whiticar, 1996a). Figure 2.9 shows Rayleigh distillation curves with calculated isotope shifts for the remaining reactant pool, in this case coal, for different fractionation factors. Considering a fractionation factor of 1.003, the isotope changes in the coal are minor due to the presence of a huge carbon pool in the form of coal. The isotope signature of the coal only changes significantly (Figure 2.9) when huge amounts of the available coal are converted to products (gas).

The isotope ratio of the generated products can be estimated by the following equation:

$$\delta^{13}C_G = \{(\delta^{13}C_0 + 1000) \cdot (1 - f^{(1/\alpha)})\}/\{(1\text{-}f) - 1000)\} \tag{2.7}$$

where $\delta^{13}C_G$ is the isotope ratio of the total (cumulative) gas generated by the conversion of kerogen (coal) to hydrocarbons. Similar to the changes for the remaining kerogen described above, the hydrocarbons generated from coal also show only slight changes in the isotope composition. The overall trend shows enrichment in the heavy isotope ^{13}C with an increasing fraction of hydrocarbons generated from the coal. The overall change

in isotope ratio expected for methane generation from coal is 3‰, related to the fractionation factor of 1.003 (Berner and Faber, 1996).

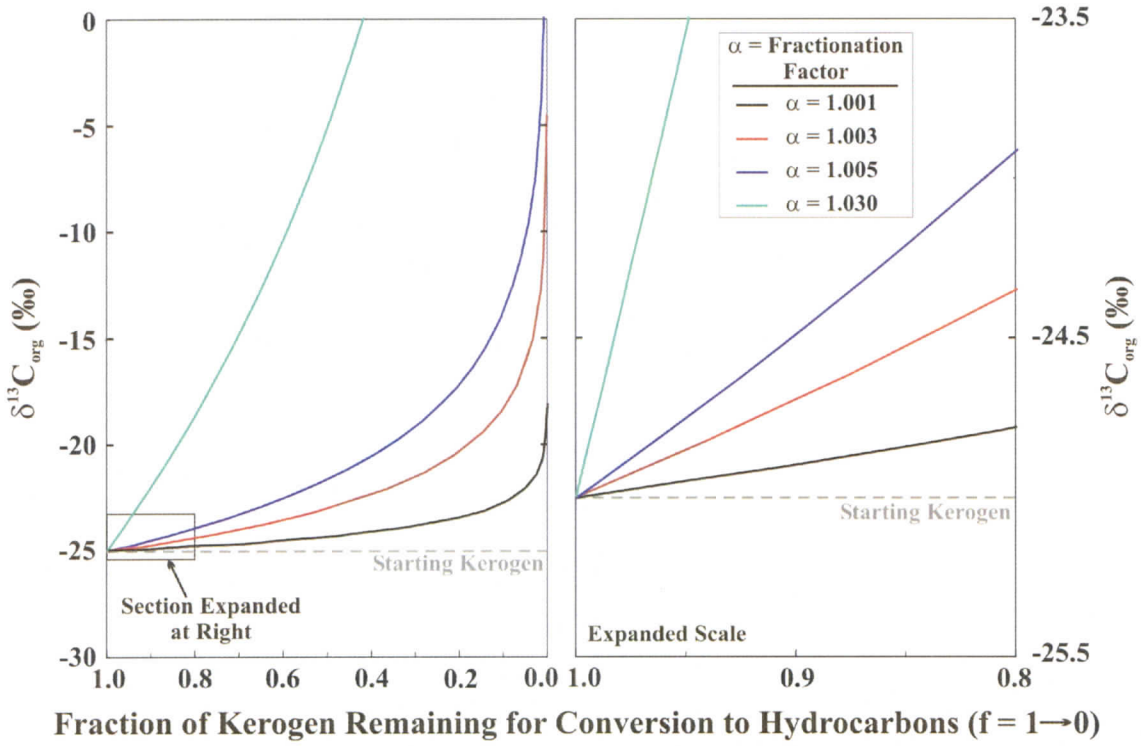


Figure 2.9: *Rayleigh distillation curves showing $\delta^{13}C$ ratio of kerogen and its variation with progressing generation and loss of gas. Initial $\delta^{13}C$ ratio of the kerogen in this example is -25‰. With decreasing fraction of kerogen remaining for the conversion to gas, the kerogen becomes relatively ^{13}C enriched, due to the loss of relatively ^{12}C enriched gases. Right side diagram shows section indicated on left side diagram in expanded scale. Curves are calculated using different fractionation factors. See text for equations and details (from Whiticar, 1996a).*

2.5.1 Carbon

The stable isotopes of carbon (^{13}C and ^{12}C) occur in nature with the following relative abundances:

^{12}C: 98.98 atom–percent

^{13}C: 1.11 atom–percent.

Coal and organic matter are derived from living plants and animals, with terrestrial plants being the most important source of organic matter for coal. Isotope analysis of plants shows that in relation to their carbon source (atmospheric CO_2: $\delta^{13}C$ = -6‰ to -8‰) terrestrial, as well as marine plants have lower $\delta^{13}C$ values between -22‰

and -33‰; they are therefore depleted in the heavy isotope ^{13}C (Park and Epstein, 1961; Whiticar, 1996a). This depletion in ^{13}C is controlled by the process of photosynthesis. The first ^{13}C discriminating effect related to the process of photosynthesis is the uptake of carbon dioxide by the plant from the atmosphere (Park and Epstein, 1961). The velocity of a gas molecule is proportional to the inverse square of its molecular weight, resulting in higher velocities for carbon dioxide molecules containing the lighter isotope ^{12}C (mass 44) than carbon dioxide molecules containing the heavy isotope ^{13}C (mass 45). Therefore ^{12}C containing carbon dioxide collides about 1.1% more frequently with plant leafs than ^{13}C containing carbon dioxide, leading to an increased uptake of ^{12}C carbon dioxide over ^{13}C carbon dioxide (e.g., Whiticar, 1996a). Another ^{13}C discriminating process takes place during the actual fixation of the carbon by enzymatic processes, again due to mobility considerations and due to the bond strength between ^{13}C and ^{12}C (Park and Epstein, 1961; Whiticar 1996a).

Coals of all geological ages show almost identical carbon isotope signatures to the plants they formed from, suggesting that organic plant material does not undergo significant carbon isotope fractionation during the process of coalification (Park and Epstein, 1961). The carbon isotope ratio of the plants is therefore preserved in coals. This implies that differences in the carbon isotope ratio of different coals are not related to coalification, but to differences in the precursor materials (Schwarzkopf, 1984). Carbon isotope fractionation reactions actually do occur during coalification, but because of the presence of such a huge carbon pool in form of coal, the changes in the isotope ratio are not detectable (Redding et al., 1980), unless high coal ranks are reached (Whiticar, 1996a). Instead carbon isotope fractionation can be observed in the products of the coalification process, in the generated gases (Redding et al., 1980).

The composition or the wetness of gases provides a first indication if the gas is either microbial or thermogenic in origin. Microbial gas generated by methyl–type fermentation or carbon dioxide reduction consists generally of only methane, whereas thermogenic gas also contains the higher gaseous hydrocarbons ethane, propane and butane (e.g., Schoell, 1980; Whiticar et al., 1986; Whiticar, 1996a). Composition alone does not identify origin, because migration, biodegradation and other secondary processes (see Chapter 2.5.3) can preferentially remove the higher hydrocarbon gases

(Sheppard, 1986; Faber et al., 1992). In addition coal is prone to generate large quantities of methane, but only small quantities of higher hydrocarbons (Whiticar, 1996a). Therefore, a second indication is needed and is provided by the carbon isotope ratio of the generated methane. The carbon isotope ratio of methane generated by microbial action is characterized by a considerable depletion in ^{13}C, due to the preferential utilization of ^{12}C by methanogens (Whiticar, 1996a); the $\delta^{13}C$ values range between -110‰ and -50‰ (Whiticar et al., 1986). The preferential utilization of ^{12}C over ^{13}C by methanogens is related to a smaller required energy to break the bond of a ^{12}C–^{12}C molecule. The ^{13}C depletion is more pronounced in the marine environment provoked by carbon dioxide reduction than in the freshwater environment due to methyl–type fermentation (Whiticar, 1996b).

Thermogenic generated methane is less depleted in ^{13}C than microbial generated methane, resulting in higher $\delta^{13}C$ values for methane (Schoell, 1980). Generally, thermogenic methane is relatively enriched in ^{13}C compared to microbial methane (Whiticar, 1999). During coalification the weakest bonds (^{12}C–^{12}C) break more frequently than the more stable bonds, resulting in depletion of ^{13}C in the generated methane relative to the source material (Whiticar, 1996a). With increasing maturity the $\delta^{13}C$ ratio generally becomes progressively more enriched in ^{13}C, because of the exhaustion of the ^{12}C pool in the source material and because of energies high enough for frequent breakage of ^{12}C–^{13}C bonds (Faber et al., 1992; Whiticar, 1994). Schoell (1980) and Whiticar (1984, 1996a, 1999) proposed a $\delta^{13}C$ (methane) based boundary between microbial and thermogenic generated methane at $\delta^{13}C$ values between -50‰ and -55‰.

The combination of chemical gas composition and the $\delta^{13}C$ ratio of methane provides a powerful tool for the distinction between microbial and thermogenic generated gas, as well as for the correlation of the gases with their source rocks (Kerogen Type). The gas composition is given in form of the concentration ratio of methane over ethane plus propane (Bernard Parameter), which can be written as follows (Bernard et al., 1978; Faber and Stahl, 1984):

$$\text{Bernard Parameter} = [C_1]/([C_2] + [C_3]) \text{ (vol.\%)} \quad (2.8)$$

This ratio provides information about the wetness of the gas, with high values indicating dry gas and low values indicating wet gas (Whiticar, 1994). The Bernard Diagram, with the Bernard Parameter in relation to the $\delta^{13}C$ ratio of methane shows distinct fields for thermogenic and microbial generated gas (Figure 2.10; Whiticar, 1994; Whiticar, 1996a):

Thermogenic generation: $\delta^{13}C$: -50‰ to -35‰
Bernard Parameter: 1 to 40

Microbial generation: $\delta^{13}C$: -100‰ to -50‰
Bernard Parameter: 200 to 100,000

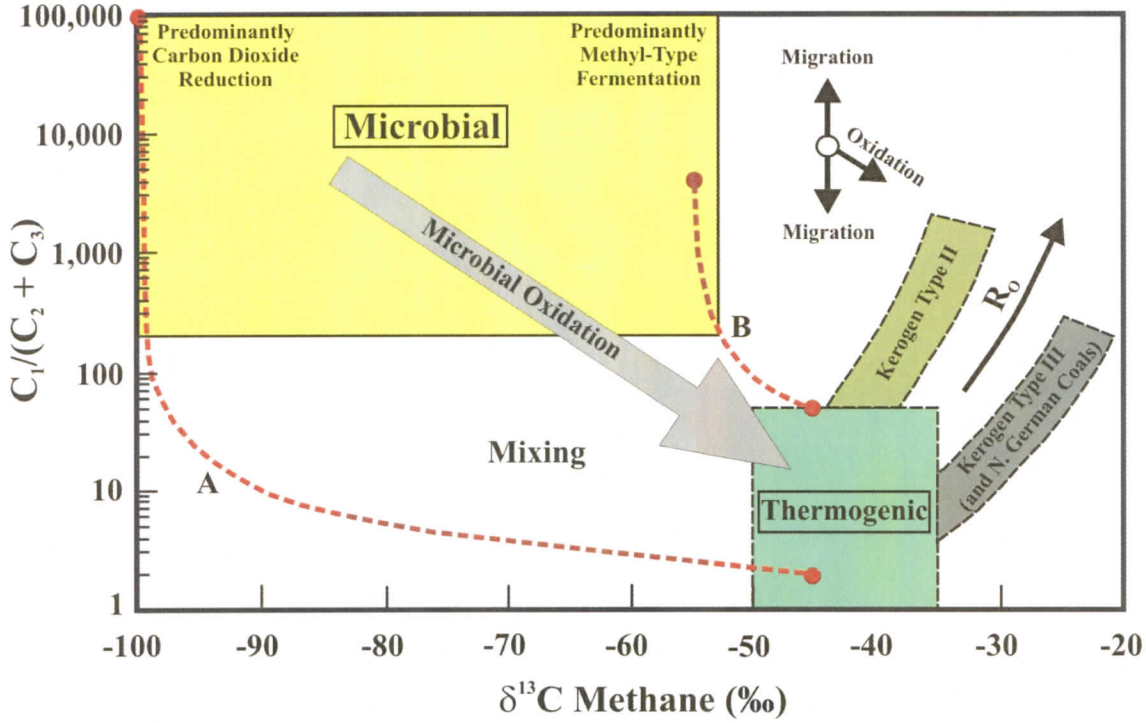


Figure 2.10: *Bernard Diagram showing $\delta^{13}C$ ratios for methane versus gas wetness (ratio of proportions of methane over ethane and propane) and distinct areas for gases of thermogenic and microbial origin. A and B represent mixing lines between gases, based on two endmembers. See text for description (modified from Whiticar, 1999).*

The more negative $\delta^{13}C$ values in the microbial gas field represent gas generated by carbon dioxide reduction, whereas the less negative values represent gas generated by methyl–type fermentation (Whiticar, 1994; Whiticar, 1996a). With increasing maturity (expressed by vitrinite reflectance, R_O) thermogenic generated gases are separated relative to their source rock material (Kerogen Type II and Type III). Gases generated

from all Kerogen Types become enriched in ^{13}C with increasing maturity, due to the exhaustion of available ^{12}C–^{12}C bonds. This trend is accelerated for Kerogen Type III gases (Whiticar, 1994; Whiticar, 1996a). In addition with the change in the carbon isotope ratio of methane, the degree of wetness decreases, so that methane becomes more dominant.

A model for the identification and quantification of microbial gas in a conventional gas system was presented by Chung et al. (1988). Methane is always isotopically lighter (more ^{12}C enriched) than the higher co–genetic hydrocarbons, whereas the concentration of ^{13}C increases with increasing carbon number; methane is isotopically lighter than ethane, ethane lighter than propane and propane lighter than butane (Chung et al., 1988). In an ideal scenario, where only co–genetic and unaltered gases are present, these gases would plot on a straight line in a natural gas plot (Figure 2.11), which relates the inverse carbon number to corresponding $\delta^{13}C$ values. The slope of this line would represent the isotope fractionation during hydrocarbon formation (Chung et al., 1988). The extrapolated intercept of this line with the y–axis represents the δ^{13} ratio of the source (Chung et al., 1988). Because microbes generate methane, but no higher hydrocarbons, the higher hydrocarbons ethane, propane and butane should not be affected by the presence of microbial gas. Methane should be shifted towards more negative $\delta^{13}C$ values by the presence of microbial gas. The difference between measured $\delta^{13}C$ and the value estimated

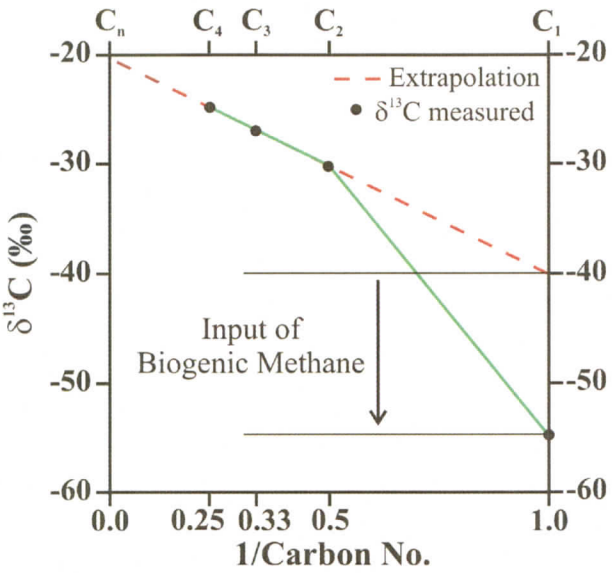


Figure 2.11: *Idealized natural gas plot showing 1/carbon number for methane, ethane, propane and butane versus corresponding $\delta^{13}C$–ratios. Black dots indicate measured samples and stippled red line represents extrapolation for the determination of $\delta^{13}C$–ratio of kerogen and $\delta^{13}C$ of pure thermogenic methane. Difference between extrapolated $\delta^{13}C$–ratio for pure thermogenic methane and actual measured $\delta^{13}C$–ratio for methane indicates input of microbial methane. In the shown example, the $\delta^{13}C$–ratio of pure thermogenic methane is -40‰ and the extrapolated $\delta^{13}C$–ratio of the kerogen is -20‰. See text for details (modified from Chung et al., 1988).*

for pure thermogenic methane by extrapolating the $\delta^{13}C$ values for ethane, propane and butane to methane (carbon number of 1.0) provides a quantitative determination of the amount of microbial gas present in the sample. Knowing both end members, $\delta^{13}C$ for pure thermogenic methane and $\delta^{13}C$ for pure microbial methane, allows the application of a mass balance calculation (Equation 2.9):

$$\delta^{13}C_{-(MIX\ AB)} = f_{(A)} \cdot \delta^{13}C_{-(A)} + (1 - f_{(A)} \cdot \delta^{13}C_{-(B)}) \qquad (2.9)$$

where $\delta^{13}C_{-(MIX\ AB)}$ is the carbon isotope ratio of the gas mixture between components A and B, $f_{(A)}$ is the fraction of component A; δ^{13}–$C_{(A)}$ is the carbon isotope ratio of component A and $\delta^{13-}C_{(B)}$ is the carbon isotope ratio of component B. Components A and B can be both of thermogenic origin or one of microbial origin. The carbon isotope ratio for microbial methane generated by methyl–type fermentation and carbon dioxide reduction is assumed to be -70‰ (Bernard et al., 1976; Rice and Claypool, 1981; Chung et al., 1988). The generation of microbial methane in coals is attributed only to methyl–type fermentation, which is assumed to have an average carbon isotope ratio of -60‰ (Whiticar, 1999). $\delta^{13}C$ for thermogenic methane is derived from the above described extrapolation. An idealized example is shown in Figure 2.11. The measured $\delta^{13}C$ value for methane is -55‰, $\delta^{13}C$ for pure microbial methane is -70‰ and based on the extrapolation the $\delta^{13}C$ value for pure thermogenic methane from this source is -40‰. Using Equation 2.9 the shown example shows a mixture of 50% thermogenic gas and 50% microbial gas. The estimated $\delta^{13}C$ value for the source is ca. -20‰.

Based on stable carbon isotope data derived from reservoir samples and from pyrolysis experiments (Stahl and Koch, 1974; Stahl and Carey, 1975; Boigk et al., 1976; Stahl, 1977; Faber, 1987; Berner and Faber, 1988; Galimov, 1988; Berner, 1989; Whiticar, 1990; Clayton, 1991; Berner et al., 1995; Berner and Faber, 1996), relationships between vitrinite reflectance and the carbon isotope ratio of methane, ethane and propane have been established. These relationships allow an estimation of the maturity of a source rock by analyzing the $\delta^{13}C$ ratio of gaseous hydrocarbons generated by a source rock, without analyzing the source rock itself.

The latest and most sophisticated model was proposed by Berner and Faber in 1996. Berner and Faber (1996) established empirical relationships for Kerogen Type II and Type III, based on data derived from dry, open–system pyrolysis experiments. The maturity estimation for Kerogen Type III is less secure, because (Whiticar, 1996a):

- only a minor fraction of Kerogen Type III will convert to hydrocarbons,
- the generation of hydrocarbons is restricted to methane with only small amounts of the higher gaseous hydrocarbons,
- kinetic isotope effects associated with Kerogen Type III are small, and
- coals retain hydrocarbons due to sorption, leading to mixing, as well as compositional and isotope fractionation during the release of the hydrocarbons.

For Kerogen Type II, Berner and Faber (1996) used a starting isotope ratio for the kerogen of -30‰. The established relationships for instantaneous methane, ethane and propane isotope ratios ($\delta^{13}C_{(I)}$) as a function of maturity (vitrinite reflectance, R_O) can be written as follows (Figure 2.12):

Methane: $$\delta^{13}C_{1(I)} = (-4.0613 \cdot R_O^5) + (34.924 \cdot R_O^4) - (113 \cdot R_O^3) + (171.26 \cdot R_O^2) - (111.86 \cdot R_O) - 20.735 \quad (2.10)$$

Ethane: $$\delta^{13}C_{2(I)} = (7.4991 \cdot R_O^6) - (81.906 \cdot R_O^5) + (354.73 \cdot R_O^4) - (772.76 \cdot R_O^3) + (881.75 \cdot R_O^2) - (482.97 \cdot R_O) + 60.083 \quad (2.11)$$

Propane: $$\delta^{13}C_{3(I)} = (-2.0174 \cdot R_O^6) + (8.294 \cdot R_O^5) + (14.76 \cdot R_O^4) - (126.87 \cdot R_O^3) + (236.04 \cdot R_O^2) - (165.11 \cdot R_O) + 3.875 \quad (2.12)$$

These relationships are valid for the following maturities (Berner and Faber, 1996):

Methane: 0.65 $\%R_O$ to 2.5 $\%R_O$,

Ethane: 0.65 $\%R_O$ to 2.0 $\%R_O$,

Propane: 0.65 $\%R_O$ to 2.0 $\%R_O$.

Equations 2.10 through 2.12 are valid only for an initial isotope ratio of the kerogen of -30‰. Berner and Faber (1996), then introduced equations to adjust Equations 2.10

through 2.12 to different, known or assumed, isotope values of source rocks. These equations are:

Methane: $$\delta^{13}C_1^* = \delta^{13}C_{1(I)} + (30 - \delta^{13}C_{org}) \quad (2.13)$$

Ethane: $$\delta^{13}C_2^* = \delta^{13}C_{2(I)} + (30 - \delta^{13}C_{org}) \quad (2.14)$$

Propane: $$\delta^{13}C_3^* = \delta^{13}C_{3(I)} + (30 - \delta^{13}C_{org}) \quad (2.15)$$

where $\delta^{13}C_{org}$ is the initial isotope ratio of the kerogen.

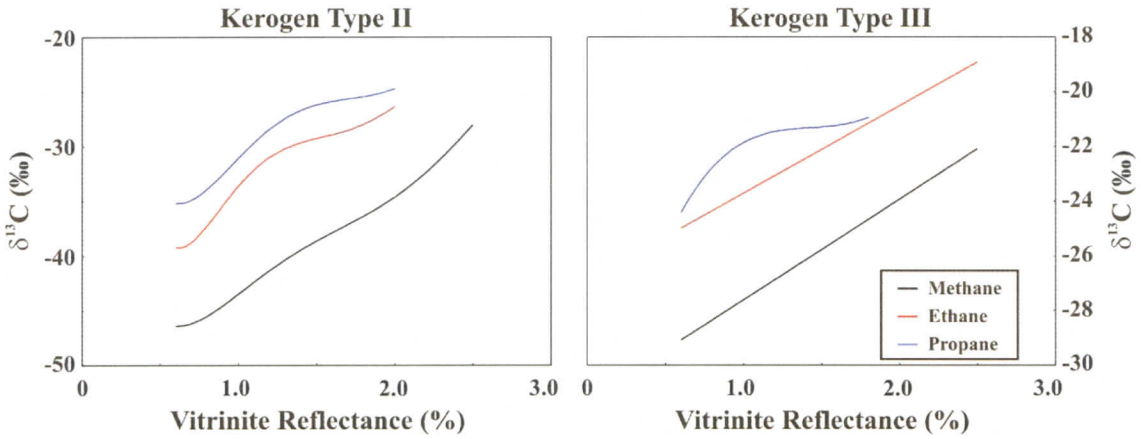


Figure 2.12: Graphic presentation of relationships between the maturity (vitrinite reflectance) of a source rock with the stable carbon isotope composition ($\delta^{13}C$) of methane, ethane and propane generated from this type of source rock. Left hand diagram shows relationships for a Kerogen Type II source rock and the right hand diagram for a Kerogen Type III source rock. See text for equations and details (modified from Berner and Faber, 1996).

For Kerogen Type III Berner and Faber (1996) fitted regression lines to the measured isotope data to derive the following empirical relationships between the carbon isotope ratio of instantaneous methane, ethane and propane ($\delta^{13}C_{(I)}$) as a function of maturity (Figure 2.12):

Methane: $$\delta^{13}C_{1(I)} = (3.684 \cdot R_O) - 31.292 \quad (2.16)$$

Ethane: $$\delta^{13}C_{2(I)} = (3.1987 \cdot R_O) - 26.901 \quad (2.17)$$

Propane: $\delta^{13}C_{3(I)} = (4.903 \cdot R_O^3) - (21.033 \cdot R_O^2) + (30.436 \cdot R_O) - 36.164$ (2.18)

The above mentioned relationships are valid for the following maturities (Berner and Faber, 1996):

Methane: 0.65 $\%R_O$ to 2.5 $\%R_O$,

Ethane: 0.65 $\%R_O$ to 2.0 $\%R_O$,

Propane: 0.65 $\%R_O$ to 1.8 $\%R_O$.

The data for methane derived by Berner and Faber (1996) covered a maturity range from 1.55 $\%R_O$ to 2.5 $\%R_O$. Extrapolation down to lower maturities of 0.6 $\%R_O$ is, however in good agreement with known reservoir data (Berner and Faber, 1996).

To correct for differences of the isotope ratios of the different landplant precursors, Berner and Faber (1996) introduced correction terms for Equations 2.16 through 2.18. These terms are (Berner et al., 1995):

Methane: -22.0‰

Ethane: -22.4‰

Propane: -22.8‰.

Therefore the correction terms can be written as (Berner and Faber, 1996):

Methane: $\delta^{13}C_1^* = \delta^{13}C_{1(I)} + (22.0 - \delta^{13}C_{org})$ (2.19)

Ethane: $\delta^{13}C_2^* = \delta^{13}C_{2(I)} + (22.4 - \delta^{13}C_{org})$ (2.20)

Propane: $\delta^{13}C_3^* = \delta^{13}C_{3(I)} + (22.8 - \delta^{13}C_{org})$ (2.21)

where $\delta^{13}C_{org}$ is the initial isotope ratio of the landplant precursors.

2.5.2 Hydrogen

In addition to carbon, stable hydrogen isotopes play an important role for the delineation of different gas types and origins. Isotope effects for hydrogen isotopes are much larger compared to carbon isotopes because of the huge mass difference between hydrogen (^{1}H) and deuterium (^{2}H; D). However, the processes leading to fractionation have similar controls as those for stable carbon isotopes (Schoell, 1980; Whiticar, 1996a). Stable hydrogen isotope values are reported versus the SMOW–standard. The uptake of hydrogen from water by plants results in isotope fractionation and in different hydrogen isotope ratios in the different organic plant compounds (Estep and Höring, 1980). Yeh and Epstein (1981) reported δD values for lipid compounds of plants between -150‰ and -250‰, which shows deuterium depletion when compared to the bulk values for entire plants with values for δD between -140‰ and -20‰). As with the carbon isotope ratio, the hydrogen isotope ratio of the plants are found in coals formed from these plants and is therefore source dominated (Redding et al., 1980).

Hydrogen isotopes are particularly useful for the distinction of the two microbial gas generation pathways. The δD values for microbial gases are between -400‰ and -150‰ (Whiticar, 1999). Gases generated by carbon dioxide reduction are more enriched in deuterium (ca. -250‰ to ca. -150‰) than gases generated by methyl–type fermentation (ca. -400‰ to ca. -290‰; Whiticar, 1999). The hydrogen isotope effects related to methanogenesis are poorly understood. An agreement exists about the transfer of hydrogen to the methane molecule during the process of carbon dioxide reduction. Water present during the reaction is considered to be the only source for the four hydrogen atoms present in the methane molecule (Whiticar, 1999). The hydrogen source for the process of methyl–type fermentation is less clear. It was commonly accepted that an intact transfer of the three hydrogens from the methyl–group to the methane molecule takes place and that the fourth hydrogen is supplied by water present during the reaction (Whiticar, 1999). But work by Waldron et al. (1988, 1999) proposed that only hydrogen from water is incorporated enzymatically into the methane molecule and that the δD ratio of methane generated by methyl–type fermentation is only controlled by the isotope ratio of the water present during the reaction.

Thermogenic methane has δD values between -275‰ and -100‰ (Whiticar, 1999), but the δD ratio shows no clear dependency on thermal maturation (Whiticar, 1994). The controls for the fractionation of hydrogen during the coalification process are similar to those described for carbon isotopes. The combination of $\delta^{13}C$ and δD ratios of methane is a useful tool in delineating the origin of gases (Figure 2.13).

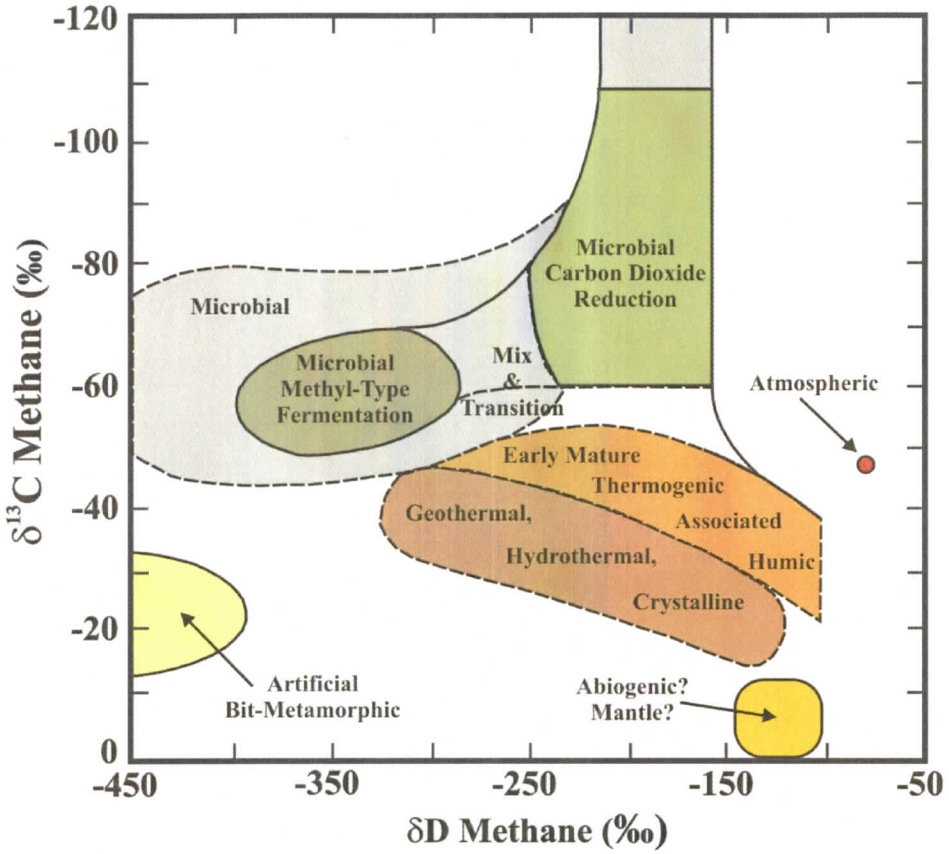


Figure 2.13: *Cross–plot of δD– and $\delta^{13}C$–ratios of methane. Based on the isotope composition of methane, different possible origins can be determined and are shown in the diagram with distinct areas. See text for details (modified from Whiticar, 1996b).*

Schwarzkopf (1984) applied carbon and hydrogen isotopes analysis for the separation of different coal macerals. For carbon the analysis showed, that inertinite (-23.4‰) and vitrinite (-23.7‰) are enriched in ^{13}C compared to liptinite (-23.9‰) and sapropelic coals (-23.4‰), which are relatively depleted in ^{13}C (Schwarzkopf, 1984; Schwarzkopf and Schoell, 1985). The analysis of hydrogen isotope ratios revealed greater separation between the different macerals. Inertinite (δD=-87‰) and vitrinite (δD= -99.2‰) are enriched in deuterium, whereas liptinite (δD=-109‰) and sapropelic coals

(δD=-122‰) are relatively depleted (Schwarzkopf, 1984; Schwarzkopf and Schoell, 1985). Figure 2.14 shows the separation of the different macerals based on their carbon and hydrogen isotope composition. Liptinite is, like modern living plants, depleted in the heavy isotopes ^{13}C and deuterium, whereas vitrinite and inertinite are depleted in the light isotopes ^{12}C and ^{1}H, probably due to their removal during early oxidation and forest fires (Schwarzkopf, 1984; Schwarzkopf and Schoell, 1985). Overall no influence of coalification on the isotope composition of the macerals was found by Schwarzkopf (1984), and therefore the isotope composition of coal depends on the isotope compositionof the macerals.

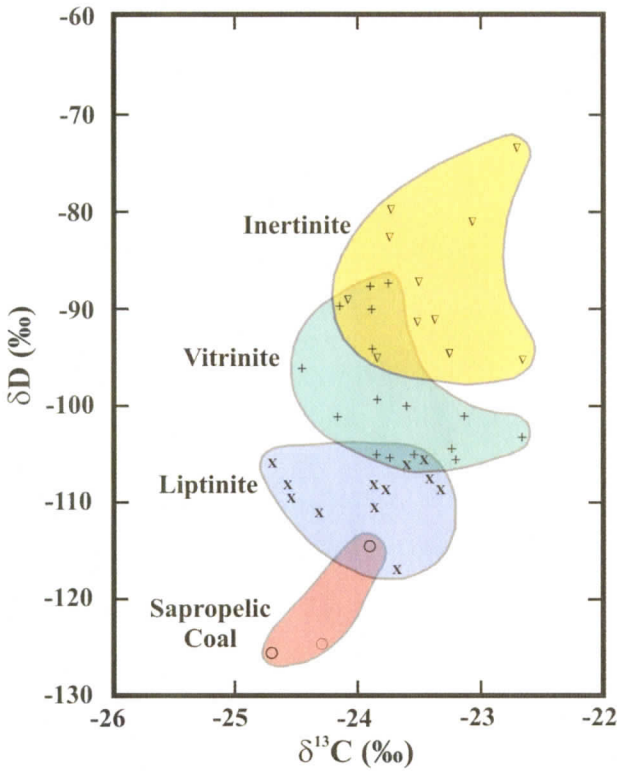


Figure 2.14: *Stable carbon and hydrogen isotope composition of different main coal maceral groups and sapropelic coal (modified from Schwarzkopf, 1984).*

2.5.3 Secondary Processes

The carbon isotope ratios of thermogenic generated hydrocarbon gases are depending on the maturity and the type of source rock. If the source rock and its maturity are known, but the carbon isotope ratios for methane, ethane or propane do not follow the Berner and Faber (1996) relationships, secondary alteration of the isotope composition of the gases is probable. These alteration processes can include mixing between thermogenic and microbial gases or between different thermogenic gases, microbial methane oxidation, adsorption/desorption and diffusion. The influence of these processes is not limited to the isotope composition, but, may also affect the chemical composition of the gas.

2.5.3a Mixing

In a conventional gas reservoir or in a coal seam, hydrocarbon gases can be mixtures of different thermogenic gases from different sources, or of thermogenic and microbial gases. If the mixture is limited to two gases, the proportions of these two gases can be calculated, where the gas composition and isotope signatures of the end members are known or can be assumed (Faber, 1987). The calculation is based on a linear mass balance (Equation 2.9).

2.5.3b Oxidation

Microbial activity not only generates gas (methanogenesis), it can also oxidize hydrocarbon gases, mainly methane, to carbon dioxide. This microbial uptake occurs under aerobic and anaerobic conditions (Barker and Fritz, 1981; Whiticar, 1996b), whereas methanogenesis is limited to anaerobic conditions (Whiticar, 1999). The anaerobic microbial methane oxidation (Equation 2.22) and aerobic microbial methane oxidation (Equation 2.23) reactions are:

$$CH_4 + SO_4^{2-} \rightarrow HCO_3^- + HS^- + H_2O \quad (2.22)$$

$$CH_4 + 2O_2 \rightarrow CO_2 + 2H_2O \quad (2.23)$$

A possible source of oxygen in coal seams, which is necessary for aerobic microbial oxidation, is oxygenated fresh waters introduced into the coal seams via recharge pathways (King and Blackburn, 1996; Aravena et al., 2003).

During the process of aerobic microbial oxidation, methane, relative to higher hydrocarbons, is preferentially consumed by bacteria, leading to a depletion of methane and a relative enrichment of carbon dioxide (Faber and Stahl, 1983, 1984; Whiticar and Faber, 1986; Faber, 1987; Whiticar, 1996b). The microbial uptake of methane is accompanied by a carbon isotope effect (Barker and Fritz, 1981; Whiticar and Faber, 1986; Whiticar, 1999). Based on laboratory measurements Whiticar and Faber (1986)

reported carbon fractionation factors ranging between 1.005 and 1.031 for microbial methane oxidation. Microbes feed preferentially on ^{12}C containing methane, with the result that the remaining methane becomes enriched in ^{13}C. In addition, the utilization of methane leaves the remaining gas wetter. The generated carbon dioxide is assumed to be ^{12}C enriched.

2.5.3c Adsorption/Desorption

Adsorption occurs mostly on the walls of the micropore network (Crosdale et al., 1998), resulting in an initial layer of adsorbed gases (Hunt, 1991). If higher pressures and space are available, multilayer adsorption may occur (Crosdale at el., 1998), whereby the initial layer is bound more strongly than the following layers (Hunt, 1991). When gases are present, adsorption will occur until the coal is gas saturated (Meissner, 1984). Desorption is required for the production of CBM and is generally achieved by lowering the pressure in a coal seam. Because coals seams act as fractured aquifers, desorption can be initiated by removing formation water out of the coal, thereby lowering the hydrostatic pressure (Rice, 1993; McLennan et al., 1995).

The processes of adsorption and desorption are accompanied by molecular and isotope effects, that alter gases in coals in the following ways (Ettinger et al., 1966; Colombo et al., 1970; Lebedev and Syngayevskiy, 1971; Friedrich and Jüntgen, 1972; Smith et al., 1985; Faber, 1987; Hunt, 1991; Yee et al., 1993; Flores, 1998; Whiticar, 1996a; Busch et al., 2004):

1. Carbon dioxide is more strongly adsorbed than methane, resulting in carbon dioxide enrichment for adsorbed gas and relative methane enrichment for desorbed gas,
2. Higher hydrocarbons are more strongly adsorbed than methane, resulting in enrichment in higher hydrocarbons for adsorbed gas and relative depletion in higher hydrocarbons for desorbed gas,
3. ^{13}C is preferentially adsorbed relative to ^{12}C, resulting in ^{13}C enrichment for adsorbed methane and relative ^{12}C enrichment for desorbed methane,
4. If coals are undersaturated with gas, all available gases will be adsorbed and therefore no fractionation, molecular, or isotopic, occurs.

Yee et al. (1993) reported increasing sorption strength from H_2 to N_2 to CH_4 to C_2H_6 to CO_2. The increasing sorption strength is related to the increasing boiling points of the different species at atmospheric pressure (Ettinger et al., 1966). Ettinger et al. (1966) also pointed out that the polarity of certain molecules is related to greater sorption strength, but this effect is secondary to the boiling point effects. Busch et al. (2004) reported preferential adsorption of methane over carbon dioxide, but only at pressures below 6MPa, opposite to the above reported greater sorption strength for carbon dioxide relative to methane.

The preferential adsorption of ^{13}C relative to ^{12}C can lead to complications when considering the overall $\delta^{13}C$ value for gas adsorbed to a coal. If during coalification and burial, i.e., during the time following gas generation, gas is lost, this lost gas should be enriched in ^{12}C, resulting in strongly ^{13}C enriched gas that is still adsorbed to the coal. A quantitative consideration of this isotope effect is extremely difficult, due to the complexity of the processes and the possible time span involved.

Colombo et al. (1970) reported ^{13}C enrichment for adsorbed methane with an average $\delta^{13}C$ difference of 5‰ between free and adsorbed methane. This value would relate to a fractionation factor for adsorption of α_C=1.005. This value has to be considered with caution, due to differences in sample collection and analytical methods in the early 1970's, relative to today's standards. Gas samples used by Colombo et al. (1970) had substantial gas loss prior to gas collection and gas analyses. The analyzed gases represent therefore late desorbed gases. Based on preferential desorption of ^{12}C, the early methane should be enriched in ^{12}C, whereas with increasing desorption this enrichment should become less pronounced. The application of vacuum on the coal samples by Colombo et al. (1970), causes a pressure reduction accompanied with strong desorption. The corresponding isotope effect should diminish due to the elevated liberation of ^{13}C enriched residual methane. As a consequence, changes in the stable carbon isotope ratio of methane should be larger in a production or desorption experiment scenario where early desorbed gases are retained and the pressure reduction is not severe.

Lebedev and Syngayevskiy (1971) measured $\delta^{13}C$ ratios of "free methane" from coal with a range from -39.2‰ to -49.5‰. The "adsorbed methane" $\delta^{13}C$ values range between -10.8‰ and -33.8‰; the measured $\delta^{13}C$ values are not available, but the

reported ^{13}C enrichment for "adsorbed methane" relative to "free methane" is in the range of several to tenths of per mil (Lebedev and Syngayevskiy, 1971).

Beutl and Lesnik (2001) and Rahn and Eiler (2001) conducted adsorption experiments for hydrogen, carbon dioxide and carbon monoxide on different substrates. Beutl and Lesnik (2001) reported no hydrogen isotope effect for the adsorption of H_2 onto vanadium/palladium alloys. Rahn and Eiler (2001) analyzed the carbon and oxygen isotope effects for carbon dioxide adsorption onto kaolinite, basalt and fluorite. The carbon isotope effect shows identical directions for all three materials with ^{13}C enrichment for the free gas phase in the range of 0.8‰ to 1.5‰ (Rahn and Eiler, 2001). These trends are reversed to expected trends, where the heavy isotope should be concentrated in the adsorbed (condensed) phase relative to the coexisting free (vapour) phase (Lindemann, 1919). Oxygen isotope fractionation showed the expected trend, with ^{18}O enrichment in the adsorbed phase relative to the free gas by 1.8‰ (Rahn and Eiler, 2001).

2.5.3d Diffusion

The process of diffusion is probably responsible for isotope fractionation, as well as for compositional changes (Leythäuser et al., 1980; Prinzhofer and Huc, 1995; Kroos and Leythäuser, 1996; Pernaton et al., 1996; Prinzhofer and Pernaton, 1997; Zhang and Kroos, 2001). Diffusion is a transport process based on the random thermal motion of individual molecules that result in a permanent redistribution of molecules in gases and liquids and to a much smaller degree in solids (Kroos and Leythäuser, 1996). If external forces and fields are absent, diffusion results in the equilibration of concentration gradients. The rate of diffusive transport is related to a concentration gradient of a compound, and can be expressed with Fick's first law of diffusion:

$$J = -D \cdot \text{grad } C \qquad (2.24)$$

where J is the diffusive flux (mass/area/time), D is the diffusion coefficient (length^2/time) and C is the volume concentration of the considered compound (mass/volume). Equation

2.24 is theoretically only valid for low concentrations and small concentration gradients (Kroos and Leythäuser, 1996), but is the basic equation for describing diffusive transport processes in the form of a mass balance equation (Fick's second law of diffusion):

$$(\partial C/\partial t) = D \cdot (\partial^2 C/\partial x^2) \qquad (2.25)$$

This law can be reformulated for the process of diffusive transport in a sedimentary (porous) media:

$$J = -D_{eff} \cdot \text{grad } C_{bulk} \qquad (2.26)$$

where D_{eff} is the effective diffusion coefficient and C_{bulk} is the bulk volume concentration (Kroos and Leythäuser, 1996). The effective diffusion coefficient reflects the impact of the porous media on the mobility of a diffusing molecule (Kroos and Leythäuser, 1996), with this mobility affected by factors like the geometry of the pore system. The above mentioned considerations are only valid for diffusive flow in the absence of temperature and pressure gradients.

Diffusion experiments typically focus on conventional gas accumulations and the evaluation of gas loss through a cap rock (mudstones and/or fine–grained sandstones) via the process of diffusion (May et al., 1968; Galimov, 1975; Fuex, 1980; Leythaeuser et al., 1980; Kroos, 1986; Kretzschmar et al., 1986; Prinzhofer and Huc, 1995; Kroos and Leythaeuser, 1996; Pernaton et al., 1996; Prinzhofer and Pernaton, 1997; Zhang and Kroos, 2001; Schloemer and Kroos, 2004). On the molecular level, the observed isotope effects as a result of the process of migration/diffusion through a sedimentary cap rock, is to deplete the higher hydrocarbons in migrated/diffused gas. This depletion tends to increase with increasing molecular size and molecular geometry (Leythaeuser et al., 1980). Kroos (1986) reported the following diffusion sequence: methane > ethane > propane > n–butane. The diffusion of branched hydrocarbons is higher than the diffusion of straight–chain hydrocarbons (Leythaeuser et al., 1980). In relation to a conventional hydrocarbon play and the pore network of a sedimentary rock, Kroos and Leythaeuser (1996) stated that aromatic hydrocarbons diffuse more rapidly if a water–saturated and

inter–connected pore network is present, whereas in cases of a discontinuously connected pore network saturated hydrocarbons migrate preferentially. In reservoir rocks, no correlation exists between diffusion and the product of porosity and permeability (Kretzschmar et al., 1986). In support of this finding, Kroos (1986) determined comparatively large diffusion coefficients for sedimentary rocks with permeabilities below the detection limit of the used analytical methods.

The fractionation of stable carbon isotopes by diffusion and migration discriminates against the heavy isotope ^{13}C, resulting in ^{12}C enriched methane in the diffusing gas (May et al., 1968; Colombo et al., 1970; Galimov, 1975; Prinzhofer and Huc, 1995; Pernaton et al., 1996; Prinzhofer and Pernaton, 1997; Zhang and Kroos, 2001; Schloemer and Kroos, 2004). Migration–related isotope changes between -3‰ and -15‰ were reported by May et al. (1968) and Colombo et al. (1970). Pernaton et al. (1996) reported values for isotope changes of -5‰ to -11‰ for water–saturated rocks and of -30‰ for dry sedimentary rocks. Similar values were reported by Prinzhofer and Pernaton (1997), with isotope changes of -3‰ to -11‰ for water–saturated rocks and of -30‰ for dry shales. These pronounced differences are not attributed to isotope effects occurring during the solubilization of methane at the gas–water interface. Fuex (1980) reported that no significant isotope effects occurs during this process.

More detailed quantification of the isotope effects due to migration/diffusion are given by Zhang and Kroos (2001) and Schloemer and Kroos (2004). Zhang and Kroos (2001) conducted diffusion experiments in water saturated rocks and showed that ^{13}C depletion in methane is strongest during the initial phase of the experiment with a value of -24.8‰; with increasing time, diffusing methane becomes relatively ^{13}C enriched (-47.8‰) and approaches the $\delta^{13}C$ value of the source gas (-39.1‰). Zhang and Kroos (2001) reported an isotope change for diffusion of -3.12‰. There was always a final offset between the $\delta^{13}C$ value of the source gas and the $\delta^{13}C$ value of the migrated methane, whereby this offset decreases with decreasing concentrations of organic material in the samples (Zhang and Kroos, 2001). This relationship cannot be expected for the diffusion of methane in coal, as the diffusion of methane in a coal requires methane to be present as a free gas. Free methane in a coal is only present when the coal is oversaturated with gas or when conditions allow desorption. Free gas present in a coal,

due to over–saturation, will be lost prior to sampling, so that the sampled gas is a product of the desorption process. When desorption occurs, the physical conditions neglect a simultaneous adsorption. Schloemer and Kroos (2004) reported that the heavier isotope species will have a lower effective diffusion coefficient and that the first gas diffusing through a rock will be depleted in heavy isotopes. In their experiments, the isotope composition of the diffused gas was consistently ^{12}C enriched relative to the source gas. Initial isotope shifts are -5.7‰ for methane and -3.4‰ for ethane. During the course of the experiment, the $\delta^{13}C$ ratio of the diffused methane approached the $\delta^{13}C$ ratio of the source gas and the isotope shifts were reduced to -2.12‰ for methane and -0.9‰ for ethane (Schloemer and Kroos, 2004). Overall the isotope fractionation for methane is twice that of ethane. For diffusion in water–saturated rocks, Schloemer and Kroos (2004) reported different results, i.e., positive isotope shifts, resulting in the enrichment of ^{13}C in the diffusing gas. They related this to the higher aqueous solubility of $^{13}CH_4$ (see also Galimov, 1975; Fuex, 1980).

Pernaton et al. (1996) conducted hydrogen isotope diffusion experiments and found that diffused methane became enriched in the heavy isotope ^{2}H. Possible explanations are that the electronic cloud for ^{2}H is smaller than for ^{1}H and therefore CH_3D would interact less with the solid of the porous medium. In addition the higher speed and smaller size of CH_3D relative to CH_4 may be factors (Pernaton et al., 1996).

Several different isotope shifts for methane diffusion through a sedimentary rock have been published. In these the isotope shifts span from -1‰ to -30‰. The differences between the isotope shifts published by Schloemer and Kroos (2004) and Pernaton et al. (1996) can be attributed to different temperatures used in the experiments (Schloemer and Kroos, 2004). Temperature dependence for the isotope effect during diffusion was also reported by Kroos (1986), who measured an increase for the diffusion coefficient for methane of the order of one magnitude as a result of a temperature increase from 30°C to 70°C during the experiments. Beside temperature, pressure also has an impact on the isotope effect of diffusion. Schloemer and Kroos (2004) conducted diffusion experiments using mudrocks and observed that increasing pressure results in decreasing effective diffusion coefficients; a pressure increase from 10MPa to 40MPa resulted in a decrease of the effective diffusion coefficient of ca. 38%. This reduction of overall molecular

mobility is attributed to an increased tortuosity, because parts of the pore system become blocked at higher pressure (Schloemer and Kroos, 2004).

Overall, isotope effects due to diffusion are complex and depend on several geological and physical parameters, such as lithology, pressure, temperature, gas content, gas composition and diffusion distance. No general fractionation factor can be assigned to the general process of diffusion, as emphasized by Prinzhofer and Huc in 1995.

Diffusion studies have been limited to clastic sedimentary rocks. Experiments using coal as a medium are rare, and do not consider stable isotopes. Furthermore, heterogeneities and the presence of fractures in the lithological units are complicating factors.

For the evaluation of diffusion coefficients, Fick's laws of diffusion (Equations 2.24 and 2.25) are applicable. Strictly, these relationships are valid when a pressure gradient is absent. However CBM is produced from wells, where a pressure gradient in the coal seams is the driving force for desorption and production. Coal seams can be found over a wide depth range, resulting in different temperature and pressure regimes. These different temperatures and pressures have to be included when considering the diffusive effect on CBM in coals. Additionally, the pore–structure of a coal depends on its geological history, as well as the structure of the cleat network, which finally determines the diffusion length. In a coal with narrowly spaced cleats the diffusion length is shorter than in a coal with widely spaced cleats, resulting in different diffusional isotope effects. Bolt and Innes (1959) suggested that "The micro–pore diffusion characteristics of coal are not mainly sensitive to chemical composition, but depend considerably upon the fine structure of the coal, which has been determined by the physical history of the seam."

Colombo et al. (1970) and Prinzhofer and Pernaton (1997) proposed the use of a diagram for the differentiation of diffusion and mixing processes in gas samples (Figure 2.15). In this diagram the concentration of ethane over methane is plotted as a function of $\delta^{13}C$ of methane. A mix of two different end members should result in a straight line (Figure 2.15), whereas diffusion should result in a substantially curved plot with positive concavity (Figure 2.15).

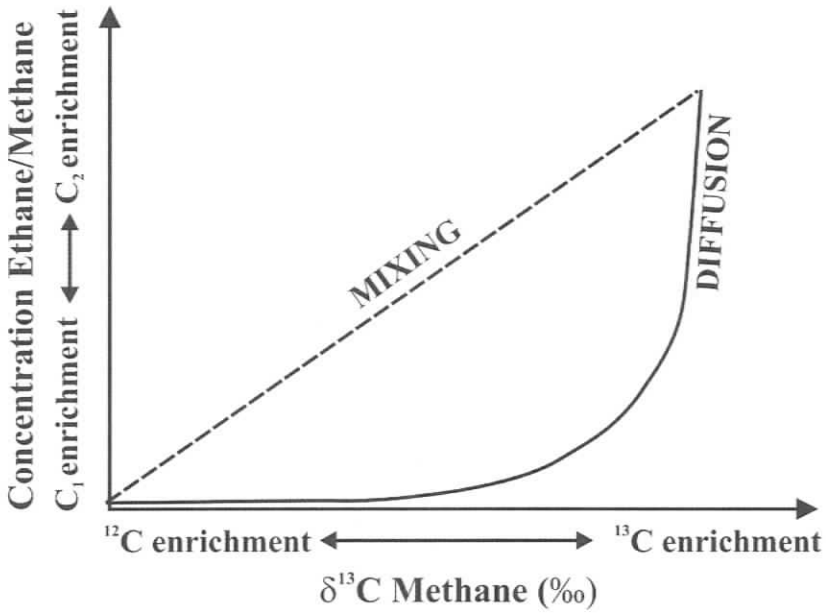


Figure 2.15: *Diffusion plot showing $\delta^{13}C$ ratio for methane versus ratio of proportions of methane over ethane. Samples plotting in a straight line indicate presence and alteration due to mixing, whereas samples plotting in a logarithmic curve indicate alteration due to the process of diffusion. See text for details (from Colombo et al., 1970 and Prinzhofer and Pernaton, 1997).*

3. Methods

3.1 Sampling

Two different strategies were used for the collection of gas samples. The strategies are related to 1) the collection of samples from producing wells and 2) the collection of samples from desorption experiments. A description of the two sample strategies is given below.

3.1.1 Production Sampling

Production samples were taken from producing CBM wells. The liberation of the gas was achieved by lowering the hydrostatic pressure in coal seams, causing the desorption of gas and the migration from the site of desorption to the well. Sampling at the well head was conducted as follows.

A deflated 50L plastic bag was pulled over a valve at the well head and attached with cable binders. Once attached, the valve was opened and the bag was fully filled with gas. The filled bag was sealed with another cable binder and removed from the valve. Gas was removed from the bag with a 30ml syringe and injected into pre–evacuated and labelled 25ml Wheaton bottles. The syringes were equipped with needles and were flushed with gas from the bag several times before filling the Wheaton bottles to minimize contaminations. The process of filling and emptying the syringes was conducted slowly to avoid fractionation at the needle tip. When the syringe was finally filled, it remained connected to the bag to allow equilibration between the gas volumes in the syringe and in the bag. The syringe was sealed by using a connected 3–port valve before removing it from the bag. The volume in the syringe was bigger than the volume of the used Wheaton bottles to provide gas for flushing the needle before injecting 25ml of gas into the pre–evacuated Wheaton bottles. The Wheaton bottles were sealed with 1cm thick silicon septa to ensure a good sealing and to prevent diffusion of the gas out of the bottle.

The large volume for the plastic bags was chosen to minimize the effect of air contamination. Deflated bags contained a minimal amount of air compared to the volume of gas introduced. The process of sealing the bag to the valve could introduce air into the bag. However, considering the amount of CBM gas in the bag, the relative amount of air was negligible. Measurements for the determination of air in the bags were not conducted.

Ideally, production samples should have been taken once a week, but, because employees of the participating energy companies carried out the sampling, the sample times were adjusted to their regular well maintenance schedule.

3.1.2 Desorption Experiment Sampling

Desorption experiment samples were collected from desorption canisters following the recovery of coal cores or cuttings from an exploration well. The implementation of a desorption experiment based on the direct method, is described in Chapter 2.4 (Figure 2.6).

Following the volumetrical measurement of the desorbed gas, gas was removed by connecting a 30ml syringe to the tubing. Syringes were equipped with three port valves to allow of the syringe to be flushed while connected to the tubing. The process of flushing and filling the syringe was conducted slowly to avoid fractionation and ideally equilibration between the two gas volumes was allowed. Thirty ml of gas were removed from the tubing and, after flushing the needle, 25 ml of gas were injected into pre–evacuated Wheaton bottles. Sample time, canister number and injected volume were recorded.

Wheaton bottles used for sampling were sealed with a 1cm thick silicon septa. Based on the set–up and the total number of canisters used in the field, a mixture of gases from different canisters can not be excluded, unless large volumes of gas were desorbed from one canister allowing the flushing of the total gas remaining in the tubing. Ideally, the canister and the tubing were flushed with an inert gas after the measurement was implemented.

The sampling schedule accounts for the fact that most of the gas desorbs from the coal early during the desorption experiment and that the volume decrease significantly over time. The initial sample schedule was modified after Ryan & Dawson (1994) and is described below:

- Immediately after the coal was sealed into the canister,
- every 30 minutes from 0 minutes to 120 minutes,
- every 5 hours from 2 hours to 22 hours,
- every 24 hours for the remaining experiment,
- immediately before the experiment is terminated.

The sampling schedule was adjusted to volume measurements. Therefore, sample times and frequencies sometimes differed from the above mentioned schedule.

3.2 Gas Chromatography–Isotope Ratio Mass Spectrometry (GC–IRMS)

The coupling of Gas Chromatography (GC) with Isotope Ratio Mass Spectrometry (IRMS) allows a compound specific, isotope ratio analysis of gas mixtures. A brief overview about the principles of GC and IRMS is given below. A schematic of a GC–IRMS is shown in Figure 3.1. For more details refer to e.g., Meier–Augenstein (1999).

A sample is transferred via a six port valve from the sample vessel (e.g. syringe) into a sample loop. The size of the sample loop selected depends on the amount of the different chemical species in the sample. From the sample loop, the gas is transferred onto a GSQ Plot column with a continuous flow of helium. The flow rate can be adjusted to achieve a better separation of the different species for subsequent isotope ratio determinations (see below). Different gas compounds are separated in the column based on their physical properties such as mass and polarity. The column is placed in an oven, which is programmed with a temperature profile. Methane and carbon dioxide, the smallest and lightest molecules, pass through the column at room temperature (first methane followed by carbon dioxide). Higher hydrocarbons such as ethane, propane,

i–butane and *n*–butane are better retained and elution requires the heating of the column. The order of elution of the considered compounds on this column is as follows:

methane → carbon dioxide → ethane → propane → *i*–butane → *n*–butane.

After separation in the column, each component is converted in an oven. The oven temperature is set and differs for the different measurements of carbon and hydrogen isotope ratios. For carbon, the temperature is set to 1080°C and hydrocarbons are oxidized in a nickel–platinum reactor to carbon dioxide. For hydrogen, the oven temperature is set to 1450°C and hydrocarbons are reduced to pure hydrogen (H_2) in an empty ceramic tube. The carbon dioxide and the hydrogen respectively are sequentially introduced into the IRMS.

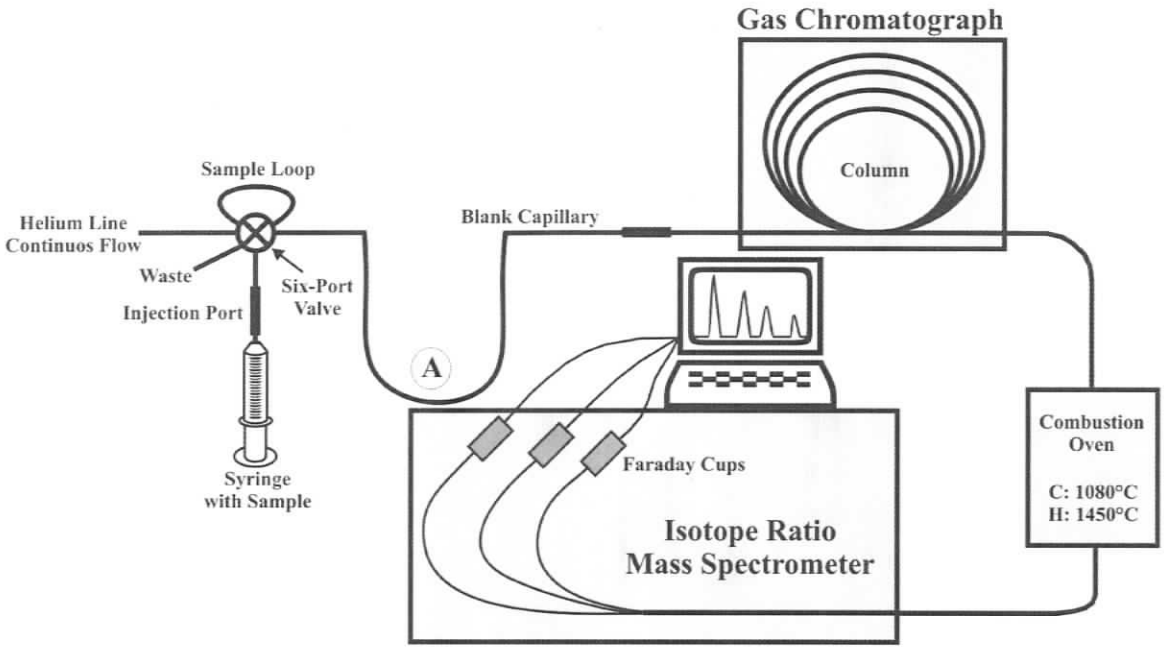


Figure 3.1: *Schematic illustration of the Gas Chromatograph–Isotope Ratio Mass Spectrometer (GC–IRMS), including its main components. C = carbon; H = hydrogen. A represents the point where gases are trapped in liquid nitrogen, if the measurement requires it.*

A mass spectrometer is divided into three main components: ion source, mass analyzer and ion detector. In the ion source, the introduced sample molecules (carbon dioxide or hydrogen), are ionized by electron bombardment. The electrons are emitted from a heated filament, normally made of tungsten or rhenium and accelerated by an electrostatic field. Generated ions are accelerated and focussed into narrow beams when leaving the ion source. In the mass analyzer, the ions in the beam are separated based on their mass/charge ratio. The beam passes through a magnetic field and is deflected into

curved paths, where the radii of these paths are proportional to the square root of the mass/charge ratio allowing a separation based on the mass of the ions. In the ion detector, the separated ions corresponding to the targeted stable isotopes are collected simultaneously in Faraday cups, passed through an amplifier and converted into electrical impulses. The electrical impulses are compared to values acquired from standards and presented by computer software in form of a chromatogram with retention time in seconds (x–axis) versus the signal's intensity in mV (y–axis). Gas chromatographic separation in a column not only affects the different chemical species, but also the different isotope species (Hoefs, 2004) resulting in a separation of carbon dioxide, respectively hydrogen, containing light and heavy isotopes. Carbon dioxide, respectively hydrogen representing the early part of a peak is relatively depleted in ^{13}C, respectively ^{2}H, and becomes continuously enriched in ^{13}C, respectively ^{2}H during the duration of the peak. Therefore, the isotope composition of a chemical compound varies across the entire peak and has to be integrated over the entire peak width to calculate the true isotope ratio.

3.3 Measurement

This chapter describes the measurement of samples. For the measurement of concentrations and of $\delta^{13}C$ values only methane, ethane, propane, *n*–butane, *i*–butane and carbon dioxide were considered. δD ratios were only determined for methane. Carbon and hydrogen measurements were conducted on a Varian 3400 gas chromatograph coupled to a Finnigan MAT Delta XL+ Isotope–Ratio–Mass–Spectrometer. Tables 3.1 and 3.2 provide parameters for the measurements of carbon and hydrogen isotopes.

Isotope ratios of different compounds were analyzed by using a GC–IRMS, and because of limited quantities of CBM samples also the concentrations of these compounds. This was achieved first by measuring standards with known concentrations. The standard gas used has the following initial composition:

- 80% methane
- 10% ethane
- 6% propane
- 4% butane.

To cover concentration differences in samples, several dilutions of this gas were measured. Resulting peak areas in relation to concentrations of the standard allowed the formulation of equations for the considered chemical compounds. These equations allowed the calculation of the relative amounts of a specific compound in an unknown sample, based on the area of the correlating peak. A calibration example for methane is shown in Figure 3.2. No calibration gases were used for carbon dioxide and *i*–butane.

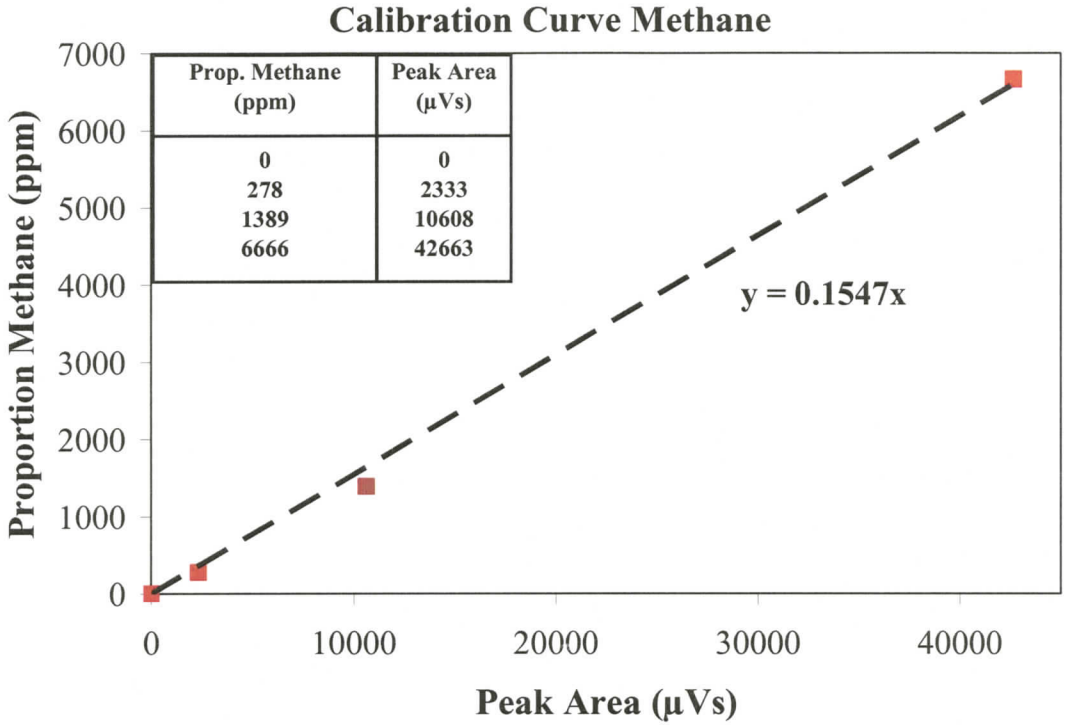


Figure 3.2: *Example of a calibration curve for methane to allow proportion measurements with the use of a GC–IRMS. The proportions of methane in different dilutions of a standard gas with known methane proportions are shown on the y–axis (actual data are shown in insert). The resulting peak areas, relative to known proportions of methane, are shown on the x–axis (actual data are shown in insert). A linear relationship exists between these two parameters and the corresponding mathematical equation to describe this relationship is shown. By applying this equation, relative proportions of methane in CBM samples can be calculated by determining the peak areas of the correlating peaks. Calibration curves were measured for methane, ethane, propane and butane. Calibration curves are subject to changes when different sample loops, flow rates and columns are applied for the measurements.*

Instead for carbon dioxide the methane equation, and for *i*–butane the *n*–butane equation, were applied. These calibration measurements also established the retention times for the different species under investigation and allowed matching of the measured peaks to the chemical compounds. Calibration measurements were conducted daily prior to the

measurement of CBM samples and every time different sample loops, different columns or different flow rates were applied.

Sub–samples were removed from sample vessels (Wheaton bottles) by injecting a similar amount of helium, allowing it to equilibrate, and then withdrawing the sub–sample. This technique avoids the creation of a negative pressure in the vessel. The volume of injected helium was recorded for the calculation of dilution factors.

Because natural gases generated from a Type III Kerogen generally have low concentrations of higher hydrocarbons (ethane to butane), measurement of the higher hydrocarbons and carbon dioxide was conducted separately from that of methane.

For the on smaller concentrations of the higher hydrocarbons and carbon dioxide, a bigger sample loop volume than used for the measurement of methane was used for the measurement of these compounds. The use of a bigger sample loop volume also introduced a quantity of methane large enough to interfere with the carbon dioxide and ethane peaks. Therefore, methane was first removed from the sample. The technique used was a liquid nitrogen trap placed on a piece of blank capillary (point A in Figure 3.1). The liquid nitrogen freezes the higher hydrocarbons and the carbon dioxide, but not methane, which was vented. After a certain time (time depends on flow rate and length of GC–column used) when the methane had passed the detectors, the capillary was removed from the liquid nitrogen trap and measurements of higher hydrocarbons were started. This method worked well for samples with smaller methane concentrations. If methane concentration exceeded a certain concentration threshold (actual concentration is unknown), it could still interfere with carbon dioxide and ethane peaks. Several different approaches were used to solve this problem and to establish the measurement of the higher hydrocarbons and carbon dioxide. These approaches included the use of different trapping liquids with different temperatures. Sample dilution to decrease the relative methane concentration in the samples is the best method to solve the problem. A negative consequence of using this approach is that low concentrations of the higher hydrocarbons and of carbon dioxide became diluted. This dilution resulted, in some cases, in intensities for these compounds below the measurement limit of 200mV. In these cases the measurement of reliable isotope ratios for these compounds was not possible. Because of the dilution, for many samples only the concentrations were measurable and isotope

ratios were considered to be unreliable. Statistical measurements and calculations were not performed because of limited quantities of CBM samples.

Table 3.1: *GC–IRMS set–up used for measurement of gas composition, proportions and $\delta^{13}C$–ratios of the different gas species.*

Carbon Measurement	
Gas Chromatograph	Varian 3400
Carrier Gas	Helium
Flow Rate	Variable
Column	GSQ PLOT (Porous Layer Open Tubular)
Column Length	30m
Temperature Profile	25°C to 160°C
Oven Temperature	1060°C
Reactor Type	Nickel Platinum
Mass Spectrometer	Finnigan MAT Delta XL+
Software	Isodat NT

Table 3.2: GC–IRMS set–up used for measurement of δD–ratios of methane.

Hydrogen Measurement	
Gas Chromatograph	Varian 3400
Carrier Gas	Helium
Flow Rate	Variable
Column	GSQ PLOT (Porous Layer Open Tubular)
Column Length	30m
Temperature Profile	25°C to 160°C
Oven Temperature	1450°C
Reactor Type	Empty Tube
Mass Spectrometer	Finnigan MAT Delta XL+
Software	Isodat NT

4. Samples

4.1 Sample Description

Over 1000 gas samples from 10 different sample sets were collected in 7 different coal–bearing basins. Three sample sets were taken from production wells (production samples) and 7 sample sets during desorption work following the drilling of exploration wells (desorption experiment samples). Only coal cores were used for the desorption experiments. Exceptions are data sets D4 and D5, which were recovered from coal fragments collected underground. Because of confidentiality agreements signed with participating companies, companies' names, sample locations and information or local names, which could lead to identification of companies or locations, have to be kept confidential. Therefore, the different sample sets are named with abbreviations P1, P2, P3, D1, D2, D3, D4, D5, D6 and D7.

A general overview about the sample sets is given in Table 4.1. Overall the samples cover coal maturity ranging from sub–bituminous coal to anthracite. Desorption experiment samples were collected over different desorption time periods, ranging from 1.5 hours to 2733 hours. Production samples cover time periods up to 6312 hours.

In the following chapters, the different sample sets are described in more detail. Sampling procedures are described in Chapter 3.1.

Table 4.1: *General information about coals under investigation and general information about type and duration of used sample methods. Ø = average; Vit = Vitrinite; Iner. = Inertinite; Lipt. = Liptinite; HV Bit.A = high volatile bituminous A; HV Bit.B = high volatile bituminous B; HV Bit.C = high volatile bituminous C; MV Bit. = medium volatile bituminous; LV Bit. = low volatile bituminous; Sub Bit.A = sub bituminous A.*

Name	Sample Type	Coal Rank	$\%R_O$ Ø	Maceral Content (Ø %)			Depth Range (m)	Canister/ Wells Quantity	Time Range (hours)
				Vit	Iner	Lipt			
P1	Prod.	n/a	n/a	n/a	n/a	n/a	n/a	3	1968
P2	Prod.	HV Bit.A-MV Bit.	1.20	n/a	n/a	n/a	136-172	5	792
P3	Prod.	Sub Bit.A-HV Bit.C	0.57	82.6	16.2	1.2	172-188	3	6312
D1	Des.	n/a	n/a	n/a	n/a	n/a	618-650	6	1.5-1535

Name	Sample Type	Coal Rank	%R_O Ø	Maceral Content (Ø %)			Depth Range (m)	Canister/ Wells Quantity	Time Range (hours)
D2	Des.	Anthracite	4.41	n/a	n/a	n/a	123-473	7	1.8-225
D3	Des.	Sub Bit.A-HV Bit.C	0.67	75.9	17.2	6.9	134-156	8	1285-1619
D4	Des.	Sub Bit.A-HV Bit.C	0.67	75.9	17.2	6.9	10*	10	1080
D5	Des.	Sub Bit.A-HV Bit.C	0.67	75.9	17.2	6.9	20*	2	168-504
D6	Des.	MV Bit.-LV Bit.	1.46	68.9	31.0	0.1	n/a	14	796-2773
D7	Des.	Sub Bit.A-HV Bit.B	0.61	76.4	19.4	4.2	1268-1312	13	480-528

4.2 Production Samples

4.2.1 Sample Set P1

Samples for sample set P1 (see Table 4.2) were collected from three different production wells in one geographic region. Well TR produces CBM from a Tertiary coal, well KV produces CBM from a Cretaceous coal and well SPI produces CBM from a coal seam, intruded by Tertiary volcanics. No data for the maturity of coal are available. The coal petrography of the intersected coals was not determined, so that values for maceral content are not available. Also the depth range for the three wells is not available. To date, samples cover a desorption time span of 1968 hours.

Table 4.2: *Rank, maturity, maceral content and depth for the different considered coals of production sample set P1, as well as maximal considered duration of production time for the different wells. Vit. = Vitrinite; Inert. = Inertinite; Lipt. = Liptinite.*

Well	Coal Rank	%R_O	Maceral Content (%)			Depth (m)	Time Elapsed (hours)
			Vit.	Inert.	Lipt.		
TR	n/a	n/a	n/a	n/a	n/a	n/a	1968
SPI	n/a	n/a	n/a	n/a	n/a	n/a	1968
KV	n/a	n/a	n/a	n/a	n/a	n/a	1968

4.2.2 Sample Set P2

Samples for sample set P2 (see Table 4.3) were collected from a CBM pilot consisting of five wells. All wells produced CBM from the same coal sequence at depths between 141m and 172m. Coal rank is high–volatile bituminous A to medium–volatile bituminous with a R_O value of 1.20%. Coal petrography of the coals was not determined, so that values for maceral content are not available. The pilot was shut in, so that only three samples per well were collected, covering a desorption time span of 792 hours.

Table 4.3: *Rank, maturity, maceral content and depth for the different considered coals from production sample set P2, as well as maximal considered duration of production time for the different wells. Vit. = Vitrinite; Inert. = Inertinite; Lipt. = Liptinite; HV Bit.A = high volatile bituminous A; MV Bit = medium volatile bituminous.*

Well	Coal Rank	%R_O	Maceral Content (%)			Depth (m)	Time Elapsed (hours)
			Vit.	Inert.	Lipt.		
100/07	HV Bit.A-MV Bit	1.20	n/a	n/a	n/a	158	792
102/02	HV Bit.A-MV Bit	1.20	n/a	n/a	n/a	149	792
102/07	HV Bit.A-MV Bit	1.20	n/a	n/a	n/a	136	792
103/02	HV Bit.A-MV Bit	1.20	n/a	n/a	n/a	172	792
104/02	HV Bit.A-MV Bit	1.20	n/a	n/a	n/a	141	792

4.2.3 Sample Set P3

Samples for sample set P3 (see Table 4.4) were collected from a CBM pilot consisting of three wells. All wells produce CBM from the same coal sequence at depths between 173m and 187m. Coal rank is sub bituminous A/high–volatile bituminous C with a R_O value of 0.70%. The coal petrography of the intersected coals is as follows: vitrinite 82.6%, inertinite 16.2%, liptinite 1.2%. To date samples cover a desorption time span of 6312 hours.

Table 4.4: Rank, maturity, maceral content and depth for the different considered coals from production sample set P3, as well as maximal considered duration of production time for the different wells. Vit. = Vitrinite; Inert. = Inertinite; Lipt. = Liptinite; HV Bit.C = high volatile bituminous C; Sub Bit.A = sub bituminous A.

Well	Coal Rank	$\%R_O$	Maceral Content (%)			Depth (m)	Time Elapsed (hours)
			Vit.	Inert.	Lipt.		
2	Sub Bit.A-HV Bit.C	0.57	82.6	16.2	1.2	187	6312
5	Sub Bit.A-HV Bit.C	0.57	82.6	16.2	1.2	173	6312
13	Sub Bit.A-HV Bit.C	0.57	82.6	16.2	1.2	183	6312

4.3 Desorption Experiment Samples

4.3.1 Sample Set D1

Samples for sample set D1 (see Table 4.5) were collected from eight desorption canisters. No data about maturity or coal rank are available. Coal petrography of the intersected coals was not determined, so that values for maceral content are not available. Desorption times range from 1.5 hours to 1535 hours. Canisters 1, 3 and 4 were terminated early due to low gas volumes. The coal cores were recovered from depths between 619m and 650m. Sample set D1 and sample set P1 were recovered from the same basin.

Table 4.5: Rank, maturity, maceral content and depth for the different considered coals from desorption experiment sample set D1, as well as maximal considered duration of desorption time for the different canisters. Vit. = Vitrinite; Inert. = Inertinite; Lipt. = Liptinite.

Canister	Coal Rank	$\%R_O$	Maceral Content (%)			Depth (m)	Time Elapsed (hours)
			Vit.	Inert.	Lipt.		
1	n/a	n/a	n/a	n/a	n/a	618.8	1.5
3	n/a	n/a	n/a	n/a	n/a	619.3	1.5
4	n/a	n/a	n/a	n/a	n/a	619.5	3.5
6	n/a	n/a	n/a	n/a	n/a	622.3	1415
7	n/a	n/a	n/a	n/a	n/a	650.0	1413
8	n/a	n/a	n/a	n/a	n/a	650.3	1535

4.3.2 Sample Set D2

Samples for sample set D2 (see Table 4.6) were collected from seven desorption canisters filled with cores recovered from two exploration holes. The coal rank is anthracite with R_O values between 4% and 4.55%. Coal petrography of the coals was not determined. Desorption times range from 1.8 hours to 225.5 hours. Canisters R17, R18, R19 and H3 were terminated early due to low gas volumes. Coal cores were recovered from depths between 123m and 473m.

Table 4.6: *Rank, maturity, maceral content and depth for the different considered coals from desorption experiment sample set D2, as well as maximal considered duration of desorption time for the different canisters. Vit. = Vitrinite; Inert. = Inertinite; Lipt. = Liptinite.*

Canister	Coal Rank	%R_O	Maceral Content (%)			Depth (m)	Time Elapsed (hours)
			Vit.	Inert.	Lipt.		
R6	Anthracite	4.41	n/a	n/a	n/a	123	225.5
R7	Anthracite	4.27	n/a	n/a	n/a	124	225.5
R17	Anthracite	4.00	n/a	n/a	n/a	465	1.8
R18	Anthracite	4.55	n/a	n/a	n/a	466	1.8
R19	Anthracite	4.41	n/a	n/a	n/a	467	2.1
R20	Anthracite	4.41	n/a	n/a	n/a	473	169
H3	Anthracite	4.41	n/a	n/a	n/a	156	14

4.3.3 Sample Set D3

Samples for sample set D3 (see Table 4.7) were collected from eight desorption canisters. Coal rank is sub bituminous A/high–volatile bituminous C with a R_O value of 0.67%. Coal petrography is as follows: vitrinite 75.9%, inertinite 17.2%, liptinite 6.9%. Desorption times range from 1285 hours to 1619 hours. Coal cores were recovered from depths between 125m and 156m.

Table 4.7: Rank, maturity, maceral content and depth for the different considered coals from desorption experiment sample set D3, as well as maximal considered duration of desorption time for the different canisters. Vit. = Vitrinite; Inert. = Inertinite; Lipt. = Liptinite; HV Bit.C = high volatile bituminous C; Sub Bit.A = sub bituminous A.

Canister	Coal Rank	%R_O	Maceral Content (%)			Depth (m)	Time Elapsed (hours)
			Vit.	Inert.	Lipt.		
5	Sub Bit.A-HV Bit.C	0.67	75.9	17.2	6.9	135	1417
6	Sub Bit.A-HV Bit.C	0.67	75.9	17.2	6.9	139	1619
7	Sub Bit.A-HV Bit.C	0.67	75.9	17.2	6.9	145	1285
8	Sub Bit.A-HV Bit.C	0.67	75.9	17.2	6.9	144	1307
9	Sub Bit.A-HV Bit.C	0.67	75.9	17.2	6.9	145	1302
10	Sub Bit.A-HV Bit.C	0.67	75.9	17.2	6.9	147	1302
11	Sub Bit.A-HV Bit.C	0.67	75.9	17.2	6.9	149	1302
12	Sub Bit.A-HV Bit.C	0.67	75.9	17.2	6.9	156	1298

4.3.4 Sample Set D4

Samples for sample set D4 (see Table 4.8) were collected from ten desorption canisters. Coal samples were recovered underground from a fresh mining surface (a fresh surface was created especially for the sampling by removing the older surface directly before sampling the coal). The depth of the coal seam is set to 10m, because the considered coal seam is the shallowest production seam in the mine. No coal cores were recovered, but ca. 500g of coal fragments with uniform grain size were sealed into the canisters. The coal rank is sub bituminous A/high volatile bituminous C with a R_O value of 0.67%. The coal petrography of the intersected coals is as follows: Vitrinite 75.9%, inertinite 17.2%, liptinite 6.9%. 1080 hours of desorption time are covered.

Table 4.8: Rank, maturity, maceral content and depth for the different considered coals from desorption experiment sample set D4, as well as maximal considered duration of desorption time for the different canisters Vit. = Vitrinite; Inert. = Inertinite; Lipt. = Liptinite; HV Bit.C = high volatile bituminous C; Sub Bit.A = sub bituminous A.

Canister	Coal Rank	%R_O	Maceral Content (%)			Depth (m)	Time Elapsed (hours)
			Vit.	Inert.	Lipt.		
1	Sub Bit.A-HV Bit.C	0.67	75.9	17.2	6.9	10*	1080
2	Sub Bit.A-HV Bit.C	0.67	75.9	17.2	6.9	10*	1080
3	Sub Bit.A-HV Bit.C	0.67	75.9	17.2	6.9	10*	1080
4	Sub Bit.A-HV Bit.C	0.67	75.9	17.2	6.9	10*	1080
5	Sub Bit.A-HV Bit.C	0.67	75.9	17.2	6.9	10*	1080
6	Sub Bit.A-HV Bit.C	0.67	75.9	17.2	6.9	10*	1080
7	Sub Bit.A-HV Bit.C	0.67	75.9	17.2	6.9	10*	1080
8	Sub Bit.A-HV Bit.C	0.67	75.9	17.2	6.9	10*	1080
9	Sub Bit.A-HV Bit.C	0.67	75.9	17.2	6.9	10*	1080
10	Sub Bit.A-HV Bit.C	0.67	75.9	17.2	6.9	10*	1080

4.3.5 Sample Set D5

Samples for sample set D5 (see Table 4.9) were collected from two desorption canisters. Coal samples were recovered underground from a fresh mining surface (a fresh surface was created especially for the sampling by removing the older surface directly before sampling the coal). The depth of the coal seam is set to 20m, because the considered coal seam is located deeper than the coal seam for sample set D4. No coal cores were recovered, but ca. 500g of coal fragments with uniform grain size were sealed into the canisters. Coal rank is sub–bituminous A/high–volatile bituminous C with a R_O value of 0.67%. Coal petrography of the intersected coals is as follows: Vitrinite 75.9%, inertinite 17.2%, liptinite 6.9%. Desorption times range from 168 hours to 504 hours. Only three gas samples were collected due to very low gas volumes. Sample set D3, sample set D4 and sample set D5 were recovered from the same coal bearing basin.

Table 4.9: Rank, maturity, maceral content and depth for the different considered coals from desorption experiment sample set D5, as well as maximal considered duration of desorption time for the different canisters. Vit. = Vitrinite; Inert. = Inertinite; Lipt. = Liptinite; HV Bit.C = high volatile bituminous C; Sub Bit.A = sub bituminous A.

Canister	Coal Rank	%R_O	Maceral Content (%)			Depth (m)	Time Elapsed (hours)
			Vit.	Inert.	Lipt.		
A	Sub Bit.A-HV Bit.C	0.67	75.9	17.2	6.9	20*	168
C	Sub Bit.A-HV Bit.C	0.67	75.9	17.2	6.9	20*	504

4.3.6 Sample Set D6

Samples for sample set D6 (see Table 4.10) were collected from 14 desorption canisters. 11 canisters were filled with coal cores and three were filled with shale cores recovered during drilling of an exploration well. Coal rank ranges from medium–volatile bituminous to low–volatile bituminous with R_O values between 1.23% and 1.77%. Average coal petrography of the coals is as follows: Vitrinite 68.9%, inertinite 31.0%, liptinite 0.1%. Desorption times range from 796 hours to 2773 hours. The depths from which the coal and shale cores were recovered is not known. Only one gas sample was collected from each of the canisters containing shale samples. No additional information about the shale is available.

Table 4.10: Rank, maturity, maceral content and depth for the different considered coals from desorption experiment sample set D6, as well as maximal considered duration of desorption time for the different canisters. Vit. = Vitrinite; Inert. = Inertinite; Lipt. = Liptinite; MV Bit = medium volatile bituminous; LV Bit = low volatile bituminous.

Canister	Coal Rank	%R_O	Maceral Content (%)			Depth (m)	Time Elapsed (hours)
			Vit.	Inert.	Lipt.		
77	LV Bit	1.55	66.2	33.8	0.0	n/a	2773
88	LV Bit	1.55	66.2	33.8	0.0	n/a	2141
90	LV Bit	1.55	66.2	33.8	0.0	n/a	1310
105	MV Bit	1.23	71.4	28.3	0.3	n/a	1461
111	LV Bit	1.77	67.5	32.5	0.0	n/a	1070
136	MV Bit	1.23	71.4	28.3	0.3	n/a	1434
153	LV Bit	1.77	67.5	32.5	0.0	n/a	796
161	LV Bit	1.77	67.5	32.5	0.0	n/a	937
188	MV Bit	1.23	71.4	28.3	0.3	n/a	1392
192	MV Bit	1.23	71.4	28.3	0.3	n/a	1330

Canister	Coal Rank	%R_O	Maceral Content (%)			Depth (m)	Time Elapsed (hours)
			Vit.	Inert.	Lipt.		
201	MV Bit	1.23	71.4	28.3	0.3	n/a	1287
215	Shale	?	/	/	/	n/a	?
220	Shale	?	/	/	/	n/a	?
224	Shale	?	/	/	/	n/a	?

4.3.7 Sample Set D7

Samples for sample set D7 (see Table 4.11) were collected from 13 desorption canisters. Coal rank ranges between sub–bituminous A/high–volatile bituminous C and high–volatile bituminous B with R_O values between 0.61% and 0.71%. Average coal petrography of the coals is as follows: Vitrinite 76.4%, inertinite 19.4%, liptinite 4.2%. Desorption times range from 480 hours to 528 hours. Coal cores were recovered from depths from 1268m to 1312m. Only two gas samples were collected from each canister. The exception was canister 17 were only one sample was collected.

Table 4.11: *Rank, maturity, maceral content and depth for the different considered coals from desorption experiment sample set D7, as well as maximal considered duration of desorption time for the different canisters. Vit. = Vitrinite; Inert. = Inertinite; Lipt. = Liptinite; HV Bit.B = high volatile bituminous B; HV Bit.C = high volatile bituminous C; Sub Bit.A = sub bituminous A.*

Canister	Coal Rank	%R_O	Maceral Content (%)			Depth (m)	Time Elapsed (hours)
			Vit.	Inert.	Lipt.		
3	HV Bit.B	0.69	70.0	25.0	5.0	1269	528
4	HV Bit.B	0.69	70.0	25.0	5.0	1274	528
5	HV Bit.B	0.69	70.0	25.0	5.0	1275	528
6	HV Bit.B	0.69	70.0	25.0	5.0	1283	504
8	HV Bit.B	0.69	70.0	25.0	5.0	1291	504
9	HV Bit.B	0.69	70.0	25.0	5.0	1300	480
10	Sub Bit.A-HV Bit.C	0.63	71.0	26.0	3.0	1307	480
11	Sub Bit.A-HV Bit.C	0.63	71.0	26.0	3.0	1308	480
13	Sub Bit.A-HV Bit.C	0.63	71.0	26.0	3.0	1309	480
15	Sub Bit.A-HV Bit.C	0.61	89.0	8.0	3.0	1310	480
16	Sub Bit.A-HV Bit.C	0.61	89.0	8.0	3.0	1311	480
17	HV Bit.B	0.71	91.0	4.0	5.0	1312	/
18	HV Bit.B	0.71	91.0	4.0	5.0	1312	480

5. Results

Results for gas composition, gas proportions, stable carbon and hydrogen isotope composition for all ten sample sets are presented here. Corresponding diagrams are located at the end of the Chapter. Results for the different sample sets are identified by canister/well number and presented versus desorption/production time. Results for ethane, propane, *n*–butane and *i*–butane, which generally occur in small proportions, are presented combined under the topic "higher hydrocarbons" with respect to gas proportions. For more detailed information, especially about the proportions of the individual higher hydrocarbons, see Appendices A to J.

Gas analyses (Chapter 3.3) are limited to gaseous hydrocarbons and carbon dioxide. Other possible components of coalbed methane, like nitrogen and carbon monoxide, are neglected. Therefore the measured proportions are normalized to the analyzed compounds, methane, ethane, propane, *n*–butane, *i*–butane and carbon dioxide and only normalized values are discussed.

Average gas composition data per sample are given in Table 5.1. Methane is the dominant species with the exception of sample set D1 (Table 5.1), where the average proportions of carbon dioxide exceeds the proportions of methane. The proportions of methane vary between 44.3% for D1 and 98.7% for P2. With the exception of sample set D1, all gases contain more than 65% methane.

The proportions of the higher gaseous hydrocarbons ethane, propane and butane (C_{2+}) are small with values below 0.5%. Sample sets D1 and D5 show elevated proportions for C_{2+} with values above 1%. High proportions of C_{2+} were only found for sample sets D6 (2.47%) and D7 (8.18%).

Carbon dioxide is the second most abundant gas species encountered in samples. The variation in proportions between the different sample sets is enormous; between 1.34% for P2 and 53.9% for D1. For sample set D6 the analysis of carbon dioxide was not possible (see Chapter 4.3.6).

Table 5.1: Gas composition of samples collected from all ten sample sets. Samples from different wells and canisters per sample set are averaged and presented per sample set. Proportions are normalized on the basis of proportions of methane, ethane, propane, n–butane, i–butane and carbon dioxide. norm. = normalized.

Sample Set	Average Proportions					
	Methane (%, norm.)	Ethane (%, norm.)	Propane (%, norm.)	*n*-Butane (%, norm.)	*i*-Butane (%, norm.)	CO_2 (%, norm.)
P1	90.4	0.32	0.001	0.000	0.0000	9.28
P2	98.7	0.01	0.003	0.000	0.0000	1.34
P3	96.1	0.15	0.127	0.172	0.0002	3.41
D1	44.3	0.50	0.554	0.801	0.0000	53.9
D2	96.8	0.43	0.001	0.000	0.0000	2.80
D3	92.3	0.26	0.005	0.000	0.0000	7.47
D4	86.6	0.05	0.036	0.003	0.0030	13.3
D5	67.2	0.00	0.000	1.092	0.0000	31.8
D6	97.5	2.31	0.152	0.009	0.0010	n/a
D7	77.3	6.98	1.150	0.051	0.0000	14.5

Legend for Tables 5.2 to 5.11:

- C_1: Methane
- C_2: Ethane
- C_3: Propane
- C_4: Butane
- C_{2+}: Higher hydrocarbons (ethane, propane, butane)
- (2): Sample Number
- (s.s.): Several samples
- ↑: Increase in proportion / increase in ^{13}C/ increase in D
- ↓: Decrease in proportion / increase in ^{12}C/ increase in ^{1}H
- →: No overall trend in relation to decrease or increase
- ∩: Distinct maximum
- F: Fluctuations
- SF: Strong fluctuations
- »: Followed by
- ⌐: Until 100% are reached
- n/a: Not available

5.1 Sample Set P1

All three wells show an overall increase in proportions of methane with increasing time (Figure 5.1; Table 5.2). The first sample for all wells has considerably lower proportions of methane than later samples, which are almost at 100%. The proportions of higher hydrocarbons are low (0% and around 0%) with the exception of sample TR1 which has almost 6% (Figure 5.2). Proportions of carbon dioxide decrease with time (Figure 5.3). The first sample per well contains high proportions (ca. 35% to ca. 65%), but proportions drop to less than 5% by the time sample 2 was taken. All wells show similar trends.

All wells show ^{12}C enrichment in methane with increasing time (Figure 5.4), with the exception of sample TR1, which shows a strongly ^{13}C enriched value of around -5‰. A similar trend is present for hydrogen isotopes in methane, with ^{1}H enrichment over time (Figure 5.5). The trend is similar for all wells, but the values for well TR show strong fluctuations over time. For higher hydrocarbons no isotope data are available. The $\delta^{13}C$ values for carbon dioxide are very similar for all wells and stay relatively stable with increasing time (Figure 5.6). For wells TR and KV a ^{13}C enrichment is present for the last samples.

Table 5.2: *Compositional and isotope results for sample set P1. Results are represented per well with minimum and maximum values for proportions and $\delta^{13}C$ and δD respectively. Proportions are normalized on the basis of proportions of methane, ethane, propane, n–butane, i–butane and carbon dioxide. Ethane, propane, n–butane and i–butane are combined under the term C_{2+} (higher hydrocarbons). Legend for symbols used for the characterization of observed trends is given above.*

Well	Species	Proportions Minimum % normalized	Proportions Maximum % normalized	Trend
TR	CH_4	56.9 (1)	99.7 (6)	↑–
TR	C_{2+}	0 (s.s.)	5.73 (1)	→
TR	CO_2	0.29 (6)	37.4 (1)	↓
SPI	CH_4	48.1 (1)	99.8 (6)	↑–
SPI	C_{2+}	0 (s.s.)	0.02 (2)	→
SPI	CO_2	0.24 (6)	51.9 (1)	↓
KV	CH_4	36.9 (1)	99.6 (6)	↑–
KV	C_{2+}	n/a	n/a	n/a
KV	CO_2	0.36 (6)	63.1 (1)	↓

Well	Species	Isotope Minimum ‰	Isotope Maximum ‰	Trend
TR	$\delta^{13}C\text{-}C_1$	-40.5 (6)	-5.1 (1)	↓
TR	$\delta D\text{-}C_1$	-195.1 (5)	-177.4 (2)	F
TR	$\delta^{13}C\text{-}C_2$	n/a	-27.8	Value only for 1 sample
TR	$\delta^{13}C\text{-}C_3$	n/a	n/a	n/a
TR	$\delta^{13}C\text{-}C_4$	n/a	n/a	n/a
TR	$\delta^{13}C\text{-}CO_2$	-10.8 (6)	-8.8 (2)	→ » ↑
SPI	$\delta^{13}C\text{-}C_1$	-36.0 (6)	-24.3 (2)	↓
SPI	$\delta D\text{-}C_1$	-182.9 (10)	-169.9 (2)	↑
SPI	$\delta^{13}C\text{-}C_2$	n/a	n/a	n/a
SPI	$\delta^{13}C\text{-}C_3$	n/a	n/a	n/a
SPI	$\delta^{13}C\text{-}C_4$	n/a	n/a	n/a
SPI	$\delta^{13}C\text{-}CO_2$	-11.0 (s.s.)	-10.8 (4,6)	→
KV	$\delta^{13}C\text{-}C_1$	-33.9 (6)	-26.0 (2)	↓
KV	$\delta D\text{-}C_1$	-177.4 (6)	-166.2 (2)	↑
KV	$\delta^{13}C\text{-}C_2$	n/a	n/a	n/a
KV	$\delta^{13}C\text{-}C_3$	n/a	n/a	n/a
KV	$\delta^{13}C\text{-}C_4$	n/a	n/a	n/a
KV	$\delta^{13}C\text{-}CO_2$	-10.9 (2)	-7.6 (6)	→ » ↑

5.2 Sample Set P2

Proportions of methane increase with increasing time for all five wells (Figure 5.1; Table 5.3). No uniform trend with time is present for the proportions of higher hydrocarbons (Figure 5.2). The differences between wells are more pronounced for early samples, whereas the later samples show less differentiation. Proportions of carbon dioxide decrease for all wells with increasing time (Figure 5.3).

All wells show a ^{12}C enrichment for methane with increasing time, with the exceptions of the last samples from wells 102/07 and 103/02, which show a slight ^{13}C enrichment. No uniform trend is present for hydrogen isotopes in methane, but early samples show a higher variation than the later ones (Figure 5.5). No isotope data are available for higher hydrocarbons. All wells show an overall trend towards ^{13}C enrichment in carbon dioxide with increasing time (Figure 5.6). Only the last sample of well 100/07 does not follow the trend and shows ^{12}C enrichment. With increasing time the differences between the wells become more pronounced.

Table 5.3: Compositional and isotope results for sample set P2. Results are represented per well with minimum and maximum values for proportions and $\delta^{13}C$ and δD respectively. Proportions are normalized on the basis of proportions of methane, ethane, propane, n–butane, i–butane and carbon dioxide. Ethane, propane, n–butane and i–butane are combined under the term C_{2+} (higher hydrocarbons). Legend for symbols used for the characterization of observed trends is given above.

Well	Species	Proportions Minimum % normalized	Proportions Maximum % normalized	Trend
100/07	CH_4	97.9 (1)	98.6 (3)	↑
100/07	C_{2+}	0.01 (2,3)	0.04 (1)	↓
100/07	CO_2	1.37 (3)	2.04 (1)	↓
102/02	CH_4	98.4 (1)	99.2 (3)	↑
102/02	C_{2+}	0 (3)	0.02 (1)	↓
102/02	CO_2	0.77 (3)	1.57 (1)	↓
102/07	CH_4	98.6 (1)	99.1 (3)	↑
102/07	C_{2+}	0 (1)	0.01 (2,3)	↑
102/07	CO_2	0.94 (3)	1.43 (1)	↓
103/02	CH_4	98.0 (1)	99.1 (3)	↑
103/02	C_{2+}	0 (1,2)	0.04 (3)	↑
103/02	CO_2	0.86 (3)	1.98 (1)	↓
104/02	CH_4	98.0 (1)	98.8 (2,3)	↑
104/02	C_{2+}	0 (2,3)	0.01 (1)	↓
104/02	CO_2	1.17 (3)	1.97 (1)	↓
Well	**Species**	**Isotope Minimum ‰**	**Isotope Maximum ‰**	**Trend**
100/07	$\delta^{13}C\text{-}C_1$	-28.2 (3)	-26.5 (1)	↓
100/07	$\delta D\text{-}C_1$	-256.7 (1)	-248.7 (3)	↑
100/07	$\delta^{13}C\text{-}C_2$	n/a	n/a	n/a
100/07	$\delta^{13}C\text{-}C_3$	n/a	n/a	n/a
100/07	$\delta^{13}C\text{-}C_4$	n/a	n/a	n/a
100/07	$\delta^{13}C\text{-}CO_2$	-11.0 (1,3)	-10.5 (2)	→
102/02	$\delta^{13}C\text{-}C_1$	-30.1 (3)	-27.2 (1)	↓
102/02	$\delta D\text{-}C_1$	-244.5 (3)	-242.8 (1)	↓
102/02	$\delta^{13}C\text{-}C_2$	n/a	n/a	n/a
102/02	$\delta^{13}C\text{-}C_3$	n/a	n/a	n/a
102/02	$\delta^{13}C\text{-}C_4$	n/a	n/a	n/a
102/02	$\delta^{13}C\text{-}CO_2$	-10.4 (1)	-8.7 (3)	↑
102/07	$\delta^{13}C\text{-}C_1$	-29.6 (2)	-27.8 (1)	↓ » ↑
102/07	$\delta D\text{-}C_1$	-238.3 (2)	-235.3 (1)	→
102/07	$\delta^{13}C\text{-}C_2$	n/a	n/a	n/a
102/07	$\delta^{13}C\text{-}C_3$	n/a	n/a	n/a
102/07	$\delta^{13}C\text{-}C_4$	n/a	n/a	n/a
102/07	$\delta^{13}C\text{-}CO_2$	-10.4 (1)	-8.8 (3)	↑
103/02	$\delta^{13}C\text{-}C_1$	-28.5 (2,3)	-26.5 (1)	↓ » →
103/02	$\delta D\text{-}C_1$	-241.0 (3)	-237.1 (1)	↓
103/02	$\delta^{13}C\text{-}C_2$	n/a	n/a	n/a
103/02	$\delta^{13}C\text{-}C_3$	n/a	n/a	n/a
103/02	$\delta^{13}C\text{-}C_4$	n/a	n/a	n/a
103/02	$\delta^{13}C\text{-}CO_2$	-10.6 (1)	-9.3 (3)	↑
104/02	$\delta^{13}C\text{-}C_1$	-27.0 (3)	-25.4 (1)	↓
104/02	$\delta D\text{-}C_1$	-247.2 (3)	-246.5 (2)	→

Well	Species	Isotope Minimum ‰	Isotope Maximum ‰	Trend
104/02	$\delta^{13}C\text{-}C_2$	n/a	n/a	n/a
104/02	$\delta^{13}C\text{-}C_3$	n/a	n/a	n/a
104/02	$\delta^{13}C\text{-}C_4$	n/a	n/a	n/a
104/02	$\delta^{13}C\text{-}CO_2$	-10.4 (1,2)	-10.2 (3)	→ » ↑

5.3 Sample Set P3

Proportions of methane for all three wells show a pronounced early increase with increasing time until proportions of almost 100% are reached (Figure 5.1; Table 5.4). Around sample 15 a slight decrease in proportions of methane occurs followed by another increase. This variation is observed in all wells and happened almost simultaneously with almost identical amplitudes. Proportions of the higher hydrocarbons show an initially strong decrease with time to very low values for all wells, followed by relatively stable values (Figure 5.2). Proportions of carbon dioxide show a decrease with increasing time, from initially very high values (ca. 20% to ca. 45%) to low values of around 0% (Figure 5.3). Differences between wells are more pronounced for early samples, whereas late samples almost are identical. Around sample 15 (for all wells), an increase in the proportions of carbon dioxide is present followed by another decrease. The increase happened simultaneously with the above described decrease in proportions of methane.

A two–stage trend with increasing time is present for $\delta^{13}C$ (methane) in all wells. Initially, up to sample 12, a ^{12}C enrichment of almost 35‰ is present, but between samples 13 and 14 a sudden jump to ^{13}C enriched values of almost 30‰ occurred (Figure 5.4). The time difference between samples 13 and 15 is seven days. Following the sudden ^{13}C increase, the values again gradually show a ^{12}C increase with increasing time. The described trend is present in all three wells, whereby the isotope jump occurred simultaneously for all wells with almost identical amplitude. δD values are only available from samples 12 onwards. Initially all wells show a ^{2}H increase with increasing time between samples 12 and 15, followed by ^{1}H enrichment from sample 15 onwards (Figure 5.5). Additional strong fluctuations occur in all three wells. Only a few scattered $\delta^{13}C$ values are available for ethane and therefore no trend can be described (Figure 5.7). $\delta^{13}C$ values for carbon dioxide show very strong fluctuations, but overall two different trends

with increasing time are apparent (Figure 5.6). Between samples 1 and 11 the values scatter around a mean value of -9 to -10‰, with no overall ^{12}C or ^{13}C enrichment is observed. From sample 13 on (no values for sample 12 are available) the values scatter around a mean value of -12 to -13‰, with again no overall ^{12}C or ^{13}C enrichment is observed.

Table 5.4: *Compositional and isotope results for sample set P3. Results are represented per well with minimum and maximum values for proportions and $\delta^{13}C$ and δD respectively. Proportions are normalized on the basis of proportions of methane, ethane, propane, n–butane, i–butane and carbon dioxide. Ethane, propane, n–butane and i–butane are combined under the term C_{2+} (higher hydrocarbons). Legend for symbols used for the characterization of observed trends is given above.*

Well	Species	Proportions Minimum % normalized	Proportions Maximum % normalized	Trend
2-24	CH_4	65.4 (1)	99.8 (26)	↑⁻ » ↓ at (15) » ↑⁻
2-24	C_{2+}	0 (s.s.)	13.7 (1)	↓ » →
2-24	CO_2	0.07 (28)	21.0 (1)	↓ » ↑ (15) » →
5-24	CH_4	42.3 (1)	99.9 (27)	↑⁻ » ↓ at (15) » ↑⁻
5-24	C_{2+}	0 (s.s.)	11.2 (1)	↓ » →
5-24	CO_2	0.05 (27)	46.5 (1)	↓ » ↑ (15) » →
13-24	CH_4	64.4 (1)	99.8 (s.s.)	↑⁻ » ↓ at (15) » ↑⁻
13-24	C_{2+}	0 (s.s.)	5.48 (1)	↓ » →
13-24	CO_2	0.08 (28)	30.1 (1)	↓ » ↑ (15) » →
Well	**Species**	**Isotope Minimum ‰**	**Isotope Maximum ‰**	**Trend**
2-24	$\delta^{13}C\text{-}C_1$	-55.7 (13)	-20.8 (1)	↓ » ↑ (14) » ↓ (15)
2-24	$\delta D\text{-}C_1$	-314.5 (3)	-239.2 (15)	↑ » ↓; SF
2-24	$\delta^{13}C\text{-}C_2$	-33.8 (13)	-19.6 (24)	→
2-24	$\delta^{13}C\text{-}C_3$	n/a	-33.2	Value only for 1 sample
2-24	$\delta^{13}C\text{-}C_4$	-30.2 (19)	-28.7 (28)	→
2-24	$\delta^{13}C\text{-}CO_2$	-12.3 (27)	-8.8 (6)	↑ » ↓; SF
5-24	$\delta^{13}C\text{-}C_1$	-55.0 (13)	-19.2 (1)	↓ » ↑ (14) » ↓ (15)
5-24	$\delta D\text{-}C_1$	-268.9 (28)	-233.6 (15)	↑ » ↓; SF
5-24	$\delta^{13}C\text{-}C_2$	-33.2 (12,13)	-23.1 (15)	→
5-24	$\delta^{13}C\text{-}C_3$	n/a	n/a	n/a
5-24	$\delta^{13}C\text{-}C_4$	n/a	n/a	n/a
5-24	$\delta^{13}C\text{-}CO_2$	-12.7 (28)	-8.8 (10)	↑ » ↓; SF
13-24	$\delta^{13}C\text{-}C_1$	-55.4 (13)	-21.2 (1)	↓ » ↑ (14) » ↓ (15)
13-24	$\delta D\text{-}C_1$	-270.3 (28)	-238.8 (14)	↑ » ↓; SF
13-24	$\delta^{13}C\text{-}C_2$	-34.2 (12)	-29.8 (27)	→
13-24	$\delta^{13}C\text{-}C_3$	n/a	n/a	n/a
13-24	$\delta^{13}C\text{-}C_4$	n/a	n/a	n/a
13-24	$\delta^{13}C\text{-}CO_2$	-12.7 (17)	-8.3 (10)	↑ » ↓; SF

5.4 Sample Set D1

Proportions of methane for canisters 6, 7 and 8 show an overall increase with increasing time until proportions of almost 100% are reached (Figure 5.8. Canisters 1, 3 and 4 were abandoned early during the desorption process and are therefore not considered here. For data and trends see Table 5.5 and Appendix D. Canisters 6 and 8 show distinctive maxima for the proportions of higher hydrocarbons, whereas canister 7 shows very strong fluctuations (Figure 5.9). Following the maximum, proportions are very low. Proportions of carbon dioxide for canisters 6, 7 and 8 decrease with increasing time approaching values of almost 0% (Figure 5.10). Early samples show fluctuations.

Canisters 6 and 8 show an initial ^{13}C enrichment for methane, followed by ^{12}C enrichment with increasing time; canister 7 shows ^{12}C enrichment with time (Figure 5.11). Differences between sample become less pronounced late in the desorption process. δD values are only available for samples from canisters 6 and 7, and because of limited data, no overall trend is apparent (Figure 5.12). No isotope data are available for ethane. $\delta^{13}C$ values for carbon dioxide show strong fluctuations with no increase in ^{12}C or ^{13}C with increasing desorption (Figure 5.13).

Table 5.5: *Compositional and isotope results for sample set D1. Results are represented per canister with minimum and maximum values for proportions and $\delta^{13}C$ and δD respectively. Proportions are normalized on the basis of proportions of methane, ethane, propane, n–butane, i–butane and carbon dioxide. Ethane, propane, n–butane and i–butane are combined under the term C_{2+} (higher hydrocarbons). Legend for symbols used for the characterization of observed trends is given above.*

Canister	Species	Proportions Minimum % normalized	Proportions Maximum % normalized	Trend
1	CH_4	13.31 (3)	22.0 (1)	↓
1	C_{2+}	0 (3)	12.8 (1)	↓
1	CO_2	65.3 (1)	98.7 (3)	↑
3	CH_4	1.01 (2)	1.87 (3)	→
3	C_{2+}	0 (3)	0.25 (1)	↓
3	CO_2	98.7 (1)	99.8 (2)	→
4	CH_4	1.12 (1)	1.34 (3)	↑
4	C_{2+}	0.20 (2,3)	0.26 (1)	↓
4	CO_2	98.6 (1)	98.8 (2)	→
6	CH_4	1.53 (1)	99.5 (8)	↑–
6	C_{2+}	0 (s.s.)	1.14 (5)	∩ (5)
6	CO_2	0.54 (8)	98.5 (1)	↓

Canister	Species	Proportions Minimum % normalized	Proportions Maximum % normalized	Trend
7	CH_4	2.56 (1)	99.7 (7)	↑–
7	C_{2+}	0 (3)	14.9 (1)	→; SF
7	CO_2	0.31 (8)	97.4 (1)	↓
8	CH_4	17.0 (4)	99.6 (8)	↑–
8	C_{2+}	0 (3)	13.8 (6)	∩ (6)
8	CO_2	0.37 (8)	81.6 (4)	↓
Canister	**Species**	**Isotope Minimum ‰**	**Isotope Maximum ‰**	**Trend**
1	$\delta^{13}C\text{-}C_1$	n/a	-43.4	Value only for 1 sample
1	$\delta D\text{-}C_1$	n/a	n/a	n/a
1	$\delta^{13}C\text{-}C_2$	n/a	-20.8	Value only for 1 sample
1	$\delta^{13}C\text{-}C_3$	n/a	n/a	n/a
1	$\delta^{13}C\text{-}C_4$	n/a	-29.1	Value only for 1 sample
1	$\delta^{13}C\text{-}CO_2$	-10.0 (3)	-9.60 (1)	↓
3	$\delta^{13}C\text{-}C_1$	n/a	n/a	n/a
3	$\delta D\text{-}C_1$	n/a	n/a	n/a
3	$\delta^{13}C\text{-}C_2$	n/a	n/a	n/a
3	$\delta^{13}C\text{-}C_3$	n/a	n/a	n/a
3	$\delta^{13}C\text{-}C_4$	n/a	n/a	n/a
3	$\delta^{13}C\text{-}CO_2$	-11.3 (3)	-10.2 (1)	↓
4	$\delta^{13}C\text{-}C_1$	n/a	n/a	n/a
4	$\delta D\text{-}C_1$	n/a	n/a	n/a
4	$\delta^{13}C\text{-}C_2$	n/a	n/a	n/a
4	$\delta^{13}C\text{-}C_3$	n/a	n/a	n/a
4	$\delta^{13}C\text{-}C_4$	n/a	n/a	n/a
4	$\delta^{13}C\text{-}CO_2$	-11.7 (3)	-10.4 (1)	↓
6	$\delta^{13}C\text{-}C_1$	-54.2 (10)	-10.8 (5)	↑ » ↓
6	$\delta D\text{-}C_1$	-267.2 (10)	-262.4 (9)	→
6	$\delta^{13}C\text{-}C_2$	n/a	n/a	n/a
6	$\delta^{13}C\text{-}C_3$	n/a	n/a	n/a
6	$\delta^{13}C\text{-}C_4$	n/a	n/a	n/a
6	$\delta^{13}C\text{-}CO_2$	-11.9 (1)	-8.9 (4)	→; SF
7	$\delta^{13}C\text{-}C_1$	-44.3 (10)	-7.8 (4)	↓
7	$\delta D\text{-}C_1$	-279.8 (10)	-287.1 (8)	→
7	$\delta^{13}C\text{-}C_2$	n/a	n/a	n/a
7	$\delta^{13}C\text{-}C_3$	n/a	-33.2	Value only for 1 sample
7	$\delta^{13}C\text{-}C_4$	-29.8 (3)	-28.7 (5)	→
7	$\delta^{13}C\text{-}CO_2$	-10.3 (3)	-9.6 (1)	→; SF
8	$\delta^{13}C\text{-}C_1$	-45.1 (1)	-6.9 (4)	↑ » ↓; F
8	$\delta D\text{-}C_1$	n/a	n/a	n/a
8	$\delta^{13}C\text{-}C_2$	n/a	n/a	n/a
8	$\delta^{13}C\text{-}C_3$	n/a	n/a	n/a
8	$\delta^{13}C\text{-}C_4$	n/a	n/a	n/a
8	$\delta^{13}C\text{-}CO_2$	-10.6 (11)	-6.6 (8)	→; SF

5.5 Sample Set D2

All canisters show an overall increase in proportions of methane with increasing time with the exceptions of canisters R18 and R20 (Figure 5.8; Table 5.6). No uniform pattern for the proportions of the higher hydrocarbons is present. Proportions are only available for canisters R6, R7 and R17. Canister R6 shows a decrease in proportions of higher hydrocarbons with time, R7 shows a distinct proportion maximum and R17 shows overall low proportions (Figure 5.9). Almost all canisters show an overall decrease in proportions of carbon dioxide with time; the only exception is canister R18, in which proportions remain constant over time (Figure 5.10).

Canisters R7 and R19 show no increase in ^{12}C or ^{13}C for methane with increasing time, whereas canisters R17, R18 and H3 show a ^{13}C enrichment; canister R6 shows initial ^{13}C enrichment with time, followed by ^{12}C enrichment (Figure 5.11). No overall trends are present for δD for methane (Figure 5.12). Only canister R6 shows a clear ^{2}H enrichment with time, whereas the other canisters show fluctuations and no clear increase in ^{2}H or ^{1}H. $\delta^{13}C$ values for ethane are only available for canisters R6 and R7, but these data show relatively stable values with increasing time (Figure 5.14). $\delta^{13}C$ values for carbon dioxide are stable with increasing time and show no increase in ^{12}C or ^{13}C (Figure 5.13).

Table 5.6: *Compositional and isotope results for sample set D2. Results are represented per canister with minimum and maximum values for proportions and $\delta^{13}C$ and δD respectively. Proportions are normalized on the basis of proportions of methane, ethane, propane, n–butane, i–butane and carbon dioxide. Ethane, propane, n–butane and i–butane are combined under the term C_{2+} (higher hydrocarbons). Legend for symbols used for the characterization of observed trends is given above.*

Canister	Species	Proportions Minimum % normalized	Proportions Maximum % normalized	Trend
R6	CH_4	89.3 (1)	98.7 (5)	↑–
R6	C_{2+}	0 (s.s.)	12.8 (1)	↓
R6	CO_2	1.29 (5)	4.48 (1)	↓
R7	CH_4	90.1 (2)	98.2 (6)	↑–
R7	C_{2+}	0 (6)	5.58 (2)	∩ (2)
R7	CO_2	1.78 (6)	4.74 (1)	↓
R17	CH_4	95.2 (1)	98.3 (3)	↑
R17	C_{2+}	0 (2,3)	0.18 (1)	→
R17	CO_2	1.71 (3)	4.65 (1)	↓
R18	CH_4	96.2 (1)	98.1 (2)	→

Canister	Species	Proportions Minimum % normalized	Proportions Maximum % normalized	Trend
R18	C_{2+}	n/a	n/a	n/a
R18	CO_2	1.90 (2)	3.76 (1)	→
R19	CH_4	96.6 (1)	98.1 (4)	↑
R19	C_{2+}	n/a	n/a	n/a
R19	CO_2	1.86 (4)	3.36 (1)	↓
R20	CH_4	93.0 (1)	98.5 (4)	→
R20	C_{2+}	n/a	n/a	n/a
R20	CO_2	1.49 (4)	7.01 (1)	↓
H3	CH_4	96.6 (1)	98.7 (6)	↑
H3	C_{2+}	n/a	n/a	n/a
H3	CO_2	1.33 (6)	3.56 (1)	↓
Canister	**Species**	**Isotope Minimum ‰**	**Isotope Maximum ‰**	**Trend**
R6	$\delta^{13}C\text{-}C_1$	-17.2 (5)	-8.2 (6)	↓ » ↑ (6)
R6	$\delta D\text{-}C_1$	-157.3 (1)	-141.3 (6)	↑; F
R6	$\delta^{13}C\text{-}C_2$	-28.7 (2)	-28.6 (1)	→
R6	$\delta^{13}C\text{-}C_3$	n/a	n/a	n/a
R6	$\delta^{13}C\text{-}C_4$	n/a	n/a	n/a
R6	$\delta^{13}C\text{-}CO_2$	-12.8 (1)	-12.0 (6)	→; F
R7	$\delta^{13}C\text{-}C_1$	-17.2 (4)	-9.9 (6)	→; SF
R7	$\delta D\text{-}C_1$	-150.7 (1,3)	-143.7 (5)	SF
R7	$\delta^{13}C\text{-}C_2$	-29.2 (1)	-28.8 (2)	→
R7	$\delta^{13}C\text{-}C_3$	n/a	n/a	n/a
R7	$\delta^{13}C\text{-}C_4$	n/a	n/a	n/a
R7	$\delta^{13}C\text{-}CO_2$	-12.8 (3)	-11.3 (4)	→; F
R17	$\delta^{13}C\text{-}C_1$	-12.2 (1)	-11.6 (3)	↑
R17	$\delta D\text{-}C_1$	-128.2 (3)	-124.5 (1)	↓
R17	$\delta^{13}C\text{-}C_2$	n/a	n/a	n/a
R17	$\delta^{13}C\text{-}C_3$	n/a	n/a	n/a
R17	$\delta^{13}C\text{-}C_4$	n/a	n/a	n/a
R17	$\delta^{13}C\text{-}CO_2$	-13.8 (1)	-12.4 (3)	↑
R18	$\delta^{13}C\text{-}C_1$	-13.6 (1)	-7.3 (3)	↑
R18	$\delta D\text{-}C_1$	-120.9 (1)	-114.9 (3)	↑
R18	$\delta^{13}C\text{-}C_2$	n/a	n/a	n/a
R18	$\delta^{13}C\text{-}C_3$	n/a	n/a	n/a
R18	$\delta^{13}C\text{-}C_4$	n/a	n/a	n/a
R18	$\delta^{13}C\text{-}CO_2$	-12.3 (2)	-12.1 (1)	→
R19	$\delta^{13}C\text{-}C_1$	-10.7 (3)	-7.5 (2)	→; SF
R19	$\delta D\text{-}C_1$	-121.8 (1)	-116.0 (2)	F
R19	$\delta^{13}C\text{-}C_2$	n/a	n/a	n/a
R19	$\delta^{13}C\text{-}C_3$	n/a	n/a	n/a
R19	$\delta^{13}C\text{-}C_4$	n/a	n/a	n/a
R19	$\delta^{13}C\text{-}CO_2$	-12.5 (4)	-12.0 (2)	→
R20	$\delta^{13}C\text{-}C_1$	-11.4 (4)	-3.3 (6)	→; SF
R20	$\delta D\text{-}C_1$	-128.5 (4)	-112.9 (6)	F
R20	$\delta^{13}C\text{-}C_2$	n/a	n/a	n/a
R20	$\delta^{13}C\text{-}C_3$	n/a	n/a	n/a

Canister	Species	Isotope Minimum ‰	Isotope Maximum ‰	Trend
R20	$\delta^{13}C\text{-}C_4$	n/a	n/a	n/a
R20	$\delta^{13}C\text{-}CO_2$	-12.6 (6)	-11.9 (3,5)	→; F
H3	$\delta^{13}C\text{-}C_1$	-11.2 (1)	-8.3 (4,5)	↑; SF
H3	$\delta D\text{-}C_1$	-141.4 (1)	-132.5 (6)	F
H3	$\delta^{13}C\text{-}C_2$	n/a	n/a	n/a
H3	$\delta^{13}C\text{-}C_3$	n/a	n/a	n/a
H3	$\delta^{13}C\text{-}C_4$	n/a	n/a	n/a
H3	$\delta^{13}C\text{-}CO_2$	-12.6 (2,3)	-12.2 (4)	→

5.6 Sample Set D3

Proportions of methane show an initial increase followed by stable values close to 100%. (Figure 5.8; Table 5.7) Later in the desorption process, proportions of methane decrease. Proportions of higher hydrocarbons are generally low with stable values over the process of desorption; an exception is canister 5 with a distinct proportions maximum (Figure 5.9). Proportions of carbon dioxide drop initially for almost all canisters followed by a period when values remain stable with increasing time (Figure 5.10). Following this period all canisters simultaneously experience a significant increase in proportions of carbon dioxide.

Following initial fluctuations, all canisters show a two–stage trend for $\delta^{13}C$ for methane (Figure 5.11). During the first stage there are no increases in ^{12}C or ^{13}C with increasing time. After the first stage, simultaneously for all canisters values become strongly enriched in ^{13}C, followed by the second stage with stable values at the ^{13}C enriched level. Values for δD (methane) show strong to very strong fluctuations, but with the exceptions of canisters 7 and 9, all canisters show an overall ^{1}H enrichment with increasing time (Figure 5.12). Values for canisters 7 and 9 are stable and show no overall increase in ^{2}H or ^{1}H over time. $\delta^{13}C$ values for ethane are only available for canisters 5, 6 and 7. Based on canisters 5 and 7 data show a ^{12}C enrichment with increasing time, but the last sample of canister 5 shows a strong ^{13}C enrichment (Figure 5.14). For carbon dioxide, the $\delta^{13}C$ values for all canisters show an initial ^{13}C enrichment followed by a gradual ^{12}C enrichment (Figure 5.13). Eventually values for all canisters become stable with no increase in ^{12}C or ^{13}C.

Table 5.7: Compositional and isotope results for sample set D3. Results are represented per canister with minimum and maximum values for proportions and $\delta^{13}C$ and δD respectively. Proportions are normalized on the basis of proportions of methane, ethane, propane, n–butane, i–butane and carbon dioxide. Ethane, propane, n–butane and i–butane are combined under the term C_{2+} (higher hydrocarbons). Legend for symbols used for the characterization of observed trends is given above.

Canister	Species	Proportions Minimum % normalized	Proportions Maximum % normalized	Trend
5	CH_4	77.8 (12)	98.2 (11)	↑ ⌐ » ↓ (11); F
5	C_{2+}	0 (s.s.)	11.6 (12)	∩ (12)
5	CO_2	1.32 (11)	21.8 (1)	↓ » ↑ (11)
6	CH_4	83.4 (12)	99.0 (4)	↑ ⌐ » ↓ (11); F
6	C_{2+}	0 (s.s.)	0.74 (12)	→
6	CO_2	1.09 (9)	15.9 (12)	↓ » ↑ (11)
7	CH_4	85.2 (12)	98.2 (7)	↑ ⌐ » ↓ (11); F
7	C_{2+}	0 (s.s.)	0.35 (11)	→
7	CO_2	1.61 (7)	14.9 (12)	↓ » ↑ (11)
8	CH_4	77.4 (12)	98.6 (7)	↑ ⌐ » ↓ (11); F
8	C_{2+}	0 (s.s.)	0.12 (11)	→
8	CO_2	1.45 (9)	22.6 (12)	↓ » ↑ (11)
9	CH_4	76.4 (1)	98.4 (9)	↑ ⌐ » ↓ (11); F
9	C_{2+}	0 (s.s.)	0.12 (11)	→
9	CO_2	1.49 (9)	23.6 (1)	↓ » ↑ (11)
10	CH_4	73.6 (12)	98.6 (8)	↑ ⌐ » ↓ (11); F
10	C_{2+}	n/a	n/a	n/a
10	CO_2	1.38 (8)	26.4 (12)	↓ » ↑ (11)
11	CH_4	48.2 (1)	98.2 (8)	↑ ⌐ » ↓ (10); F
11	C_{2+}	n/a	n/a	n/a
11	CO_2	1.82 (8)	51.8 (1)	↓ » ↑ (10)
12	CH_4	67.9 (11)	98.4 (8)	↑ ⌐ » ↓ (9); F
12	C_{2+}	n/a	n/a	n/a
12	CO_2	1.61 (8)	28.6 (10)	↓ » ↑ (8)
Canister	**Species**	**Isotope Minimum ‰**	**Isotope Maximum ‰**	**Trend**
5	$\delta^{13}C\text{-}C_1$	-75.9 (1)	-41.7 (14)	→ » ↑ (11) » → (12)
5	$\delta D\text{-}C_1$	-207.2 (2)	-199.0 (3)	↓; F
5	$\delta^{13}C\text{-}C_2$	-28.7 (13)	-11.9 (14)	↓ » ↑
5	$\delta^{13}C\text{-}C_3$	n/a	-26.8	Value only for 1 sample
5	$\delta^{13}C\text{-}C_4$	n/a	n/a	n/a
5	$\delta^{13}C\text{-}CO_2$	-11.8 (12)	5.5 (7)	↓ » → (12)
6	$\delta^{13}C\text{-}C_1$	-81.1 (1)	-41.8 (12)	→ » ↑ (11) » → (12)
6	$\delta D\text{-}C_1$	-210.3 (1)	-186.6 (10)	↓; F
6	$\delta^{13}C\text{-}C_2$	n/a	-25.3	Value only for 1 sample
6	$\delta^{13}C\text{-}C_3$	n/a	n/a	n/a
6	$\delta^{13}C\text{-}C_4$	n/a	n/a	n/a
6	$\delta^{13}C\text{-}CO_2$	-16.8 (2)	5.1 (8)	↓ » → (12)
7	$\delta^{13}C\text{-}C_1$	-67.9 (11)	-40.1 (12)	→ » ↑ (11) » → (12)
7	$\delta D\text{-}C_1$	-205.6 (4)	-190.6 (3)	F » →
7	$\delta^{13}C\text{-}C_2$	-21.2 (11)	-19.8 (9)	↓
7	$\delta^{13}C\text{-}C_3$	n/a	n/a	n/a
7	$\delta^{13}C\text{-}C_4$	n/a	n/a	n/a

Canister	Species	Isotope Minimum ‰	Isotope Maximum ‰	Trend
7	$\delta^{13}C\text{-}CO_2$	-11.5 912,14)	8.1 (8)	↓ » → (12)
8	$\delta^{13}C\text{-}C_1$	-74.7 (1)	-41.4 (13)	→ » ↑ (11) » → (12)
8	$\delta D\text{-}C_1$	-207.6 (12)	-187.6 (8)	↓; F
8	$\delta^{13}C\text{-}C_2$	n/a	n/a	n/a
8	$\delta^{13}C\text{-}C_3$	n/a	n/a	n/a
8	$\delta^{13}C\text{-}C_4$	n/a	n/a	n/a
8	$\delta^{13}C\text{-}CO_2$	-11.9 (12)	9.0 (8)	↓ » → (12)
9	$\delta^{13}C\text{-}C_1$	-79.3 (1)	-41.5 (12)	→ » ↑ (11) » → (12)
9	$\delta D\text{-}C_1$	-202.0 (1)	-189.6 (3)	→; F
9	$\delta^{13}C\text{-}C_2$	n/a	n/a	n/a
9	$\delta^{13}C\text{-}C_3$	n/a	n/a	n/a
9	$\delta^{13}C\text{-}C_4$	n/a	n/a	n/a
9	$\delta^{13}C\text{-}CO_2$	-11.6 (13)	8.7 (8)	↓ » → (12)
10	$\delta^{13}C\text{-}C_1$	-71.1 (1)	-41.5 (12)	→ » ↑ (11) » → (12)
10	$\delta D\text{-}C_1$	-204.1 (14)	-188.9 (8)	F » ↓ » →
10	$\delta^{13}C\text{-}C_2$	n/a	n/a	n/a
10	$\delta^{13}C\text{-}C_3$	n/a	n/a	n/a
10	$\delta^{13}C\text{-}C_4$	n/a	n/a	n/a
10	$\delta^{13}C\text{-}CO_2$	-11.6 (14)	0.8 (9)	↓ » → (12)
11	$\delta^{13}C\text{-}C_1$	-77.6 (1)	-47.6 (12,13)	→ » ↑ (10) » → (12)
11	$\delta D\text{-}C_1$	-211.0 (12)	-189.9 (8)	F » ↓
11	$\delta^{13}C\text{-}C_2$	n/a	n/a	n/a
11	$\delta^{13}C\text{-}C_3$	n/a	n/a	n/a
11	$\delta^{13}C\text{-}C_4$	n/a	n/a	n/a
11	$\delta^{13}C\text{-}CO_2$	-11.5 (12)	0.7 (9)	↓ » → (12)
12	$\delta^{13}C\text{-}C_1$	-73.5 (7)	-49.6 (8)	→ » ↑ (8)
12	$\delta D\text{-}C_1$	-203.0 (11)	-176.2 (2)	F » ↓
12	$\delta^{13}C\text{-}C_2$	n/a	n/a	n/a
12	$\delta^{13}C\text{-}C_3$	n/a	n/a	n/a
12	$\delta^{13}C\text{-}C_4$	n/a	n/a	n/a
12	$\delta^{13}C\text{-}CO_2$	-11.6 (10)	-6.3 (5)	↓ » → (12)

5.7 Sample Set D4

Proportions of methane start high and are similar for all 10 canisters (Figure 5.8; Table 5.8). With increasing time proportions decrease and the differences between the different canisters become pronounced. All canisters show distinct maxima (but low proportions) for higher hydrocarbons early in the desorption process, with the exception of canister 10, which shows stable values with no increase or decrease with increasing time (Figure 5.9). Early values for proportions of carbon dioxide are low and similar for

all canisters, but with increasing time the proportions increase for all canisters (Figure 5.10). Differences between canisters become more pronounced with increasing time.

$\delta^{13}C$ values for methane show extreme fluctuations, but overall a ^{13}C enrichment with increasing time is observed for canisters 1 to 6; canisters 7 to 10 show no overall increase in ^{12}C or ^{13}C (Figure 5.11). For δD (methane) no overall trend is present with time (Figure 5.12). All canisters show extreme fluctuations with the exception of canisters 4, 7 and 9. No values are available for $\delta^{13}C$ for ethane. $\delta^{13}C$ values for carbon dioxide, despite strong fluctuations, show an overall ^{12}C enrichment with increasing time (Figure 5.13).

Table 5.8: *Compositional and isotope results for sample set D4. Results are represented per canister with minimum and maximum values for proportions and $\delta^{13}C$ and δD respectively. Proportions are normalized on the basis of proportions of methane, ethane, propane, n–butane, i–butane and carbon dioxide. Ethane, propane, n–butane and i–butane are combined under the term C_{2+} (higher hydrocarbons). Legend for symbols used for the characterization of observed trends is given above.*

Canister	Species	Proportions Minimum % normalized	Proportions Maximum % normalized	Trend
1	CH_4	48.7 (16)	99.9 (1)	↓
1	C_{2+}	0 (s.s.)	0.04 (2)	∩ (2) » →
1	CO_2	0.09 (1)	51.3 (16)	↑
2	CH_4	34.9 (16)	93.5 (1)	↓
2	C_{2+}	0 (s.s.)	0.08 (4)	∩ (4) » →
2	CO_2	3.54 (3)	65.1 (16)	↑
3	CH_4	69.1 (16)	98.6 (1)	↓
3	C_{2+}	0 (s.s.)	0.47 (3)	∩ (3) » →
3	CO_2	1.36 (1)	30.9 (16)	↑
4	CH_4	79.0 (16)	95.9 (2)	↓
4	C_{2+}	0 (s.s.)	0.32 (2)	∩ (2) » →
4	CO_2	0.66 (1)	21.0 (16)	↑
5	CH_4	68.4 (16)	98.6 (1)	↓
5	C_{2+}	0 (s.s.)	0.18 (3)	∩ (3) » →
5	CO_2	1.40 (1)	31.6 (16)	↑
6	CH_4	45.2 (16)	99.3 (1)	↓
6	C_{2+}	0 (s.s.)	0.90	∩ (3) » →
6	CO_2	0.73 (1)	54.8 (16)	↑
7	CH_4	89.7 (14)	99.0 (1)	↓
7	C_{2+}	0 (s.s.)	0.26 (3)	∩ (3) » →
7	CO_2	0.96 (1)	10.3 (14)	↑; F
8	CH_4	0.7 (16)	99.1 (1)	↓
8	C_{2+}	0 (s.s.)	0.34 (2)	∩ (2) » →
8	CO_2	0.92 (1)	99.3 (16)	↑
9	CH_4	91.8 (12)	98.6 (1)	↓
9	C_{2+}	0 (s.s.)	0.19 (3)	∩ (3) » →
9	CO_2	1.44 (1)	6.07 (8)	↑; F
10	CH_4	1.40 (16)	99.1 (1)	↓

Canister	Species	Proportions Minimum % normalized	Proportions Maximum % normalized	Trend
10	C_{2+}	0 (s.s.)	0.08 (12)	→
10	CO_2	0.94 (1)	98.6 (16)	↑; F
Canister	**Species**	**Isotope Minimum ‰**	**Isotope Maximum ‰**	**Trend**
1	$\delta^{13}C\text{-}C_1$	-62.5 (1)	-40.1 (11)	↑; F
1	$\delta D\text{-}C_1$	-239.1 (6)	-189.1 (10)	↑ » ↓
1	$\delta^{13}C\text{-}C_2$	n/a	n/a	n/a
1	$\delta^{13}C\text{-}C_3$	n/a	n/a	n/a
1	$\delta^{13}C\text{-}C_4$	n/a	n/a	n/a
1	$\delta^{13}C\text{-}CO_2$	-39.9 (14)	-3.7 (1)	↓; SF
2	$\delta^{13}C\text{-}C_1$	-61.8 (1)	-37.7 (16)	↑; F
2	$\delta D\text{-}C_1$	-248.8 (6)	-168.2 (14)	↑ » ↓
2	$\delta^{13}C\text{-}C_2$	n/a	n/a	n/a
2	$\delta^{13}C\text{-}C_3$	n/a	n/a	n/a
2	$\delta^{13}C\text{-}C_4$	n/a	-25.0	Value only for 1 sample
2	$\delta^{13}C\text{-}CO_2$	-39.5 (14)	-3.0 (2)	↓; SF
3	$\delta^{13}C\text{-}C_1$	-62.4 (1)	-43.5 (16)	↑; F
3	$\delta D\text{-}C_1$	-247.6 (6)	-206.9 (12)	SF
3	$\delta^{13}C\text{-}C_2$	n/a	n/a	n/a
3	$\delta^{13}C\text{-}C_3$	n/a	n/a	n/a
3	$\delta^{13}C\text{-}C_4$	n/a	n/a	n/a
3	$\delta^{13}C\text{-}CO_2$	-29.4 (9)	-0.2 (7)	↓; SF
4	$\delta^{13}C\text{-}C_1$	-61.9 (1)	-52.3 (16)	↑; F
4	$\delta D\text{-}C_1$	-252.2 (6)	-241.2 (16)	→
4	$\delta^{13}C\text{-}C_2$	n/a	n/a	n/a
4	$\delta^{13}C\text{-}C_3$	n/a	-24.0	Value only for 1 sample
4	$\delta^{13}C\text{-}C_4$	n/a	n/a	n/a
4	$\delta^{13}C\text{-}CO_2$	-22.1 (14)	-1.0 (2)	↓; SF
5	$\delta^{13}C\text{-}C_1$	-62.4 (3)	-44.6 (16)	↑; F
5	$\delta D\text{-}C_1$	-249.1 (6)	-120.6 (14)	↑ » ↓; SF
5	$\delta^{13}C\text{-}C_2$	n/a	n/a	n/a
5	$\delta^{13}C\text{-}C_3$	n/a	n/a	n/a
5	$\delta^{13}C\text{-}C_4$	n/a	n/a	n/a
5	$\delta^{13}C\text{-}CO_2$	-41.2 (16)	-1.3 (1)	↓; SF
6	$\delta^{13}C\text{-}C_1$	-61.5 (1)	-29.6 (16)	↑; F
6	$\delta D\text{-}C_1$	-248.5 (6)	-135.6 (16)	SF » ↑
6	$\delta^{13}C\text{-}C_2$	n/a	n/a	n/a
6	$\delta^{13}C\text{-}C_3$	n/a	n/a	n/a
6	$\delta^{13}C\text{-}C_4$	n/a	n/a	n/a
6	$\delta^{13}C\text{-}CO_2$	-30.0 (8)	-4.5 (2)	↓; SF
7	$\delta^{13}C\text{-}C_1$	-63.3 (2)	-59.0 (9)	→; F
7	$\delta D\text{-}C_1$	-251.7 (14)	-247.2 (12)	→
7	$\delta^{13}C\text{-}C_2$	n/a	n/a	n/a
7	$\delta^{13}C\text{-}C_3$	n/a	n/a	n/a
7	$\delta^{13}C\text{-}C_4$	n/a0.5 (2)	n/a	n/a
7	$\delta^{13}C\text{-}CO_2$	-27.4 (10)		↓; SF
8	$\delta^{13}C\text{-}C_1$	-62. (1) (6)	--46.5 (10)	→; F

Canister	Species	Isotope Minimum ‰	Isotope Maximum ‰	Trend
8	$\delta D\text{-}C_1$	-257.7 (6)	-168.6 (10)	↑
8	$\delta^{13}C\text{-}C_2$	n/a	n/a	n/a
8	$\delta^{13}C\text{-}C_3$	n/a	n/a	n/a
8	$\delta^{13}C\text{-}C_4$	n/a	n/a	n/a
8	$\delta^{13}C\text{-}CO_2$	-38.2 (16)	-1.1 (2)	↓; SF
9	$\delta^{13}C\text{-}C_1$	-63.2 (2)	-60.8 (16)	→; F
9	$\delta D\text{-}C_1$	-250.8 (6)	-248.7 (10)	→
9	$\delta^{13}C\text{-}C_2$	n/a	n/a	n/a
9	$\delta^{13}C\text{-}C_3$	n/a	-24.6	Value only for 1 sample
9	$\delta^{13}C\text{-}C_4$	n/a	n/a	n/a
9	$\delta^{13}C\text{-}CO_2$	-25.1 (10)	0.4 (3)	↓; SF
10	$\delta^{13}C\text{-}C_1$	-61.7 (1)	-41.3 (12)	→; F
10	$\delta D\text{-}C_1$	-		
10	$\delta^{13}C\text{-}C_2$	n/a	n/a	n/a
10	$\delta^{13}C\text{-}C_3$	n/a	n/a (12)	SFn/a
10	$\delta^{13}C\text{-}C_4$	n/a	n/a	n/a
10	$\delta^{13}C\text{-}CO_2$	-37.6 (16)	2.5 (1)	↓; SF

5.8 Sample Set D5

Only three samples from two canisters are available and therefore only canister C is considered here. Proportions of methane show an increase with increasing time (Figure 5.8; Table 5.9). Proportions for higher hydrocarbons are not available. Proportions of carbon dioxide decrease with increasing time (Figure 5.10).

$\delta^{13}C$ values for methane show ^{12}C enrichment with increasing time (Figure 5.11), whereas δD values show a ^{2}H enrichment (Figure 5.12). Values for $\delta^{13}C$ (ethane) are not available. For carbon dioxide a slight ^{13}C enrichment is observed (Figure 5.13).

Table 5.9: *Compositional and isotope results for sample set D. Results are represented per canister with minimum and maximum values for proportions and $\delta^{13}C$ and δD respectively. Proportions are normalized on the basis of proportions of methane, ethane, propane, n–butane, i–butane and carbon dioxide. Ethane, propane, n–butane and i–butane are combined under the term C_{2+} (higher hydrocarbons). Legend for symbols used for the characterization of observed trends is given above.*

Canister	Species	Proportions Minimum % normalized	Proportions Maximum % normalized	Trend
A	CH_4	n/a	70.6	Only 1 sample
A	C_{2+}	n/a	n/a	Only 1 sample
A	CO_2	n/a	26.1	Only 1 sample

Canister	Species	Proportions Minimum % normalized	Proportions Maximum % normalized	Trend
C	CH_4	61.2 (1)	69.7 (2)	↑
C	C_{2+}	n/a	n/a	n/a
C	CO_2	30.4 (2)	38.8 (1)	↓
Canister	**Species**	**Isotope Minimum ‰**	**Isotope Maximum ‰**	**Trend**
A	$\delta^{13}C\text{-}C_1$	n/a	-50.1	Only 1 sample
A	$\delta D\text{-}C_1$	n/a	-219.1	Only 1 sample
A	$\delta^{13}C\text{-}C_2$	n/a	n/a	n/a
A	$\delta^{13}C\text{-}C_3$	n/a	n/a	n/a
A	$\delta^{13}C\text{-}C_4$	n/a	-28.2	Only 1 sample
A	$\delta^{13}C\text{-}CO_2$	n/a	-11.0	Only 1 sample
C	$\delta^{13}C\text{-}C_1$	-50.5 (1)	-46.8 (2)↑	↑
C	$\delta D\text{-}C_1$	-209.7 (1)	-202.0 (2)	
C	$\delta^{13}C\text{-}C_2$	n/a	n/a	n/a
C	$\delta^{13}C\text{-}C_3$	n/a	n/a	n/a
C	$\delta^{13}C\text{-}C_4$	n/a	n/a	n/a
C	$\delta^{13}C\text{-}CO_2$	-11.1 (1)	-11.0 (2)	→

5.9 Sample Set D6

Sample set D6 contained large proportions of carbon dioxide. During the analyzes, the carbon dioxide peak interfered with the methane peak, so that reliable results (proportions and $\delta^{13}C$ for methane and carbon dioxide) were not obtained. Therefore, the carbon dioxide was removed from samples by injecting KOH solution into the sample vessels. This treatment allowed proportions of methane and $\delta^{13}C$ values to be measured, but eliminated the possibility of measuring carbon dioxide. Therefore, the values are normalized to methane, ethane, propane, *n*–butane and *i*–butane only. Exceptions are canisters 77, 88 and 90.

Canisters 136, 188, 192 and 201 show decreases in proportions of methane with increasing time, whereas canisters 77, 88, 90, 105, 11, 153 and 161 have stable values (Figure 5.8; Table 5.10). The proportions of higher hydrocarbons from canisters 77, 88, 90, 105, 111 and 161 do not increase or decrease with increasing time, whereas an increase with time was observed for canisters 136, 153, 188, 192 and 201 (Figure 5.9).

The overall trend related to $\delta^{13}C$ values for methane is an enrichment in ^{13}C with increasing time, with more pronounced enrichments during the early desorption process (Figure 5.11). δD values for methane were only available for canisters 77, 88 and 90 and these results show no overall trend with increasing time (Figure 5.12). $\delta^{13}C$ values for ethane show an overall trend of ^{13}C enrichment with increasing time, though early enrichment is more pronounced (Figure 5.14). Exceptions are canisters 90 and 111, with strongly fluctuating values. Reliable isotope data for carbon dioxide are only available for canisters 77, 88 and 90 and all these canisters show an overall ^{13}C enrichment with increasing time, with pronounced early enrichment (Figure 5.13)

Table 5.10: *Compositional and isotope results for sample set D6. Results are represented per canister with minimum and maximum values for proportions and $\delta^{13}C$ and δD respectively. Proportions are normalized on the basis of proportions of methane, ethane, propane, n–butane, i–butane and carbon dioxide. Ethane, propane, n–butane and i–butane are combined under the term C_{2+} (higher hydrocarbons). Legend for symbols used for the characterization of observed trends is given above.*

Canister	Species	Proportions Minimum % normalized	Proportions Maximum % normalized	Trend
77	CH_4	99.6 (s.s.)	99.7 (s.s.)	→
77	C_{2+}	0.28 (1)	0.36 (2)	→
77	CO_2	n/a	n/a	n/a
88	CH_4	99.8 (s.s.)	99.8 (s.s.)	→
88	C_{2+}	0.19 (1)	0.21 (2)	→
88	CO_2	n/a	n/a	n/a
90	CH_4	99.9 (s.s.)	100 (s.s.)	→
90	C_{2+}	0.03 (2)	0.08 (4)	→
90	CO_2	n/a	n/a	n/a
105	CH_4	91.4 (5)	96.1 (2)	→
105	C_{2+}	3.85 (2)	8.63 (5)	→
105	CO_2	n/a	n/a	n/a
111	CH_4	99.6 (s.s.)	99.8 (s.s.)	→
111	C_{2+}	0.22 (1)	0.36 (7)	→
111	CO_2	n/a	n/a	n/a
136	CH_4	91.9 (6)	97.6 (3)	↓
136	C_{2+}	2.43 (3)	8.08 (6)	↑; F
136	CO_2	n/a	n/a	n/a
153	CH_4	98.6 (s.s.)	99.1 (s.s.)	→
153	C_{2+}	0.93 (1)	1.39 (3)	↑; F
153	CO_2	n/a	n/a	n/a
161	CH_4	99.5 (s.s.)	99.9 (s.s.)	→
161	C_{2+}	0.12 (1)	0.46 (2)	∩ (2) » →
161	CO_2	n/a	n/a	n/a
188	CH_4	95.2 (6)	97.4 (1)	↓
188	C_{2+}	2.55 (1)	4.82 (6)	↑
188	CO_2	n/a	n/a	n/a
192	CH_4	91.3 (6)	97.7 (1)	↓

Canister	Species	Proportions Minimum % normalized	Proportions Maximum % normalized	Trend
192	C_{2+}	2.26 (1)	8.74 (6)	↑
192	CO_2	n/a	n/a	n/a
201	CH_4	95.7 (4)	97.1 (1)	↓
201	C_{2+}	2.87 (1)	4.29 (4)	↑
201	CO_2	n/a	n/a	n/a
215	CH_4	n/a	95.5	Only 1 sample
215	C_{2+}	n/a	4.55	Only 1 sample
215	CO_2	n/a	n/a	n/a
220	CH_4	n/a	87.7	Only 1 sample
220	C_{2+}	n/a	12.3	Only 1 sample
220	CO_2	n/a	n/a	n/a
224	CH_4	n/a	91.1	Only 1 sample
224	C_{2+}	n/a	8.88	Only 1 sample
224	CO_2	n/a	n/a	n/a
Canister	**Species**	**Isotope Minimum ‰**	**Isotope Maximum ‰**	**Trend**
77	$\delta^{13}C\text{-}C_1$	-57.2 (2)	-55.5 (1,6)	↑
77	$\delta D\text{-}C_1$	-302.5 (1)	-271.8 (5)	↑ » →
77	$\delta^{13}C\text{-}C_2$	-24.9 (1)	-22.8 (6)	↑ » →
77	$\delta^{13}C\text{-}C_3$	n/a	n/a	n/a
77	$\delta^{13}C\text{-}C_4$	n/a	n/a	n/a
77	$\delta^{13}C\text{-}CO_2$	-29.0 (1)	-13.8 (5)	↑
88	$\delta^{13}C\text{-}C_1$	-52.8 (1)	-48.7 (6)	↑ ↓
88	$\delta D\text{-}C_1$	-253.7 (4)	-243.4 (5)	→
88	$\delta^{13}C\text{-}C_2$	-13.5 (1)	-10.8 (5)	↑ » →
88	$\delta^{13}C\text{-}C_3$	n/a	n/a	n/a
88	$\delta^{13}C\text{-}C_4$	n/a	n/a	n/a
88	$\delta^{13}C\text{-}CO_2$	-14.8 (1)	-5.6 (3)	↑ ↓
90	$\delta^{13}C\text{-}C_1$	-52.4 (1)	-50.1 (5)	↑
90	$\delta D\text{-}C_1$	-251.6 (3)	-248.3 (5)	→
90	$\delta^{13}C\text{-}C_2$	-13.4 (4)	-9.0 (2)	SF
90	$\delta^{13}C\text{-}C_3$	n/a	-31.7	Value only for 1 sample
90	$\delta^{13}C\text{-}C_4$	n/a	n/a	n/a
90	$\delta^{13}C\text{-}CO_2$	-5.2 (1)	1.5 (4)	↑ ↓
105	$\delta^{13}C\text{-}C_1$	-38.8 (1)	-33.2 (5)	↑
105	$\delta D\text{-}C_1$	n/a	n/a	n/a
105	$\delta^{13}C\text{-}C_2$	-26.8 (1)	-25.3 (5)	↑ » →
105	$\delta^{13}C\text{-}C_3$	-22.7 (2)	-21.8 (5)	↑
105	$\delta^{13}C\text{-}C_4$	n/a	n/a	n/a
105	$\delta^{13}C\text{-}CO_2$	n/a	n/a	n/a
111	$\delta^{13}C\text{-}C_1$	-45.0 (2)	-40.0 (4)	↑
111	$\delta D\text{-}C_1$	n/a	n/a	n/a
111	$\delta^{13}C\text{-}C_2$	-20.0 (6)	-11.7 (5)	SF
111	$\delta^{13}C\text{-}C_3$	-18.2 (5)	-12.8 (7)	↑
111	$\delta^{13}C\text{-}C_4$	n/a	n/a	n/a
111	$\delta^{13}C\text{-}CO_2$	-10.6 (1)	0.3 (4)	↑ ↓
136	$\delta^{13}C\text{-}C_1$	-54.5 (1)	-40.0 (6)	↑
136	$\delta D\text{-}C_1$	n/a	n/a	n/a

Canister	Species	Isotope Minimum ‰	Isotope Maximum ‰	Trend
136	$\delta^{13}C\text{-}C_2$	-26.7 (2)	-23.2 (6)	↑ » →
136	$\delta^{13}C\text{-}C_3$	-31.3 (2)	-20.9 (4)	SF
136	$\delta^{13}C\text{-}C_4$	n/a	n/a	n/a
136	$\delta^{13}C\text{-}CO_2$	n/a	n/a	n/a
153	$\delta^{13}C\text{-}C_1$	-39.8 (1)	-33.0 (6)	↑
153	$\delta D\text{-}C_1$	n/a	n/a	n/a
153	$\delta^{13}C\text{-}C_2$	-21.4 (1)	-20.1 (6)	↑ » →
153	$\delta^{13}C\text{-}C_3$	n/a	n/a	n/a
153	$\delta^{13}C\text{-}C_4$	n/a	n/a	n/a
153	$\delta^{13}C\text{-}CO_2$	n/a	n/a	n/a
161	$\delta^{13}C\text{-}C_1$	-44.7 (1)	-41.3 (5)	↑
161	$\delta D\text{-}C_1$	n/a	n/a	n/a
161	$\delta^{13}C\text{-}C_2$	-14.6 (3)	-13.5 (5)	↑
161	$\delta^{13}C\text{-}C_3$	n/a	n/a	n/a
161	$\delta^{13}C\text{-}C_4$	n/a	n/a	n/a
161	$\delta^{13}C\text{-}CO_2$	n/a	n/a	n/a
188	$\delta^{13}C\text{-}C_1$	-49.8 (1)	-41.9 (6)	↑
188	$\delta D\text{-}C_1$	n/a	n/a	n/a
188	$\delta^{13}C\text{-}C_2$	-27.4 (1,3)	-25.2 (4)	↑
188	$\delta^{13}C\text{-}C_3$	-21.6 (1)	-20.9 (5,6)	↑
188	$\delta^{13}C\text{-}C_4$	n/a	n/a	n/a
188	$\delta^{13}C\text{-}CO_2$	n/a	n/a	n/a
192	$\delta^{13}C\text{-}C_1$	-42.6 (1)	-27.9 (6)	↑
192	$\delta D\text{-}C_1$	n/a	n/a	n/a
192	$\delta^{13}C\text{-}C_2$	-25.7 (3)	-25.2 (4)	F
192	$\delta^{13}C\text{-}C_3$	-20.2 (1)	-19.3 (6)	↑
192	$\delta^{13}C\text{-}C_4$	n/a	n/a	n/a
192	$\delta^{13}C\text{-}CO_2$	n/a	n/a	n/a
201	$\delta^{13}C\text{-}C_1$	-44.7 (1)	-42.4 (4)	↑
201	$\delta D\text{-}C_1$	n/a	n/a	n/a
201	$\delta^{13}C\text{-}C_2$	-25.3 (1)	-23.9 (4)	↑
201	$\delta^{13}C\text{-}C_3$	-20.4 (3)	-19.5 (4)	→ » ↑
201	$\delta^{13}C\text{-}C_4$	n/a	n/a	n/a
201	$\delta^{13}C\text{-}CO_2$	n/a	n/a	n/a
215	$\delta^{13}C\text{-}C_1$	n/a	-37.0	Only 1 sample
215	$\delta D\text{-}C_1$	n/a	n/a	n/a
215	$\delta^{13}C\text{-}C_2$	n/a	-37.4	Only 1 sample
215	$\delta^{13}C\text{-}C_3$	n/a	-35.2	Only 1 sample
215	$\delta^{13}C\text{-}C_4$	n/a	n/a	n/a
215	$\delta^{13}C\text{-}CO_2$	n/a	-26.5	Only 1 sample
220	$\delta^{13}C\text{-}C_1$	n/a	-45.3	Only 1 sample
220	$\delta D\text{-}C_1$	n/a	n/a	n/a
220	$\delta^{13}C\text{-}C_2$	n/a	-33.2	Only 1 sample
220	$\delta^{13}C\text{-}C_3$	n/a	-31.9	Only 1 sample
220	$\delta^{13}C\text{-}C_4$	n/a	-36.9	Only 1 sample
220	$\delta^{13}C\text{-}CO_2$	n/a	-26.6	Only 1 sample
224	$\delta^{13}C\text{-}C_1$	n/a	-47.9	Only 1 sample
224	$\delta D\text{-}C_1$	n/a	n/a	n/a

Canister	Species	Isotope Minimum ‰	Isotope Maximum ‰	Trend
224	$\delta^{13}C\text{-}C_2$	n/a	-30.2	Only 1 sample
224	$\delta^{13}C\text{-}C_3$	n/a	-29.7	Only 1 sample
224	$\delta^{13}C\text{-}C_4$	n/a	-29.9	Only 1 sample
224	$\delta^{13}C\text{-}CO_2$	n/a	-13.36	Only 1 sample

5.10 Sample Set D7

Proportions of methane show a minor increase with increasing time for canisters 3, 4, 5, 6, 9, 10, 11, 13 and 15, but a minor decrease for canisters 8, 16 and 18 (Figure 5.8; Table 5.11). The proportions of the higher hydrocarbons increases for all canisters with increasing time (Figure 5.9), and the proportions of carbon dioxide decrease with increasing time for all canisters (Figure 5.10).

A minor ^{13}C enrichment for methane is present with increasing time for all canisters (Figure 5.11). δD values for methane show a minor ^{2}H enrichment with increasing time for canisters 5, 8, 13, 15 and 18, whereas the values for canisters 3, 4, 10, 11 and 16 show an ^{1}H enrichment (Figure 5.12). Values for canisters 6 and 9 are stable and show no increase in ^{2}H or ^{1}H. $\delta^{13}C$ values for ethane show an overall slight ^{13}C enrichment with increasing time (Figure 5.14). Exceptions are canisters 13 with stable values, and 3, with ^{12}C enrichment with increasing time. Carbon dioxide shows only very small variations in $\delta^{13}C$ values, with an overall trend to ^{13}C enrichment with increasing time (Figure 5.13).

Table 5.11: *Compositional and isotope results for sample set D7. Results are represented per canister with minimum and maximum values for proportions and $\delta^{13}C$ and δD respectively. Proportions are normalized on the basis of proportions of methane, ethane, propane, n–butane, i–butane and carbon dioxide. Ethane, propane, n–butane and i–butane are combined under the term C_{2+} (higher hydrocarbons). Legend for symbols used for the characterization of observed trends is given above.*

Canister	Species	Proportions Minimum % normalized	Proportions Maximum % normalized	Trend
3	CH_4	79.1 (1)	81.2 (2)	↑
3	C_{2+}	2.80 (1)	3.35 (2)	↑
3	CO_2	15.4 (2)	18.1 (1)	↓
4	CH_4	73.8 (1)	75.1 (2)	↑
4	C_{2+}	8.45 (1)	10.3 (2)	↑
4	CO_2	14.7 (2)	17.8 (1)	↓

Canister	Species	Proportions Minimum % normalized	Proportions Maximum % normalized	Trend
5	CH_4	76.7 (1)	78.3 (2)	↑
5	C_{2+}	7.54 (1)	9.50 (2)	↑
5	CO_2	12.2 (2)	15.7 (1)	↓
6	CH_4	69.8 (1)	73.8 (2)	↑
6	C_{2+}	5.77 (1)	6.84 (2)	↑
6	CO_2	19.3 (2)	24.4 (1)	↓
8	CH_4	74.7 (2)	72.4 (1)	↓
8	C_{2+}	6.00 (1)	8.41 (2)	↑
8	CO_2	18.2 (2)	19.3 (1)	↓
9	CH_4	71.5 (1)	75.1 (2)	↑
9	C_{2+}	6.69 (1)	8.51 (2)	↑
9	CO_2	16.4 (2)	21.9 (1)	↓
10	CH_4	77.2 (1)	78.7 (2)	↑
10	C_{2+}	8.82 (1)	11.1 (2)	↑
10	CO_2	10.2 (2)	14.0 (1)	↓
11	CH_4	77.6 (1)	78.5 (2)	↑
11	C_{2+}	8.98 (1)	12.0 (2)	↑
11	CO_2	9.60 (2)	13.4 (1)	↓
13	CH_4	80.3 (1)	80.6 (2)	↑
13	C_{2+}	7.67 (1)	10.1 (2)	↑
13	CO_2	9.36 (2)	12.0 (1)	↓
15	CH_4	79.0 (1)	79.1 (2)	↑
15	C_{2+}	9.15 (1)	11.7 (2)	↑
15	CO_2	9.18 (2)	11.2 (1)	↓
16	CH_4	78.6 (2)	79.8 (1)	↓
16	C_{2+}	8.23 (1)	11.3 (2)	↑
16	CO_2	10.0 (2)	12.0 (1)	↓
17	CH_4	n/a	79.9	Only 1 sample
17	C_{2+}	n/a	6.82	Only 1 sample
17	CO_2	n/a	13.3	Only 1 sample
18	CH_4	80.3 (2)	80.9 (1)	↓
18	C_{2+}	5.97 (1)	8.64 (2)	↑
18	CO_2	11.1 (2)	13.2 (1)	↓
Canister	**Species**	**Isotope Minimum ‰**	**Isotope Maximum ‰**	**Trend**
3	$\delta^{13}C\text{-}C_1$	-41.8 (10	-39.4 (2)	↑
3	$\delta D\text{-}C_1$	-181.6 (2)	-180.0 (1)	↓
3	$\delta^{13}C\text{-}C_2$	-25.0 (2)	-25.8 (1)	↓
3	$\delta^{13}C\text{-}C_3$	-27.2 (2)	-26.9 (1)	↓
3	$\delta^{13}C\text{-}C_4$	n/a	-27.8	Value only for 1 sample
3	$\delta^{13}C\text{-}CO_2$	-20.4 (2)	-20.1 (1)	↓
4	$\delta^{13}C\text{-}C_1$	-37.7 (1)	-36.3 (2)	↑
4	$\delta D\text{-}C_1$	-179.7 (2)	-179.4 (1)	↓
4	$\delta^{13}C\text{-}C_2$	-29.4 (1)	-28.8 (2)	↑
4	$\delta^{13}C\text{-}C_3$	-28.0 (2)	-27.9 (1)	↓
4	$\delta^{13}C\text{-}C_4$	n/a	n/a	n/a
4	$\delta^{13}C\text{-}CO_2$	-15.0 (1)	-14.7 (2)	↑
5	$\delta^{13}C\text{-}C_1$	-36.4 (1)	-34.2 (2)	↑
5	$\delta D\text{-}C_1$	-181.3 (1)	-181.0 (2)	↑

Canister	Species	Isotope Minimum ‰	Isotope Maximum ‰	Trend
5	$\delta^{13}C\text{-}C_2$	-29.0 (1)	-28.8 (2)	↑
5	$\delta^{13}C\text{-}C_3$	-28.0 (1)	-27.9 (2)	↑
5	$\delta^{13}C\text{-}C_4$	n/a	n/a	n/a
5	$\delta^{13}C\text{-}CO_2$	-14.0 (2)	-13.6 (1)	↓
6	$\delta^{13}C\text{-}C_1$	-37.6 (1)	-35.9 (2)	↑
6	$\delta D\text{-}C_1$	-187.5	-187.5	→
6	$\delta^{13}C\text{-}C_2$	-30.8 (1)	-30.7 (2)	↑
6	$\delta^{13}C\text{-}C_3$	-29.6	-29.6	→
6	$\delta^{13}C\text{-}C_4$	n/a	n/a	n/a
6	$\delta^{13}C\text{-}CO_2$	-5.6 (1)	-5.0 (2)	↑
8	$\delta^{13}C\text{-}C_1$	-37.0 (1)	-35.3 (2)	↑
8	$\delta D\text{-}C_1$	-187.9 (1)	-185.0 (2)	↑
8	$\delta^{13}C\text{-}C_2$	-30.9 (1)	-30.6 (2)	↑
8	$\delta^{13}C\text{-}C_3$	-29.9 (2)	-29.8 (1)	↓
8	$\delta^{13}C\text{-}C_4$	n/a	n/a	n/a
8	$\delta^{13}C\text{-}CO_2$	-7.0 (1)	-6.7 (2)	↑
9	$\delta^{13}C\text{-}C_1$	-36.4 (1)	-35.3 (2)	↑
9	$\delta D\text{-}C_1$	-178.6	-178.6	→
9	$\delta^{13}C\text{-}C_2$	-29.7 (1)	-29.5 (2)	↑
9	$\delta^{13}C\text{-}C_3$	-29.6 (2)	-29.5 (1)	↓
9	$\delta^{13}C\text{-}C_4$	n/a	n/a	n/a
9	$\delta^{13}C\text{-}CO_2$	-7.6 (1)	-7.0 (2)	↑
10	$\delta^{13}C\text{-}C_1$	-32.3 (1)	-29.0 (2)	↑
10	$\delta D\text{-}C_1$	-167.1 (2)	-165.5 (1)	↓
10	$\delta^{13}C\text{-}C_2$	-28.4 (1)	-27.7 (2)	↑
10	$\delta^{13}C\text{-}C_3$	-27.2 (1)	-26.8 (2)	↑
10	$\delta^{13}C\text{-}C_4$	n/a	n/a	n/a
10	$\delta^{13}C\text{-}CO_2$	-4.9 (1)	-4.1 (2)	↑
11	$\delta^{13}C\text{-}C_1$	-31.4 (1)	-27.9 (2)	↑
11	$\delta D\text{-}C_1$	-165.1 (2)	-165.5 (1)	↓
11	$\delta^{13}C\text{-}C_2$	-28.4 (1)	-27.6 (2)	↑
11	$\delta^{13}C\text{-}C_3$	-27.1 (1)	-26.6 (2)	↑
11	$\delta^{13}C\text{-}C_4$	n/a	n/a	n/a
11	$\delta^{13}C\text{-}CO_2$	-4.3 (1)	-3.7 (2)	↑
13	$\delta^{13}C\text{-}C_1$	-32.4 (1)	-29.4 (2)	↑
13	$\delta D\text{-}C_1$	-167.0 (1)	-163.7 (2)	↑
13	$\delta^{13}C\text{-}C_2$	-28.0	-28.0	→
13	$\delta^{13}C\text{-}C_3$	-26.9	-26.9	→
13	$\delta^{13}C\text{-}C_4$	n/a	-28.7	Value only for 1 sample
13	$\delta^{13}C\text{-}CO_2$	-4.0 (1)	-3.4 (2)	↑
15	$\delta^{13}C\text{-}C_1$	-31.9 (1)	-29.1 (2)	↑
15	$\delta D\text{-}C_1$	-165.3 (1)	-164.7 (2)	↑
15	$\delta^{13}C\text{-}C_2$	-27.8 (1)	-27.4 (2)	↑
15	$\delta^{13}C\text{-}C_3$	-26.9 (1)	-26.8 (2)	↑
15	$\delta^{13}C\text{-}C_4$	n/a	n/a	n/a
15	$\delta^{13}C\text{-}CO_2$	-3.3 (1)	-3.2 (2)	↑
16	$\delta^{13}C\text{-}C_1$	-32.7 (1)	-29.4 (2)	↑
16	$\delta D\text{-}C_1$	-167.0 (2)	-166.6 (1)	↓

Canister	Species	Isotope Minimum ‰	Isotope Maximum ‰	Trend
16	$\delta^{13}C\text{-}C_2$	-28.2 (1)	-27.6 (2)	↑
16	$\delta^{13}C\text{-}C_3$	-26.8	-26.8	→
16	$\delta^{13}C\text{-}C_4$	n/a	n/a	n/a
16	$\delta^{13}C\text{-}CO_2$	-3.2 (1)	-2.9 (2)	↑
17	$\delta^{13}C\text{-}C_1$	n/a	-34.2	Only 1 sample
17	$\delta D\text{-}C_1$	n/a	-167.4	Only 1 sample
17	$\delta^{13}C\text{-}C_2$	n/a	-27.8	Only 1 sample
17	$\delta^{13}C\text{-}C_3$	n/a	-27.1	Only 1 sample
17	$\delta^{13}C\text{-}C_4$	n/a	n/a	n/a
17	$\delta^{13}C\text{-}CO_2$	n/a	-3.4	Only 1 sample
18	$\delta^{13}C\text{-}C_1$	-34.7 (1)	-31.9 (2)	↑
18	$\delta D\text{-}C_1$	-170.3 (1)	-166.9 (2)	↑
18	$\delta^{13}C\text{-}C_2$	-27.3 (1)	-27.2 (2)	↑
18	$\delta^{13}C\text{-}C_3$	-26.3 (1)	-25.9 (2)	↑
18	$\delta^{13}C\text{-}C_4$	n/a	n/a	n/a
18	$\delta^{13}C\text{-}CO_2$	-3.1 (1)	-2.5 (2)	↑

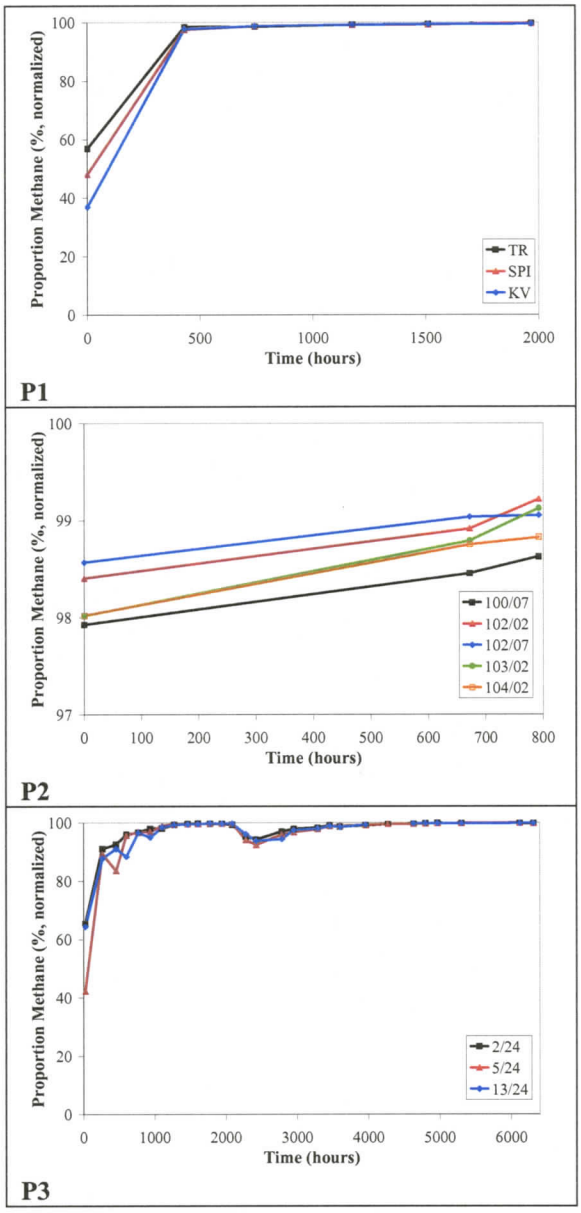


Figure 5.1: *Proportions of methane for samples from production sample sets P1, P2 and P3 presented versus production time. First available sample is set to 0 hours. Proportions are normalized on the basis of proportions of methane, ethane, propane, n–butane, i–butane and carbon dioxide. For discussion of data see text. Note the different scales.*

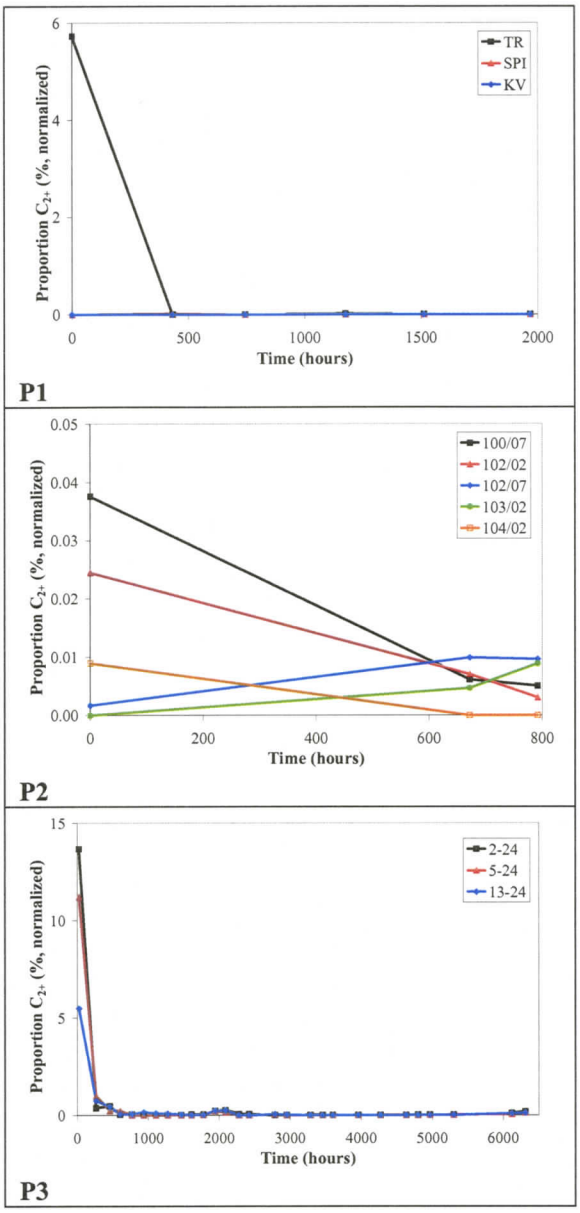


Figure 5.2: *Proportions of higher hydrocarbons (ethane, propane, n–butane and i–butane) for samples from production sample sets P1, P2 and P3 presented versus production time. First available sample is set to 0 hours. Proportions are normalized on the basis of proportions of methane, ethane, propane, n–butane, i–butane and carbon dioxide. For discussion of data see text. Note the different scales.*

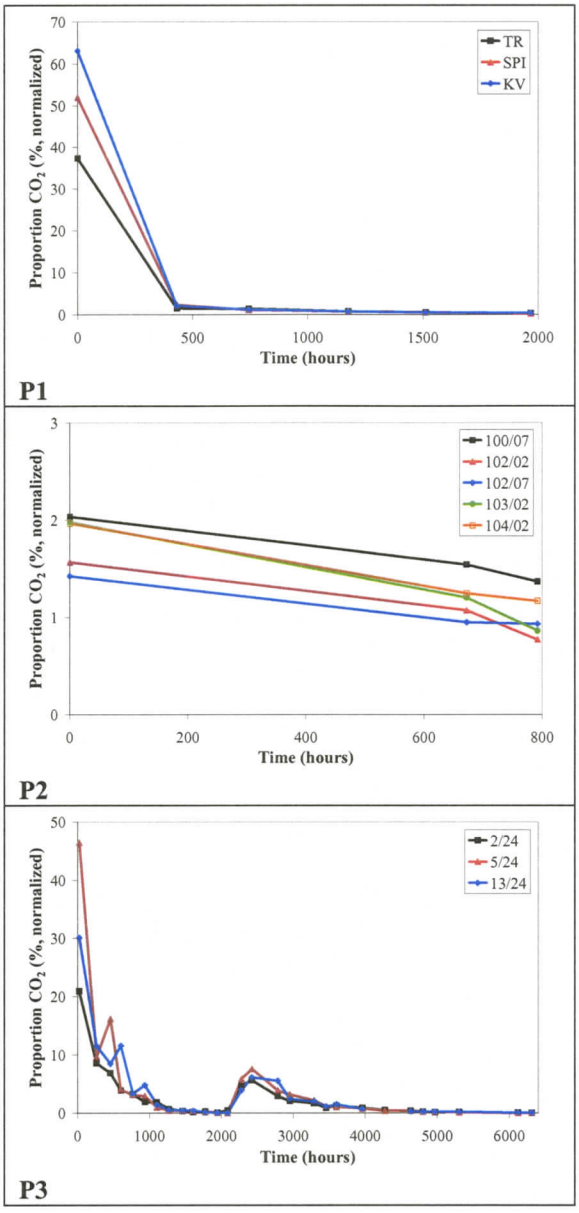


Figure 5.3: *Proportions of carbon dioxide for samples from production sample sets P1, P2 and P3 presented versus production time. First available sample is set to 0 hours. Proportions are normalized on the basis of proportions of methane, ethane, propane, n–butane, i–butane and carbon dioxide. For discussion of data see text. Note the different scales.*

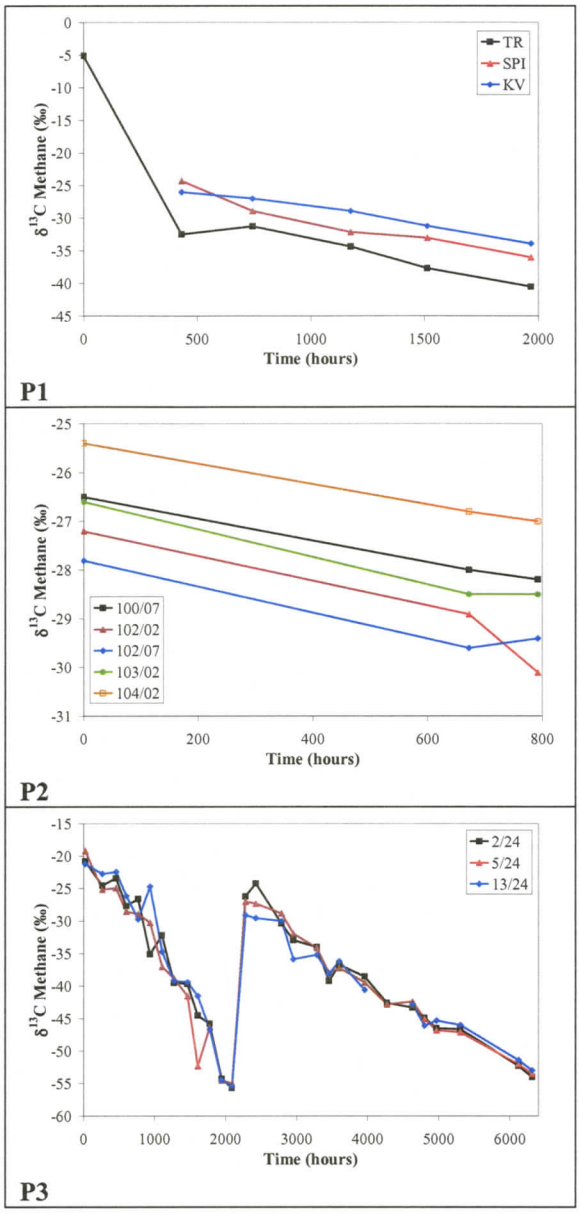


Figure 5.4: *$\delta^{13}C$ ratios for methane from samples of production sample sets P1, P2 and P3 presented versus production time. First available sample is set to 0 hours. For discussion of data see text. Note the different scales.*

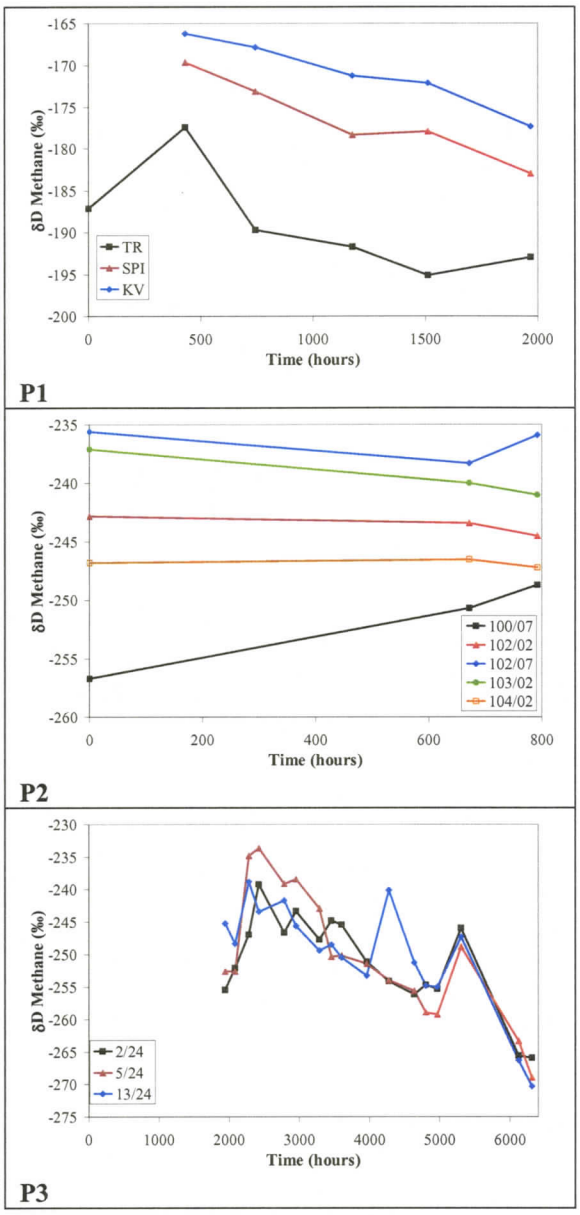


Figure 5.5: *δD ratios for methane from samples of production sample sets P1, P2 and P3 presented versus production time. First available sample is set to 0 hours. For discussion of data see text. Note the different scales.*

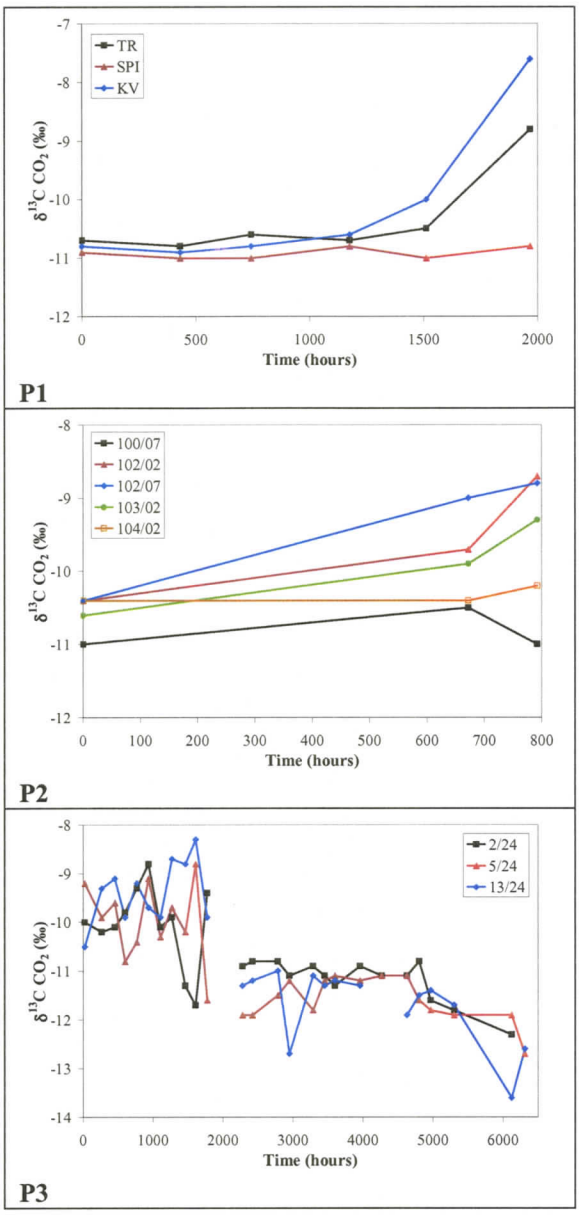


Figure 5.6: *$\delta^{13}C$ ratios for carbon dioxide from samples of production sample sets P1, P2 and P3 presented versus production time. First available sample is set to 0 hours. For discussion of data see text. Note the different scales.*

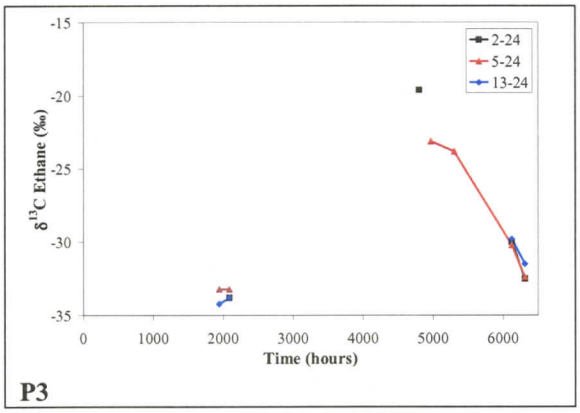


Figure 5.7: *$\delta^{13}C$ ratios for ethane from samples of production sample sets P3 presented versus production time. First available sample is set to 0 hours. Results for samples from production scenarios P1 and P2 are not available. For discussion of data see text.*

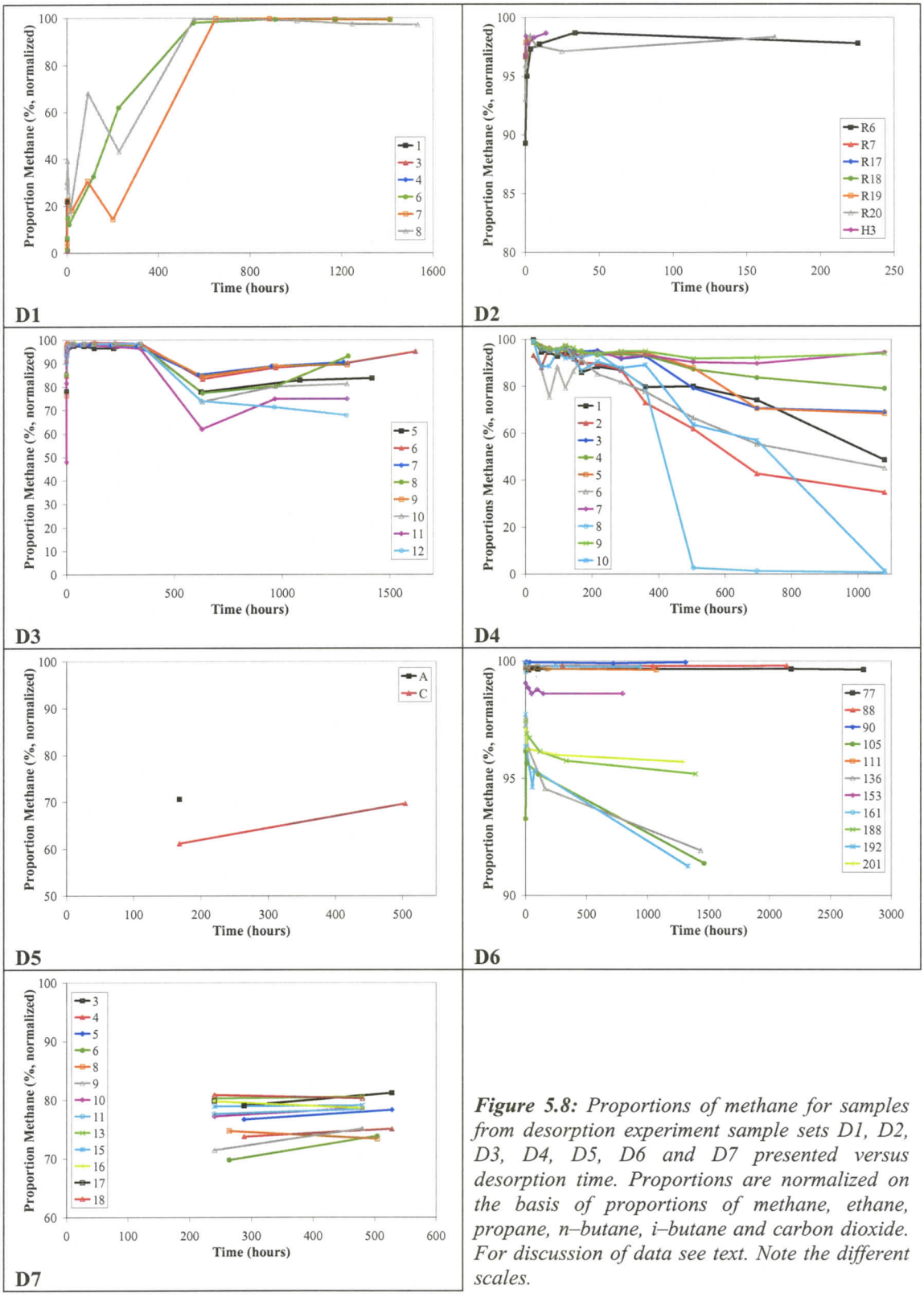


Figure 5.8: *Proportions of methane for samples from desorption experiment sample sets D1, D2, D3, D4, D5, D6 and D7 presented versus desorption time. Proportions are normalized on the basis of proportions of methane, ethane, propane, n–butane, i–butane and carbon dioxide. For discussion of data see text. Note the different scales.*

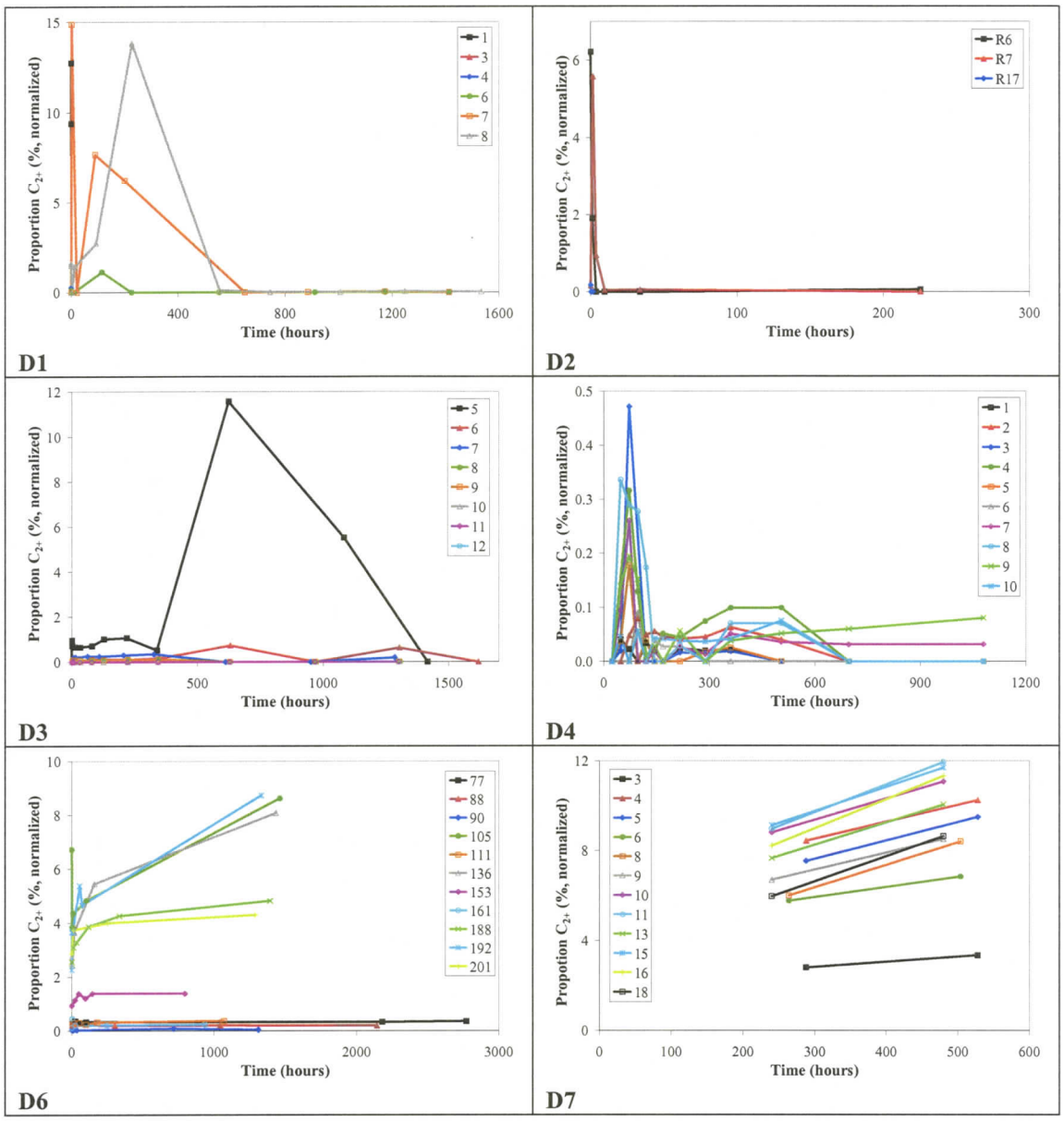


Figure 5.9: *Proportions of higher hydrocarbons (ethane, propane, n–butane and i–butane) for samples from desorption experiment sample sets D1, D2, D3, D4, D6 and D7 presented versus desorption time. No results are available for desorption experiment sample set D5. Proportions are normalized on the basis of proportions of methane, ethane, propane, n–butane, i–butane and carbon dioxide. For discussion of data see text. Note the different scales.*

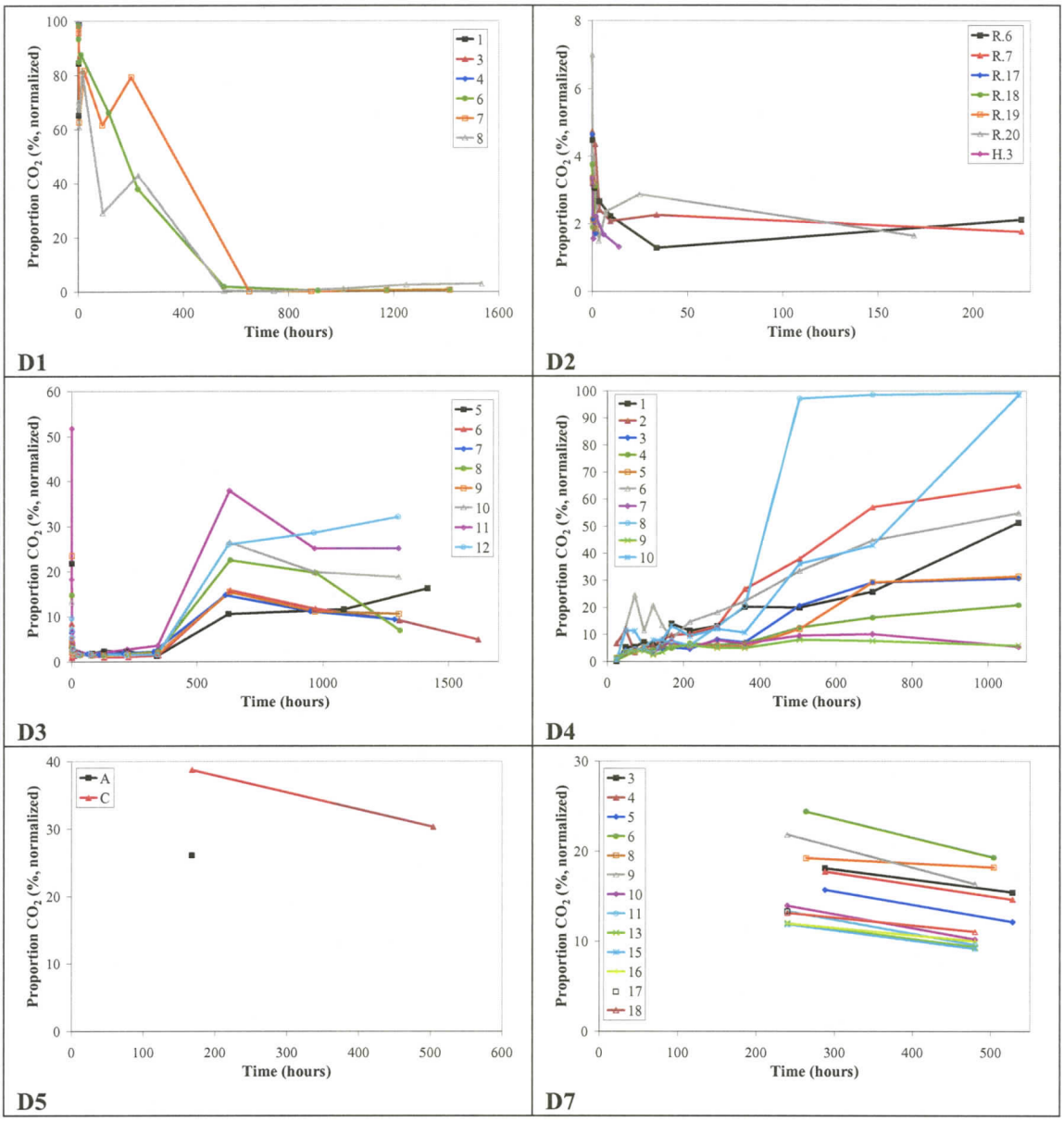


Figure 5.10: *Proportions of carbon dioxide for samples from desorption experiment sample sets D1, D2, D3, D4, D5 and D7 presented versus desorption time. No results are available for desorption experiment sample set D6. Proportions are normalized on the basis of proportions of methane, ethane, propane, n–butane, i–butane and carbon dioxide. For discussion of data see text. Note the different scales.*

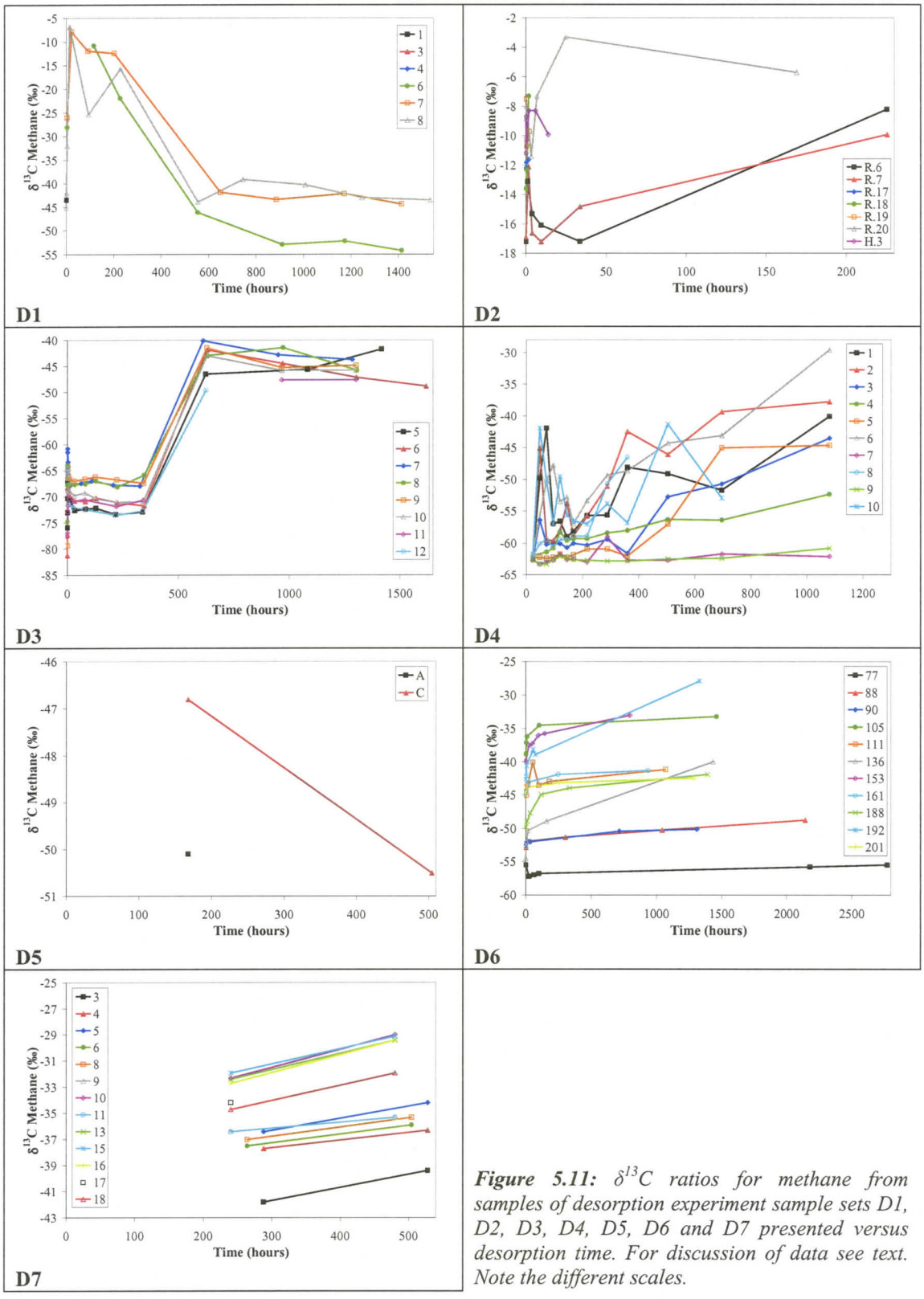


Figure 5.11: *$\delta^{13}C$ ratios for methane from samples of desorption experiment sample sets D1, D2, D3, D4, D5, D6 and D7 presented versus desorption time. For discussion of data see text. Note the different scales.*

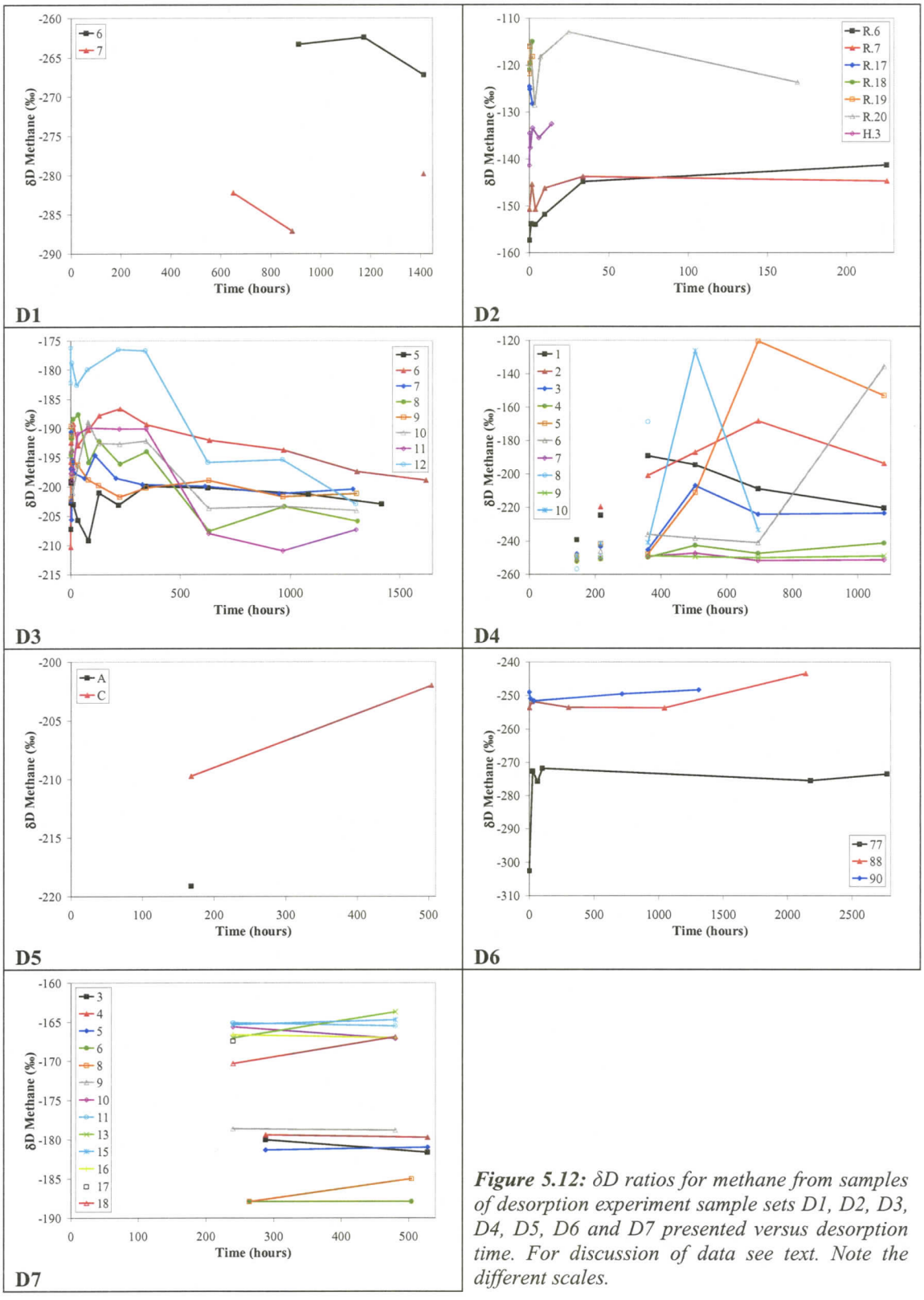


Figure 5.12: *δD ratios for methane from samples of desorption experiment sample sets D1, D2, D3, D4, D5, D6 and D7 presented versus desorption time. For discussion of data see text. Note the different scales.*

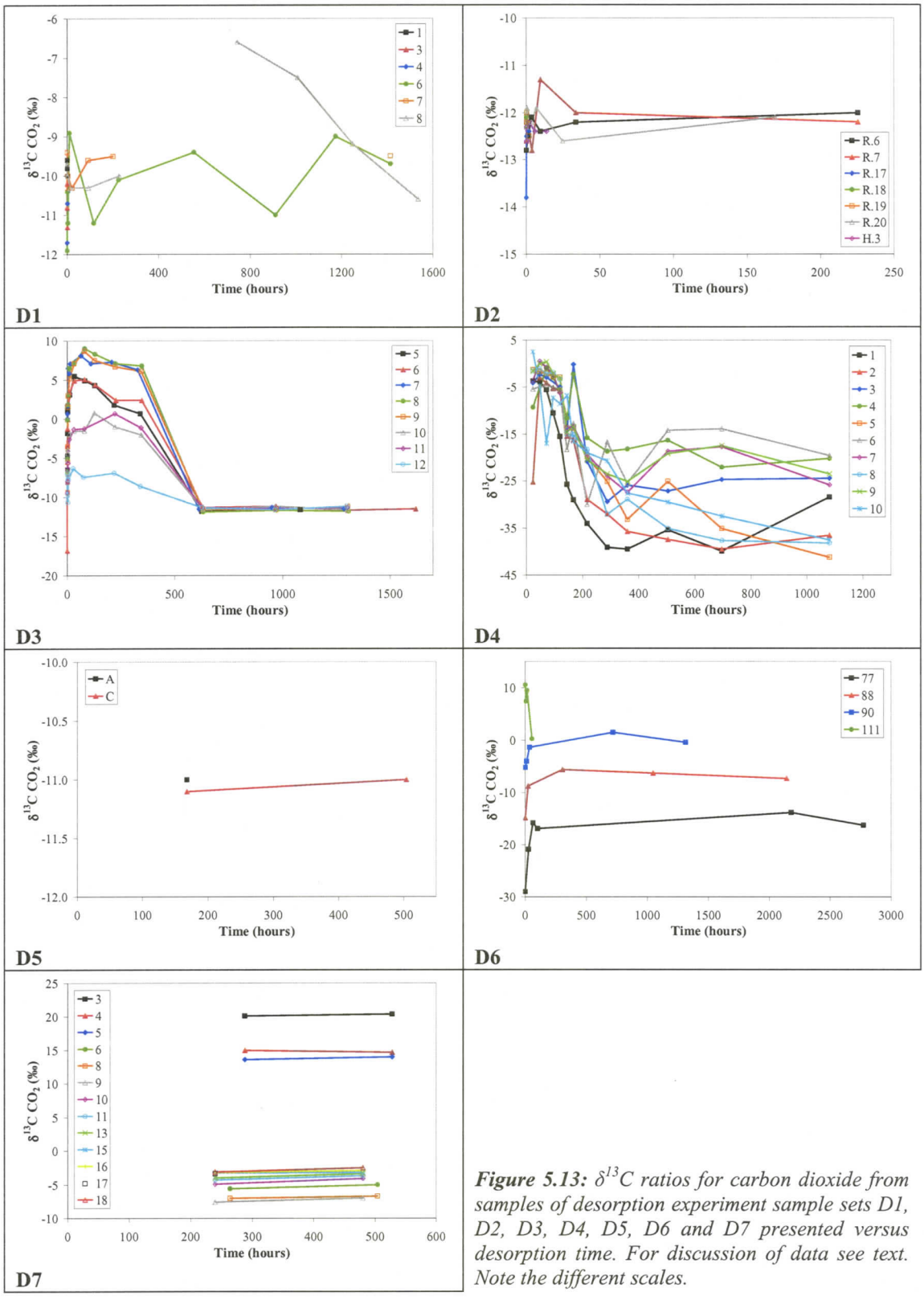


Figure 5.13: *$\delta^{13}C$ ratios for carbon dioxide from samples of desorption experiment sample sets D1, D2, D3, D4, D5, D6 and D7 presented versus desorption time. For discussion of data see text. Note the different scales.*

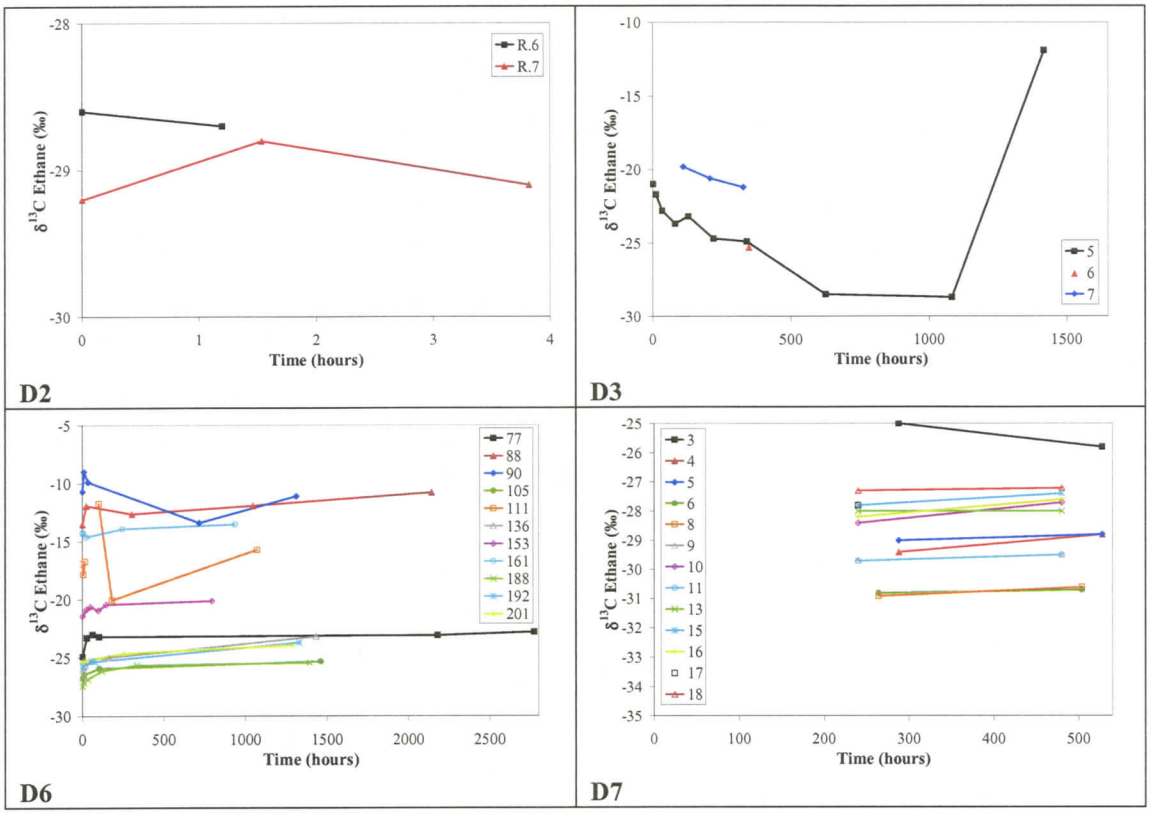


Figure 5.14: *$\delta^{13}C$ ratios for ethane from samples of desorption experiment sample sets D2, D3, D6 and D7 presented versus desorption time. Results for desorption experiment sample sets D1, D4 and D5 are not available. For discussion of data see text. Note the different scales.*

6. Discussion

6.1 Coal–Gas Relationships

Coal is a complex sedimentary rock with a complex geological and geochemical history. Based on coal composition and maturation history, no coal is like any other. Therefore, it can be assumed that methane generated from coal shows a dependency on coal parameters like maturity and maceral composition and on geological parameters like sample depth.

Based on my experimental data dependencies on maturity, maceral composition and depth are tested and, the influence of these parameters on the stable carbon and hydrogen isotope composition of CBM can be determined.

For this purpose maturity, maceral composition and depth are plotted versus the values t_{START}, t_{END} and $t_{WEIGHTED}$ (t_{WGH}) of the carbon and hydrogen isotope composition of methane. The value t_{START} is defined as the $\delta^{13}C$ and δD values for methane available from the earliest sample per well or canister of each sample set. Ideally that should be the first sample taken, but due to the fact that some samples have proportions of methane too low for analysis, especially for δD analysis, the value t_{START} can be the second sample or even a later sample (see Appendix A to J for details). The value t_{END} is defined as the $\delta^{13}C$ and δD values for methane from the latest available sample per well or canister for each sample set. For the value t_{WGH} the individual $\delta^{13}C$ and δD values are set into relation with the proportions of methane of corresponding samples, based on the following relationships:

$$t_{WEIGHTED}\,(\delta^{13}C) = (\delta^{13}C\ a \cdot [CH_4\ a]) + (\delta^{13}C\ b \cdot [CH_4\ b]) + \ldots + (\delta^{13}C\ n \cdot [CH_4\ n])/\ \Sigma\,[CH_4\ a \rightarrow n] \quad (6.1)$$

$$t_{WEIGHTED}\,(\delta D) = (\delta D\ a \cdot [CH_4\ a]) + (\delta D\ b \cdot [CH_4\ b]) + \ldots + (\delta D\ n \cdot [CH_4\ n])/\ \Sigma\,[CH_4\ a \rightarrow n] \quad (6.2)$$

where n equals the number of samples.

6.1.1 Influence of Maturity on Isotope Ratios

Methane generated from organic matter becomes ^{13}C and ^{2}H enriched with increasing maturity (e.g., Rice, 1993; Whiticar, 1994). A higher frequency of chemical bond rupture involving heavy isotopes (^{13}C, ^{2}H) requires higher energy. With increasing maturity, more energy, in the form of heat, is present, high enough for the more frequent rupture of bonds involving heavy isotopes. The rupture of bonds involving heavier isotopes is liberating methane enriched in ^{13}C and ^{2}H.

The gas samples analyzed for this study were taken from coals ranging in maturity between 0.57%R_O (per cent vitrinite reflectance) and 4.41%R_O. Based on this large range, a relationship between $\delta^{13}C$ and δD for methane and vitrinite reflectance can be expected. High mature coals (high %R_O values) should correspond to ^{13}C and ^{2}H enriched methane and low mature coals (low %R_O values) should correspond to ^{12}C and ^{1}H enriched methane.

A relationship between vitrinite reflectance and the carbon isotope composition of methane is apparent (Figure 6.1). The greatest ^{13}C enrichment is found in methane from high mature coals, whereas methane from low mature coals is ^{12}C enriched. However, $\delta^{13}C$ values for methane from

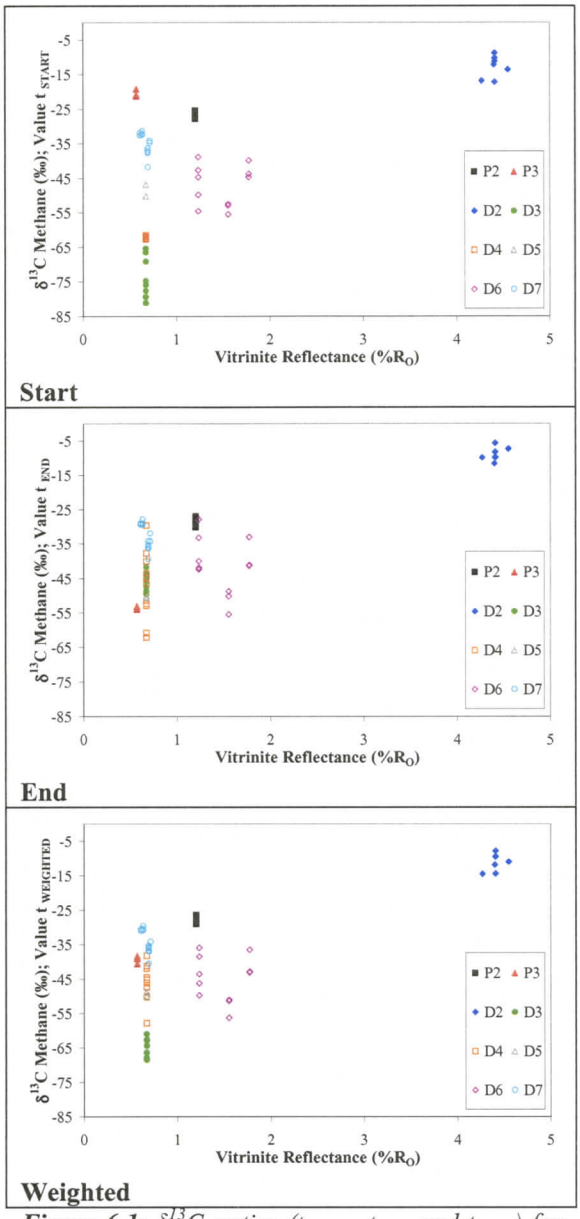


Figure 6.1: *$\delta^{13}C$–ratios (t_{START}, t_{END} and t_{WGH}) for methane from production and desorption experiment samples presented versus maturity (vitrinite reflectance) of the corresponding coals. t_{START} represents the first sample available per well or canister respectively, t_{END} represents the last sample available per well, or canister respectively. For calculation of value t_{WGH} see text. No results are available for sample sets P1 and D1.*

samples of low mature coals show extreme variations and cannot be mathematically described.

A relationship between vitrinite reflectance and the hydrogen isotope composition of methane is also apparent (Figure 6.2). Strong ^{2}H enrichment corresponds to mature coals and ^{1}H enrichment to immature coals. However, δD values for methane from samples of low mature coals show extreme variations and the establishment of an equation to describe this relationship is therefore not possible.

$\delta^{13}C$ and δD for methane show a correlation with vitrinite reflectance. However, the extreme variations within single sample sets for low maturity coals ($\%R_O$ <2) indicate possible alteration of the isotope composition of methane. The responsible processes may have included isotope effects due to oxidation, adsorption, desorption, diffusion, microbial methane generation or the presence of thermogenic gas from different sources. Knowledge about the isotope effects associated with these processes is needed for a more complete consideration of possible relationships between CBM isotope compositions and vitrinite reflectance.

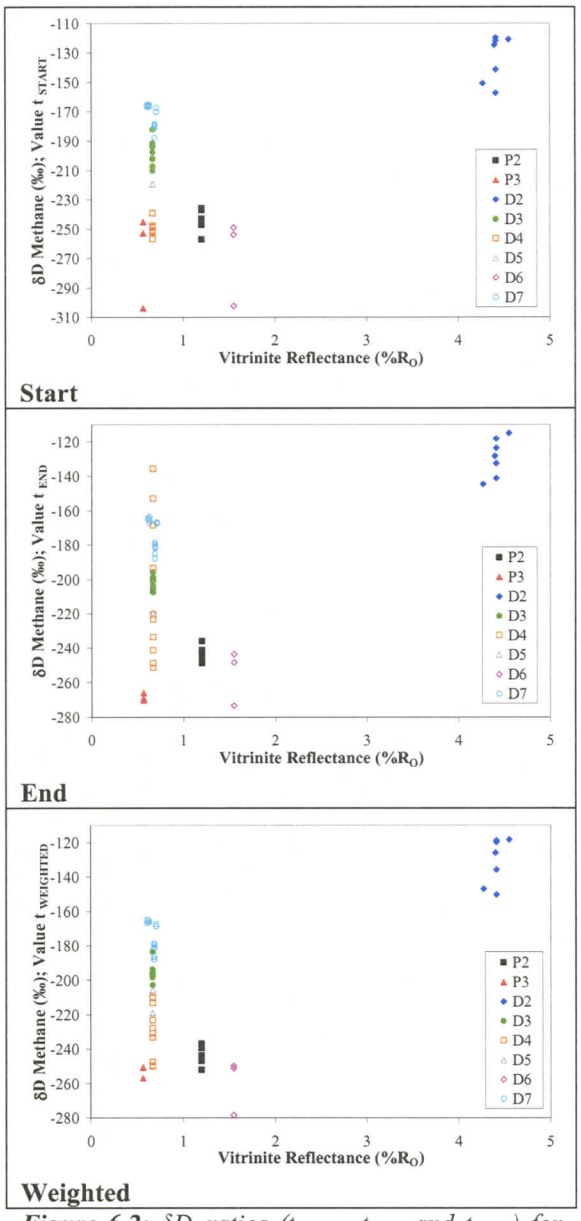


Figure 6.2: *δD–ratios (t_{START}, t_{END} and t_{WGH}) for methane from production and desorption experiment samples presented versus maturity (vitrinite reflectance) of the corresponding coals. t_{START} represents the first sample available per well or canister respectively, t_{END} represents the last sample available per well, or canister respectively. For calculation of value t_{WGH} see text. No results are available for sample sets P1 and D1. Note the different scales.*

6.1.2 Influence of Maceral Composition on Isotope Ratios

Coals of all geological ages have $\delta^{13}C_{coal}$ values ranging between -27‰ and -22‰ (Whiticar, 1996a) and δD_{coal} values ranging from -170‰ to -70‰ (Redding et al., 1980). These values are strongly related to the precursor material of coal, mainly terrestrial plants with $\delta^{13}C_{plant}$ values between -33‰ and -22‰ and δD_{plant} values between -175‰ and -75‰ (Whiticar, 1996a). Coalification influences the isotope composition of the coal, but the pool of available carbon is so huge, that isotope effects are not detectable in the coal itself (Redding et al., 1980). Schwarzkopf (1984) analyzed the stable carbon and hydrogen isotope composition of the macerals vitrinite, liptinite and inertinite, which are shown in Table 6.1. Coalification has no influence on the isotope composition of the different macerals (Schwarzkopf, 1984) and, the bulk isotope composition of coal, depends on the $\delta^{13}C$ values of the macerals present in the coal.

Table 6.1: *Stable carbon and hydrogen isotope ratios of macerals vitrinite, liptinite and inertinite. Values from Schwarzkopf (1984).*

Maceral	$\delta^{13}C$ (‰)	δD (‰)
Vitrinite	-23.4	-87
Liptinite	-23.7	-99.2
Inertinite	-23.9	-109

That leads to the question as to whether the $\delta^{13}C$ and δD differences between the different macerals influence or control the isotope composition of CBM as was mentioned by Rice (1993). It could be assumed that a liptinite–rich coal would generate methane more enriched in ^{12}C and ^{1}H, than a liptinite–poor coal. Similar an inertinite–rich coal would generate methane more enriched in ^{13}C and ^{2}H, than inertinite–poor coal. The maceral compositions of coals in this study are shown in Table 6.2.

Table 6.2: Minimum and maximum amounts of the macerals vitrinite, liptinite and inertinite in coals considered in this study.

Maceral	Minimum Amounts (%)	Maximum Amounts (%)
Vitrinite	68.9	87.6
Liptinite	0.1	6.9
Inertinite	16.2	31.0

Maceral composition data are not available for sample sets P1, P2, D1 and D2.

6.1.2a Vitrinite

Neither for $\delta^{13}C$ (Figure 6.3) nor for δD (Figure 6.4) could a relation with the amount of vitrinite be established. The stable carbon and hydrogen isotope ratios of methane are not dependent on the relative abundance of vitrinite. Samples from different sample sets behaved completely different. The strong variations within the different sample sets (Figures 6.3 and 6.4) indicate that other processes have altered the isotopic composition of methane. These processes may include oxidation, adsorption, desorption, diffusion, as well as mixing with microbial gas or thermogenic gas from other sources. Knowledge of the isotope effects related to these processes is needed. The incorporation of these fractionation effects may reveal a relation between amounts of vitrinite and $\delta^{13}C$, respectively δD.

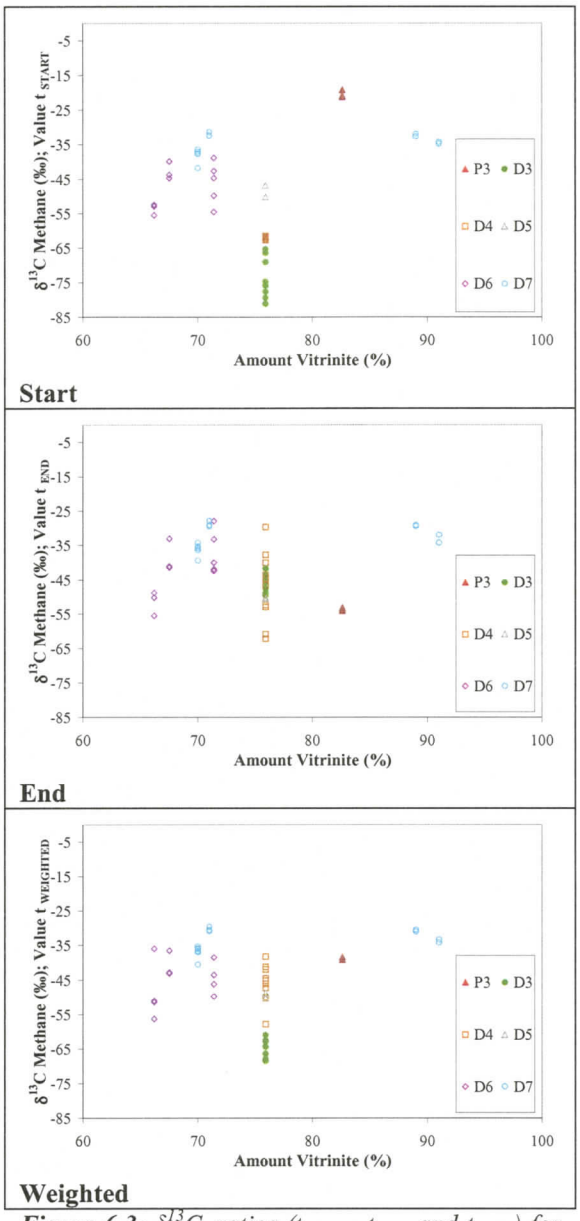


Figure 6.3: *$\delta^{13}C$–ratios (t_{START}, t_{END} and t_{WGH}) for methane from production and desorption experiment samples presented versus amount of vitrinite in the corresponding coals. t_{START} represents the first sample available per well or canister respectively, t_{END} represents the last sample available per well, or canister respectively. For calculation of value t_{WGH} see text. No results are available for sample sets P1, P2, D1 and D2.*

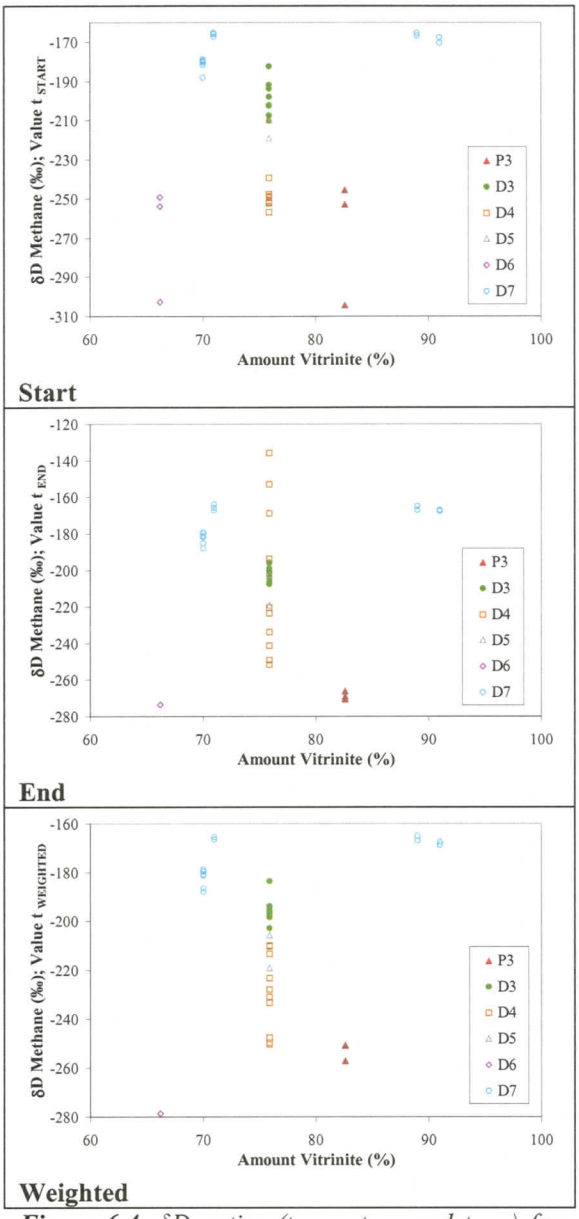


Figure 6.4: *δD–ratios (t_{START}, t_{END} and t_{WGH}) for methane from production and desorption experiment samples presented versus amount of vitrinite in the corresponding coals. t_{START} represents the first sample available per well or canister respectively, t_{END} represents the last sample available per well, or canister respectively. For calculation of value t_{WGH} see text. No results are available for sample sets P1, P2, D1 and D2. Note the differences in scale.*

6.1.2b Liptinite

A linear correlation of $\delta^{13}C$ of methane with the amount of liptinite in the corresponding coals is observed for t_{START} (Figure 6.5); the only exception is sample set D6. A similar, although less pronounced relationship as observed for $\delta^{13}C$, is also observed for δD with the exceptions of sample sets P3 and D6 (Figure 6.6).

Early values (t_{START}) of $\delta^{13}C$ and δD for methane show the expected trend of ^{12}C, respectively ^{1}H enrichment with increasing amount of liptinite in the coal. For $\delta^{13}C$ this trend can not be observed for t_{END} and t_{WGH}, whereas for δD the trend still is observable for t_{WGH}, but not for t_{END}. Because of strong variations for $\delta^{13}C$ and δD for methane the described trends could be the result of other processes alterating the stable carbon and hydrogen isotope ratios. These effects may also explain the increased variation within sample sets with increasing liptinite, because sample sets D3, D4 and D5 have the highest amounts of liptinite of all considered coals. Strong variations are present for $\delta^{13}C$ and δD in almost all sample sets, again indicating the likely presence of processes, which altered the isotope ratios of methane.

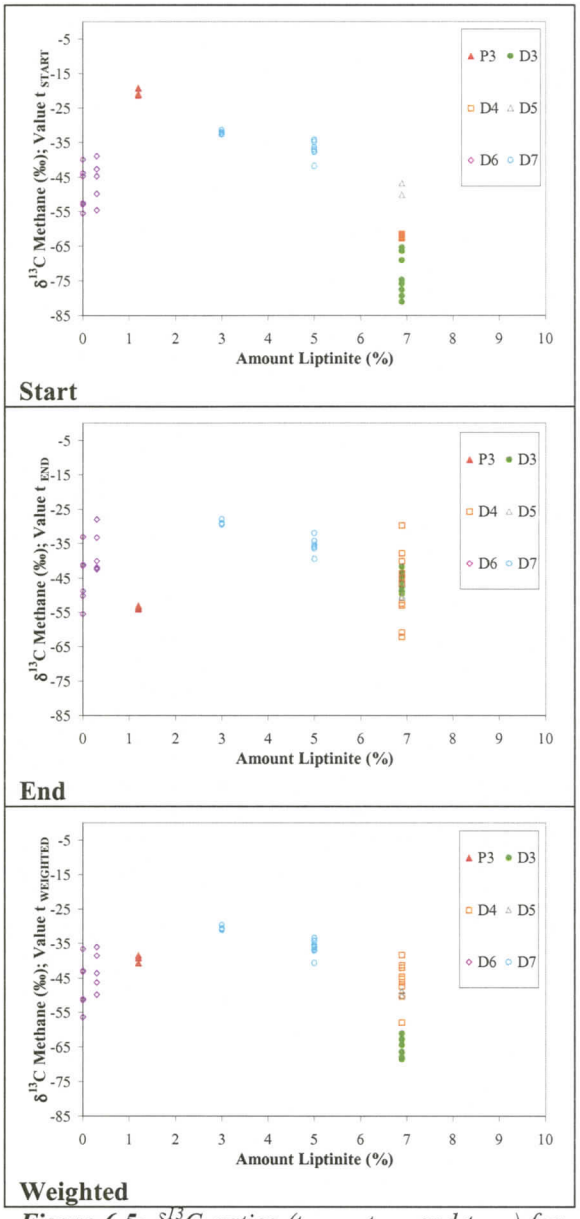


Figure 6.5: *$\delta^{13}C$–ratios (t_{START}, t_{END} and t_{WGH}) for methane from production and desorption experiment samples presented versus amount of liptinite in the corresponding coals. t_{START} represents the first sample available per well or canister respectively, t_{END} represents the last sample available per well, or canister respectively. For calculation of value t_{WGH} see text. No results are available for sample sets P1, P2, D1 and D2.*

Sample set D7 shows the largest variation in the amount of liptinite of all considered coals (3% to 5%) and even within this sample set ^{12}C enrichment correlates with increasing amounts of liptinite. The highest ^{12}C enrichment, from samples of sample set D3, correlates to the highest amount of liptinite (6.9%) of all considered coals. ^{12}C enrichment due to other processes cannot, however be ruled out. Especially when considering t_{START} values for sample set D3 it is obvious that the variation in $\delta^{13}C$ for methane is extremely large. When including sample sets D4 and D5 from the same basin with identical amounts of liptinite, the variation becomes even larger (Figure 6.5). The establishment of an equation to describe the observed trend is not possible, because of the huge variations of $\delta^{13}C$ observed within the individual sample sets.

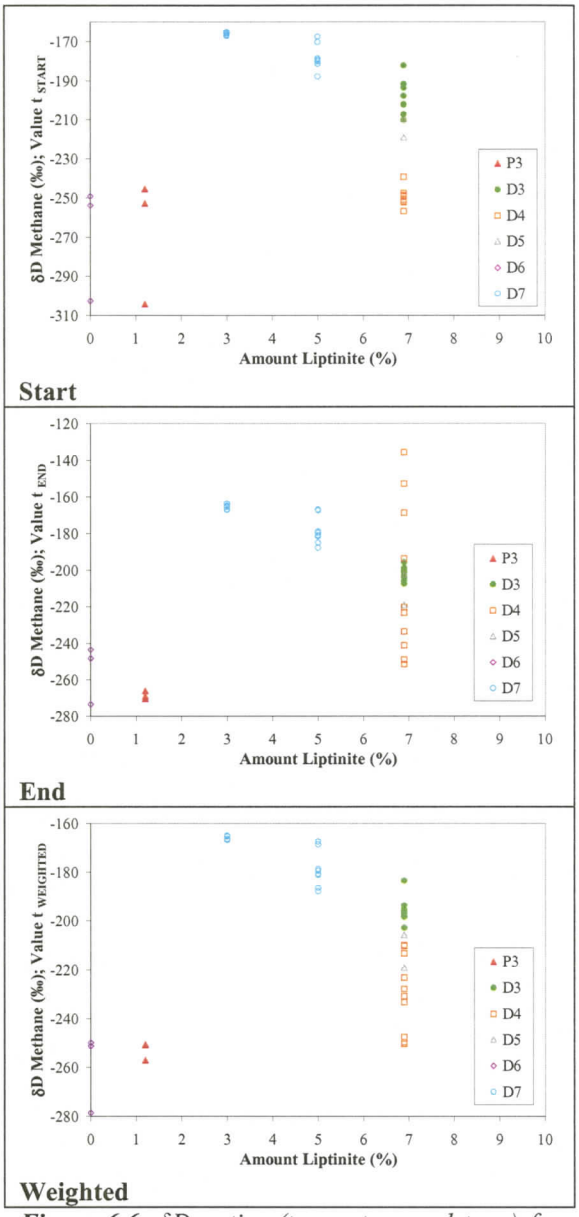


Figure 6.6: *δD–ratios (t_{START}, t_{END} and t_{WGH}) for methane from production and desorption experiment samples presented versus amount of liptinite in the corresponding coals. t_{START} represents the first sample available per well or canister respectively, t_{END} represents the last sample available per well, or canister respectively. For calculation of value t_{WGH} see text. No results are available for sample sets P1, P2, D1 and D2. Note the differences in scale.*

6.1.2c Inertinite

The stable carbon (Figure 6.7) and stable hydrogen isotope ratios (Figure 6.8) are independent on the amount of inertinite. Even within sample set D7, with a variation in amounts of inertinite of 22%, no inertinite–isotope dependencies are observed.

No relationship between $\delta^{13}C$, δD and the amounts of inertinite were observed. Extreme variations of $\delta^{13}C$ and δD, indicate a possible alteration of the stable carbon and hydrogen isotope ratios for methane as the result of secondary processes.

6.1.3 Influence of Depth on Isotope Ratios

Coal rank increases with increasing depth or burial (Taylor et al., 1998). Increase in temperature with depth exerts an isotope effect on the products generated from organic matter. If heat capacity is a constant, a temperature increase represents an increase in energy. This increase can enhance the rupture of chemical bonds in organic matter, e.g., peat and coal, leading to the generation and liberation of water, methane and other volatiles. In addition, it can be expected that methane generated at greater depth is more enriched in ^{13}C and ^{2}H than methane generated at shallower depths (Friedrich & Jüntgen, 1972). No constant geothermal gradient can be assumed for sample sets and no bottom–hole temperatures are available, resulting in the fact that a direct comparison of the different sample sets is not possible. Another complication is that the present depth of a coal seam does not necessarily represent the maximal depth of burial the coal has experienced. Therefore, the present depth does not

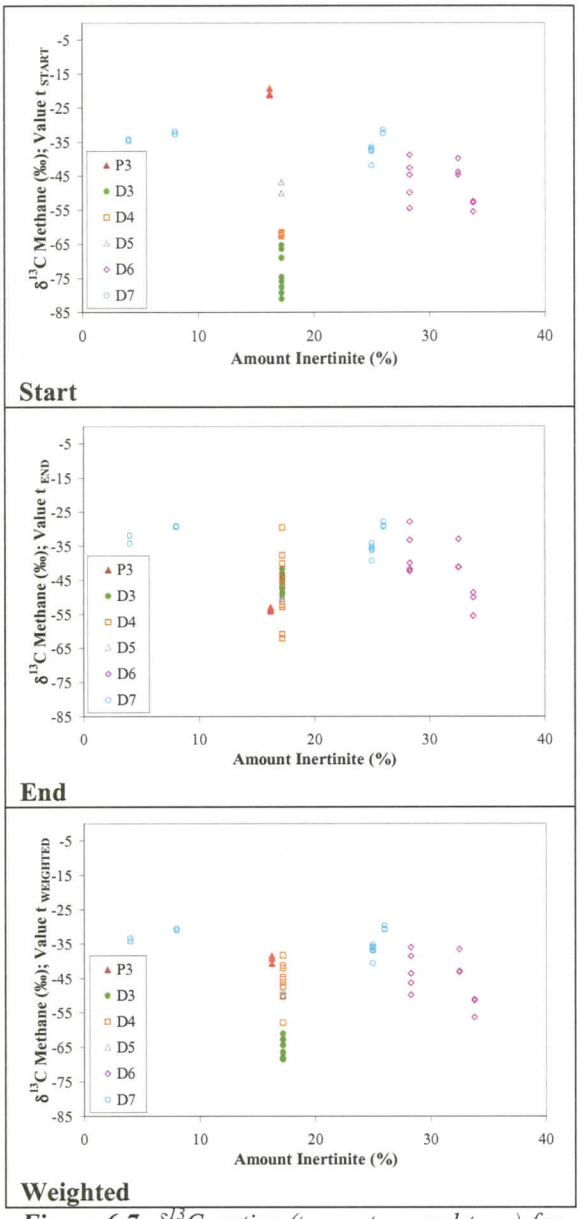


Figure 6.7: *$\delta^{13}C$–ratios (t_{START}, t_{END} and t_{WGH}) for methane from production and desorption experiment samples presented versus amount of inertinite in the corresponding coals. t_{START} represents the first sample available per well or canister respectively, t_{END} represents the last sample available per well, or canister respectively. For calculation of value t_{WGH} see text. No results are available for sample sets P1, P2, D1 and D2.*

necessarily have to correlate with $\delta^{13}C$ and δD values for methane generated from this coal. In the case of an uplifted coal seam, the ^{13}C and ^{2}H enrichment in methane would be expected to be higher than the present depth would imply.

Another factor which could influence and alter the isotope composition of methane at shallower depths is the presence of primary or secondary microbial methane. Primary generation of microbial gas (see Chapter 2.2.1 for more details) takes place early during diagenesis (Rooney et al., 1995). Microbial gas generation will be inhibited when temperatures cross a certain threshold. Depending on the geothermal gradient, this geopasteurization depth will be reached in different depths. Secondary generation of microbial gas can take place in every coal, regardless of coal rank, when the coals are uplifted to shallower depths were the present conditions allow microbial activity (Scott, 1993).

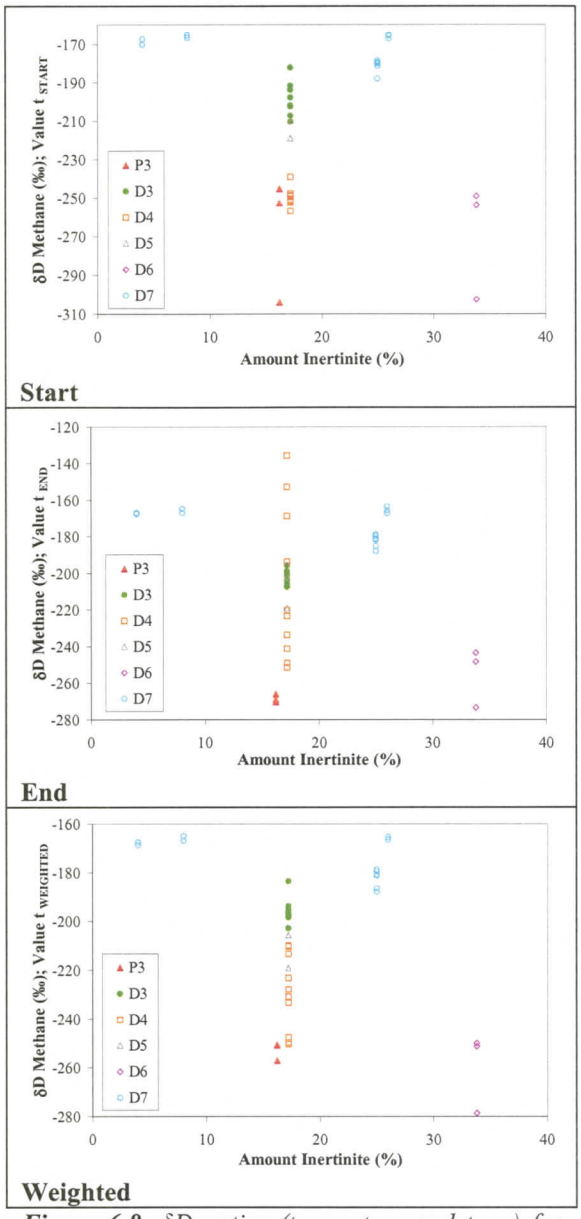


Figure 6.8: *δD–ratios (t_{START}, t_{END} and t_{WGH}) for methane from production and desorption experiment samples presented versus amount of inertinite in the corresponding coals. t_{START} represents the first sample available per well or canister respectively, t_{END} represents the last sample available per well, or canister respectively. For calculation of value t_{WGH} see text. No results are available for sample sets P1, P2, D1 and D2. Note the differences in scale.*

Beside these complications and exceptions, a relationship between present day depth and $\delta^{13}C$ and δD for methane can be assumed with ^{12}C and ^{1}H enriched methane correlating to shallow depths and ^{13}C and ^{2}H enriched methane correlating to greater depths. Strong ^{12}C and ^{1}H enrichment should be expected in the methane when microbial gas generation is present. The range of present depth for all considered

scenarios is between 10m and 1551m. Depth data are not available for sample sets P1 and D6.

For $\delta^{13}C$ (Figure 6.9) and δD (Figure 6.10) of methane no consistent trend versus depth is observed. Therefore, depth appears to have no influence on the stable carbon and hydrogen isotope ratios of methane.

^{12}C enrichments in methane are observed in samples from shallow depths (Figure 6.9). This possibly indicates the presence of microbial methane. Only methane extracted from very mature coals ($\%R_O \geq 4$; sample set D2) do not show this indication (Figure 6.9). Alternatively, the methane isotope ratios are altered by the presence of other processes.

The δD range of microbial methane is between -400‰ and -150‰, whereas thermogenic methane ranges from ca. -300‰ to ca. -100‰ (Whiticar, 1996b). Interestingly, when applying a δD value of -150‰ as an upper boundary for the occurrence of microbial methane, almost all samples fall in the field, which indicates the possible presence of microbial generated methane (more negative than -150‰; Figure 6.10). Alternatively, the observed ^{1}H enrichment for methane may have resulted from an isotope effect related to other processes. The only exception is methane

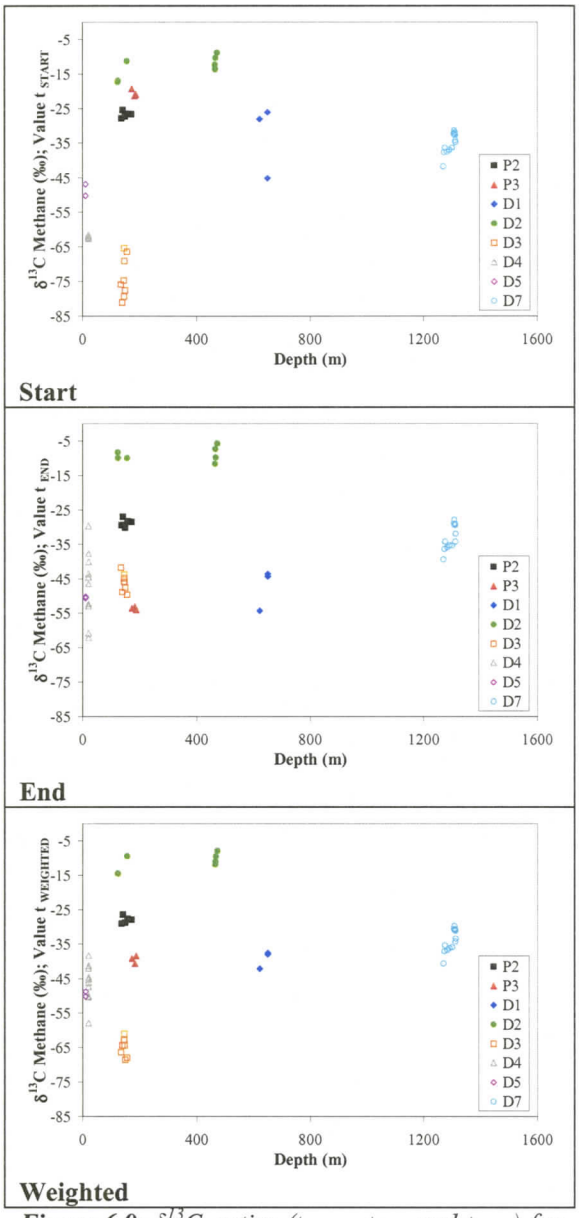


Figure 6.9: *$\delta^{13}C$–ratios (t_{START}, t_{END} and t_{WGH}) for methane from production and desorption experiment samples presented versus depth of the corresponding coals. t_{START} represents the first sample available per well or canister respectively, t_{END} represents the last sample available per well, or canister respectively. For calculation of value t_{WGH} see text. No results are available for sample sets P1 and D6.*

from sample set D2 coals (Figure 6.10), which are extremely mature with values of 4%R_O and higher. Sample set D2 shows the highest ^2H enrichment in methane (Figure 6.10).

6.2 Gas Classification

For conventional Kerogen Type I and Type II, gas classifications are possible and widely used for the characterization of gas generation pathways and the identification of secondary processes like mixing, oxidation and migration. Because coal can be a source and reservoir rock (Levine, 1993; Hunt, 1995), it is commonly assumed that CBM is of thermogenic origin, generated from the coal itself only (Jüntgen & Karweil, 1966a; van Heek et al., 1971; Jüntgen & Klein, 1975; Das et al., 1991; Rice, 1993; Flores, 1998) with possible admixtures of early and late microbial generated methane (Rice, 1992, 1993; Aravena et al., 2003; Kotarba & Lewan, 2004). The presence of thermogenic hydrocarbons generated from other sources that have migrated into a coal seam cannot be ruled out. Niemann et al. (2005), found indications in CBM gases for gas generated from a Kerogen Type II shale (see Chapter 6.2.2b).

It is uncertain if the geochemical approach for gas characterization and classification of conventional Kerogen Type

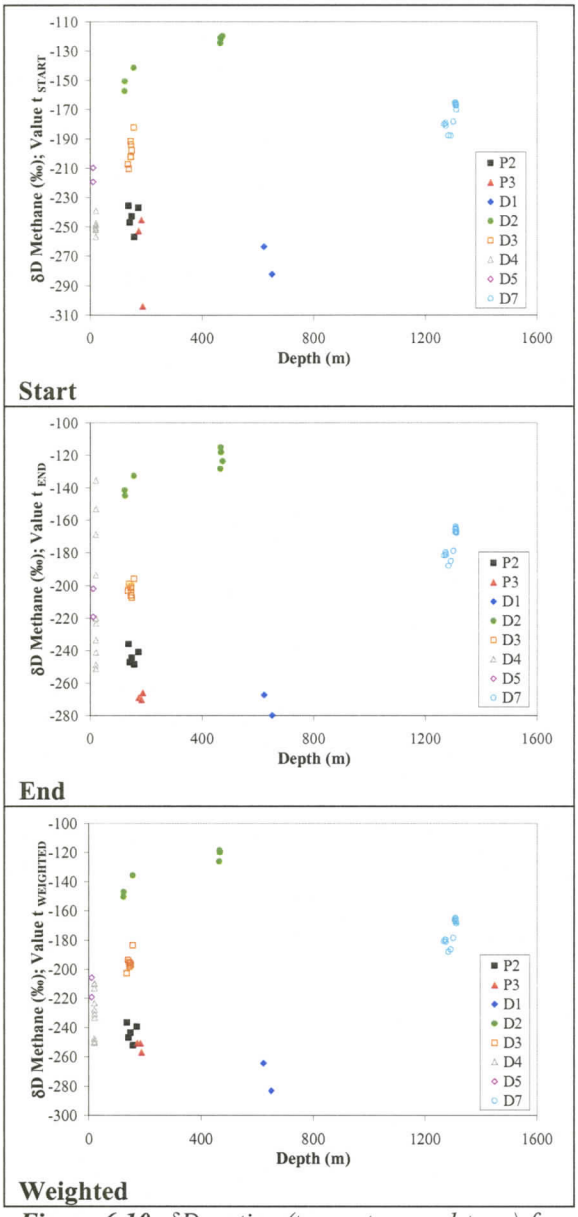


Figure 6.10: *δD–ratios (t_{START}, t_{END} and t_{WGH}) for methane from production and desorption experiment samples presented versus depth of the corresponding coals. t_{START} represents the first sample available per well or canister respectively, t_{END} represents the last sample available per well, or canister respectively. For calculation of value t_{WGH} see text. No results are available for sample sets P1 and D6. Note the differences in scale.*

I and Type II, i.e., thermogenic gas, can also be applied to CBM. This includes the questions of gas origins and the identification, separation and characterization of secondary processes like mixture, oxidation, adsorption, desorption, migration and diffusion. This chapter uses chemical composition and stable isotope signature to classify the CBM gases.

6.2.1 Gas Origin: Primary Effects

6.2.1a Composition

Gases generated from humic coals during coalification, include methane, higher gaseous hydrocarbons, carbon dioxide, carbon monoxide, nitrogen and hydrogen sulphide (Hunt, 1995). Only the most abundant species, i.e., methane (CH_4), higher gaseous hydrocarbons (C_{2+}) and carbon dioxide (CO_2) are considered here. CH_4 is quantitatively the most important gas generated from coal. Generally there are only small contributions of C_{2+} and CO_2 (Rice, 1993; Hunt, 1995). Kopp et al. (2000) reported general proportions of C_{2+} in CBM of only a few per cent. Gas concentrations in coals reported by Jüntgen and Karweil (1966a) and Rice (1993) are shown in Table 6.3.

Table 6.3: *Proportions of methane (CH_4), higher hydrocarbons (C_{2+}) and carbon dioxide (CO_2) in gases encountered in coal gases. Data from Jüntgen and Karweil (1966a) represent selected bituminous coals of Germany. Data from Rice (1993) represent gases from CBM basins worldwide. For Rice (1993): C_{2+} maximum from Upper Carboniferous of Germany; CO_2 maximum from Upper Carboniferous of Poland.*

Gas Species	Jüntgen and Karweil (1966a)	Rice (1993)
CH_4	Up to 100 Vol.%	n/a
C_{2+}	Up to 15 Vol.%	0% to 70.5%
CO_2	Up to 90 Vol.%	0% to 99%

The generation of thermogenic CH_4 begins at temperatures of ca. 70°C (Hunt, 1995), which correlates to the coal rank of high–volatile bituminous and with vitrinite reflectance values of less than 0.6%R_O (Rice, 1993). CH_4 generation becomes quantitatively important at temperatures above 110°C (van Heek et al., 1971), correlating to the medium–volatile bituminous coal rank and 1.3%R_O to 1.4%R_O (Tissot & Welte,

1978; Hunt, 1995). At temperatures of 150°C, the maximum of thermogenic CH_4 generation is reached (Rice, 1993; Hunt, 1995), although generation continues up to temperatures of above 200°C (Hunt, 1995). The generation of C_{2+} commences around 70°C, but is essentially over at temperatures of above 130°C (Hunt, 1995), corresponding to 1.5%R_O to 1.6%R_O. The peak generation of CO_2 occurs at maturities of 1.3%R_O to 1.4%R_O, i.e., ca. 110°C (Tissot & Welte, 1978; Hunt, 1995). Generation is concluded before the onset of the anthracite stage, i.e., ca. 170°C (Taylor et al., 1998).

The following gas compositions can be predicted for coals of different maturity (temperature ranges mentioned below from Hunt, 1995 and Taylor et al., 1998):

1. Gases encountered in low rank coals, i.e., lignite and sub–bituminous coal (%R_O >0.6%; temperature below ca. 70°C), should contain high proportions of CO_2 and low proportions of C_{2+}. Large proportions of CH_4 should be of microbial origin (see Chapter 6.2.2a).
2. Gases encountered in medium rank coals, i.e., bituminous coal (maturity 0.6%R_O to ca. 1.9%R_O; temperature ca. 70°C to 170°C), should contain large proportions of thermogenic CH_4, and higher abundances of C_{2+} and CO_2. Depending on the adsorption history, gases from these coals may also contain earlier generated microbial CH_4 that was adsorbed onto the coal.
3. Gases encountered in high rank coals, i.e., semi–anthracite and anthracite (maturity ca. 1.9%R_O to >4%R_O; temperature 170°C to 250°C), should contain large proportions of thermogenic CH_4 and only small contributions of C_{2+} and CO_2. Based on the adsorption history, these gases can reach higher proportions if adsorbed on the coal earlier during the coalification process. This could also include microbial generated CH_4.

It is important to emphasize the interpretative challenges related to the gas adsorption capacity of coal. Due to the inherent retentive capacity of coal, mixtures between gases of different origins (thermogenic, microbial) and mixtures of gases generated at different stages of the coalification process are possible (Whiticar, 1996a).

Based on the analyzed samples, proportions of CH_4, CO_2 and C_{2+} show no correlation with the maturity of the different coals. Therefore the above mentioned

assumptions are not justified, or more likely, the gas compositions of the analyzed samples do not represent the gas composition of the final stage of coalification, but represent a mixture of gases generated during the entire or during parts of the coalification process, which were retained by the coal due to adsorption. Therefore an accurate estimation of gases expected in coals of certain maturities is not possible.

In Table 6.4 the average maturities ($\%R_O$) for the coals in this study are shown in relation to the average gas composition (CH_4, C_{2+} and CO_2) and the average amounts of liptinite. Maturity values are only available for sample sets P2, P3, D2, D3, D4, D5, D6 and D7.

Table 6.4: *Average maturities of coals considered for the different sample sets in relation to average gas composition and average amounts of liptinite in the considered coals. Proportions are normalized on the basis of proportions of methane, ethane, propane, n–butane, i–butane and carbon dioxide. Ethane, propane, n–butane and i–butane are combined under the term C_{2+} (higher hydrocarbons). norm. = normalized.*

Sample Set	Average Maturity ($\%R_O$)	Average Proportions			
		CH_4 (%, norm.)	C_{2+} (%, norm.)	CO_2 (%, norm.)	Liptinite (%)
P3	0.57	96.1	0.45	3.41	1.2
D7	0.61	77.3	8.18	14.5	4.2
D3	0.67	92.3	0.27	7.47	6.9
D4	0.67	86.6	0.09	13.3	6.9
D5	0.67	67.2	1.09	31.8	6.9
P2	1.20	98.7	0.01	1.34	n/a
D6	1.46	97.5	2.49	n/a	0.1
D2	4.41	96.8	0.43	2.80	n/a
P1	n/a	90.4	0.32	9.28	n/a
D1	n/a	44.3	1.86	53.9	n/a

Methane

High proportions of CH_4 are found for low, medium and high rank coals. Proportions of over 70% CH_4 are found for all sample sets with the exceptions of sample sets D1 and D5 (Table 6.4 and Figure 6.11). Coals for sample set D1 were recovered during exploration drilling, but this well was shut down shortly after the completion of the desorption work, due to insufficient recoverable CBM. Gas sampling and following analyzes indicated problems related to the apparatus used on the wellsite for the

volumetric determination of desorbed CBM. Because of confidentiality reasons, these problems cannot be discussed here in more detail.

Coals for sample set D5 were recovered underground from an exposed coal face. A fresh surface was produced ca. 50cm to ca. 60cm behind the old face. However, because the old surface had been exposed to the atmosphere for a substantial amount of time (S. Gardener, communication), gas may have been lost. This assumption is supported by the fact that almost no gas was recovered from the desorption canisters. Sample set D3 was collected during exploration drilling in the same coal basin in close proximity to the mine site, indicating the presence of CBM in the coals. Another indication for gas loss is the elevated proportion of CO_2, which could be explained by later stage desorption.

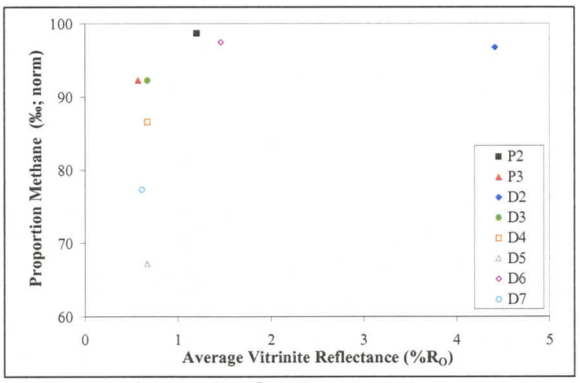


Figure 6.11: *Methane proportions versus maturity (%R_O) of the corresponding coals for production sample sets P2 and P3 and for desorption experiment sample sets D2, D3, D4, D5, D6 and D7. No data are available for sample sets P1 and D1. Shown are averaged proportions and maturities per well, respectively canister. Proportions are normalized on the basis of methane, ethane, propane, n–butane, i–butane and carbon dioxide proportions.*

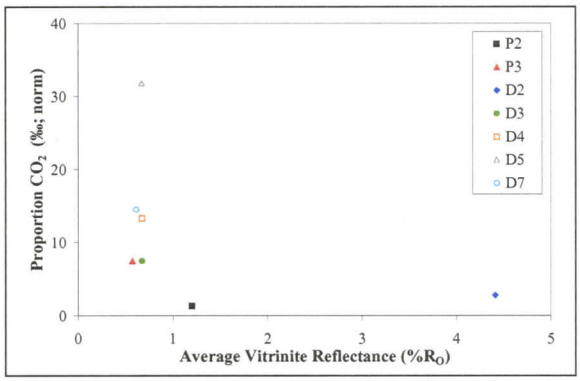


Figure 6.12: *Proportions of carbon dioxide versus maturity (%R_O) of the corresponding coals for production sample sets P2 and P3 and for desorption experiment sample sets D2, D3, D4, D5 and D7. No data are available for sample sets P1, D1 and D6. Shown are averaged proportions and maturities per well, respectively canister. Proportions are normalized on the basis of proportions of methane, ethane, propane, n–butane, i–butane and carbon dioxide.*

Carbon Dioxide

Maturity appears to have little if any dependency on carbon dioxide. Coals with maturites of ≤1.20%R_O have proportions of CO_2 between 3.41% and 14.5% (except sample set D5; Table 6.4 and Figure 6.12), whereas the proportions for coals with maturities ≥1.46%R_O have proportions

between 1.34% and 2.8%. These differences are not significant. For example comparing sample set P3 from low rank coals (0.57%R_O) with sample set D2 from high rank coals (4.41%R_O), the difference is only 0.61%.

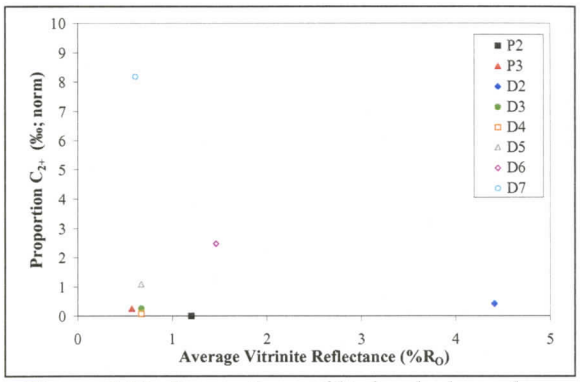


Figure 6.13: *Proportions of higher hydrocarbons (ethane, propane, n–butane and i–butane) versus maturity (%R_O) of the corresponding coals for production sample sets P2 and P3 and for desorption experiment sample sets D2, D3, D4, D5, D6 and D7. No data are available for sample sets P1 and D1. Shown are averaged proportions and maturities per well, respectively canister. Proportions are normalized on the basis of proportions of methane, ethane, propane, n–butane, i–butane and carbon dioxide.*

Higher Hydrocarbon Gases

C_{2+} content shows no relationship on maturity. Hydrogen–rich coals, i.e., those with higher amounts of liptinite, are prone to the generation of higher hydrocarbons (Hunt, 1991; Rice, 1993). Therefore, a correlation between high liptinite content and high C_{2+} abundances should be expected for liptinite rich coals.

C_{2+} proportions are low with values below 1.9% (Table 6.4 and Figure 6.13). The exceptions are sample sets D6 and D7 with 2.49% and 8.18% of C_{2+}. A cross–plot of liptinite versus C_{2+} shows no clear relationship (Figure 6.14). Based on the low amounts of liptinite in sample sets D6 and D7, the high proportions of C_{2+} are not likely to be generated from these coals alone. Both coal systems are underlain by thick organic rich shale sequences (Kerogen Type II) and an admixture of gas generated form these shales is a likely scenario for the explanation of these high proportions of C_{2+} (Chapter 6.2.2b).

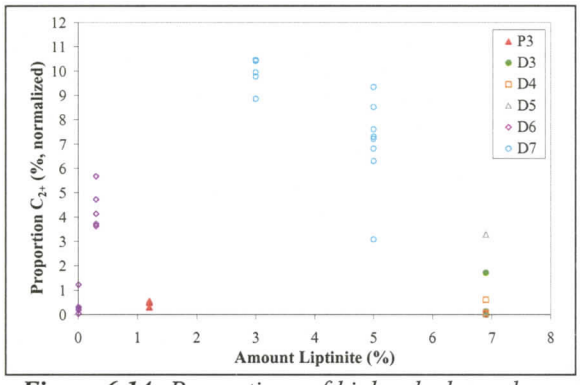


Figure 6.14: *Proportions of higher hydrocarbons (C_{2+}; ethane, propane, n–butane and i–butane) presented versus proportions of liptinite in the corresponding coals. Proportions are normalized on the basis of proportions of methane, ethane, propane, n–butane, i–butane and carbon dioxide. No results are available for sample sets P1, P2, D1 and D2.*

6.2.1b $\delta^{13}C$ (CH_4) Estimation

For most samples in this study the maturities of the source rocks are known and therefore, $\delta^{13}C$–$\%R_O$ relationships can be applied for an estimation of the primary unaltered carbon isotope composition for methane, ethane and propane generated from the considered source rocks.

The $\delta^{13}C$–$\%R_O$ relationships presented by Berner and Faber (1996) are empirical, based on data derived from dry, open–system pyrolysis experiments. The calibration limits for the relationships by Berner and Faber (1996) are given in Table 6.5.

Table 6.5: *Calibration limits for the relationships between maturity and the stable carbon isotope ratios of methane, ethane and propane by Berner and Faber (1996).*

Species	Calibration Minimum ($\%R_O$)	Calibration Maximum ($\%R_O$)
Methane	0.6	2.5
Ethane	0.6	2.0
Propane	0.6	1.8

The relationships for methane, ethane and propane generated from a Kerogen Type III source rock (Equations 2.16 for methane, 2.17 for ethane and 2.18 for propane) allow the estimation of $\delta^{13}C$ values for instantaneous methane, ethane and propane, whereby instantaneous refers to the composition of gases generated at any given maturity (Berner & Faber, 1996). This is in contrast with cumulative gas. Gases encountered in coals do not represent ideal instantaneous accumulations, because of adsorption and retention of gases generated at different maturities. An approach using cumulative values could also be in error, because the relative proportions of the different gas species lost and stored during the coalification and burial/uplift histories are not known. It has to be assumed that gas is lost during coalification, burial and uplift, because during coalification more gas may be generated then can be adsorbed by the coal. Additionally not all gas present in a coal can be extracted for analyzes and residual gas will remain adsorbed onto the coal (see Chapter 2.4). Despite these difficulties a comparison between calculated and analyzed values is reasonable and may provide information about direction

and magnitude of secondary processes, altering the primary isotope compositions of methane, ethane and propane.

The relationships from Berner and Faber (1996) for a Kerogen Type III are graphically shown in Figure 6.15. The estimated isotope compositions of methane, ethane and propane for the maturities of the considered coals are given in Table 6.6. A more detailed presentation in regard to the different sample sets is given in Appendix K. The lowest maturity encountered in the considered coals is 0.57%R_O (sample set P3) and the highest maturity is 4.51%R_O (sample set D2). These sample sets will not be included in the following discussion, because they are outside the calibration limits for the $\delta^{13}C$–%R_O relationships by Berner and Faber (1996).

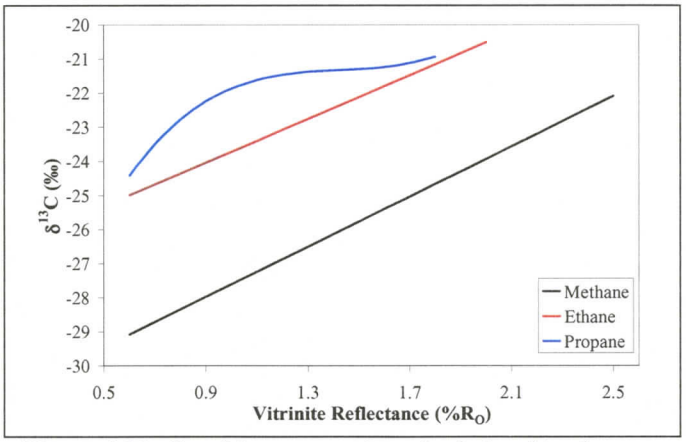


Figure 6.15: *Graphic presentation of relationships between the maturity (vitrinite reflectance) of a Kerogen Type III source rock with the stable carbon isotope composition ($\delta^{13}C$) of methane, ethane and propane generated from this type of source rock. See text for equations and details (modified from Berner and Faber, 1996).*

Table 6.6: *Estimated $\delta^{13}C$ values for methane, ethane and propane, based on maturities of coals considered for all ten sample sets. Calculations were performed by using maturity–$\delta^{13}C$ relationships by Berner and Faber (1996). Maturities below 0.6%R_O and above 2.5%R_O are not included, because the applied maturity–$\delta^{13}C$ relationships by Berner and Faber (1996) are not calibrated for these maturity ranges.*

Maturity (%R_O)	$\delta^{13}C$ Methane (‰)	$\delta^{13}C$ Ethane (‰)	$\delta^{13}C$ Propane (‰)
0.61	-29.0	-25.0	-24.3
0.63	-29.0	-24.9	-24.1
0.67	-28.9	-24.8	-23.7
0.69	-28.8	-24.7	-23.6
0.71	-28.7	-24.6	-23.4
1.20	-26.9	-23.1	-21.5
1.23	-26.8	-23.0	-21.4
1.46	-25.9	-22.2	-21.3
1.55	-25.6	-21.9	-21.3
1.77	-24.8	-21.2	-21.0

The calculated $\delta^{13}C$ ratios become ^{13}C enriched for a given maturity from methane to ethane to propane indicating the presence of gases from a single source

(Chung et al., 1988). In Table 6.7, calculated carbon isotope ratios for primary methane, ethane and propane derived from a Kerogen Type III source rock are shown. These values are calculated by applying $\delta^{13}C$–$\%R_O$ relationships by Berner and Faber (1996) for the lowest and highest maturities encountered in coals for this study lying within the calibration range mentioned in Table 6.5 (0.61$\%R_O$ and 1.77$\%R_O$).

Table 6.7: *Calculated carbon isotope ratios for methane, ethane and propane derived from a Kerogen Type III source rock. Calculations are performed by applying the lowest and highest maturities encountered in coals from this study to $\delta^{13}C$–$\%R_O$ relationships for methane, ethane and propane by Berner and Faber (1996).*

Species	**$\delta^{13}C$ calculated for 0.61$\%R_O$ (‰)**	**$\delta^{13}C$ calculated for 1.77$\%R_O$ (‰)**
Methane	-29.0	-24.3
Ethane	-25.0	-21.2
Propane	-24.3	-21.0

The overall isotope range between highest and lowest considered maturity are 4.8‰ for methane, 3.7‰ for ethane and 3.3‰ for propane.

6.2.1c Comparison: Calculated vs. Measured Carbon Isotope Ratios

A graphical comparison between modeled and measured values is given for methane in Figure 6.16, for ethane in Figure 6.17 and for propane in Figure 6.18. The calculated and measured values, as well as the calculated differences ($\Delta\delta^{13}C$) are presented for methane in Appendix L, for ethane in Appendix M and for propane in Appendix N.

$\delta^{13}C$ values of methane from CBM samples shows slight to extreme differences relative to the values calculated by applying the $\delta^{13}C$–$\%R_O$ relationship for methane by Berner and Faber (1996). Methane is ^{12}C enriched relative to the modeled $\delta^{13}C$ values. Samples from two production sample sets (P2 and P3) are the exceptions, with relative ^{13}C enrichments. This indicates that the measured $\delta^{13}C$ values for methane do not represent primary gas generation. Rather they are altered due to the presence of microbial

generated methane or due to secondary processes. For ethane and propane no conclusive trends were observed.

Methane

For methane, measured values are more ^{12}C enriched than the calculated values. For t_{START} values (Figure 6.16) only sample set P2 shows $\delta^{13}C$ values equal or more ^{13}C enriched than the calculated values. Samples set P3 shows ^{13}C enrichment, but is not discussed here, because the maturity falls below the calibration limit (Berner and Faber, 1996). It is interesting that sample sets P2 and P3 were taken from production wells, whereas all other samples came from desorption experiments (Chapter 6.3). The overall observed $\delta^{13}C$ differences between modeled and measured values cover a range of >50‰.

These differences become less pronounced when considering $\delta^{13}C$ values for t_{END} (Figure 6.16), but still cover more than 33‰. Overall, values from more individual samples are comparable to the calculated values, including samples from sample sets D4, D5 and D7, whereas sample set D6 is still more ^{12}C enriched than the calculated values.

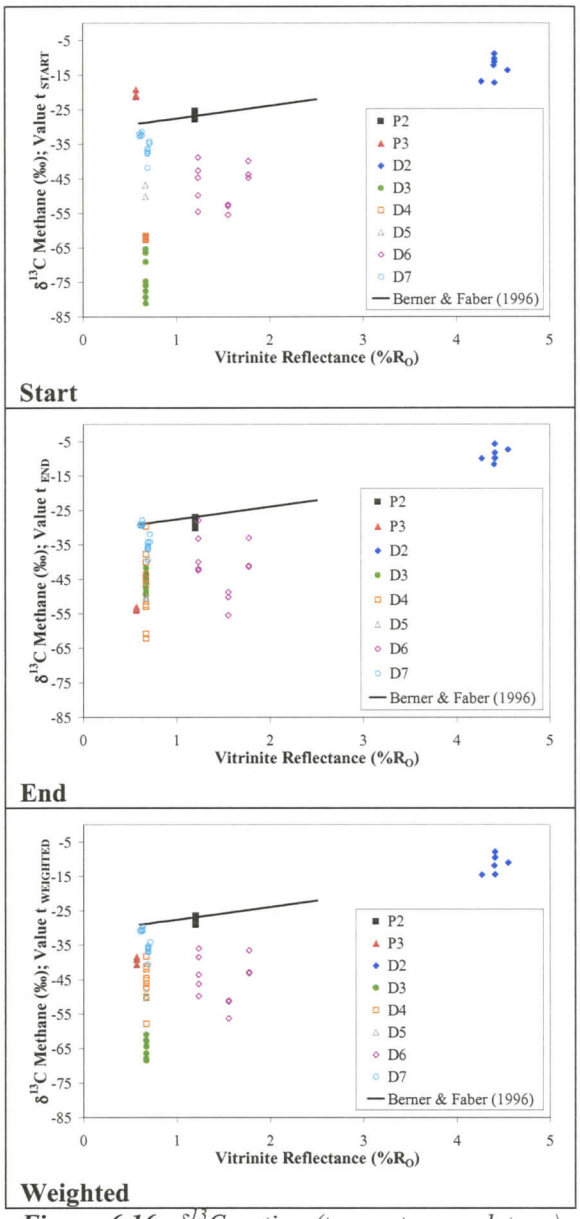


Figure 6.16: *$\delta^{13}C$–ratios (t_{START}, t_{END} and t_{WGH}) for methane from production and desorption experiment samples presented versus maturity (vitrinite reflectance) of the corresponding coals. t_{START} represents the first sample available per well or canister respectively, t_{END} represents the last sample available per well, or canister respectively. For calculation of value t_{WGH} see text. Also shown is line representing relationship between maturity of a Kerogen Type III source rock and $\delta^{13}C$–ratio for methane expected to be generated from this type of source rock (after Berner and Faber, 1996). No results are available for sample sets P1 and D1.*

For t_{WGH} values (Figure 6.16), only sample sets D2 and D7 are similar to the calculated values, while only sample set P2 shows a relative ^{13}C enrichment. The overall differences between calculated and measured $\delta^{13}C$ values cover a range of ca. 40‰.

Ethane

For ethane the overall differences between calculated and measured $\delta^{13}C$ values become smaller. For t_{START} (Figure 6.17) all values scatter around the calculated values with differences from +11‰ to -6‰. $\delta^{13}C$ values for t_{END} (Figure 6.17) show differences from the calculated $\delta^{13}C$ values in the range of ca. -13‰ to ca. -6‰. For t_{WGH} values (Figure 6.17) the overall differences between calculated and measured $\delta^{13}C$ values are in the range of -1‰ to -6‰.

Propane

t_{START} values (Figure 6.18) for sample set D7 are ^{12}C enriched relative to the calculated $\delta^{13}C$ values with a maximum difference of 6.2‰. The overall differences are smaller for sample set D6, but show both, ^{12}C and ^{13}C enrichment relative to the

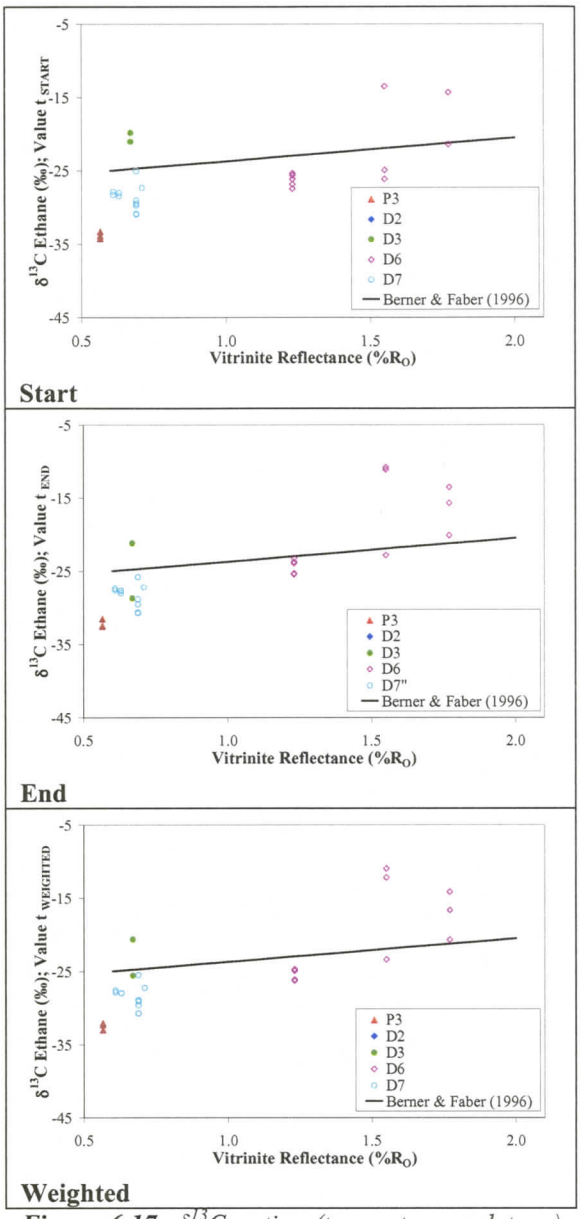


Figure 6.17: *$\delta^{13}C$–ratios (t_{START}, t_{END} and t_{WGH}) for ethane from production and desorption experiment samples presented versus maturity (vitrinite reflectance) of the corresponding coals. t_{START} represents the first sample available per well or canister respectively, t_{END} represents the last sample available per well, or canister respectively. For calculation of value t_{WGH} see text. Also shown is graph representing relationship between maturity of a Kerogen Type III source rock and $\delta^{13}C$–ratio for ethane expected to be generated from this type of source rock (after Berner and Faber, 1996). No results are available for sample sets P1, P2, D1, D4 and D5.*

calculated $\delta^{13}C$ values; $\delta^{13}C$ values range between -1‰ and +3‰.

For t_{END} (Figure 6.18), $\delta^{13}C$ values of sample set D7 show ^{12}C enrichment relative to the calculated values with a maximum difference of 6.3‰. $\delta^{13}C$ values of sample set D6 are shifted towards greater ^{13}C enrichment with only one sample showing 0.4‰ ^{12}C enrichment relative to the calculated $\delta^{13}C$ values. The maximum ^{13}C enrichment for the other samples is 2.8‰.

For t_{WGH} values (Figure 6.18), sample set D7 shows ^{12}C enrichment relative to calculated $\delta^{13}C$ values with a maximum enrichment of 6.3‰. The range of $\delta^{13}C$ values from sample set D6 is increased, but ^{12}C and ^{13}C enrichment, relative to calculated $\delta^{13}C$ values, is present. The maximum differences are 0.8‰ for ^{12}C enrichment and 5.4‰ for ^{13}C enrichment.

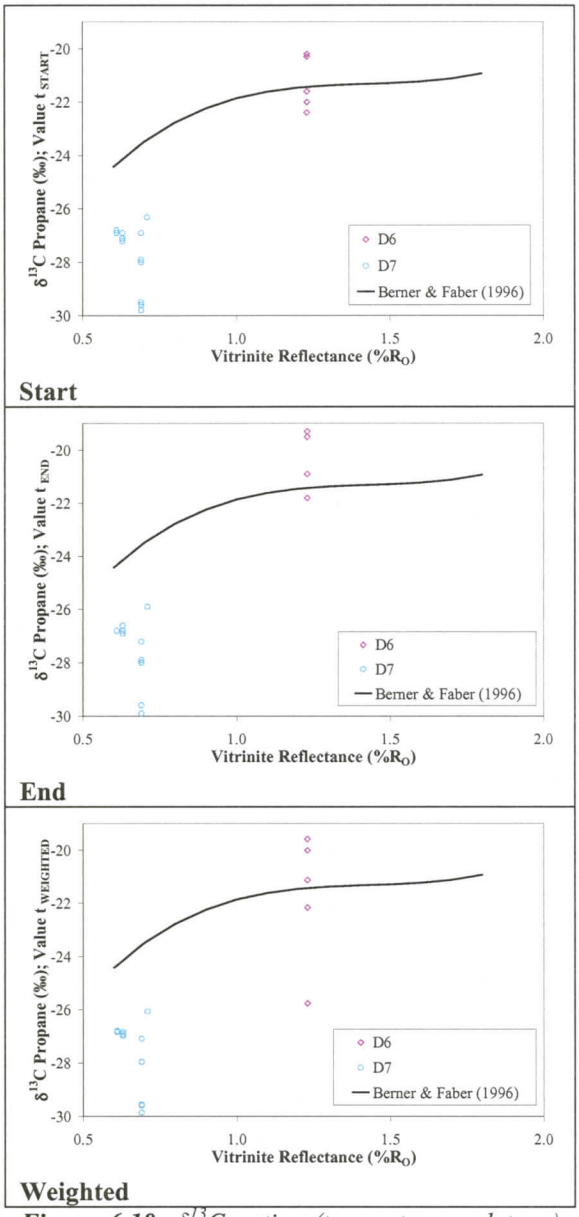


Figure 6.18: *$\delta^{13}C$–ratios (t_{START}, t_{END} and t_{WGH}) for propane from samples of desorption experiments D6 and D7 presented versus maturity (vitrinite reflectance) of the corresponding coals. t_{START} represents the first sample available per well or canister respectively, t_{END} represents the last sample available per well, or canister respectively. For calculation of value t_{WGH} see text. Also shown is graph representing relationship between maturity of a Kerogen Type III source rock and $\delta^{13}C$–ratio for propane expected to be generated from this type of source rock (after Berner and Faber, 1996). No results are available for sample sets P1, P2, P3, D1, D2, D3, D4 and D5.*

6.2.1d Gas Classification Approach

A classical approach for the classification of natural gases includes the use of the Bernard Diagram and the carbon–hydrogen (CD) Diagram (see Chapter 2.5). Both diagrams are commonly used for conventional gases for the identification of gas generation processes (microbial or

thermogenic), separation of microbial processes (carbon dioxide reduction or methyl–type fermentation) and the identification of secondary processes (mixing, migration and oxidation). For both types of diagrams, the different data points per well or canister are plotted connected, representing the evolution of the considered values with increasing production or desorption time. The variations of the single parameters (proportions of methane, proportions of higher hydrocarbon, $\delta^{13}C$ for methane and δD for methane) with increasing production or desorption time are shown in Figures 5.1, 5.2, 5.4, 5.5, 5.8, 5.9, 5.11 and 5.12.

Bernard Diagram

Considering the analyzed data, it is possible in some cases to distinguish between microbia or thermogenic gas by using the Bernard Diagram (Figure 6.19).

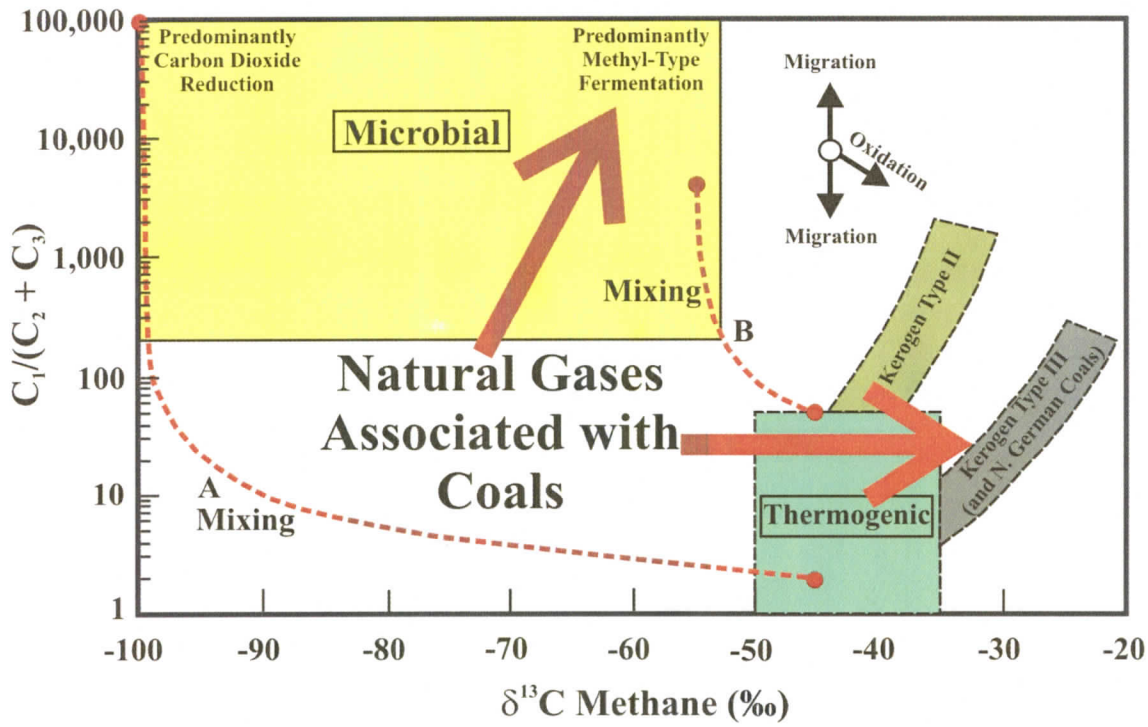


Figure 6.19: *Bernard Diagram indicating areas where natural gases associated with coal are expected to plot (methyl–type fermentation and Kerogen Type III areas). For discussion of diagram see text (modified from Whiticar, 1996a and 1999).*

The evolution of the measured values ($\delta^{13}C$–CH_4 and Bernard Parameter) with production or desorption time, shows that these values change extremely, indicating the presence of molecular and isotope ratio altering processes. Because of these complications, a definitive interpretation of the gas origin of the CBM samples is difficult. Samples, which contain no higher hydrocarbons, have an undefined Bernard Parameter. Therefore, the Bernard Parameter is arbitrarily set to 10^5, which represents a CH_4 rich sample. The application of the Bernard Diagram for the identification of different gas generation pathways for CBM gases is questionable, and new approaches for gas classification will be necessary, incorporating the effect of secondary processes and attendant molecular and isotope effects.

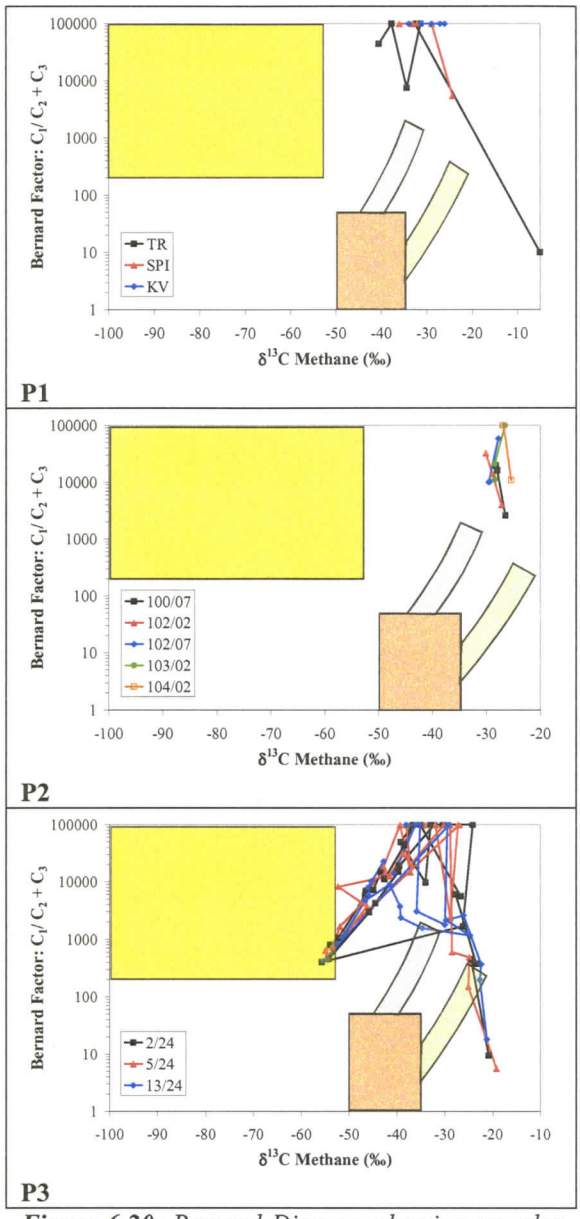


Figure 6.20: *Bernard Diagram showing samples from production sample sets P1, P2 and P3. Diagram is modified from Whiticar (1999). For explanations of different areas see Figure 6.19. Note the different scales.*

Samples from production sample sets P1, P2 and P3 (Figure 6.20) indicate a dry gas with a wet gas component only for sample set P3 (Figure 6.20). Gases from sample sets P1 (Figure 6.20) and P2 (Figure 6.20) show no evidence for a contribution of microbial gas, but show strong indications of migrated thermogenic gas, i.e., the carbon isotope ratios resemble more a migrated Kerogen Type II gas, than the expected Kerogen Type III gas. Based on the data for sample set P3 a microbial gas contribution is possible.

Data from sample set D1 and high mature sample set D2 (Figure 6.21) show a strong thermogenic imprint. Data from sample set D3 (Figure 6.21) show a strong microbial component, but overall scatter is large. Based on the Bernard Diagram a mixture of microbial and thermogenic gas is indicated for sample set D4 (Figure 6.21). For sample set D5 (Figure 6.21) the three data points show no indication of higher hydrocarbons and, based on the $\delta^{13}C$ values for methane indicate a mixture of microbial and thermogenic gas. Based on the Bernard Diagrams sample sets D6 and D7 (Figure 6.21) resemble thermogenic gas, with some D6 samples indicate a mixture of microbial and thermogenic gas.

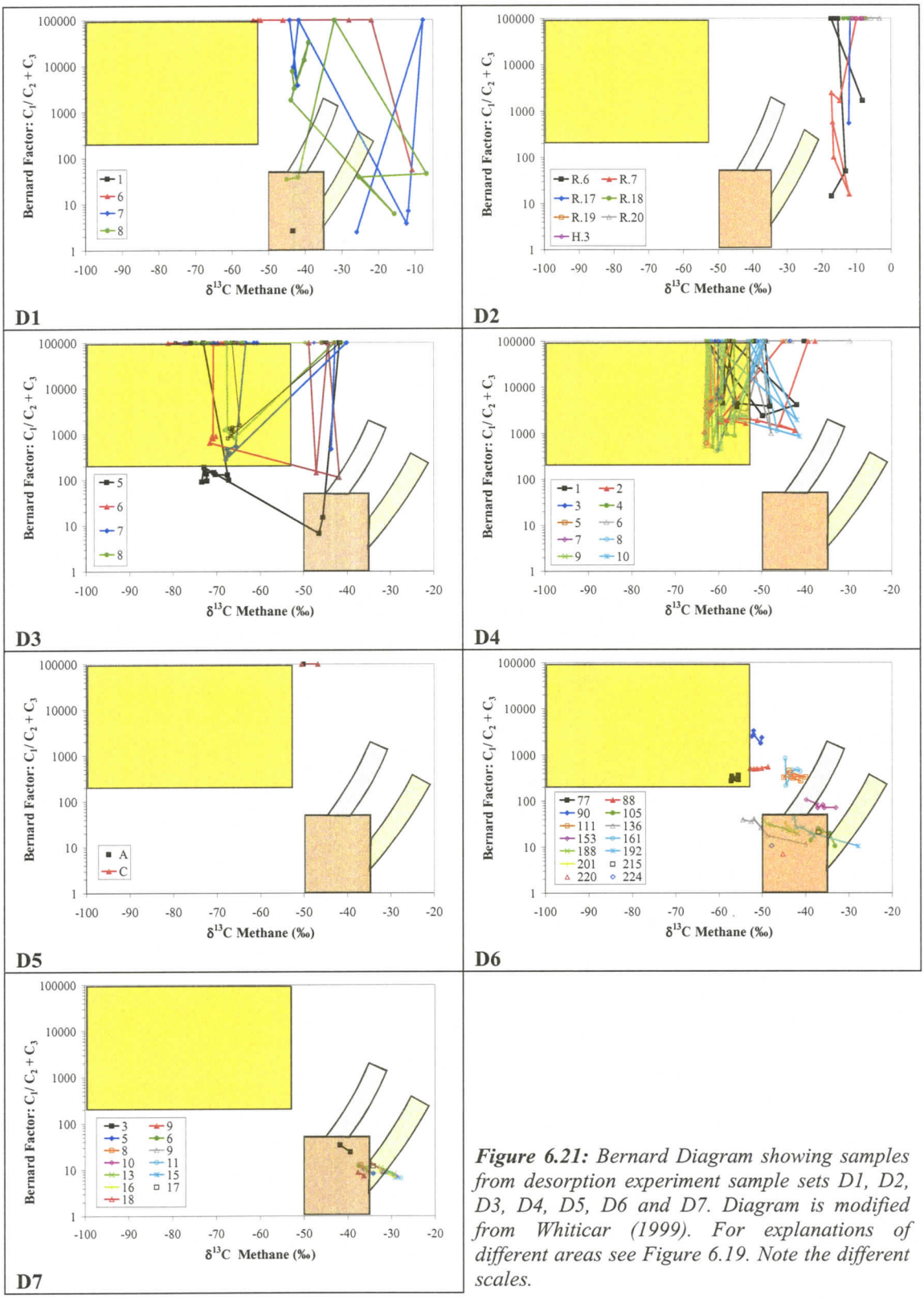


Figure 6.21: *Bernard Diagram showing samples from desorption experiment sample sets D1, D2, D3, D4, D5, D6 and D7. Diagram is modified from Whiticar (1999). For explanations of different areas see Figure 6.19. Note the different scales.*

CD Diagram

The CD Diagram (Whiticar et al., 1986) correlates $\delta^{13}C$ and δD ratios of methane (Figure 6.22). Methane, genetically related to coal or humic Kerogen, occupies distinct regions within the diagram, including regions indicating methyl–type fermentation and thermogenic (humic) gas generation (Whiticar, 1996a). The region within the CD Diagram representing thermogenic gases generated from humic kerogen is defined by methane from the Westphalian of Northern Germany (M. Whiticar, personal communication). Other accumulations of methane from coals, e.g., USA, are known to exhibit different values.

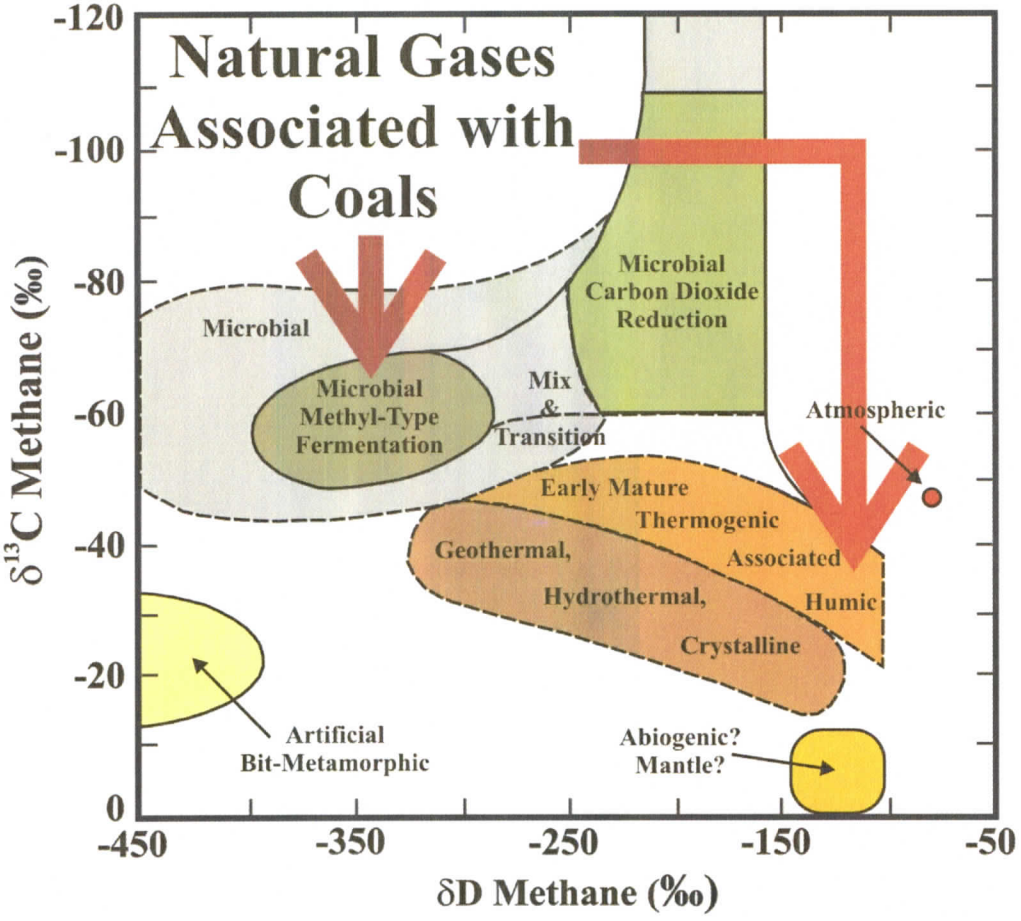


Figure 6.22: *$\delta^{13}C$–δD (methane) Diagram indicating areas where natural gases associated with coal are expected to plot (methyl–type fermentation and humic kerogen areas). For discussion of diagram see text (modified from Whiticar, 1996a and 1999).*

Based on the CD Diagram, a definitive classification of the analyzed CBM samples in terms of origin is difficult. The measured data most likely do not represent the primary isotope composition of the generated gases. Based on the CD Diagrams, certain gases would have to be interpreted as of abiogenic and mantle derived origin, whereas others are of geothermal, hydrothermal and crystalline origin, which is unreasonable for gases known to be generated from coal. The evolution of $\delta^{13}C$ and δD values with production and desorption time indicates the presence of isotope ratio altering processes. These complications make it difficult to assign the origin of the analyzed gases based on the CD Diagram. The use of the CD Diagram for the differentiation of different gas generation pathways for CBM gases is questionable, and new approaches for gas classification will be necessary, incorporating the effect of secondary processes and attendant molecular and isotope effects.

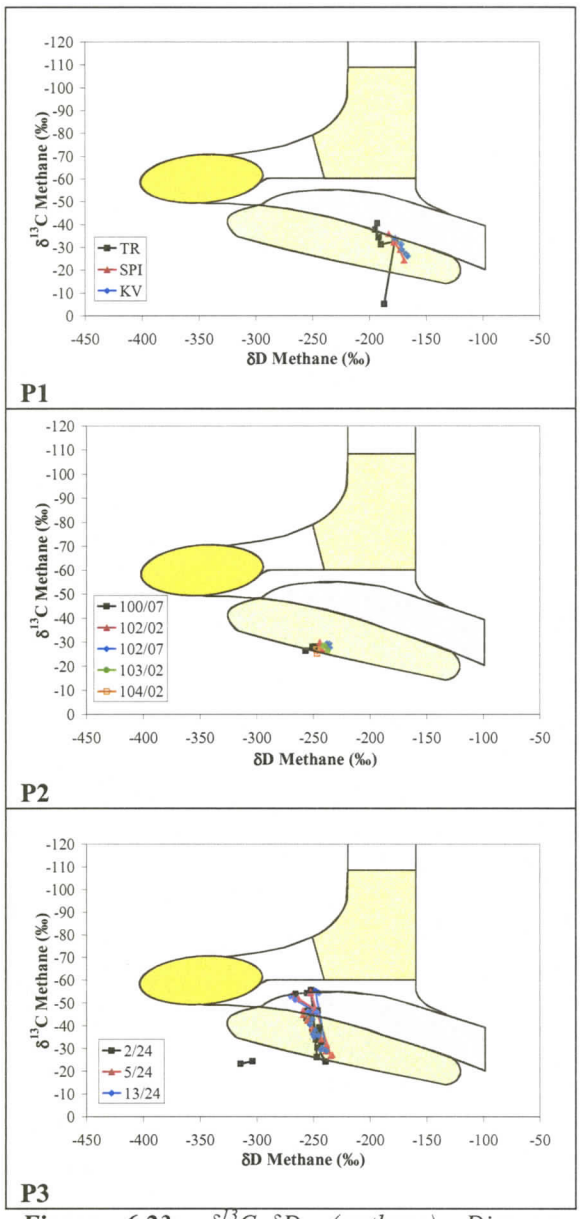


Figure 6.23: *$\delta^{13}C$–δD (methane) Diagram showing samples from production sample sets P1, P2 and P3. Diagram is modified from Whiticar (1999). For explanations of different areas see Figure 6.22.*

None of the samples from production sample sets P1, P2 and P3 plot in the expected regions for gases derived from coals or Kerogen Type III (Figure 6.23). Sample sets P1, P2 and P3 would be interpreted as gases of geothermal, hydrothermal and crystalline origin, which is unreasonable for gases known to be generated by coals or Kerogen Type III source rocks. Some data from sample set P1 indicate thermogenic origin. This is more pronounced for sample set P3,

but still most of the data points plot in the geothermal, hydrothermal and crystalline origin region. Interestingly, samples from all production scenarios plot left to the humic thermogenic region, indicating ^{2}H depletion. This ^{2}H depletion could be attributed to differences in the stable hydrogen isotope ratios of the precursor materials and the water involved during gas generation. None of the samples from the production scenarios show any indication for the presence of microbial gas.

Samples from all desorption experiment sample sets (exception is sample set D2) show methane $\delta^{13}C$ values too enriched in ^{12}C expected for a typical coal or a humic source (Figure 6.24). Sample sets D1, D2 and D7 could be interpreted as gases of geothermal, hydrothermal and crystalline origin, which is unreasonable for CBM gas. Indications for thermogenic generated methane are found for some sample sets D1, D3, D4, D5, D6, D7, and microbial gas contributions are observed for sample sets D3, D4 and D6. Microbial gas contribution in sample set D3 would be generated by carbon dioxide reduction, a process which is not considered an associated pathway for the generation of microbial gas from coal or from a Kerogen Type III source (Whiticar, 1996a). Some data from sample set D2 actually plot in the data range, which is thought to represent a possible abiogenic and mantle derived origin, which is not possible for methane known to be derived from coal or Kerogen Type III source rocks. Samples from desorption experiment sample sets also indicate ^{2}H depletion relative to the region indicating humic gases in the CD Diagram (Figure 6.24). This ^{2}H depletion could be attributed to differences in the stable hydrogen isotope ratios of the precursor materials and the water involved during gas generation.

In summary the classical approach for gas classification using Bernard Diagram and CD Diagram cannot be readily applied to CBM. This conclusion is discussed earlier by Smith et al. (1985) and Kotarba and Lewan (2004). However this has not been substantiated by production and desorption experiments. Due to the effect of secondary processes and attendant molecular and isotope effects new approaches for gas classification have to be necessitated.

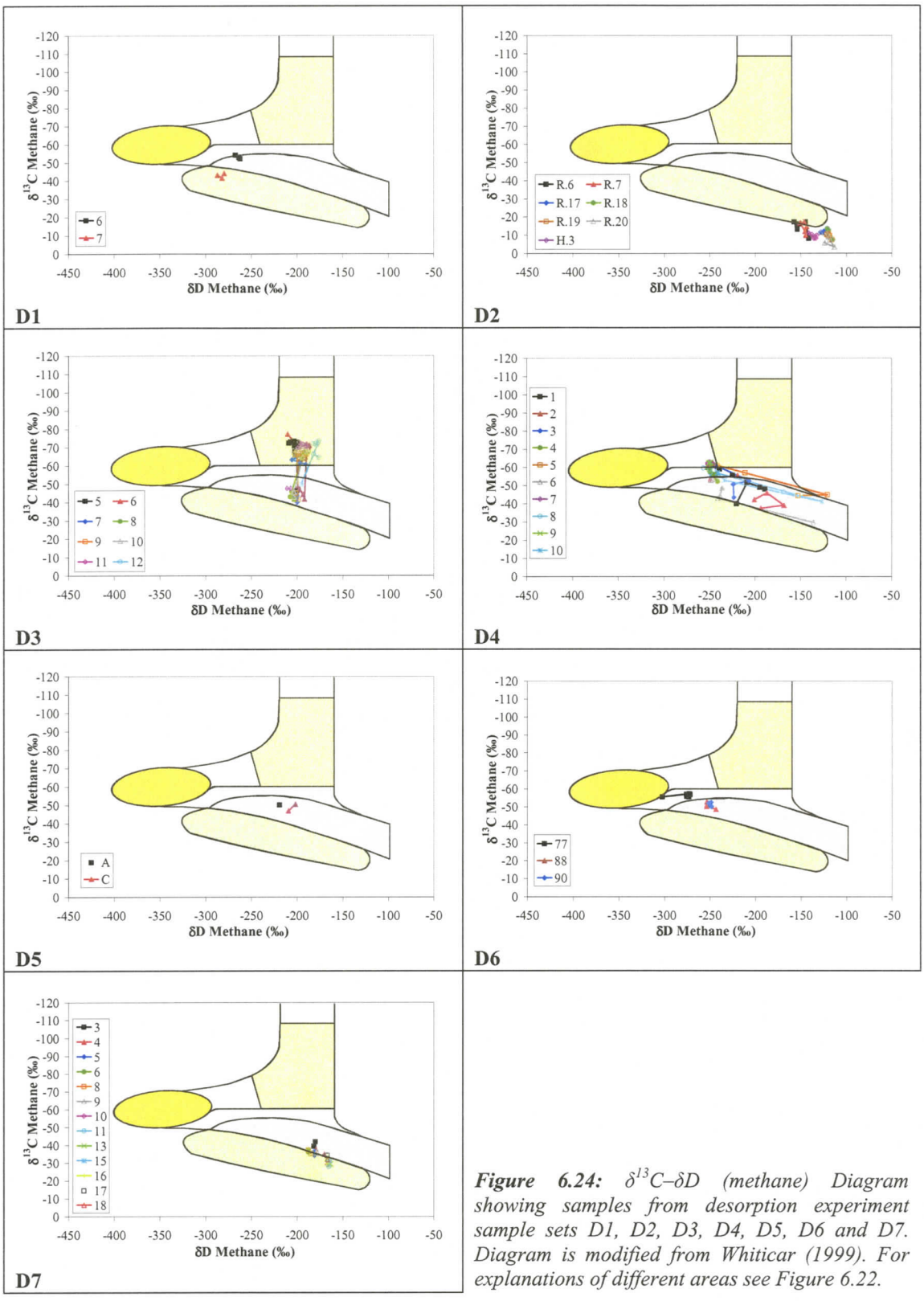


Figure 6.24: *$\delta^{13}C$–δD (methane) Diagram showing samples from desorption experiment sample sets D1, D2, D3, D4, D5, D6 and D7. Diagram is modified from Whiticar (1999). For explanations of different areas see Figure 6.22.*

6.2.2 Secondary Alteration Effects

A main conclusion of the previous discussions is the importance of secondary processes for the interpretation of CBM. Molecular and isotope fractionations as a result of these effects change the compositional and isotope appearance of CBM so much, that a classification is not reasonable without the incorporation of these effects. Additionally, the presence and the significant impact of secondary processes on the molecular and isotope composition of CBM gases indicate that results and findings from coal pyrolysis experiments cannot be applied easily for the geochemical consideration of CBM gases. Coal pyrolysis experiments consider the generation of gas from coal, but do not take secondary processes, e.g., mixing, adsorption, desorption, oxidation and diffusion, into account.

6.2.2a Mixture of Coal Gas with Microbial Gas

Natural Gas Plots

Higher hydrocarbons in the CBM samples are present in low proportions excepting sample sets D6 and D7. Therefore the approach of using natural gas plots (Chung et al., 1988) described in Chapter 2.5 will only be applied to sample sets D6 and D7. Natural gas plots (Chung et al., 1988) for these two sample sets are show in Figure 6.25, using t_{WGH} values for methane and ethane. $\delta^{13}C$ values for propane are not available for samples from either sample set. Determination of primary $\delta^{13}C$ ratios for methane is achieved by process of extrapolation described in Chapter 2.5. The calculation

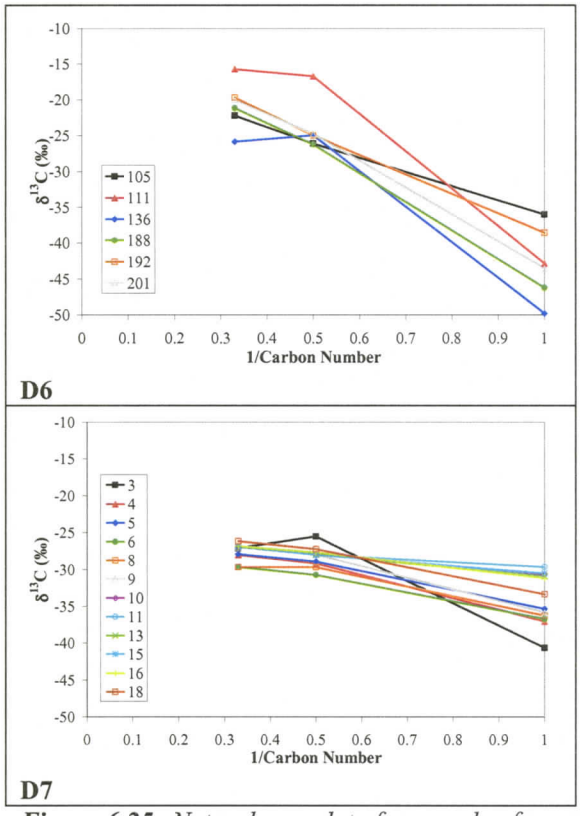


Figure 6.25: *Natural gas plots for samples from desorption experiment sample sets D6 and D7. See text for discussion. Diagram is modified after Chung et al., 1988.*

of the fractions of thermogenic and biogenic gas is performed by applying the following linear mass balance equation:

$$\delta^{13}C_{-(T/M)} = f_{(T)} \cdot \delta^{13}C_{-(T)} + (1 - f_{(T)} \cdot \delta^{13}C_{-(M)}) \quad (6.3)$$

where $\delta^{13}C_{-(T/M)}$ is the carbon isotope ratio of the gas mixture between thermogenic (T) and microbial (M) generated gas, $f_{(T)}$ is the fraction of thermogenic methane; $\delta^{13}C_{-(T)}$ is the carbon isotope ratio of thermogenic methane and $\delta^{13}C_{(M)}$ is the carbon isotope ratio of microbial methane. The carbon isotope ratio for microbial generated methane generated by methyl–type fermentation is assumed to be -60‰ (Whiticar, 1999).

Microbial methane is suspected in sample sets D6 and D7. Based on the described approach the CBM gases could be described as mixtures of thermogenic gas generated from a Kerogen Type III source rock and microbial gas, with variable proportions of microbial gas, and as pure thermogenic gas generated from a Kerogen Type III source rock. Calculated fractions of thermogenic and microbial methane from sample sets D6 and D7 are presented in Figure 6.26 and Appendix O.

Natural gas plot data from sample set D6 (Figure 6.25) show steep slopes, indicating large isotope fractionation during the formation of the hydrocarbons (Chung et al., 1988). For sample set D6 the calculated proportions (Equation 6.3; Figure 6.26; Appendix O) for microbial gas range between none (canister 192) and 44% (canister 111).It appears that these strong variations are based on the $\delta^{13}C$ ratio of methane. Canisters from sample set D6 with ^{12}C enriched extrapolated $\delta^{13}C$ values are ignored.

Natural gas plot data from sample set D7 (Figure 6.25) show only small differences in $\delta^{13}C$ for ethane and propane. The slope of the gas plots is flat, indicating only small isotope effects during the generation of the hydrocarbons (Chung et al., 1988). The calculated fractions of thermogenic and microbial gas from sample set D7 show no or only small contributions of microbial gas with a maximum contribution of 22%.

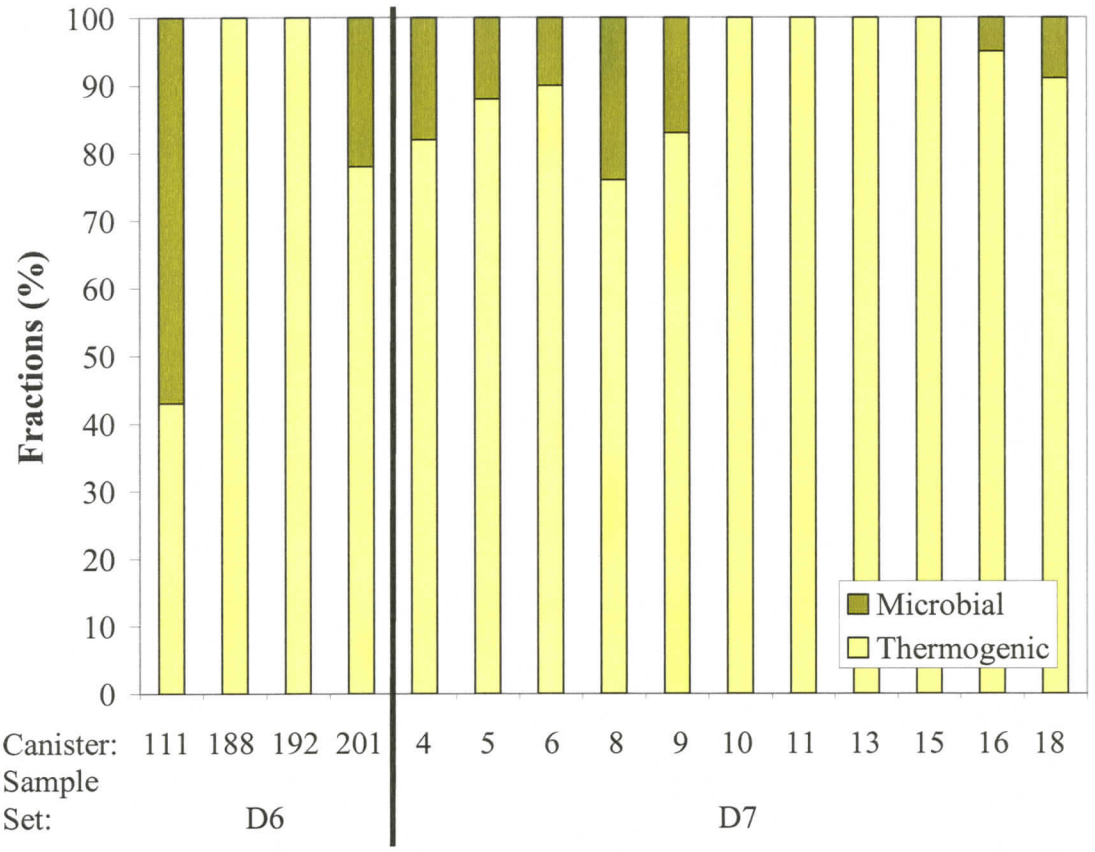


Figure 6.26: *Calculated fractions of thermogenic and microbial gas in sample sets D6 and D7. Calculations are based on natural gas plots and are performed following description by Chung et al. (1988). Calculations of proportions of thermogenic and microbial gas are performed by applying a mass–balance equation (see text for equation). See text for discussion.*

$\delta^{13}C$–%R_O Relationships

Microbial generated hydrocarbons consist mostly of methane. Therefore, in a mix of thermogenic and microbial gas, the $\delta^{13}C$ ratio of methane should represent a mix of the two end members. A comparison of estimated $\delta^{13}C$ values for methane generated from a Kerogen Type III source rock, based on maturity of the correlating coal and the relationships by Berner and Faber (1996), and the measured $\delta^{13}C$ values for methane provide indications about the presence of microbial methane. A quantitative consideration is possible by applying a mass balance (Equation 6.3) with the calculated $\delta^{13}C$ values as the initial value for methane, the measured $\delta^{13}C$ values as the microbial–thermogenic methane mix and a value of -60‰ for pure microbial methane generated by methyl–type fermentation.

Microbial methane is suspected in sample sets P3, D3, D4, D5, D6 and D7 and based on the described approach the CBM gases could be described as mixtures of thermogenic gas generated from a Kerogen Type III source rock and microbial gases, with variable proportions of microbial gas, and pure thermogenic gases generated from a Kerogen Type III source rock, as well as pure microbial gases. Calculated fractions of thermogenic and microbial methane in samples from these sample sets are presented in Figure 6.27 and Appendix P.

Calculated fractions of thermogenic and microbial gas from sample set P2 show an almost pure thermogenic gas, with microbial gas proportions of maximal 5%. Sample set D3 shows methane of only microbial origin. Gases from samples of sample set D4 show variations between 2% and 70% for thermogenic generated methane. Sample set D5 shows a mixture of thermogenic and microbial gas with fractions for thermogenic methane between 30% and 40%. Coals for sample sets D4 and D5 were taken underground from the same coal mine, but from different seams. Averaging the fractions of thermogenic and microbial gas from the different canisters of sample set D4 shows values of 58% thermogenic gas, which is similar to the value calculated for sample set D5 with 50%. This similarity leads to a comparison between sample sets D3, D4 and D5, which all originated from the same coal bearing basin. The spacing between the different sample locations is 1 kilometer. For sample set D3 coal cores recovered during drilling were used, whereas for sample sets D4 and D5 coal fragments (>4mm) were used. Gases collected from sample set D4 and D5 show proportions of thermogenic gas of ca. 50% to 60%, while sample set D3 shows proportions of 100% for microbial gas. A possible explanation for this discrepancy can be found in the methods of coal recovery. Recovery by wire–line drilling results in fresh coal cores, which are sealed into desorption canisters as early as possible after coring. Therefore, early desorbing gas is collected. The early desorbing methane is thought to be ^{12}C enriched, due to the desorption effect that discriminates against ^{13}C (e.g., Whiticar, 1996a). The coal collected underground was exposed to the atmosphere for a substantial amount of time, leading to a loss of gas, particularly methane. The lost gas should be ^{12}C enriched, leaving the remaining adsorbed methane ^{12}C depleted. The relative ^{13}C enrichment for methane from the exposed coals would lead to a reduced proportion of microbial gas, because of the

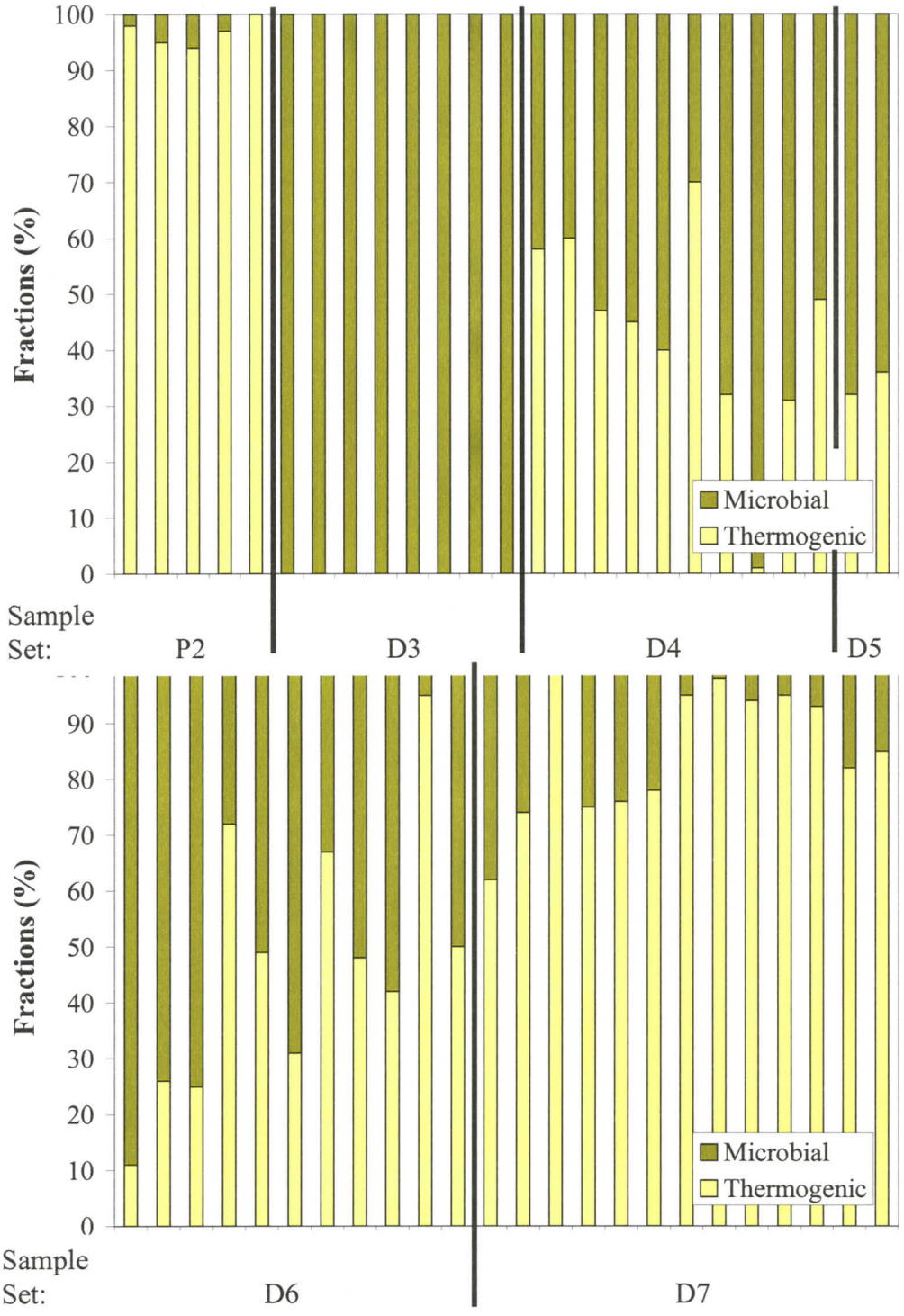


Figure 6.27: *Calculated fractions of thermogenic and microbial gas in CBM samples. A shows sample sets P2, D3, D4 and D5. B shows sample sets D6 and D7. Calculations are based on a comparison between measured $\delta^{13}C$ ratios for methane with $\delta^{13}C$–$\%R_O$ relationship for methane from Berner and Faber (1996). Calculations of proportions of thermogenic and microbial gas are performed by applying a mass–balance equation (see text for equation). See text for discussion.*

correlation of ^{12}C enrichment with microbial methane. This decrease in the proportion of microbial gas is found sample sets D4 and D5 relative to D3, which experienced a loss of gas with methane enriched in ^{12}C.

For sample set D6 thermogenic gas varies between 11% and 96%. For sample set D7 thermogenic gas ranges between 60% and 100%.

The above described possible mixtures of thermogenic and microbial gas, and especially the calculated quantities, have to be considered with extreme caution, because they are based on ^{12}C enrichment in methane of analyzed samples relative to calculated or extrapolated and therefore assumed $\delta^{13}C$ values. ^{12}C enrichment can also be the result of isotope fractionation. The processes of desorption and diffusion can also lead to a ^{12}C enrichment in methane (e.g., Pernaton et al., 1996).

For sample sets D6 and D7, both considered approaches are applied and therefore, a comparison between the two methods is possible (Figure 6.28 and Appendix Q). For the estimation of the original $\delta^{13}C$ value of methane Chung et al. (1988) uses natural gas plots, where the extrapolation of the $\delta^{13}C$ values for ethane, propane and butane allows a determination of the original $\delta^{13}C$ value of methane. By using a mass balance (Equation 6.3) with the original $\delta^{13}C$ value and the measured $\delta^{13}C$ value of methane, the proportion of thermogenic methane in the sample can be calculated. Berner & Faber (1996) uses empirical relationships between the maturity of a source rock and the $\delta^{13}C$ value of methane generated from this source for the determination of the original $\delta^{13}C$ value of methane. Also a mass balance (Equation 6.3), the modeled $\delta^{13}C$

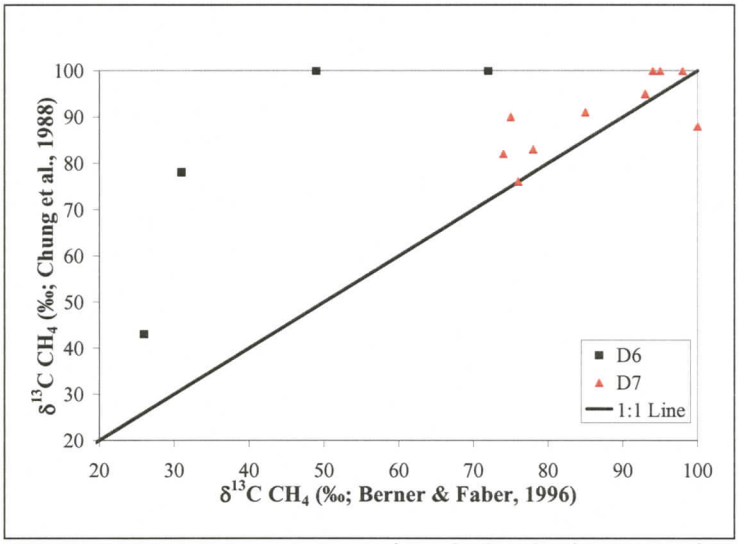


Figure 6.28: *Comparison of calculated fractions for thermogenic gas generated from a Kerogen Type III source rock based on the approaches by Chung et al. (1988) and Berner and Faber (1996) for sample sets D6 and D7. See text for description of both approaches*

value of methane and the measured $\delta^{13}C$ value of methane are used for the calculation of the proportion of thermogenic methane.

Both methods show similar results. The relative dominance of thermogenic over microbial gas for most of the considered canisters is found using both methods. For sample set D7 the data points for $\delta^{13}C$ ratios for methane calculated by using the two different approaches by Chung et al. (1988) and Berner and Faber (1996) plot closer to the shown 1:1 line (Figure 6.28), indicating no or only small differences for the calculated fractions of thermogenic gas. For sample set D6 the differences for the calculated fractions of thermogenic methane are greater between the two approaches by Chung et al. (1988) and Berner and Faber (1996; Figure 6.28), whereby the calculated fractions of thermogenic gas using the approach by Chung et al. (1988) exceed the calculated fractions using the approach by Berner and Faber (1996). The calculated differences between the primary $\delta^{13}C$ values for methane derived from the methods by Chung et al. (1988) and Berner and Faber (1996) are shown for sample sets D6 and D7 in Appendix R.

Hydrocarbons generated by microbes consist mostly of methane and therefore, when having a thermogenic–microbial gas mixture, the higher hydrocarbons generated by the thermogenic source, should not be influenced by the admixture of microbial gas. However, the calculated $\delta^{13}C$ values for methane derived by the method of Chung et al. (1988), which were derived by using the measured $\delta^{13}C$ values for ethane, propane and butane, show ^{12}C enrichment relative to the values calculated by using the method of Berner and Faber (1996) and these values. Assuming now that the $\delta^{13}C$ values for methane derived by using the Berner & Faber (1996) approach are the true "original" values, the measured $\delta^{13}C$ values for ethane and propane can not be original values, but have to be altered. For the gas plots presented in this chapter only $\delta^{13}C$ values for ethane and propane were available and consequently used for the extrapolation and determination of the original $\delta^{13}C$ values of methane.

The calculated $\delta^{13}C$ values for ethane and propane, based on $\delta^{13}C$–$\%R_O$ relationships for a Kerogen Type III source rock by Berner and Faber (1996) are presented in Appendix S. The measured ethane and propane $\delta^{13}C$ values show ^{12}C enrichment relative to the calculated values. The differences between calculated and

measured ethane and propane $\delta^{13}C$ ratios show a shift towards ^{12}C enrichment of the same magnitude. The ^{12}C enrichment for ethane and propane cannot be attributed to an admixture of microbial gas. This ^{12}C enrichment requires a source to generate higher hydrocarbons with $\delta^{13}C$ ratios more ^{12}C enriched than expected for coal or Kerogen Type III source rocks. A potential source rock is Kerogen Type II shale, and a thick succession of such shales is located beneath the coal seams considered for sample set D7. The considered shales are known to be a source of gas and oil. A detailed discussion of this topic is given in chapter6.2.2b.

The presented model indicates the possible mixture of three components in sample set D7. The types of gases in this mixture are CBM, microbial gas and gas generated from a Kerogen Type II source rock. The presence of this mixture would imply that besides methane, the higher hydrocarbons ethane and propane also migrated into the coals, were they became retained by the coal. This model assumes that the gases are not altered by secondary processes, but the presence of secondary processes like desorption and diffusion is likely, which would change the isotope signature of methane, resulting in ^{12}C enrichment. If the ^{12}C enrichment is only the result of isotope effects due to secondary processes, than the results would also imply that not only the methane isotope ratio, but also the ethane and propane isotope ratios are influenced by these isotope effects.

The application of the described methods by Chung et al. (1988) and Berner and Faber (1996) for the determination of fractions of thermogenic and microbial gas in a gas mixture is possible, but attention has to be paid to secondary processes and sample collection. Not only the type of secondary process with its specific direction and magnitude of isotope effects is important for the interpretation of data, but also a possible loss of gas, particularly methane, from the coal prior to recovery, has to be considered. A loss of such methane, which is relatively ^{12}C enriched would lead to an underestimation of the microbial gas fraction.

6.2.2b Mixture of CBM Gas with Kerogen Type II Gas

$\delta^{13}C$–$\%R_O$ Relationships for Gases Generated from Kerogen Type II and Kerogen Type III Source Rocks

Not only mixtures of thermogenic gas derived from coal and microbial gas are likely, but also mixtures of thermogenic gases generated from Kerogen Type III and Kerogen Type II sources are possible. Based on sample sets D6 and D7 a model is proposed, where thermogenic gas (methane, ethane and propane), generated from a Kerogen Type II source rocks migrated into coals. The model is based on relative ^{12}C enrichments in all three hydrocarbon species, resulting in $\delta^{13}C$ values divergent for a coal or Kerogen Type III source rock.

For sample sets D7 and D6 a mixture of gases generated from a Kerogen Type III and Type II source rock is possible. Overall $\delta^{13}C$ ratios for methane, ethane and propane from sample set D7 show ^{12}C enrichment relative to a Kerogen Type III source and ^{13}C enrichment relative to a Kerogen Type II source. $\delta^{13}C$ ratios for methane from sample set D6 show ^{12}C enrichment relative to methane generated from a Kerogen Type II source rock, whereas $\delta^{13}C$ ratios for ethane and propane show partly ^{13}C enrichment relative to $\delta^{13}C$ ratios calculated for these gases generated from a Kerogen Type III source.

Comparisons of measured $\delta^{13}C$ ratios and calculated $\delta^{13}C$ ratios ($\delta^{13}C$–$\%R_O$ relationships for Kerogen Type II and Type III by Berner and Faber, 1996) are shown for methane in Figure 6.29, for ethane in Figure 6.30 and for propane in Figure 6.31.

An estimation of the fractions of the Kerogen Type III and Type II source rock gases is calculated using the measured $\delta^{13}C$ values (t_{WGH}) for methane, ethane and propane, as well as the calculated values expected for methane, ethane and propane generated from Kerogen Type II and Type III source rocks, derived from $\delta^{13}C$–$\%R_O$ relationships from Berner and Faber (1996). For the calculation of fractions of Kerogen Type II and Type III derived gases a linear mass balance (Equation 6.3) is used. The calculations were made assuming that no microbial methane is present in the samples and that isotope effects due to secondary processes did not occur.

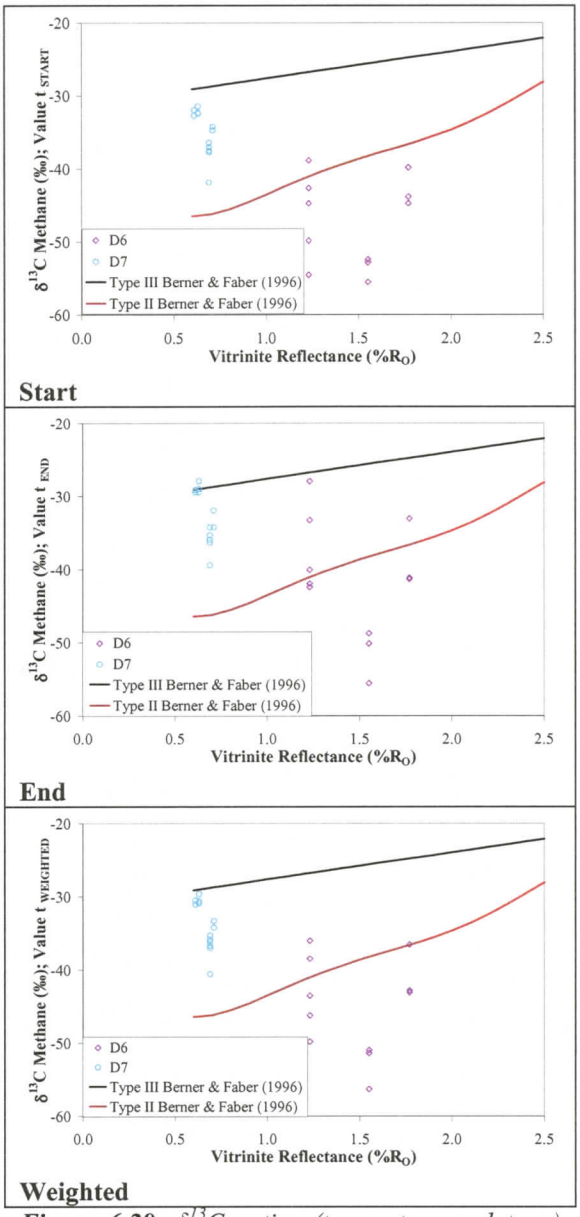


Figure 6.29: *$\delta^{13}C$–ratios (t_{START}, t_{END} and t_{WGH}) for methane from samples of desorption experiment sample sets D6 and D7 presented versus maturity (vitrinite reflectance) of the corresponding coals. t_{START} represents the first sample available per canister, t_{END} represents the last sample available per canister. For calculation of value t_{WGH} see text. Also shown are $\delta^{13}C$–maturity relationships for methane generated from a Kerogen Type II and Kerogen Type III source rock from Berner and Faber (1996). For equations see text.*

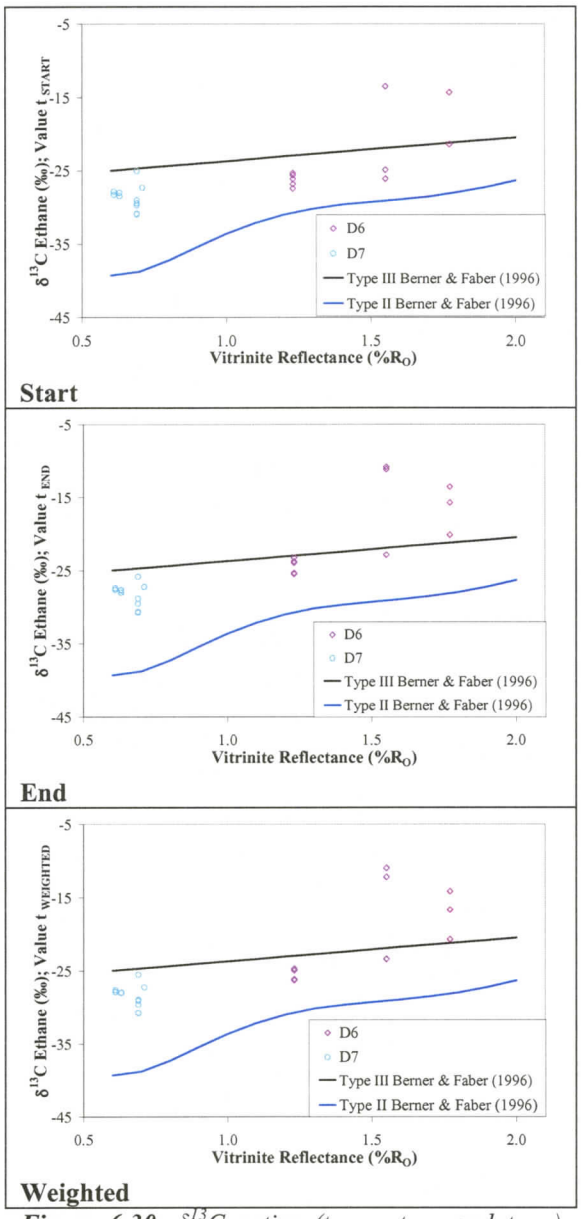


Figure 6.30: *$\delta^{13}C$–ratios (t_{START}, t_{END} and t_{WGH}) for ethane from samples of desorption experiment sample sets D6 and D7 presented versus maturity (vitrinite reflectance) of the corresponding coals. t_{START} represents the first sample available per canister, t_{END} represents the last sample available per canister. For calculation of value t_{WGH} see text. Also shown are $\delta^{13}C$–maturity relationships for ethane generated from a Kerogen Type II and Kerogen Type III source rock from Berner and Faber (1996). For equations see text.*

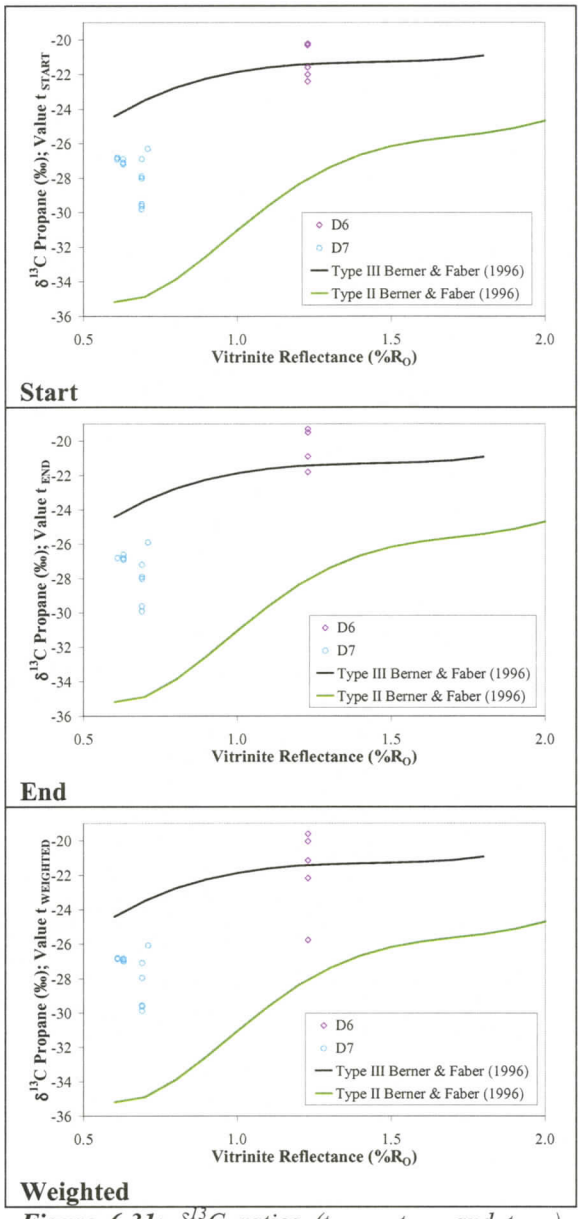


Figure 6.31: *$\delta^{13}C$–ratios (t_{START}, t_{END} and t_{WGH}) for propane from samples of desorption experiment sample sets D6 and D7 presented versus maturity (vitrinite reflectance) of the corresponding coals. t_{START} represents the first sample available per canister, t_{END} represents the last sample available per canister. For calculation of value t_{WGH} see text. Also shown are $\delta^{13}C$–maturity relationships for propane generated from a Kerogen Type II and Kerogen Type III source rock from Berner and Faber (1996). For equations see text.*

Under these idealized conditions, sample sets D6 and D7 show indications for the presence of thermogenic gas, generated from a Kerogen Type II source rock, based on the isotope ratios of methane, ethane and propane. The results for these calculations are presented in Figure 6.32 and Appendix T (methane), Figure 6.33 and Appendix U (ethane) and Figure 6.34 and Appendix V (propane).

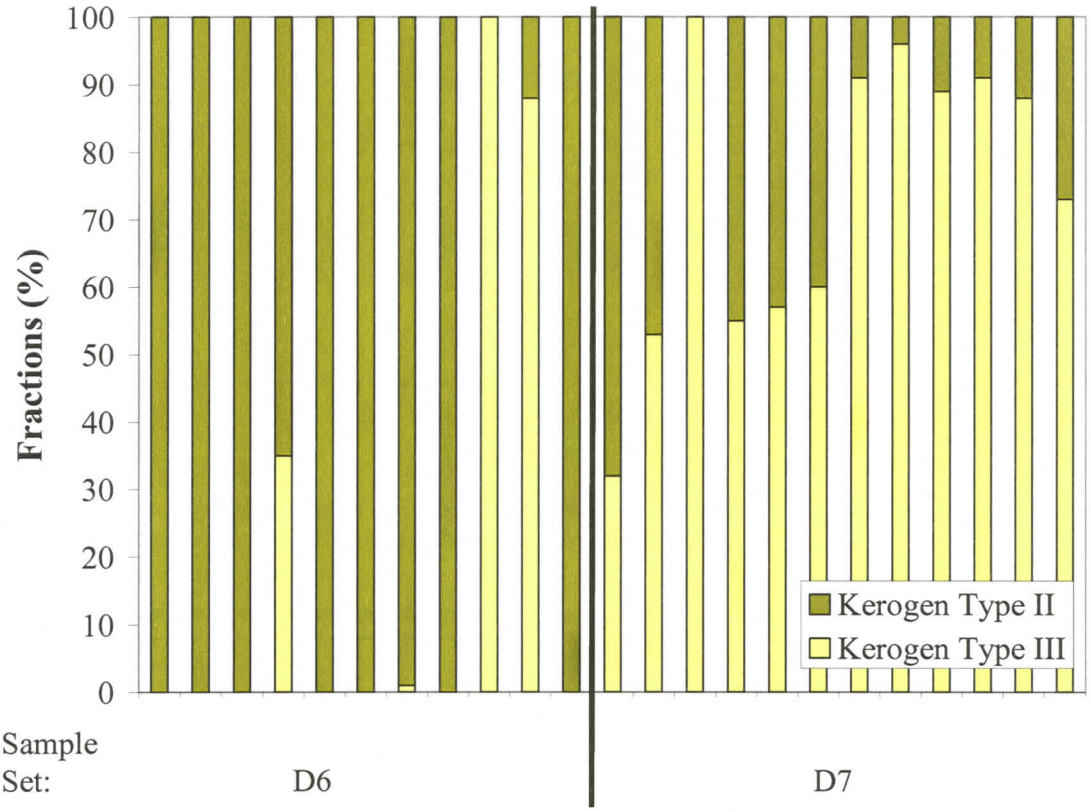


Figure 6.32: *Calculated fractions of methane generated from a Kerogen Type III and Kerogen Type II source rock in sample sets D6 and D7. Calculations are based on $\delta^{13}C$–$\%R_O$ relationships for methane by Berner and Faber (1996). Calculations of proportions of thermogenic and microbial gas are performed by applying a mass–balance equation (see text for equation). See text for discussion.*

Sample set D6 shows high contributions of Kerogen Type II derived methane with an average proportion of 80%. Sample set D7 show varying contributions of methane derived from a Kerogen Type II source ranging from none to 68% (average 26%). Ethane from sample set D6 contrasts with higher contributions of Kerogen Type III derived gas (average 84%). Sample set D7 shows contributions of gas derived from Kerogen Type II source rocks between none and 43% (average 25%). Propane from

sample set D6 shows contributions of gas derived from Kerogen Type II between none and 100% (average 30%). For sample set D7, the average contribution of gases derived from Kerogen Type II is 21%. The calculated fractions for gas derived from a Kerogen Type II source rock, based on the isotope composition of the three considered hydrocarbons is presented in Appendix W.

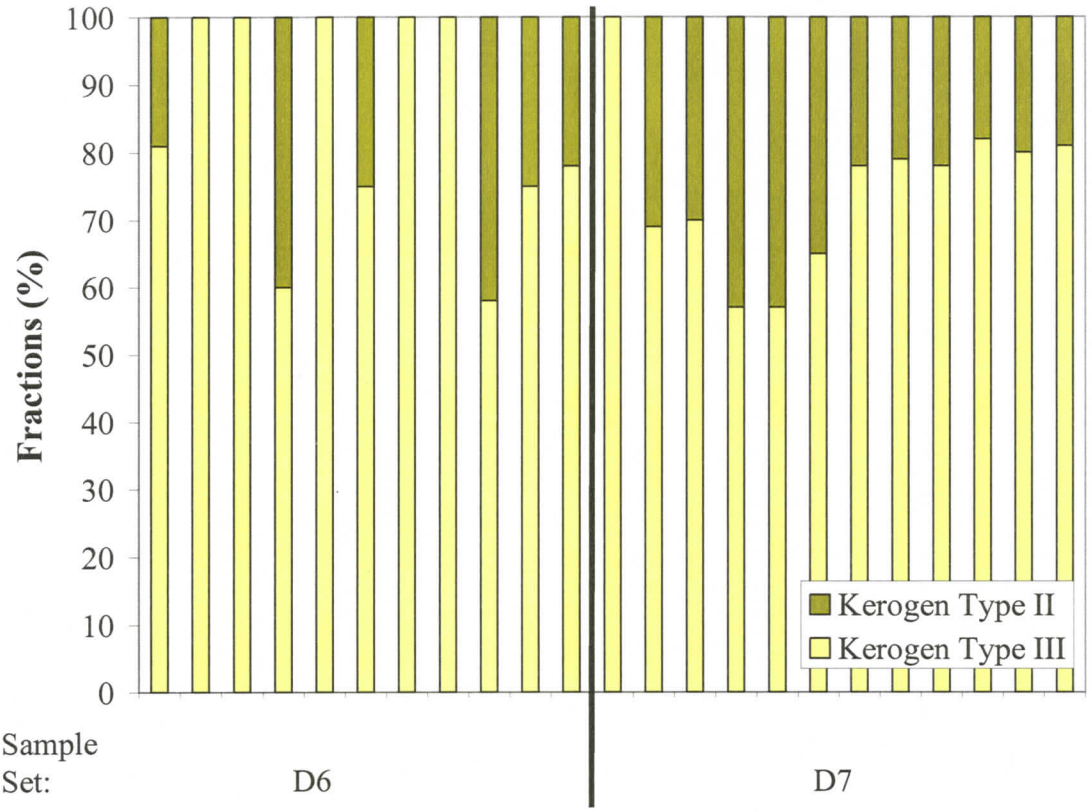


Figure 6.33: *Calculated fractions of ethane generated from a Kerogen Type III and Kerogen Type II source rock in sample sets D6 and D7. Calculations are based on $\delta^{13}C$–$\%R_O$ relationships for ethane by Berner and Faber (1996). Calculations of proportions of thermogenic and microbial gas are performed by applying a mass–balance equation (see text for equation). See text for discussion.*

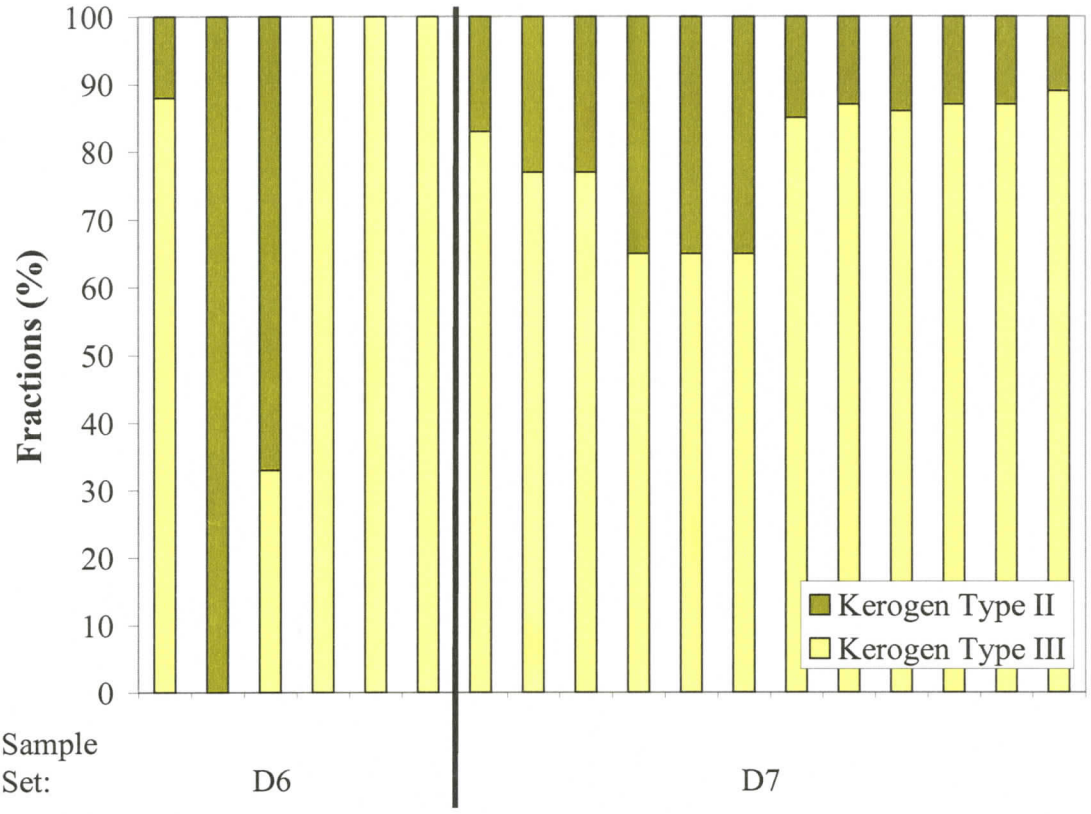


Figure 6.34: *Calculated fractions of propane generated from a Kerogen Type III and Kerogen Type II source rock in sample sets D6 and D7. Calculations are based on $\delta^{13}C$–$\%R_O$ relationships for propane by Berner and Faber (1996). Calculations of proportions of thermogenic and microbial gas are performed by applying a mass–balance equation (see text for equation). See text for discussion.*

The observed strong differences of contributions of gases derived from Kerogen Type II source rocks based on the calculations using $\delta^{13}C$ ratios of methane, ethane and propane indicate that for a scenario of gas mixing from two different thermogenic sources (Kerogen Type II and Type III), not all coal samples and coal seams are affected by the intrusion of Kerogen Type II gas in the same way. Some coals and coal seams would have to contain higher proportions of Kerogen Type II derived gas than others. These differences could indicate differences in the different considered coal samples, e.g., gas saturation and diffusivity.

For a scenario where the observed isotope compositions of methane, ethane and propane are the results of isotope alteration due to secondary processes, these alterations have a different impact on the different hydrocarbons methane, ethane and propane.

These possible differences in isotope alteration would have to be related to physical parameters, e.g., gas saturation and diffusivity.

Comparison of Liptinite Content in Coals with Molecular and Isotope Composition of Methane, Ethane and Propane

Indications for the presence of gases derived from Kerogen Type II source rocks are also observed by considering the proportions of higher hydrocarbons relative to the amount of liptinite present in the coal.

Gases generated from a humic coal are dry with only minor contributions of the higher gaseous hydrocarbons ethane, propane and butane (Levine, 1993; Rice, 1993; Hunt, 1995; Whiticar, 1996a). Exceptions are sapropelic coals and coals with a high amount of the maceral liptinite, which, because of its high hydrogen content, is more prone for the generation of higher hydrocarbons (Tissot & Welte, 1978; Schwarzkopf, 1984; Hunt, 1995; Whiticar, 1996a). The generation of higher hydrocarbons takes place for a humic coal normally during the stage of catagenesis at temperatures between ca. 70°C and ca. 130°C (Hunt, 1995). These temperatures correlate to vitrinite reflectance values between ca. 0.6 and ca. 1.6%R_O (Tissot & Welte, 1978; Hunt, 1995; Taylor et al., 1998). These implications lead to the following expectations:

1. Coals with maturities lower than ca. 0.6%R_O should have generated only low proportions of higher hydrocarbons,
2. Coals with maturities higher than ca. 1.6%R_O should have generated higher proportions of higher hydrocarbons during their history,
3. Coals with low amounts of liptinite should have generated only minor proportions of higher hydrocarbons,
4. Coals with high amounts of liptinite should have generated high proportions of higher hydrocarbons.

Amounts of liptinite, maturities and average proportions of higher hydrocarbons (ethane, propane, *n*–butane and *i*–butane) for sample sets D6 and D7 are presented in Appendix X.

Sample Set D6

For sample set D6, a mixture of gases generated from a Kerogen Type II and Type III source cannot be ruled out. An admixture of C_{2+} rich Kerogen Type II gas could explain observed high proportions of C_{2+} hydrocarbons in some canisters. ^{12}C enrichment, especially in methane, could also be explained by an admixture of isotopic light Kerogen Type II gas. Coals from sample set D6 are underlain by thick successions of Kerogen Type II shales and a mixture of gases generated by Kerogen Type II and Type III source rocks can be assumed.

Based on a maturity of 1.23%R_O to 1.77%R_O for coals from sample set D6 the generation of higher gaseous hydrocarbons (C_{2+}) is possible (Hunt, 1995), but the small amounts of liptinite in these coals (0.3%) indicate that the generation potential for C_{2+} hydrocarbons from liptinites is limited (Tissot & Welte, 1978; Schwarzkopf, 1984; Hunt, 1995; Whiticar, 1996a). The presence of elevated amounts of inertinite, which have the lowest generation potential for hydrocarbons for all macerals and a limitation to methane (Taylor et al., 1998), supports this assumption.

The average proportion of C_{2+} hydrocarbons for the different canisters of sample set D6 show strong variations between 0.05 and 5.68% with an overall average proportion of 2.21%. The proportions of C_{2+} hydrocarbons from sample set D6 with 0% liptinite are very low as expected, but samples from coals with 0.3% liptinite show unexpectedly high amounts between 2.21% and 5.68%. Post–maturation amounts of liptinite of only 0.3% in the coals should not have the ability for the generation of such large quantities of C_{2+} hydrocarbons. Liptinites become thermally destroyed during coalification and cannot be separated from other macerals. Therefore pre–maturation amounts of liptinites might have been higher. If the elevated proportions of C_{2+} hydrocarbons are the result of an admixture of Kerogen Type II derived gases, the question arises why only the coals with elevated amounts of liptinite contained gases high in C_{2+} hydrocarbons and not also the coals with low amounts of liptinite. A likely explanation is an exaggeration for the proportions of C_{2+} hydrocarbons based on the performed normalization. Carbon dioxide had to be removed from samples of sample set D6 and therefore, the normalization of the measured proportions are on the basis of

hydrocarbons only. Because of the presence of carbon dioxide in the samples the normalized proportions for the hydrocarbons are exaggerated.

It is likely that the proportions of C_{2+} hydrocarbons are actually in the expected range and that the elevated values for the mentioned coals are the result of the reported elevated amounts of liptinite in these coals. If this would be the case, the reported ^{12}C enrichments for methane, ethane and propane relative to a gas generated from a Kerogen Type III source rock would have to be attributed to isotope alteration due to secondary processes. This isotope alteration would therefore, mostly affect methane and to a lesser degree ethane and propane.

Sample Set D7

The potential of early stage C_{2+} hydrocarbons generation for coals from sample set D7 is indicated by the maturities of the coals (0.61%R_O and 0.71%R_O; Hunt, 1995). The expected proportions of C_{2+} hydrocarbons should be low; based on the low maturities the generation of significant proportions of C_{2+} hydrocarbons should not be expected (Hunt, 1995). The present depth of these coals and assuming a normal geothermal gradient of 3°C/100m, the present day temperatures (ca. 40°C) are too low for the generation of significant proportions of C_{2+} hydrocarbons. Hunt (1995) reported that the earliest occurrence of C_{2+} hydrocarbons relates to temperatures of ca. 50°C, but significant proportions are generated at temperatures between 70°C and 130°C. Potential for the generation of C_{2+} hydrocarbons is indicated by the relatively high amounts of liptinite (3% to 5%) in coals from sample set D7. Hunt (1995) and Taylor et al. (1998) reported a necessary amount of liptinites in coal of 15% for the generation of liquid hydrocarbons in addition to gas. Based on this information, coals from sample set D7 have the potential for the generation of elevated quantities of C_{2+} hydrocarbons.

Sample set D7 shows 3.1% to 10.5% (average 8.3%) C_{2+} hydrocarbons. There is no correlation between the amount of liptinite in the coals and the proportions of C_{2+} hydrocarbons. The lowest proportions of C_{2+} hydrocarbons is found in samples from a coal with high amounts of liptinite (5%), whereas the highest proportions of C_{2+} hydrocarbons are found in samples from a coal with lower amounts of liptinite (3%).

There is no relationship between the maturities of the coals and the proportions of C_{2+} hydrocarbons.

The following facts can be derived from measured compositional and isotope values for sample set D7:

1. The measured proportions of C_{2+} hydrocarbons (average 8.3%) are higher than expected for a gas generated from a humic coal of low maturity and relatively low amounts of liptinite (ca. 1%; Whiticar 1996a),
2. The isotope compositions of methane, ethane and propane (for t_{START}, t_{END} and t_{WGH}) show ^{12}C enrichment (for methane: -29.0‰ to -41.8‰) relative to a gas generated from a Kerogen Type III source rock (for methane: -29.0‰ to -28.7‰; values based on maturities of 0.61%R_O to 0.71%R_O using $\delta^{13}C$–%R_O relationships by Berner and Faber, 1996).

Based on these findings, it is not likely that the relatively high proportions of C_{2+} hydrocarbons and the relative ^{12}C enrichments for methane, ethane and propane in sample set D7 are generated from coals, but from external sources.

Considering the possibility of an admixture of gases from an underlying source, these gases have to fulfill the following criteria:

1. Methane, ethane and propane should be more ^{12}C enriched than gases generated from a Kerogen Type III source rock,
2. The proportions of C_{2+} hydrocarbons should be higher than expected for a gas generated from a Kerogen Type III source rock.

Samples for sample set D7 come from coal seams, which are underlain by Kerogen Type II shales. This Kerogen Type II source rock is a possible source for admixed gases. Gases generated from a Kerogen Type II source rock show the following characteristics:

1. High proportions of C_{2+} hydrocarbons (ca. 13%; Hunt, 1995),
2. Based on maturities of 0.61%R_O to 0.71 %R_O, $\delta^{13}C$ values for methane, ethane and propane are more ^{12}C enriched than a gas generated from a Kerogen Type III source

(for methane: -46.1‰ and heavier; based on relationships by Berner and Faber, 1996).

Therefore, a shale (Kerogen Type II) would fulfill the necessary requirements and is considered to be a likely source for gases migrated into the coal seams. In Figures 6.29, 6.30 and 6.31 it is shown that the measured $\delta^{13}C$ values for methane, ethane and propane plot between the calculated values for gases generated from a Kerogen Type III and Type II source, indicating a possible mixture of gases generated by these two types of sources rocks.

An alternative explanation of the measured data includes that the measured amounts of macerals are not representative for the coal. To explain the elevated proportions of C_{2+} hydrocarbons higher amounts of liptinite are required, or alternatively the presence of substances with a high potential for the generation of C_{2+} hydrocarbons, e.g., resinites and sapropelic materials. In this scenario, the ^{12}C enrichment for methane, ethane and propane would be only attributed to a possible admixture of microbial gas and isotope alteration due to secondary processes.

Sample Set D7: Depth–$\delta^{13}C$ Methane Relationships

A relationship between $\delta^{13}C$ methane (, t_{START}, t_{END} and t_{WGH}) and depth (Figure 6.35) is observed. The deepest samples show the greatest ^{13}C enrichment, whereas a relative depletion in ^{13}C is observed with decreasing depth. Analogue $\delta^{13}C$depth relationships are not observed for ethane (Figure 6.36) and propane (Figure 6.37). These observations indicate that if Kerogen Type II derived gases migrated into and were adsorbed onto coals, then methane behaves differently from ethane and propane.

Migration of methane through the coal seams with the isotope effect of adsorption is a possible explanation for the isotope–depth relationship observed for methane. Adsorption discriminates against the light isotope ^{12}C, resulting in relative ^{13}C enrichment in the adsorbed methane and relative ^{12}C enrichment in the non–adsorbed methane (Lebedev and Syngayevskiy, 1971; Faber, 1987; Whiticar, 1996a). Therefore, based on the maturity range of the considered coals for sample set D7 between 0.61%R_O

and 0.71%R_O and the presence of a gas generating Kerogen Type II source rock, the following model for the explanation of the observed ^{12}C enriched $\delta^{13}C$ values for methane and the observed trend of ^{12}C enrichment in methane with decreasing depth can be proposed. For this model certain conditions have to be applied:

1. Coal seams have to be initially undersaturated with gas,
2. Coal seams will become gas saturated with migrating gas from Kerogen Type II source, leaving free gas behind,
3. Compositional and isotope effects due to migration and diffusion are of minor importance.

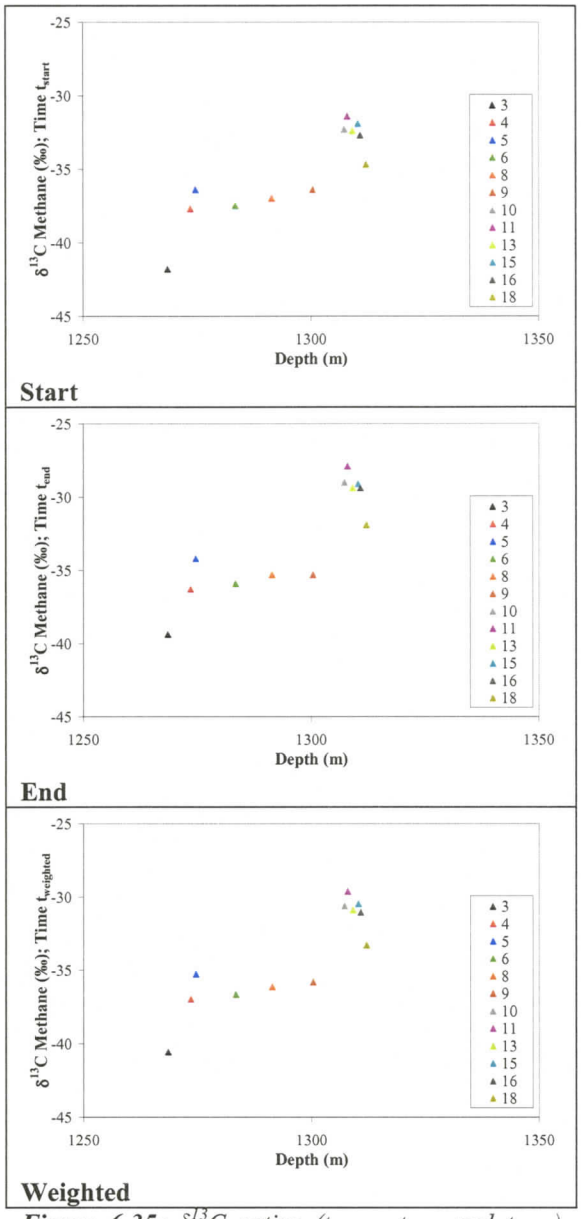


Figure 6.35: *$\delta^{13}C$–ratios (t_{START}, t_{END} and t_{WGH}) for methane from samples of desorption experiment sample set D7 presented versus depth of the corresponding coals. t_{START} represents the first sample available per canister, t_{END} represents the last sample available per canister. For calculation of value t_{WGH} see text. For discussion see text.*

The model includes three coal seams (I, II and III) underlain by a shale (Figure 6.38). Gases generated in all three coals are dry and the $\delta^{13}C$ values for methane are between -29.0‰ and -28.7‰. Gases generated in the shale are wet and $\delta^{13}C$ values for methane are -46.1‰ or heavier. The maturity of the shale is assumed to be as high as the highest maturity reported for the overlying coal seams (0.71%R_O). In the model, the possible interaction with microbial gas is neglected. The gases generated in the different coal seams become immediately adsorbed onto the coal, and leaves the coal undersaturated. The gases generated in the shale migrate into the overlying coal seam I, where the gas becomes partly adsorbed onto

the coal. Coal seam I becomes saturated with gas, leaving free gas present in the coal seam. The process of adsorption is accompanied by an isotope effect with the preferential adsorption of ^{13}C. C_{2+} hydrocarbons also become, relative to methane, preferentially adsorbed onto the coal resulting in the observed C_{2+} proportions. The remaining ^{12}C enriched non adsorbed methane and non adsorbed C_{2+} hydrocarbons in coal seam I continue to migrate. When reaching coal seam II, again adsorption and molecular and isotope partition occurs. Adsorption of ethane and propane also occurs at this stage. Coal seam II becomes saturated with gas, leaving free gas in the seam. Because the gas, which became adsorbed onto coal seam II was already depleted in ^{13}C, methane adsorbed onto coal seam II is more ^{12}C enriched, than coal seam I. The remaining free gas, now strongly ^{12}C enriched, continues to migrate. When reaching coal seam III adsorption occurs. Because of the earlier ^{12}C enrichment the methane now adsorbing onto coal seam III is strongly ^{12}C enriched. The overall result is an elevated proportion of C_{2+} hydrocarbons in the different coal seams and ^{13}C enriched methane adsorbed onto coals at greater depths.

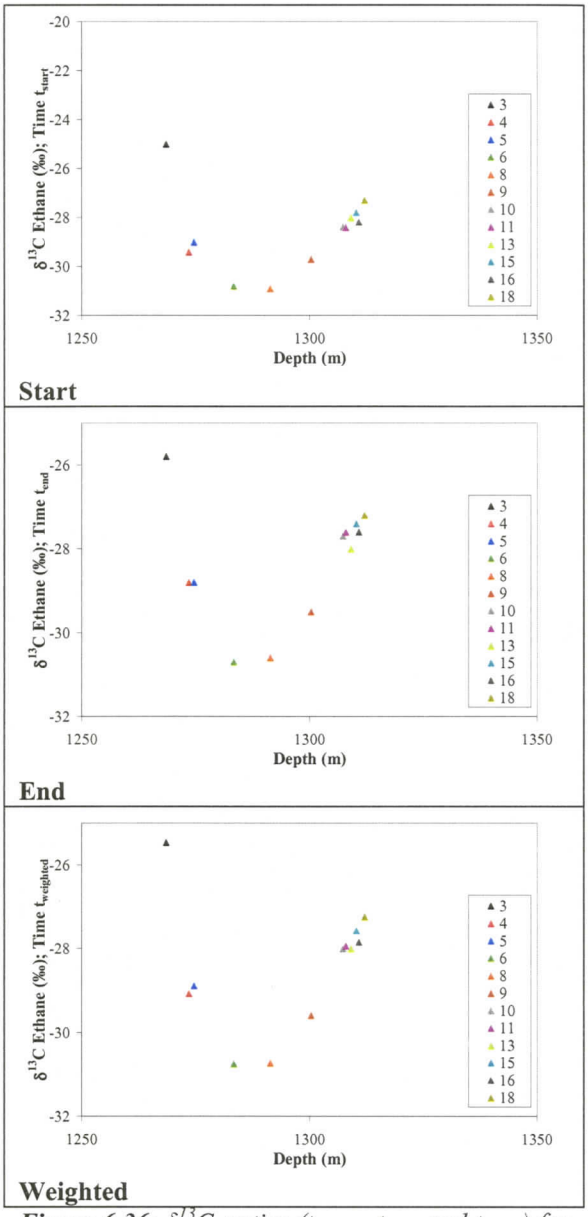


Figure 6.36: *$\delta^{13}C$–ratios (t_{START}, t_{END} and t_{WGH}) for ethane from samples of desorption experiment sample set D7 presented versus depth of the corresponding coals. t_{START} represents the first sample available per canister, t_{END} represents the last sample available per canister. For calculation of value t_{WGH} see text. For discussion see text.*

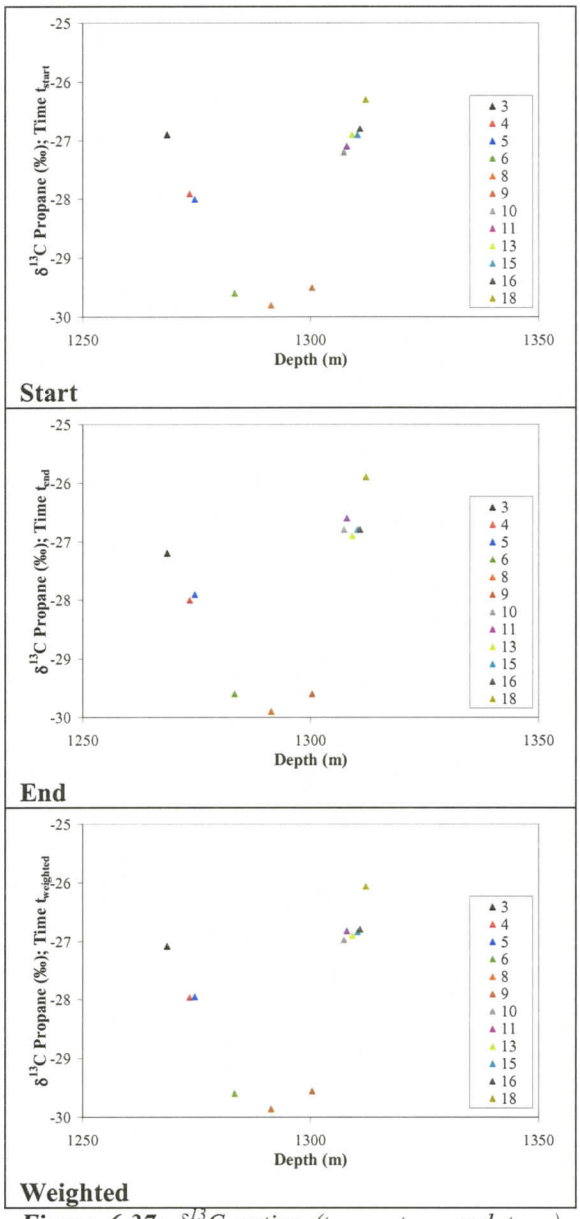


Figure 6.37: *$\delta^{13}C$–ratios (t_{START}, t_{END} and t_{WGH}) for propane from samples of desorption experiment sample set D7 presented versus depth of the corresponding coals. t_{START} represents the first sample available per canister, t_{END} represents the last sample available per canister. For calculation of value t_{WGH} see text. For discussion see text.*

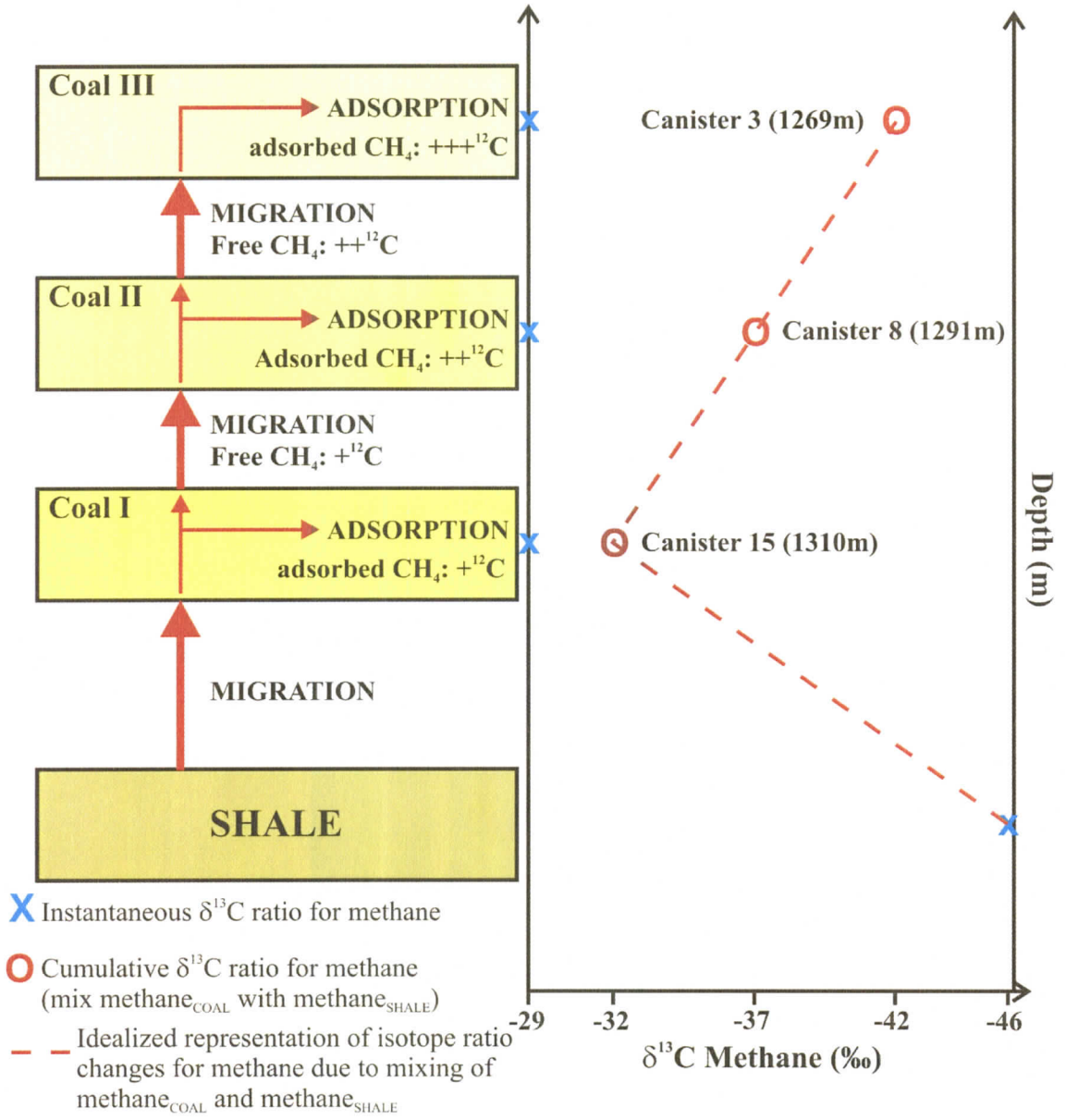


Figure 6.38: *Idealized and schematic model for mixture of methane generated from a Kerogen Type III and methane from a Kerogen Type III source rock from samples of sample set D7. CH_4 = methane; + = medium; ++ = strong; +++ = very strong Stippled red line does not represent an actual mixing line, but illustrates the changes for the $\delta^{13}C$ ratio for methane. See text for discussion.*

The model is not able to account for the presented ethane and propane $\delta^{13}C$ values (Figures 6.36 and 6.37). If $\delta^{13}C$ ratios of ethane and propane would be similarly affected by adsorption, a similar $\delta^{13}C$–depth trend should be observed. The lack of a relationship at all, may indicate that adsorption only has an isotope effect on methane, or that the direction (^{12}C or ^{13}C enrichment) and magnitude is different for methane and ethane/propane. The $\delta^{13}C$ ratio of methane may be influenced by the presence of

microbial gas, whereas ethane and propane are not influenced, also resulting in differences between the gas species.

6.2.2c Mixture of CBM Gas A with CBM Gas B

At higher coal ranks (medium volatile bituminous and higher) the possibility occurs that coals generate more gas than they can store (Rice, 1993). When such a deeply located coal seam is gas saturated, the remaining non adsorbed free gas will migrate out of the coal. This migration can lead to the formation of gas reservoirs in suitable reservoir rocks (Rice, 1993), or when reaching a coal undersaturated in gas, the migrating gas becomes adsorbed by the coal leading to a mixture of different CBM gases.

Because of the similarities of gas composition and stable carbon isotope ratios of gases generated by different coals or Kerogen Type III source rocks, the identification of mixing between two CBM gases is difficult.

The bulk carbon isotope composition of coals from North America and Europe is limited to $\delta^{13}C_{coal}$ values between -22‰ and -27‰ (Schwarzkopf & Schoell, 1985). For maturities below the rank of meta–anthracite, maturity does not appear to have an influence on the stable carbon isotope ratio of the coal (Redding et al., 1980), whereas coals of higher ranks show a trend towards ^{13}C enrichment (Hoefs & Frey, 1976; Berner & Faber, 1996). Applying the established $\delta^{13}C$–$\%R_O$ relationships by Berner and Faber (1996) between maturity of a source rock and expected $\delta^{13}C$ ratio for methane, generated from this source, shows that the expected isotope ratio of the generated methane shows only a difference of 7‰ (-29.1‰ to -22.1‰) for a considered range of maturity from $0.6\%R_O$ to $2.5\%R_O$. For a scenario of a high volatile A bituminous coal ($0.7\%R_O$) underlain by a low volatile bituminous coal ($1.6\%R_O$), the differences between the expected carbon isotope ratio for methane would be only 3.3‰. Therefore, the expected carbon isotope ratios for methane generated from different coals are expected to be very similar and differentiate by maximal 7‰, unless high rank coals are present. No relationships for the calculation of $\delta^{13}C$ for methane, based on the maturity of such high rank coals, are available. The expected gas composition for gases generated from different humic coals is also considered to be similar, with predominantly methane and

only minor contributions of higher gaseous hydrocarbons (Levine, 1993; Rice, 1993; Hunt, 1995; Whiticar, 1996a).

Methane t_{WGH} values for all sample sets (Appendix Y) show ^{12}C enrichment, relative to $\delta^{13}C$ values for methane expected to be generated from the canister coals. These ^{12}C enrichments are likely to be the result of isotope effects due to secondary processes and the admixture of microbial and/or Kerogen Type II derived gas.

6.2.2d Microbial Oxidation of Methane

The presence of microbial methane oxidation in coal seams is likely, but it is difficult to detect evidence for this process from analyses of gas composition and the $\delta^{13}C$ ratios of methane from samples derived from desorption experiments or from producing wells. Trends indicating microbial methane oxidation may be masked by molecular and isotope effects due to other processes.

A recent study by Ulrich et al. (2005) investigated the microbial generation of methane in coals from the Powder River basin in Wyoming, USA. Scanning electron microscope analyses of these coals showed that bacteria responsible for gas generation are located in fractions and cleats within the coal and that the physical size of these bacteria is too big to reach the pores within the coal (Ulrich et al., 2005). The pore system within a coal is the actual place where adsorption and desorption, and therefore the storage of methane, occurs (Rice, 1993; Beamish & Crosdale, 1995). Therefore, if microbial oxidation of methane takes place in a coal seam, the methane has to be present as a free gas in fractures and cleats, allowing the uptake by the bacteria present there. Free gas in a coal will be the first gas migrating out of the coal during the recovery of the coal for desorption experiments, or during the production of CBM from a coal seam. When considering gas samples recovered from desorption experiments, the free gas will already be lost from the coal prior to sealing the coal into desorption canisters. Depending on migration distances, free gas should already be lost from samples taken from wells already producing CBM for a substantial amount of time. Therefore, in all analyzed samples for this study no free gas should be present in the samples. Additionally, the pool of available methane in CBM is so large that substantial proportions of methane have to

be oxidized, in order to recognize a relative depletion in methane and a corresponding enrichment for carbon dioxide. The scenario of large–scale microbial methane oxidation in coal is unlikely, because most of the gas stored in a coal is adsorbed onto the internal surface of the coal particles in the pore system (Yee et al., 1993; Crosdale et al., 1998), away from the actual location of the oxidizing bacteria. When CBM is produced, either in a production or desorption experiment scenario, the stored gas will desorb and diffuse into the fracture and cleat network of the coal. At this point microbial uptake of this free methane can occur.

Faber (1987), Berner (1989) and Whiticar (1990, 1994, 1996a) proposed two approaches for the identification of microbial oxidation of methane, using the Bernard Diagram and a cross–plot of $\delta^{13}C$ methane versus $\delta^{13}C$ ethane. These approaches will be applied to the data presented in this study, to see if microbial methane oxidation is present and if it can be detected.

A gas pool affected by microbial methane oxidation becomes 1) relatively depleted in methane, i.e., becomes wetter, 2) enriched in carbon dioxide and 3) the residual methane becomes relatively enriched in ^{13}C. In this study most samples are methane rich and the methane is ^{12}C enriched, relative to primary $\delta^{13}C$ ratios for methane generated from a Kerogen Type III source rock, especially samples collected during desorption experiments. No trends indicating microbial methane oxidation (see Figure 6.19) can be observed in the Bernard Diagrams (Figures 6.20 and 6.21); trends may be masked due to other processes, i.e., adsorption, desorption and diffusion.

Support for the lack of observed microbial oxidation of methane is provided by a cross–plot for the carbon isotope compositions of methane and ethane (Figure 6.39). This plot shows the effects on the $\delta^{13}C$ values for methane and ethane as a result of admixture of different thermogenic gases, admixture of microbial gas and microbial methane oxidation. The relationship "unaltered" in Figure 6.39 represents the primary $\delta^{13}C$ values for unaltered methane and ethane, for maturities between 0.57%R_O and 4.55%R_O ($\delta^{13}C$–%R_O relationships for methane and ethane generated from a Kerogen Type III source rock by Berner and Faber, 1996). Shown in Figure 6.39 are t_{WGH} values for methane and ethane plus maturities of the corresponding coals (shown in identical colours). A shift towards ^{13}C enriched methane values away from the "unaltered" line (parallel to the

corresponding maturity) would indicate the presence of microbial oxidation processes, but this is not the case. Almost all samples show strong ^{12}C enrichment for methane and ethane. An exception is the high maturity sample set D2, which shows ^{12}C enrichment only for ethane. However, these samples are beyond the calibrated range of a maximum maturity of 2.5%R_O for methane and 2.0%R_O for ethane. Methane carbon isotope ratios for higher maturities, especially for maturities of 4%R_O or higher, would be more ^{13}C enriched than indicated by the plotted relationship (Hoefs & Frey, 1976; Berner & Faber, 1996), therefore implying that methane from samples of sample set D2 are also ^{12}C enriched.

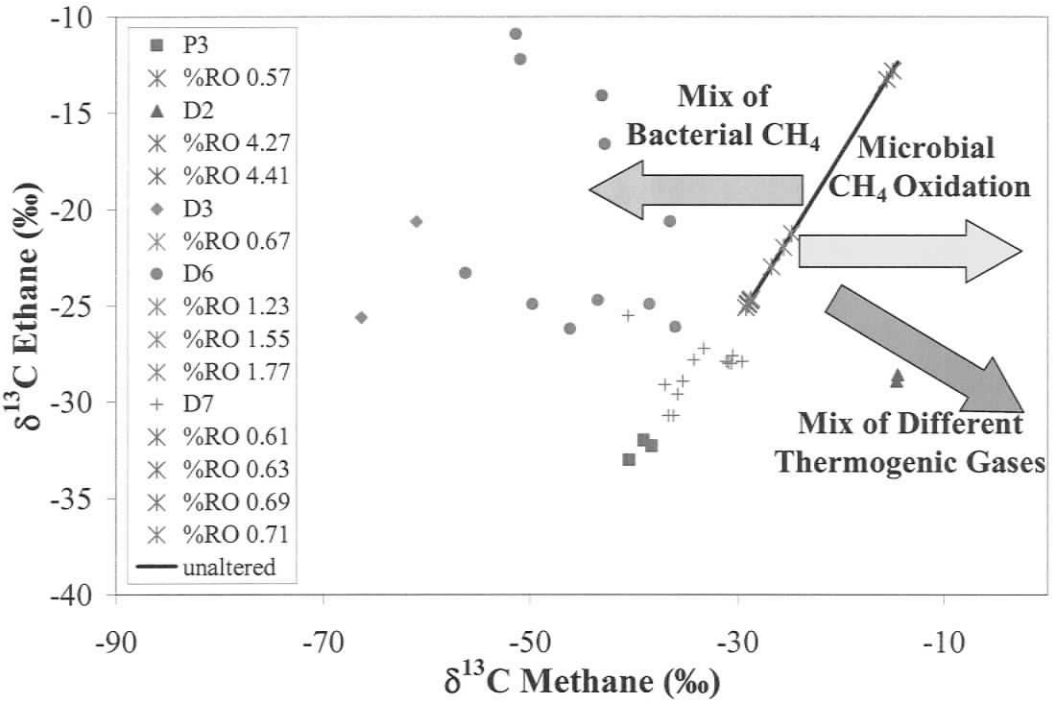


Figure 6.39: *$\delta^{13}C$ methane–$\delta^{13}C$ ethane plot showing expected isotope trends for methane and ethane due to processes of admixture of bacterial methane, mixture of different thermogenic gases and microbial methane oxidation. Shown are results from production and desorption experiment sample sets P3, D2, D3, D6 and D7, together with vitrinite reflectance values of the corresponding coals. No results for the other sample sets are available. Black line indicates unaltered gases (methane and ethane) with increasing maturity (modified from Berner and Faber, 1996).*

The proportions of carbon dioxide in samples from production and desorption experiment sample sets (exceptions are D3 and D4) decrease with increasing time (Figures 5.3 and 5.10). This relative decrease indicates that carbon dioxide generation due to methane oxidation is not present or not detectable by considering proportions of carbon

dioxide in CBM samples. Microbial methane oxidation can be assumed based on increasing proportions of carbon dioxide in sample sets D3 and D4 (Figure 5.10) This is because it is not clear if the observed increase of proportions of carbon dioxide is a result of carbon dioxide generation due to methane oxidation, or if it is carbon dioxide, desorbing naturally from the coal.

6.2.2e Adsorption and Desorption

The molecular and isotopic characteristics of CBM, are influenced by gas generation, mixing (microbial and thermogenic generated gas), adsorption, desorption and diffusion. The interaction of these processes has implications for the compositional and isotope systematics of CBM. The repeated occurrence of these processes during the evolution of a coal seam and its burial history lead to extreme complications.

During early coalification, early thermogenic gas is generated. These gases can be retarded by the coal due to its sorptive ability. With increasing coal rank the sorption capacity of a coal increases initially, until at higher coal ranks the sorption capacity decreases. Increasing burial, leading to hydrostatic pressure increase, also results in increasing sorption capacity. Therefore, pre–coalification microbial and early thermogenic gases are adsorbed onto the coal sometimes as a gas mixture. The molecular composition of this gas and the isotope ratio of methane depend on the proportions of these different gases. When these proportions or end member compositions are not known, then an exact evaluation of composition and the carbon isotope ratio of methane can not be made.

As long as a coal is undersaturated with gas, molecular and isotope effects due to the process of adsorption will not be expressed, because all available gas will be adsorbed onto the coal. That changes once the generation of thermogenic gas exceeds the sorption capacity of the coal. At this point coal cannot totally adsorb the available quantities of gas so that molecular and isotope effects may occur. In this case the adsorbed gas fraction will become enriched in carbon dioxide and higher hydrocarbons relative to methane and the adsorbed methane will become enriched in ^{13}C over ^{12}C. The remaining non–adsorbed gas will therefore be relatively enriched in methane that is relatively enriched in ^{12}C. If

the coal seam is overlain by a seal rock, then this free gas could remain trapped in the coal, stored in cleats and fractures. When the desorption capacity increases again, for example due to further burial, this stored free gas can be adsorbed onto the coal. Depending on the fraction of gas becoming adsorbed, molecular and isotope effects might occur. It is likely that this free gas will be mixed with thermogenic gas generated continuously by the coal. If no seal rock is present, then the surplus gas, plus gas generated continuously by the coal, will migrate out of the coal seam, depleting the gas pool in ^{12}C enriched methane. This migrating gas can become adsorbed onto overlying coal seams that are able to adsorb gas. The gas pool of these coals is enriched in ^{12}C enriched methane.

A schematic representation of the coal sorption capacity (Figure 6.40) shows that sorption initially increases with increasing depth due to pressure increase. This increase stops once temperatures are high enough to counteract the effect of increasing pressure. The effect of increasing pressure is displaced by the effect of increasing temperature on the sorption capacity with further increase in temperature with greater burial. Decreasing pressure due to uplift can result in a decrease in sorption capacity. Such a reduction in sorption capacity, either due to temperature increase or pressure decrease, results in the desorption of gas, accompanied by molecular and isotope effects. The desorbing gas will be enriched in methane relative to other gases with this methane being relatively ^{12}C enriched. If a seal rock is present, this desorbed and

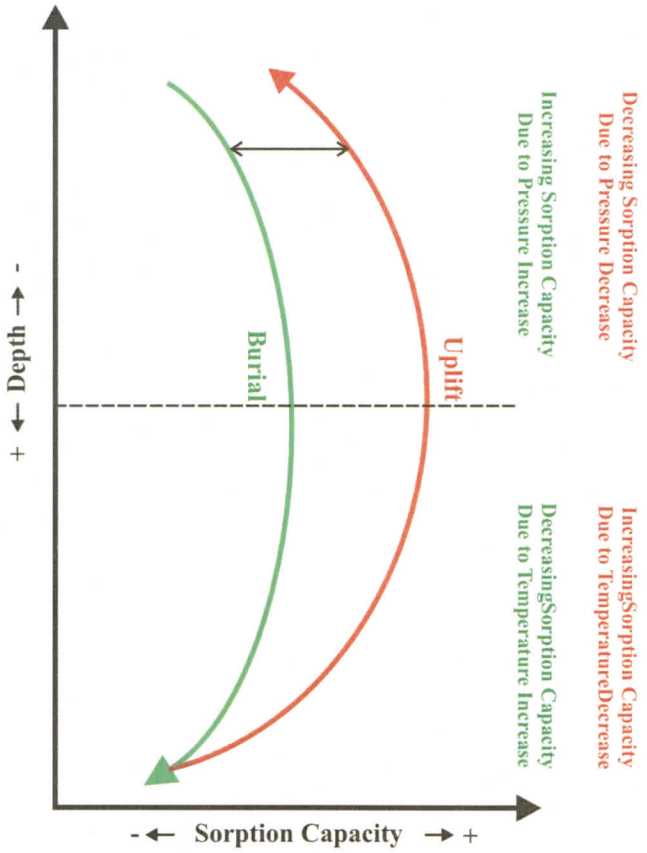


Figure 6.40: Idealized diagram showing effect of temperature and pressure on the sorption capacity of coal during burial and uplift. See text for discussion.

now free gas will be stored in the coal and may become re–adsorbed onto the coal when the sorption capacity increases again. Without a seal rock this gas will migrate out of the coal and will be lost from the gas pool. The residual adsorbed gas is depleted in methane, and enriched in ^{13}C. The possibility of an admixture of gases generated from different types of source rocks (Kerogen Type I, Type II) also present, would be a source for molecular and isotope effects.

Repeated burial and uplift, every time accompanied by adsorption and desorption, can result in continuous depletion of the gas pool in ^{12}C enriched methane. An additional complication can occur when coals are uplifted into an environment suitable for post–coalification generation of microbial gas, enriching the gas pool in relatively ^{12}C enriched methane.

This multitude of processes and their possible interactions leads to a variety of molecular and isotope ratios of gases, especially for methane, stored in coal seams. Therefore qualitative and quantitative considerations of CBM systematics are difficult. Because of these complications and especially because of the lack of knowledge about the molecular and isotope effects (for example, no fractionation factors are published for adsorption and desorption of methane) a differentiation of the different processes is not possible. Therefore, the relative impact of the described processes, gas generation, mixing, adsorption and desorption, can not be determined.

During the production and sampling of CBM (production and desorption experiments) not all gas adsorbed onto the coal is removed and measured. Therefore, the recovered gas will not represent the mean composition of the total overall adsorbed gas. The isotope ratios of the different gas species may also be different to the mean values of the adsorbed gases. Regardless of the molecular composition and the isotope ratios of the adsorbed gases, fractionation effects may occur when desorption is initiated for either production or for desorption experiments. Early desorbing gas is expected to be relatively enriched in methane and that methane is expected to be relatively enriched in ^{12}C. With increasing desorption time, the relative proportions of carbon dioxide and higher hydrocarbons should increase, as well as the ^{13}C content of methane. Carbon dioxide is expected to desorb quickly when the right conditions are present, leading to volume increases in the coal, which may be responsible for catastrophic gas outbursts in

underground mines (for example Smith & Gould, 1980; Flores, 1998). Therefore, the proportions of carbon dioxide in desorbing CBM should show a strong increase at a certain time.

Indications for desorption are found in the data from the different sample sets. The observed methane isotope variations in the data cannot be attributed to gas generation itself. Secondary processes, i.e. mixing, diffusion and processes occurring during the geological history of coal must have had an impact on the molecular and isotope composition of the analyzed CBM samples. These processes compound the process of desorption. The fractionation effects for these processes cannot be isolated and it is therefore not possible to delineate the impact of desorption.

Overall, the analyzes data show large variations for molecular and isotope composition of methane, higher hydrocarbons and carbon dioxide. As mentioned the methane isotope variations cannot be attributed to gas generation itself. The $\delta^{13}C$ variation is 7‰ between sample maturities of 0.6%R_O and 2.5%R_O whereas the observed variation is over 40‰. Therefore secondary processes have must have an impact on the composition. The different observed trends include those expected for the process of desorption. Production/desorption time may have been too short for the desorption of larger proportions of the strongly bound higher hydrocarbons and carbon dioxide. Hence no indications for the presence of desorption are observed from the development of the proportions of higher hydrocarbons and carbon dioxide with increasing production/desorption time. Based on the storage of gas adsorbed onto the coal, all analyzed gases are desorbed gases and should therefore have been subjected to some degree of fractionation due to desorption.

Desorbed gases diffuse from the spot of desorption into the fracture and cleat network within the coal. This process is responsible for molecular and isotope fractionation. The fact that diffusion and desorption show fractionation effects in the same direction (e.g. ^{12}C enrichment for early desorbed/diffused methane) makes their differentiation difficult. In addition, the physical conditions in a coal seam and during the process of desorption (desorption experiment) should be included. Changes in pressure and temperature, due to weather or altitude, during the process of desorption can have an impact on the actual process. Changes in pressure and temperature lead to accelerated

desorption (lower pressure and/or higher temperatures) or to the re–adsorption of already desorbed gas, stored in the headspace of a canister, (higher pressure and/or lower temperatures) onto the coal. These processes would again have a fractionation effect.

Stable Carbon and Hydrogen Isotopes

Many different trends for the carbon isotope composition of methane can be observed in the data. It should be emphasized that there is a general difference between samples from production scenarios (Figure 5.4) and samples from desorption experiment scenarios (Figure 5.11).

All samples from production scenarios show ^{12}C enrichment for methane with increasing production time (Figure 5.4). This trend is opposite to the expected trend of ^{13}C enrichment with time for desorption. Most samples from desorption experiments scenarios show the expected ^{13}C enrichment with increasing desorption time (Figure 5.11). Exceptions are sample sets D1, D3 and D4, which are assumed to have *in situ* generation of microbial methane.

The carbon isotope composition of methane from canisters R6 and R7 of sample set D2 (Figure 5.11) show after an initial ^{12}C enrichment the expected ^{13}C enrichment with increasing desorption time. Methane from canister R20 shows the opposite trend, with an initial ^{13}C enrichment followed by ^{12}C enrichment. This difference in trends might be related to differences in the geological and physical characteristics of the related coals. Overall, the $\delta^{13}C$ ratios for methane from sample set D2 are extremely enriched in the heavy isotope ^{13}C with values more positive than -4‰ (Figure 5.11). Based on maturities of 4%R_O or more, these coals have a complex history and the ^{13}C enriched methane might be the result of repeated gas loss, including ^{12}C enriched methane due to repeated desorption processes and associated migration of these desorbed gases out of the coal.

δD ratios for methane show no conclusive trends (Figures 5.5 and 5.12). Carbon isotope data for the heavier hydrocarbons are limited and only a few results are available for ethane (Figures 5.7 and 5.14). These data show a wide range of absolute values and no conclusive trend with increasing time is observed. Carbon isotope ratios for carbon

dioxide show only small variations with increasing production/desorption time and no conclusive trends (Figures 5.6 and 5.13). An exception is sample set D6 that shows an initial ^{12}C enrichment with increasing desorption time, as is expected for desorption. This trend is more pronounced during the early desorption, whereas the later samples show less variation with time, almost reaching constant $\delta^{13}C$ ratios. $\delta^{13}C$ ratios for carbon dioxide from sample set D3 converge simultaneously to almost identical values around -11‰ (Figure 5.13). The sudden ^{12}C increase correlates with elevated proportions of carbon dioxide (Figure 5.10). A possible contamination of the canisters during the desorption experiment with air is possible (B. Ryan, personal communications).

Molecular composition

Methane contents are high (Figures 5.1 and 5.8). If lower proportions are measured for early collected samples (sample sets P1, P3 and D1) then this may be related to sampling problems. These low values correlate to higher proportions of carbon dioxide (Figures 5.3 and 5.10) and higher hydrocarbons (Figures 5.2 and 5.9). This is expected, because all presented proportions are normalized to 100% on the volume basis of methane, ethane, propane, *n*–butane, *i*–butane and carbon dioxide.

Coals for sample set D4 were collected underground and, due to decreased pressure conditions, have already experienced desorption and the general loss of gas including relatively ^{12}C enriched methane. Therefore it is likely that the observed decrease in the proportion of methane (Figure 5.8), which correlates to a strong increase in the proportion for carbon dioxide (Figure 5.10), is related to the effect of late desorption of carbon dioxide and/or the previous loss of methane. The overall differences in the proportions of carbon dioxide are large within sample set D4 (Figure 5.10), despite the fact that the related coals were all sampled from the same coal seam at approximately the same location, i.e., the geological and physical characteristics of these samples are similar. The fact that samples from certain canisters of sample set D4, especially canisters 4, 7 and 9, do not show decreasing proportions of methane with increasing desorption time (Figure 5.8) might be the result of *in situ* generation of microbial methane in the canister. The canisters that show consistently high proportions of methane also show

consistently ^{12}C enriched methane (Figure 5.11). In contrast, the samples from the other canisters of sample set D4 show ^{13}C enrichment with increasing time, as it is expected for the process of desorption. The proportions of higher hydrocarbons (ethane, propane, *n*–butane and *i*–butane are combined) for these samples is generally very low (Figure 5.9), but they show a distinct maximum very early during the considered desorption time.

6.2.2f Diffusion/Migration

The application of fractionation effects for the diffusion of methane could theoretically allow the quantification of this process for CBM and a better quantitative understanding of the impact of processes like adsorption and desorption. However this is difficult because of the following reasons:

1. Reported fractionation effects were measured for methane and ethane diffusion through fine–grained sedimentary rocks (shale, sandstone), not through coal,
2. Observed isotope effect due to adsorption of methane onto organic material in sedimentary rocks during diffusion (Zhang and Kroos, 2001) is not expected in coals ,
3. Reported fractionation effects for methane diffusion through sedimentary rocks range between -2.22‰ and -30‰,
4. Diffusion length varies, based on the cleat and fracture network in the different coals; these parameter are unknown,
5. The isotope composition of the initial gas desorbing from the coal is not known,
6. The earliest gas desorbing from and diffusing out of coal can not be collected and its isotope composition is therefore unknown,
7. Water saturation of the different sample sets is unknown,
8. Actual pressure and temperature conditions for the seams are unknown,
9. It is not clear how much impact the desorption of methane prior to diffusion has on the isotope composition of the methane and how much influence pressure and temperature have on this isotope effect.

CBM gases have to be subjected to molecular and isotope effects due to diffusion, but based on the evolution of these parameters with time and classical approaches, no

conclusive evidence for diffusion are observed. Classical approaches for the delineation of diffusion are not useful for CBM gases and new approaches, which integrate the multitude of processes altering the molecular and isotope composition of CBM have to be developed.

Variations in $\delta^{13}C$ values for methane over time (Figure 5.4) do not show expected trends for diffusion in samples from production scenarios. Some samples from desorption experiments (Figure 5.11) show an overall trend that would be expected for diffusion.

Initially strong ^{12}C enriched methane was measured for sample sets D3, D4, D6 and D7 (Figure 5.11). The initial $\delta^{13}C$ values for methane from sample set D3 are between ca. -65‰ and ca. -73‰ (Figure 5.11) and therefore, relative to primary methane generated from coal, ^{12}C enriched. These values stay constant for a desorption time of around 400 hours. At a desorption time of around 400 hours, the $\delta^{13}C$ values for all canisters show a strong and sudden ^{13}C enrichment for methane to values between ca. -40‰ and ca. -50‰. The ^{13}C enrichment for methane is expected. However, when considering the experimental results of diffusion studies (see Chapter 2.5.3d), the initially ^{12}C enriched methane becomes quickly ^{13}C enriched causing a steep slope in a time versus $\delta^{13}C$ (methane) diagram (Figure 5.11). The magnitude of this ^{13}C enrichment decreases with time and the $\delta^{13}C$ values for methane slowly approach the $\delta^{13}C$ value of the used source methane.

Sample set D4 shows strong fluctuations in methane $\delta^{13}C$ ratios with time. Overall ^{13}C enrichment is observed, but not strongly expressed due to masking.

Sample set D6 shows for most canisters the expected trend of initially light methane, the strong early ^{13}C enrichment and the decrease in magnitude for this increase later in time (Figure 5.11). Initial $\delta^{13}C$ ratios for methane range between ca. -58‰ and ca. -36‰, whereas the final samples show $\delta^{13}C$ values between -55‰ and -30‰. When assuming that the final $\delta^{13}C$ values for methane are isotopically close to the primary $\delta^{13}C$ values for methane generated from a Kerogen Type III source rock, the observed differences are too large to be attributed only to gas generation from coal.

The analyzed $\delta^{13}C$ ratios for methane from sample set D7 show the methane of early samples being relatively ^{12}C enriched and methane of the later samples enriched in

^{13}C (Figure 5.11). The correlating desorption times for these samples indicate that the first samples were taken relatively late during the desorption process. The observed small differences in $\delta^{13}C$ for methane of 1‰ to 3‰ could indicate isotope effects during late stages of diffusion.

Pernaton et al. (1996) observed that stable hydrogen isotopes have the opposite trend to carbon isotopes during the diffusion of methane through sedimentary rocks. This means that the initial diffused methane is ^{2}H enriched. This trend is not observed for the analyzed hydrogen isotope compositions of samples from desorption experiments (Figure 5.12). Overall, the methane hydrogen isotope ratios show no or only slight variations with increasing time.

The stable carbon isotope ratios for ethane show no or only minor variations with increasing time (Figures 5.7 and 5.14).

The diagram for the determination of the presence of diffusion in natural gases proposed by Colombo et al. (1970) and Prinzhofer and Pernaton (1997) (Figure 2.15; see Chapter 2.5.3d) expresses mixing of two gas pools represented by an almost straight line (see Prinzhofer & Pernaton, 1996 for details). Diffusion would be expressed in this diagram by data plotting on an exponential curve (see Figure 2.15). Based on Figure 6.41 no evidence for diffusion can be observed for samples from production scenarios. With the exceptions of sample sets D6 and D7, no sample set

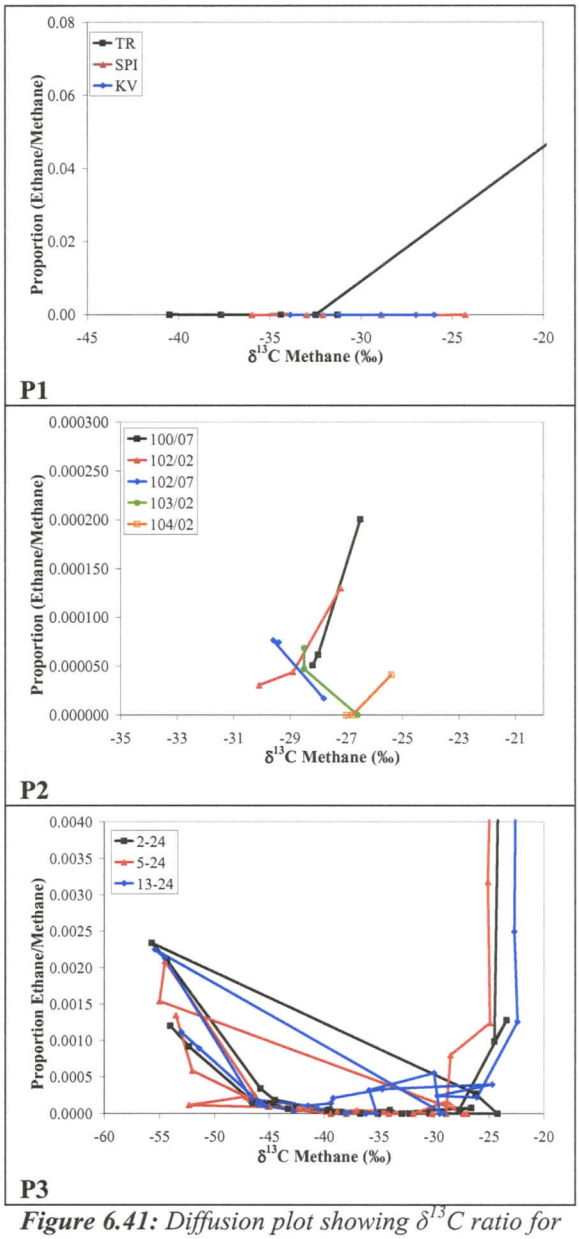


Figure 6.41: *Diffusion plot showing $\delta^{13}C$ ratio for methane versus ratio of proportions of methane over ethane for samples of production sample sets P1, P2 and P3. See text for details (diagram from Colombo et al., 1970 and Prinzhofer and Pernaton, 1997).*

shows a conclusive trend either for diffusion or mixing (Figure 6.42). Sample sets D6 and D7 are thought to contain a mixture of gases generated from a Kerogen Type II and Kerogen Type III source rock. Based on the diagrams in Figure 6.42, the data suggest mixing between thermogenic and microbial gas. Gases generated from a Kerogen Type II source rock contain relatively large proportions of higher hydrocarbons, which can be observed in the diagrams for sample sets D6 and D7 relative to the other sample sets. In addition, methane generated from a Kerogen Type II source rock is relatively enriched in ^{12}C. Isotopic ^{12}C enriched methane correlates with low proportions of ethane. This isotopic light methane represents the early methane, whereas with increasing time the carbon isotope ratio for methane becomes ^{13}C enriched and the gas becomes enriched in ethane. This is not expected for a mixture of gases generated from a Kerogen Type II and a Kerogen Type III source rock, where high proportions of ethane should correlate with isotopic light methane (Kerogen Type II) and low proportions of ethane with isotopic heavy methane (Kerogen Type III). A mixture of thermogenic gas generated by a Kerogen Type III source rock and microbial gas in sample sets D6 and D7 is possible, but it is uncertain, because multiple processes can alter the molecular and isotope composition of the gas. Therefore, the use of the diagram for the identification of mixing and diffusion proposed by Colombo et al. (1970) and Prinzhofer and Pernaton (1997) is not useful for CBM gas classification.

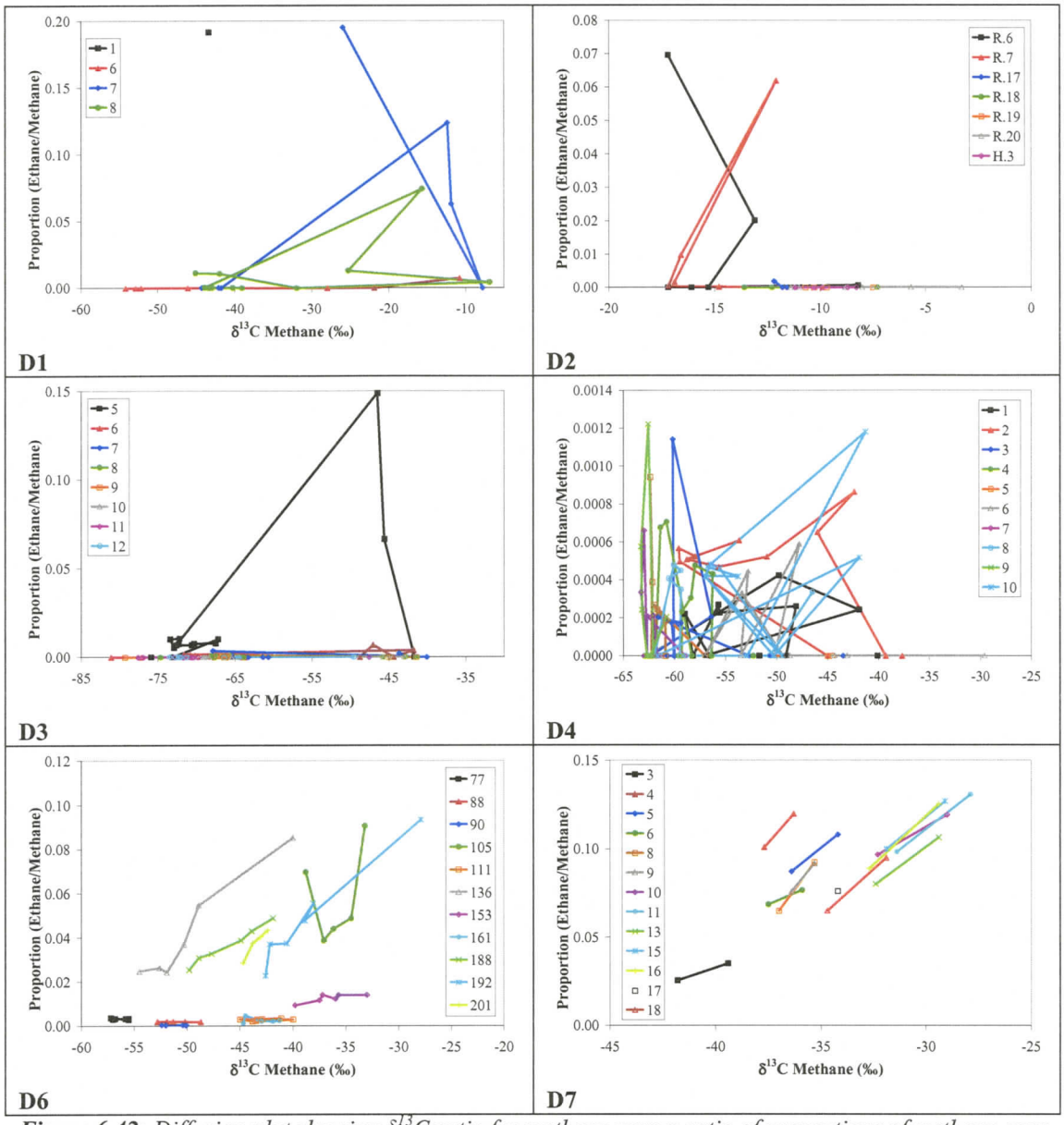


Figure 6.42: *Diffusion plot showing $\delta^{13}C$ ratio for methane versus ratio of proportions of methane over ethane for samples of desorption experiment sample sets D1, D2, D3, D4, D6 and D7. See text for details. No results are available for sample set D5 (diagram from Colombo et al., 1970 and Prinzhofer and Pernaton, 1997).*

6.3 Production vs. Desorption Experiment

Gases collected from producing wells and from coal cores during a desorption experiments should be affected by the same secondary processes. The gas has first to desorb from the coal, then to diffuse into the fractures and cleats and from there to migrate to the well heads or to the head spaces of the desorption canisters. However, the actual physical setting in which these secondary processes take place is quite different for a production scenario and for a desorption experiment scenario. Therefore, differences in extent and magnitude of isotope effects due to secondary processes should be expected for gases collected from these two scenarios.

Coal cores used for desorption experiments are subjected to a pressure drop, i.e., from hydrostatic to atmospheric pressure. Due to this pressure reduction a proportion of the adsorbed gas desorbs from the coal, with only residual gas left adsorbed onto the coal. Additionally, the reduced pressure is applied on the entire coal core. During the recovery of the coal core a substantial proportion of gas is already lost which consists of free gas, if present, and early desorbed gas.

Coal cores used for desorption experiments vary in size, but usually the canisters allow a maximum core size of 1 foot length and a diameter of 3 inches to 4 inches. Therefore, the quantity of coal is limited. This leads to a limitation of migration length. Diffusion length is controlled by the spacing of the cleat network inside the coal and if these cleats are open or closed due to the precipitation of minerals on the cleat surfaces. Laubach et al. (1998) reported that cleat spacing is on the order of centimetres and therefore close enough that several cleats or fractures are present and recognizable in coal cores. The process and especially the length of diffusion should not be impacted by considering coal cores instead of considering an entire coal seam or larger parts of a coal seam. Therefore, only relatively short path length diffusion is expected for coal cores and coal seams. Migration distances inside the fracture or cleat network are reduced in coal cores, but no significant isotope effect is reported for mass movement of gas as a Darcy flow, which takes place inside the fracture and cleat network (McLennan et al., 1995).

The actual production of CBM from coal seams underground under a reduced pressure is achieved by lowering the hydrostatic pressure inside a coal seam. The total

pressure decrease is much smaller when compared with the pressure decrease for a desorption experiment scenario. The magnitude of pressure reduction depends on the success of water removal from the coal seam, i.e. recharge with meteoric waters. In comparison to a desorption experiment, the elevated pressure in a production scenario leads to the desorption of a much smaller fraction of gas from the coal, leaving larger quantities of gas actually adsorbed onto the coal. In addition, the reduced pressure is not applied uniformly to the coal, resulting in a pressure gradient, with relatively low pressure at and around the well bore and relatively high pressure further away from the well. A result of this pressure gradient is that different proportions of adsorbed gas are allowed to desorb from the coal, and the proportion is a function of pressure and therefore in a production scenario of distance to the well bore. This distance depends on a multitude of parameters, i.e., gas saturation, development of cleat and fracture network, water recharge and diffusivity, and therefore varies for different coal seams.

All wells in this study had been subjected to hydraulic fracturing, where several substances (gaseous, liquid and solid) are pumped into a coal seam under enormous pressure to create artificial fractures. These artificially created fractures can increase the flow of gas, desorbed from the coal and diffused out of the coal matrix into the cleat and fracture network, to the well bore. Additionally, these artificial fractures allow the access of coal further away from the well bore in terms of water removal and consequently pressure reduction, desorption of gas and finally production of this gas. Naturally, the amount of coal accessed under a production scenario is much larger then for a desorption experiment, resulting among other things in the mixing of gases desorbing from different locations of the coal seam.

It has to be mentioned here again, that economic production of CBM is only possible, when the diffusivity of the coals is high enough to allow diffusion of substantial quantities of gas desorbed from the coal to the fracture and cleat network. If the diffusivity is too low, only small quantities of gas actually diffuse into the fracture and cleat network, limiting the production of the well.

6.3.1 CBM Samples from Production Scenarios

The methane stable carbon isotope composition as a function of increasing production time shows similar trends for all eleven wells from the three production scenarios P1, P2 and P3 (Figure 5.4). The abrupt isotope shift observed for data from sample set P3 is important and is discussed more in Chapter 6.4. Initial $\delta^{13}C$ values show relatively ^{13}C enriched methane and a progressive ^{12}C enrichment with increasing production time. These start values represent the first sample taken from these wells and not the actual start of production. Production from the wells of sample set P3 actually started on January 21st, 2004, almost four months prior to the first sampling. Times for the start of production of wells from sample sets P1 and P2 are not available, as these wells were already under production before the first sampling was conducted. The isotope shift for samples from all three sample sets is identical in direction (^{12}C enrichment), but the magnitude varies between the different sample sets.

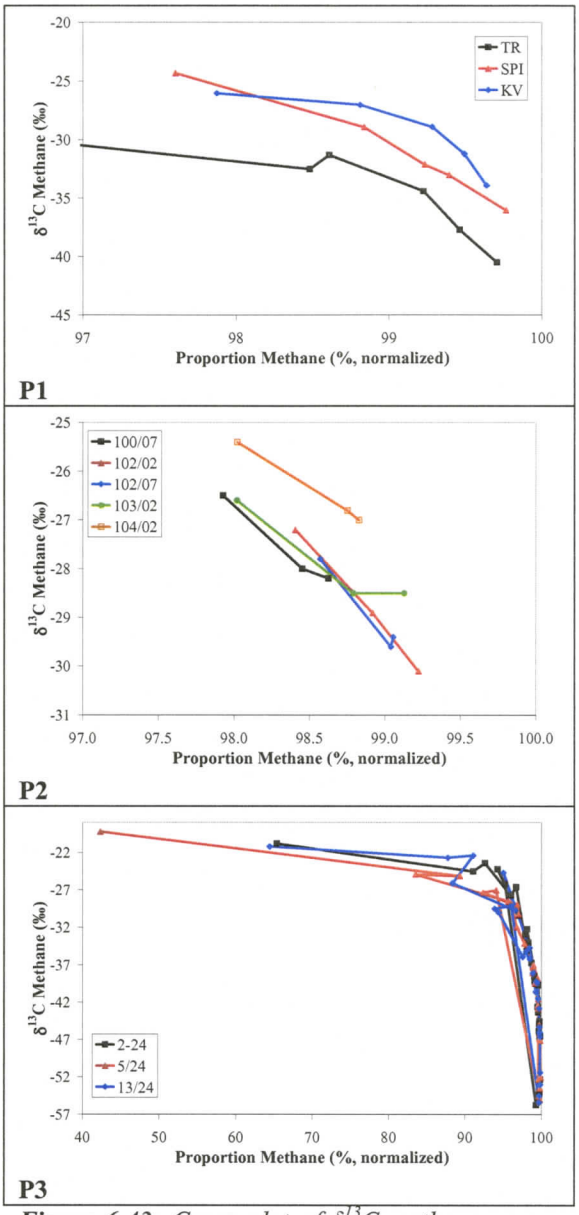


Figure 6.43: *Cross–plot of $\delta^{13}C$ methane versus proportions of methane for samples of production sample sets P1, P2 and P3. Proportions are normalized on the basis of proportions of methane, ethane, propane, n–butane, i–butane and carbon dioxide. See text for discussion.*

The correlating proportions of methane for samples from the production sample sets (Figure 5.1) show a correlation with the $\delta^{13}C$ ratio of methane. A cross plot between proportions of methane and $\delta^{13}C$ ratios of methane is presented in Figure 6.43. Relatively low proportions of methane

correlate with relatively ^{12}C depleted methane, whereas relatively high proportions of methane correlate with ^{12}C enriched methane. The shapes of the resulting curves are relatively similar within wells from the same sample set, but show considerable differences between the different sample sets.

δD ratios of methane from sample sets P1 and P3 show ^{1}H enrichment with increasing production time (Figure 5.5), similar to the trend observed for $\delta^{13}C$ ratios of methane. Methane δD ratios for sample set P2 shows no conclusive trend with increasing production time (Figure 5.5).

Available $\delta^{13}C$ ratios for ethane show no conclusive trend with increasing production time (Figure 5.7). Proportions of ethane correlate with $\delta^{13}C$ for ethane (Figure 6.44). Relatively ^{12}C depleted ethane correlates with relatively low proportions of ethane, whereas relatively ^{12}C enriched ethane correlates with relatively high proportions of ethane (Figure 6.44).

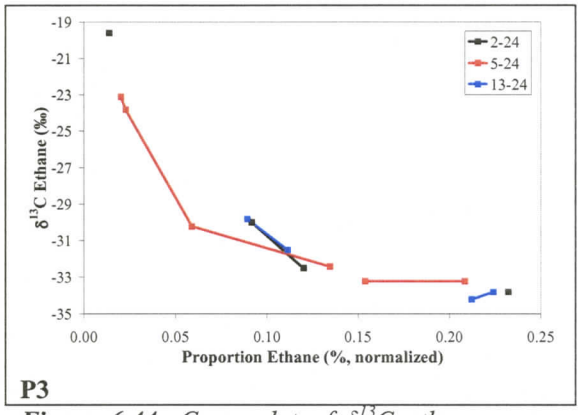


Figure 6.44: *Cross–plot of $\delta^{13}C$ ethane versus proportions of ethane for samples of production sample set P3. Proportions are normalized on the basis of proportions of methane, ethane, propane, n–butane, i–butane and carbon dioxide. No results are available for sample sets P1 and P2. See text for discussion.*

For $\delta^{13}C$ ratios of carbon dioxide, no conclusive trend with increasing production time is observed (Figure 5.7). In addition, no trend between $\delta^{13}C$ ratios for carbon dioxide and proportions of carbon dioxide is observed (Figure 6.45).

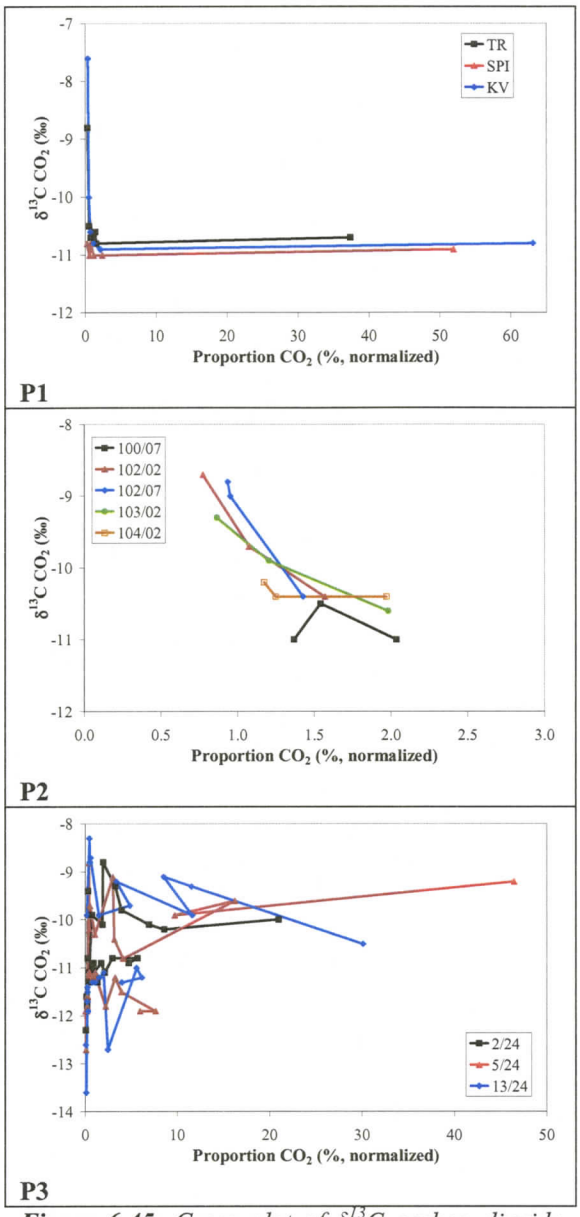


Figure 6.45: *Cross–plot of $\delta^{13}C$ carbon dioxide versus proportions of carbon dioxide for samples of production sample sets P1, P2 and P3. Proportions are normalized on the basis of proportions of methane, ethane, propane, n–butane, i–butane and carbon dioxide. See text for discussion.*

6.3.2 CBM Samples from Desorption Experiment Scenarios

Unlike the production study, samples from desorption experiment scenarios show a series of different trends of $\delta^{13}C$ for methane with increasing desorption time (Figure 5.11). Methane from samples of sample sets D1, D4, D5, D6 and D7 shows relative ^{12}C enrichment with increasing desorption time (Figure 5.11). Sample set D2 shows two different trends, 1) initial ^{12}C enrichment for methane followed by ^{12}C depletion and 2) initial ^{13}C enrichment followed by ^{13}C depletion (Figure 5.11). Sample set D3 shows a two–stage trend, with relatively stable $\delta^{13}C$ ratios for methane around -70‰ and around -45‰ separated by an abrupt ^{12}C enrichment for methane (Figure 5.11).

For sample sets D1, D4, D5 and D6 a correlation between $\delta^{13}C$ ratios of methane and proportions of methane is observed (Figure 6.46). Relatively ^{13}C enriched methane correlates with relatively low proportions of methane and relatively ^{13}C depleted methane with relatively high proportions of methane (Figure 6.46). For desorption experiment samples, relative to production samples, this relationship is less pronounced and accompanied by greater variations (Figure 6.46).

Stable hydrogen isotope ratios for samples from desorption experiment studies show no conclusive trend with increasing desorption time (Figure 5.12). Stable carbon isotope ratios of ethane show no conclusive trends with increasing desorption time (Figure 5.14). A correlation of ethane $\delta^{13}C$ ratios with proportions of ethane shows for sample sets D2, D6 and D7 relatively ^{13}C enriched ethane related to relatively high proportions of ethane and relatively ^{13}C depleted ethane related to relatively low proportions of ethane (Figure 6.47).

For the stable carbon isotope composition of carbon dioxide a relative ^{12}C enrichment is observed with increasing desorption time for sample sets D3 and D4 (Figure 5.13). For sample sets D1, D2, D5, D6 and D7 no trend is observed between $\delta^{13}C$ ratios of carbon dioxide and desorption time (Figure 5.13).

The observed two–stage trend for $\delta^{13}C$ ratios of methane with increasing desorption time (Figure 5.11) is also observed for $\delta^{13}C$ ratios of carbon dioxide for sample set D3 (Figure 5.13). The first stage is represented by strong variations between the different canisters and ^{12}C enrichment of carbon dioxide with increasing time. The

second stage is characterized by almost identical $\delta^{13}C$ values for carbon dioxide from all canisters with values of ca. -11.5‰. No conclusive trend between $\delta^{13}C$ for carbon dioxide and proportions of carbon dioxide is observed (Figure 6.48).

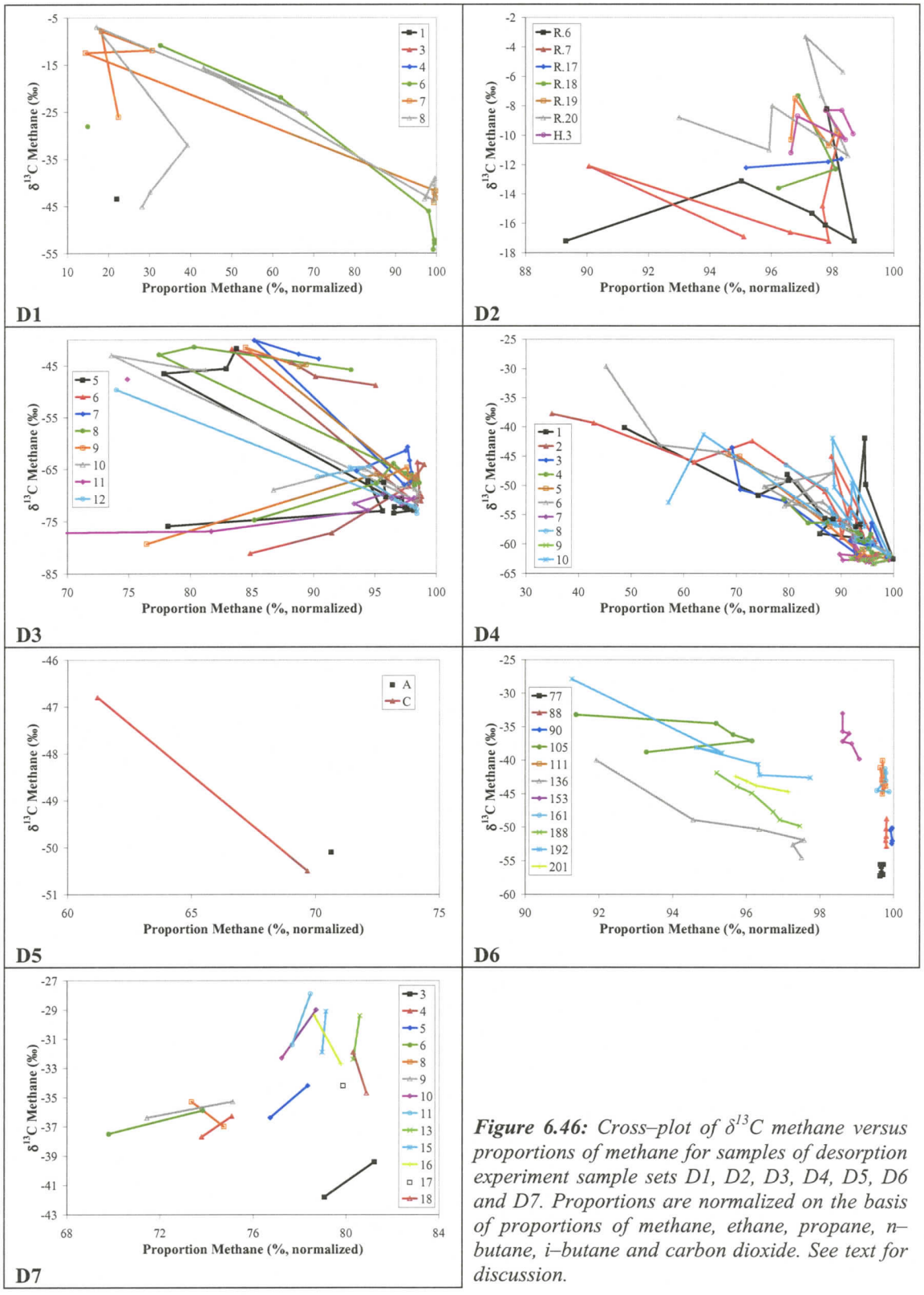


Figure 6.46: *Cross–plot of $\delta^{13}C$ methane versus proportions of methane for samples of desorption experiment sample sets D1, D2, D3, D4, D5, D6 and D7. Proportions are normalized on the basis of proportions of methane, ethane, propane, n–butane, i–butane and carbon dioxide. See text for discussion.*

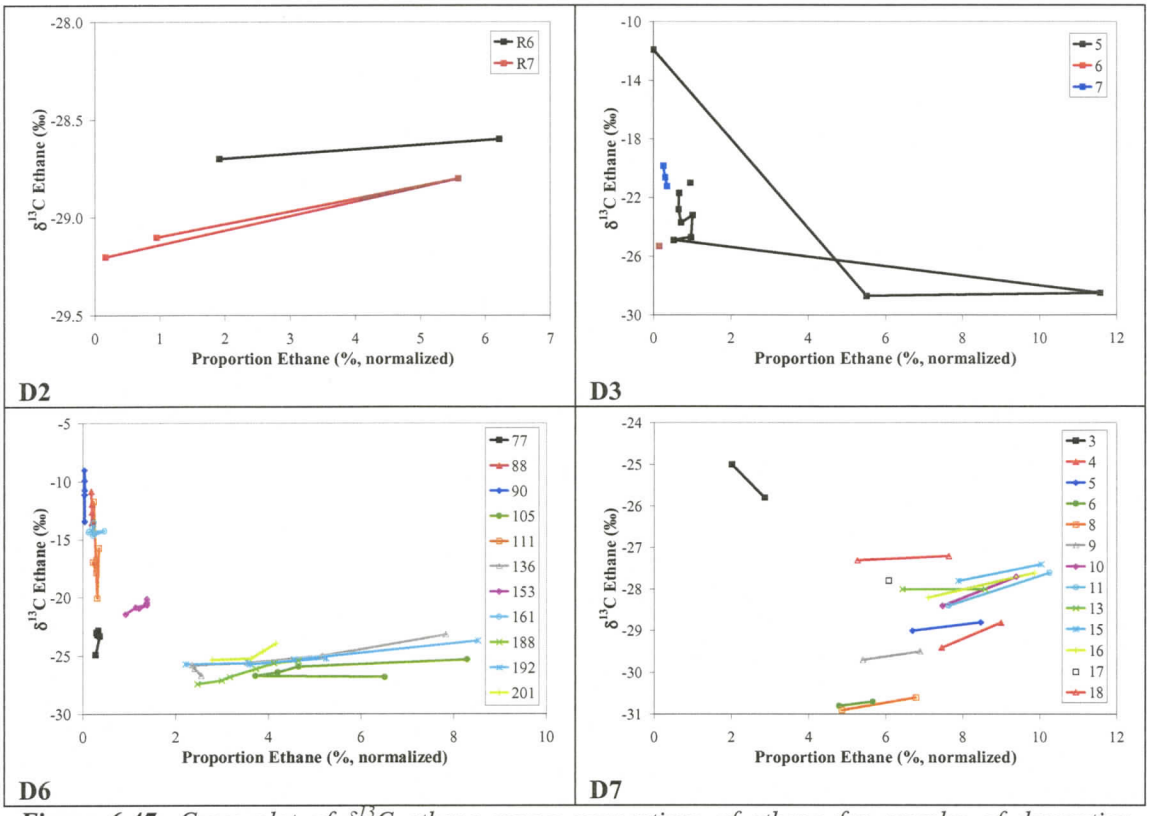


Figure 6.47: *Cross–plot of $\delta^{13}C$ ethane versus proportions of ethane for samples of desorption experiment sample sets D2, D3, D6 and D7. Proportions are normalized on the basis of proportions of methane, ethane, propane, n–butane, i–butane and carbon dioxide. No results are available for sample sets D1, D4 and D5. See text for discussion.*

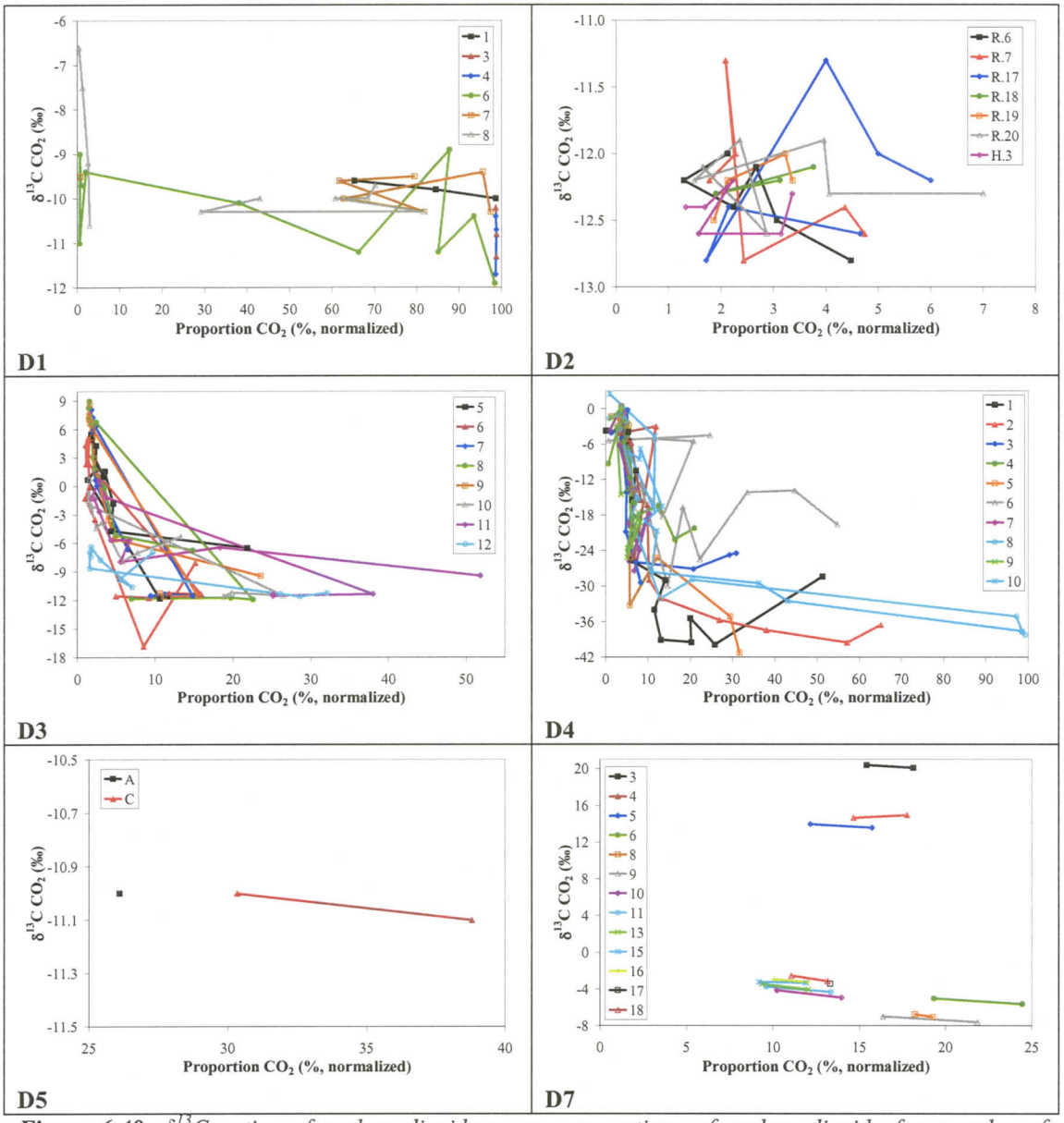


Figure 6.48: *$\delta^{13}C$–ratios of carbon dioxide versus proportions of carbon dioxide for samples of desorption experiment sample sets D1, D2, D3, D4, D5 and D7. Proportions are normalized on the basis of proportions of methane, ethane, propane, n–butane, i–butane and carbon dioxide. No results are available for sample set D6. See text for discussion.*

6.3.3 Systematic of CBM Production from Producing Wells

Stable carbon isotope compositions of methane from desorption experiment samples and from production samples show opposite trends with increasing desorption/production time. Methane from production scenarios shows ^{12}C enrichment with increasing production time (Figure 5.4), whereas methane from desorption experiments shows, in most cases, ^{13}C enrichment with increasing desorption time (Figure 5.11). For both scenarios, relative ^{12}C enriched methane correlates to relatively high proportions of methane, whereas relative ^{13}C enriched methane correlates to relatively low proportions of methane (Figures 6.43 and 6.46).

Based on the molecular and isotope effect due to desorption and diffusion, early desorbed and diffused gas should be relatively enriched in methane and this methane should be relatively enriched in ^{12}C. Late desorbed and diffused gas should contain higher proportions of higher hydrocarbons and carbon dioxide and therefore, relatively lower proportions of methane. The methane should be relatively enriched in ^{13}C. These correlations are observed in CBM gases from desorption experiments. The opposite trend is observed for CBM gases from production studies with early gas relatively depleted in methane and this methane relatively enriched in ^{13}C and late gas relatively enriched in methane and this methane relatively ^{13}C depleted.

The proportions of methane and the $\delta^{13}C$ ratios of methane from production studies do not show the expected trends for desorption and diffusion, but these processes must have occurred for gas collected during CBM production and therefore another process or other processes are responsible for the observed trend. This process or these processes have to alter the isotope ratio of the present methane in a way that it becomes initially ^{13}C enriched or circumstances are present, which allow the desorption and diffusion not only of early ^{12}C enriched methane, but also of late ^{13}C enriched methane at similar times.

A process, which would allow the desorption of early and late methane at roughly the same time is accelerated desorption and diffusion due to hydraulic fracturing. Hydraulic fracturing creates artificial fractures in coal seams, radiating away from the well bore. Due to these fractures, pathways for enhanced gas flow towards the well bore

are generated. Additionally, the required pumping of water out of the coal seam to establish desorption, may now effectively reach areas further away from the well bore, resulting in reduced pressure in these areas and consequently in the desorption of CBM, which, after diffusion, will migrate towards the well bore via the generated artificial fractures. The effect of the applied pressure during the fracturing process is greatest close to the well bore and decreases with increasing distance from the well bore. The dependency of the impact of hydraulic fracturing on distance from the well bore has several implications for CBM.

The resulting implications are schematically shown in Figure 6.49. Shown is the schematic view of a coal seam and the physical effects as a result of pumping of gas and water out of the coal seam, plus the impact of the process of hydraulic fracturing.

The numbers in Figure 6.49, provide examples of the proportions of gas allowed to desorb under the present physical conditions, relative to the total gas adsorbed onto these coals. Because more coal volume can be accessed further away from the well bore, relatively larger overall quantities of gas are produced from coal further away from the well bore. The physical characteristics of the coal itself and the success of the hydraulic fracturing determine the distance of these regions away from the well bore. Due to the removal of water, the impact of reduced pressure will be greatest close to the well bore and decreases with increasing distance from the well bore. This pressure gradient has implications for gas desorption. Close to the well bore, overall small quantities may be produced due to the limited volume of coal, but these gases represent of large fraction of the overall adsorbed CBM gases in this area. With increasing distance from the well bore, the overall desorbing and produced quantities of CBM gases are greater, relative to the area close to the well bore, because of larger coal volumes, but these gases represent only a small fraction of the overall adsorbed CBM gases in these areas. Additionally, because of the lower pressure close to the well bore, large quantities of the total adsorbed gas may desorb in short time. If, due to a continuous removal of water, the pressure will drop further, more gas will desorb from the coal. In regions where the pressure reduction is insufficient desorption can not be established (0% in Figure 6.49).

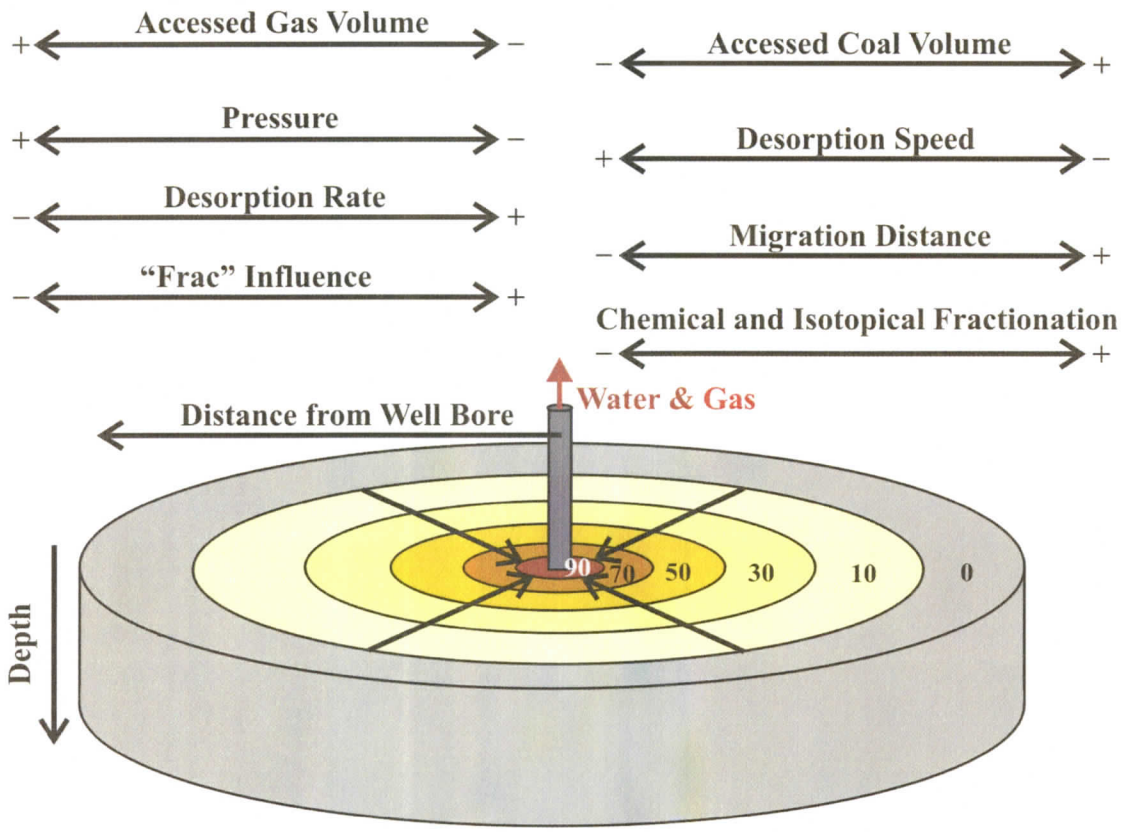


Figure 6.49: *Idealized model of a coal seam showing the effect of water and gas production, as well as the influence of hydraulic fracturing on selected physical and chemical parameters. See text for discussions.*

The arrows in Figure 6.49 indicate schematically the direction of the gas and water flow towards the well bore and out of the well. The migration distance (gas flow) increases naturally with increasing distance from the well bore.

The impact of hydraulic fracturing decreases with increasing distance from the well bore. The aperture of the created artificial fractures will be widest close to the well bore and decrease towards zero with increasing distance away from the well bore. Besides major fractures, also smaller and micro–fractures, are generated during hydraulic fracturing and these smaller fractures are concentrated in coal relatively close to the well bore. These smaller and micro–fractures might reduce the natural spacing of the cleat and fracture network in these coals, resulting in smaller diffusion lengths.

A conceptual model is presented to explain the observed molecular and isotope trends for CBM production samples (Figure 6.50). The presented model is limited to a

qualitative consideration. A quantitative consideration is currently not possible because of the following reasons:

1. Fractionation factors for desorption and diffusion are not known
2. The influence of pressure on the degree of isotope partioning associated with desorption and diffusion is not known
3. The actual pressure reduction in the coal seam and the pressure gradient throughout the coal seam are not known
4. The extent (spacing, aperture and length) of natural and artificially created fractures is not known
5. Molecular and isotope composition of the "original" gas, adsorbed onto the coal is not known.

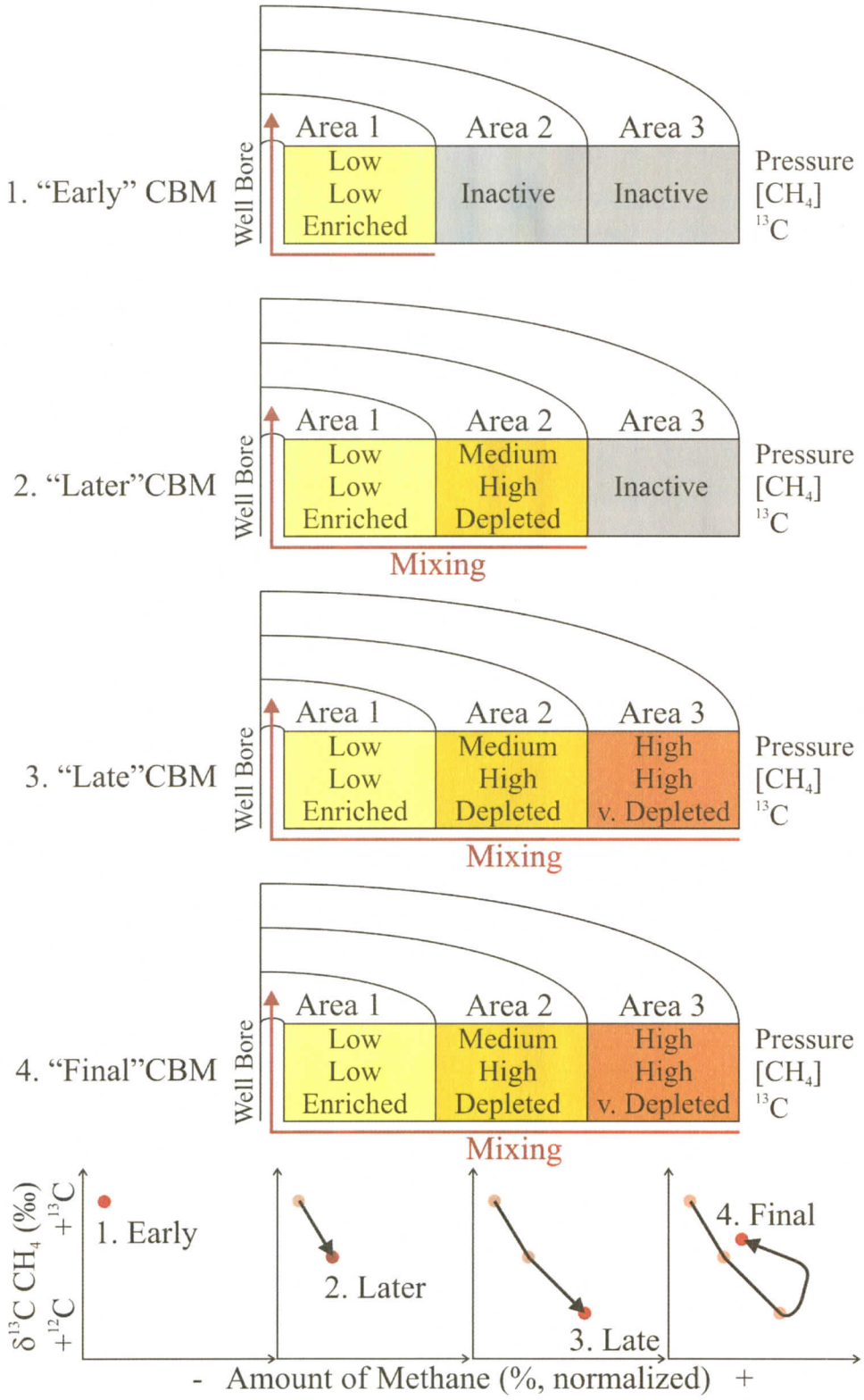


Figure 6.50: *Idealized model for isotope and compositional development of methane during the production of CBM. Actual distances of Areas 1, 2 and 3 are not known and should differ strongly between different coal seams. Vol. = Volume. See text for discussion.*

Stage 1: "Early" CBM

The first gas produced desorbed from coal relatively close to the well bore with a relatively limited coal volume (Volume 1 in Figure 6.50; Volumes 2 and 3 are inactive at this point). Actual distances are not known and may vary from coal to coal. Because of the strong impact of hydraulic fracturing and the strongly reduced pressure, this gas should be relatively depleted in methane with elevated proportions of higher hydrocarbons and carbon dioxide. In addition, the methane should be enriched in ^{13}C, because relatively large proportions of methane are able to desorb. No or only a small isotope shifts, relative to total adsorbed gas, are expected. Due to the artificially created fractures and micro–fractures and the resulting closer cleat spacing, the isotope shift due to diffusion should also be relatively small. Relatively small proportions of methane and elevated proportions of higher hydrocarbons and carbon dioxide, as well as methane relatively enriched in ^{13}C are observed for early produced CBM samples.

Stage 2: "Mid Stage" CBM

Relatively later produced CBM (Mid Stage) samples should be a mixture of gases desorbing from coal relatively close to the well bore (Volume 1) and from coal further away from the well bore (Volume 2 in Figure 6.50; Volume 3 is inactive). Coal in Volume 2 is, relative to coal from Volume 1, exposed to an elevated pressure. Coal in Volume 2 represent a greater volume than coal in Volume 1 and the overall produced gas volume should increase, but due to the elevated pressure, these gases represent only relatively small fractions of the total adsorbed gas. The desorbing gas should be relatively enriched in methane with smaller proportions of higher hydrocarbons and carbon dioxide. Methane should be, relative to Volume 1, more enriched in ^{12}C, due to the fact that ^{13}C is more strongly adsorbed than ^{12}C and requires lower pressures for desorption. Overall, the isotope shifts due to desorption and diffusion, relative to total adsorbed gas, are expected to be greater for gases from Volume 2, relative to gas from Volume 1, because of the decreased influence of hydraulic fracturing. Gases from Volume 2 mix during their migration towards the well bore with gases from Volume 1. Relative to gases entirely

originated from Volume 1, this mixed gas should be relatively enriched in methane and this methane should be relatively more ^{12}C enriched. This is enhanced by the access of large volumes of gas from Volume 2, due to the relatively larger volume of coal. The predicted increase in the proportion of methane, the decrease for the proportions of higher hydrocarbons and carbon dioxide, as well as the relative ^{12}C enrichment for methane are observed in the later produced CBM samples.

Stage 3: "Late" CBM

Gases, even later produced from a coal seam should include late gases from Volumes 1 and 2 and gases desorbing from the coal of Volume 3 (Figure 6.50). The coal in Volume 3 experiences only a relatively low pressure reduction, resulting in the desorption of almost exclusively methane strongly enriched in ^{12}C. The affected volume of coal in Volume 3 is greater than the volume for Volume 2, resulting in the desorption and production of huge proportions of methane, but which represent only a small fraction of the total adsorbed volume of gas. The proportions of higher hydrocarbons and carbon dioxide are predicted to be low, because the pressure reduction is insufficient for the desorption of these gas species. The admixture of this gas from Volume 3 to the gases from Volumes 1 and 2 should lead to an overall enrichment of methane in the late produced gas and this methane should be even more ^{12}C enriched than the previously produced methane. This trend is enhanced by the access of large volumes of gas from Volume 3, due to the relatively larger volume of coal. These predicted trends are observed in the late gas samples from all considered production scenarios.

Stage 4: "Final "CBM

Considering these sequences of events over an extended period of time leads to the following (Stage 4 in Figure 6.50). With increased removal of water, assuming no influx of meteoric water, and the production of CBM from the coal seam, gas from Volume 1 should become even more depleted in methane and enriched in higher hydrocarbons and carbon dioxide. Methane should be strongly enriched in ^{13}C. Gases

from Volumes 2 and 3 now also experience a greater pressure reduction, resulting in relative methane depletion and enrichment of higher hydrocarbons and carbon dioxide. Methane becomes progressively ^{13}C enriched. Assuming that no "early" gas from volumes further away from the well bore are admixed to the pool of "late" gas, the mix of late gases from Volumes 1, 2 and 3 should become relatively enriched in higher hydrocarbons and carbon dioxide and the methane should become relatively ^{13}C enriched. If the presented model is valid, very late produced CBM should show the described trends of carbon dioxide and higher hydrocarbon enrichment, as well as ^{13}C enrichment for methane as show in Figure 6.50 (Stage 4). More CBM samples, especially from the late stages of CBM production, representing stage 4 in Figure 6.50, are required for the evaluation of the presented model.

6.4 Sample set P3

Sample set P3 reveals unexpected and particular molecular and isotope trends and has to be considered separately and in more detail.

6.4.1 Compositional Aspects

Initially, proportions of methane are relatively low, but increase steadily with increasing production time until values of almost 100% methane are reached (Figure 6.51). After a production time of 2088 hours (sample 13) the proportions of methane decrease and at sample 15 (2424 hours) the maximum of this decrease is reached. Following this, the proportions of methane increase again to values of almost 100%.

The proportions of higher hydrocarbons are initially relatively high, but decrease with increasing production time (Figure 6.51). An increase in proportions of higher hydrocarbons is observed between desorption times of 1776 hours (sample 11) and 2280 hours (sample 14). Following sample 14, up to sample 26, the proportions of higher hydrocarbons are again low. For samples 27 (6120 hours) and 28 (6312 hours) another increase in the proportion of higher hydrocarbons is observed.

The proportion of carbon dioxide are also initially relatively high (Figure 6.51), but decreases steadily with increasing production time. Following sample 13 (2088 hours), the proportions of carbon dioxide increase again until a maximum is reached at sample 15 (2424 hours). Following this maximum the proportions of carbon dioxide decrease with increasing production time

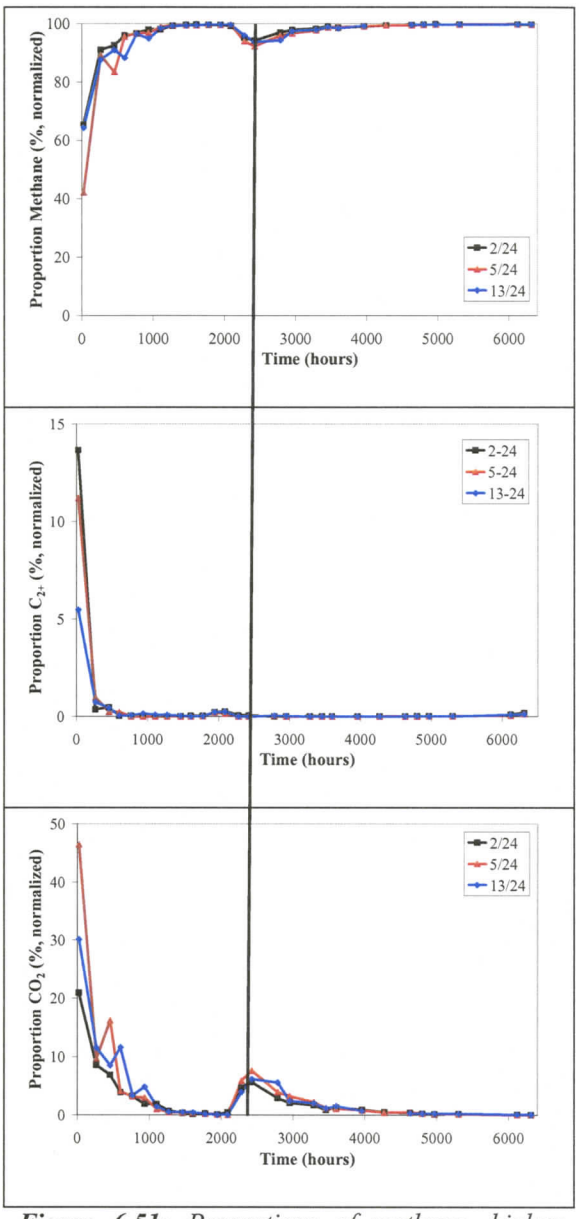


Figure 6.51: *Proportions of methane, higher hydrocarbons (C_{2+}; ethane, propane, n–butane and i–butane) and carbon dioxide of samples from production sample set P3 presented versus production time. Proportions are normalized on the basis of proportions of methane, ethane, propane, n–butane, i–butane and carbon dioxide. Black line represents sample 15 (2424 hours). See text for discussion.*

6.4.2 Isotope Aspects

Initial $\delta^{13}C$ ratios for methane are relatively enriched in ^{13}C (Figure 6.52). Up to sample 14 (2280 hours) methane becomes progressively enriched in ^{12}C. Between samples 14 and 15 (2424 hours) methane abruptly becomes enriched in ^{13}C. Following sample 15, methane becomes again progressively enriched in ^{12}C. The observed trends occur simultaneously for samples from all three wells with similar overall $\delta^{13}C$ ratios for methane.

δD ratios for methane are available for samples 12 to 28 from all three wells. Methane becomes enriched in ^{2}H up to samples 15 (wells 2/24 and 5/24) and sample 14 (well 13/24) (Figure 6.52). Following samples 15, respectively 14, δD ratios for methane show strong variations, but overall ^{1}H enrichment with increasing production time is observed. The $\delta D–CH_4$ time trend is observed simultaneously for all wells.

Up to sample 11 (1776 hours) $\delta^{13}C$ ratios for carbon dioxide show strong fluctuations around a mean value of -9.5‰ to -10‰ and no trend is observed with increasing time (Figure 6.52). Following sample 14 up to sample 24 the overall fluctuations of $\delta^{13}C$ ratios for carbon dioxide are smaller between a mean value of -10.5‰ and -11‰. Following sample 25 enrichment in ^{12}C for carbon dioxide is observed. The described trends are observed simultaneously for all wells.

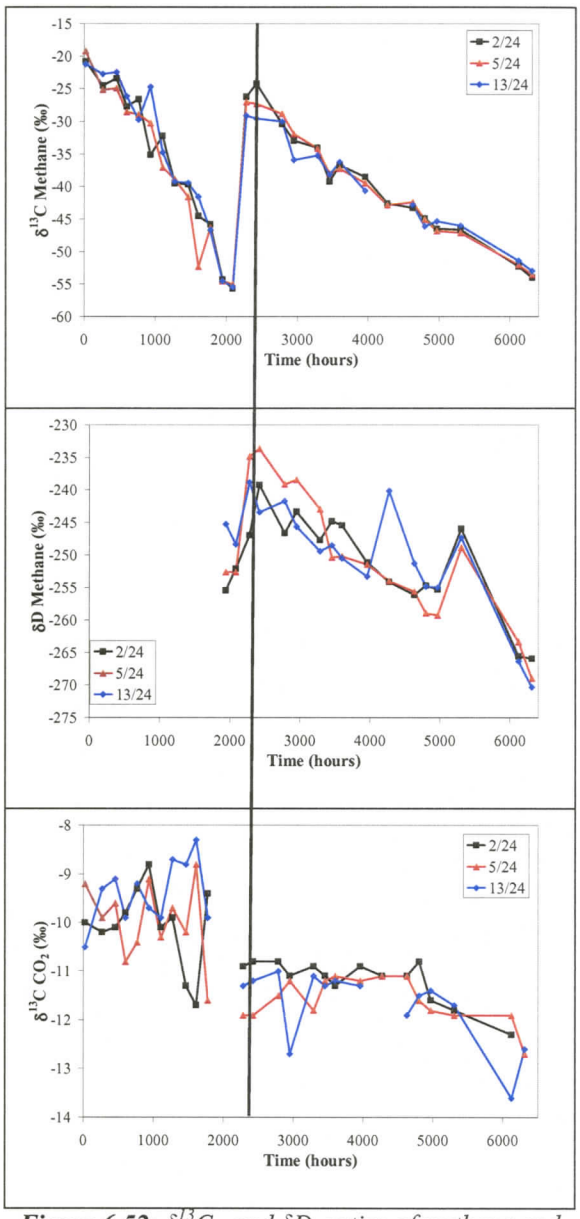


Figure 6.52: *$\delta^{13}C$– and δD–ratios of methane and $\delta^{13}C$–ratios of carbon dioxide of samples from production sample set P3 presented versus production time. Black line represents sample 14 (2280 hours). See text for discussion.*

6.4.3 Modelation of CBM Production for Sample Set P3

A schematic model is presented to explain the observed molecular and isotope trends for CBM samples of sample set P3 between samples 11 (1776 hours) and 15 (2424 hours) (Figure 6.53). The observed molecular and isotope changes occurred during a short time frame of eight days (192 hours). Therefore, the process, or the processes, responsible for the observed changes, occurred suddenly.

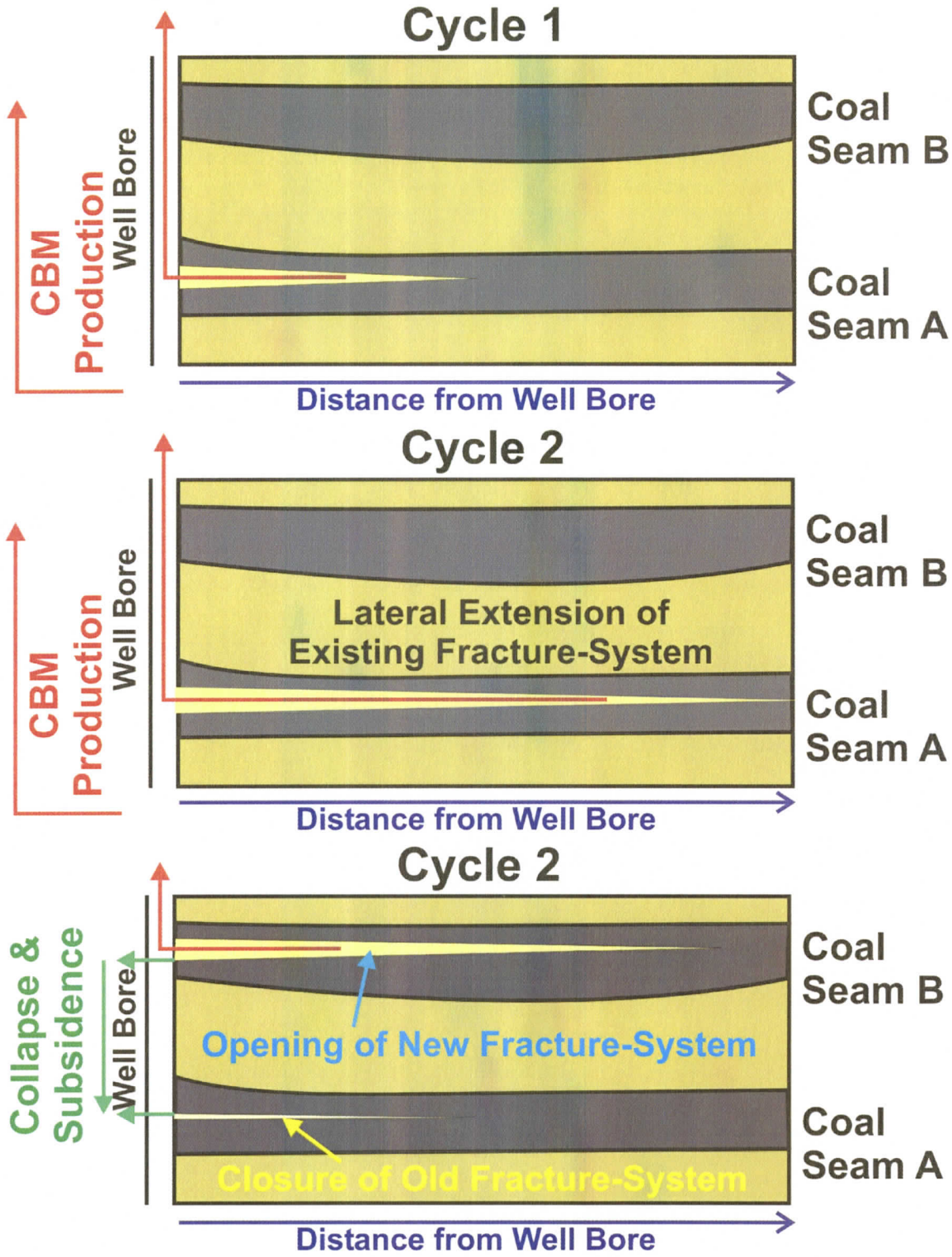


Figure 6.53: *Idealized model showing closing and opening of fracture systems in coal seams and lateral extension of fracture system as a result of the production of CBM from wells of production sample sets P3. See text for discussion.*

The first cycle of ^{13}C depletion for methane (samples 1 to 13) indicates mixing from different areas of the coal seam as described in Figure 6.50 and Chapter 6.3. If cycle 2 (samples 14 to 28) is also a result of the mentioned mixing process than the gas has to come from a different location of the same coal seam, or from a different coal seam, previously not or only slightly affected by the production of CBM. A continuous production of gas from the areas responsible for the first cycle would not result in the observed trends and changes for sample set P3. To access gas from different coal areas or different coal seams, new fractures or fracture systems have to be opened and previously open fractures have to become closed.

Harpalani and Schraufnagel (1990) and George & Barakat (2001) reported shrinkage processes in coal as an effect of gas desorption and release. This shrinkage process might have been the initiation of the collapse of one fracture system and the opening of a new one (Figure 6.53). This new fracture system might occur in the same coal seam, or as shown in Figure 6.53 in a different coal seam. The fracture system responsible for production of gases from cycle 1 becomes closed and a new fracture system opens. Due to the presence of the new fracture system, water removal from coal seam B is now possible resulting in pressure reduction and production of CBM from this coal seam (Cycle 2). CBM production from this new fracture system would also undergo the processes described in Chapter 6.3 and Figure 6.50.

It is not necessary that the new fracture system opens because of a closing process. Due to pressure differences throughout a coal seam, the existing fracture system may become extended (Figure 6.53). This extension may occur lateral or angular relative to the existing system. As a result of these extensions, coal not or only slightly affected by CBM production (Cycle 1) is subjected to decreased pressure, resulting in desorption and the production of CBM (Cycle 2). The production of CBM of Cycle 2 follows the principles of the mixing model (Figure 6.50; Chapter 6.3.3).

The processes of opening of a new fracture system or extension of the existing one have to occur quickly, because the measured gas flow for all three wells does not show significant variations for the 7 days between August 21st, 2004 (sample 13) and August 28th, 2004 (sample 14) as shown in Figure 6.54. No other events, such as heavy rainfall, earthquakes, etc., were reported.

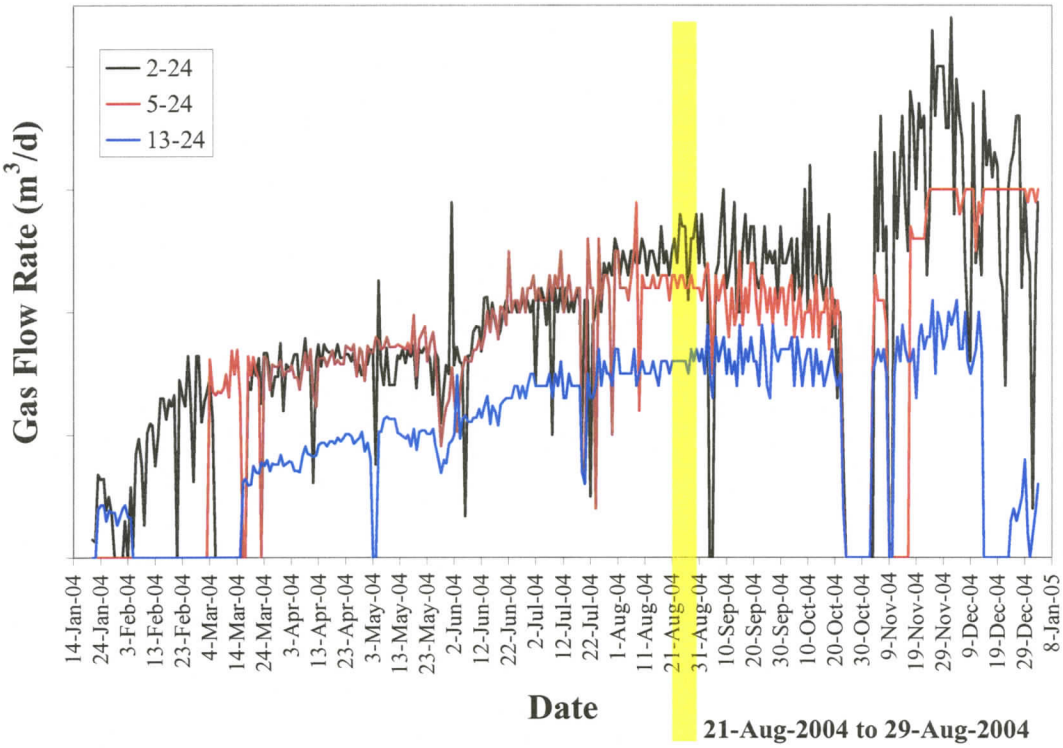


Figure 6.54: *Gas production volumes for the considered three wells of production sample set P3 between January 14th 2004 and January 8th 2005. Yellow area indicates time period between August 21st and August 29th 2004, where in samples from all three wells major compositional and isotope changes are observed. See text for discussion.*

Because the described trends and changes occurred simultaneously in all three wells, a large–scale process is required to explain the observed trends. The wells were drilled in a triangular set–up with a distance of a couple of hundred meters between the wells, but all three wells produce CBM from the same coal seams (Figure 6.55). Therefore, opening the new fracture–system or extending the existing one have to affect a large area. Due to the presence of the fracture system, water removal from coal seam B is now possible resulting in pressure reduction and production of CBM from this coal seam (cycle 2).

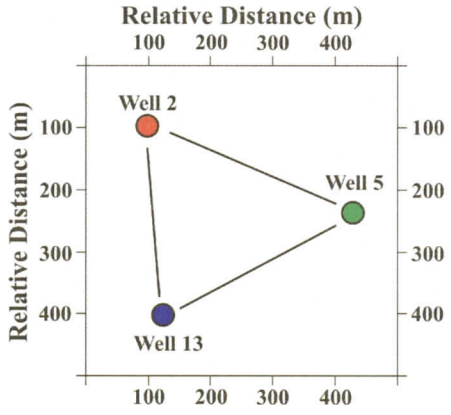


Figure 6.55: *Conceptual and relative map for the set up of the three wells considered for production scenario P3. Location, exact distance between the wells and further details about these wells are confidential. Reported distances between the wells are several hundred meters.*

The above described processes of opening and closing of fracture systems and extending an existing fracture system are able to explain the observed trends and changes from samples from production sample set P3.

7. Synthesis

7.1 Coal–Gas Relationships

Influence of Maturity on Isotope Ratios

A dependency of the stable carbon isotope ratio for methane on the maturity of coal can be established from the presented data, where the greatest ^{13}C enrichment for methane is found in high mature coals. Methane from low mature coals is relatively depleted in ^{13}C. $\delta^{13}C$ ratios of methane from low mature coals show strong variations and therefore, a mathematical description of this relationship is not possible.

For stable hydrogen isotope ratios of methane a dependency on the maturity of coal can also be established. ^{2}H enrichment is found in methane from high mature coals, whereas methane from low mature coals is relatively depleted in ^{2}H. The establishment of an equation to describe this relationship mathematically is not possible, because of the strong variations in δD ratios of methane from low mature coals.

Influence of Maceral Composition on Isotope Ratios

Vitrinite

Stable carbon and hydrogen isotope ratios of methane show no dependency on the relative abundance of vitrinite in coal.

Liptinite

Early $\delta^{13}C$ ratios of methane (t_{START}) show a dependency on the relative abundances of liptinite in coal. High amounts of liptinite correspond to relative ^{13}C depletion for methane, whereas low amounts of liptinite correlate to methane relatively enriched in ^{13}C. This dependency is not present anymore for late $\delta^{13}C$ ratios of methane (t_{END}) and weighted values (t_{WGH}).

A similar, although less pronounced dependency is observed for early and late stable hydrogen isotope ratios of methane, where relatively ^{2}H depleted methane

corresponds to coals with high abundances of liptinite. This relationship is not present for t_{WGH}.

The establishment of an equation to describe the observed relationship between $\delta^{13}C$, and δD respectively, on the relative abundances of liptinite mathematically is not possible, because of strong variations for $\delta^{13}C$ ratios of methane within the individual sample sets.

Inertinite

The stable carbon and hydrogen isotope ratios of methane are independent on the relative abundances of inertinite in corresponding coals.

Influence of Depth on Isotope Ratios

For the stable carbon and isotope ratios of methane no relationship with present day depth of the corresponding coal is observed. Therefore, depth of sampling appears to have no influence on $\delta^{13}C$ and δD ratios of methane.

7.2 Primary Effects

Composition

The proportions of methane, higher hydrocarbons and carbon dioxide in CBM show no correlation with the maturity of the corresponding coals and differ from gas compositions expected to be generated from coals of different maturities. Therefore, it is likely that the gas compositions of the analyzed samples do not represent the gas compositions representing the final stage of coalification, experienced by the corresponding coal. CBM samples represent a mixture of gases generated during the entire or during parts of the coalification process, which were retained by the coal due to adsorption. An accurate estimation of gas compositions expected in coals of certain maturities is therefore not possible.

Comparison: Calculated vs. Measured Carbon Isotope Ratios

The stable carbon isotope ratios of methane from CBM samples shows strong differences relative to modeled values calculated by applying a $\delta^{13}C$–$\%R_O$ relationship for methane generated from a Kerogen Type III source rock by Berner and Faber (1996). Methane from CBM samples is generally ^{13}C depleted relative to the modeled $\delta^{13}C$ ratios. These differences of up to 50‰ indicate that the measured $\delta^{13}C$ ratios for methane from CBM samples do not represent primary gas generation. CBM samples are likely altered due to the presence of microbial methane and/or due to secondary processes.

For ethane and propane from CBM samples no conclusive trends are observed.

Gas Classification Approach

Bernard Diagram

In Figure 7.1 it is shown that it is possible in some cases to distinguish between microbial and thermogenic gas. Overall, $\delta^{13}C$ ratios for methane and Bernard Parameters change extremely within the different sample sets indicating the presence of molecular and isotope ratio altering processes.

The application of the Bernard Diagram for the identification of different gas generation pathways for CBM gases is questionable, and new approaches for gas classification will be necessary, incorporating the effect of secondary processes and attendant molecular and isotope effects.

CD Diagram

Based on the CD Diagram (Figure 7.2), a definitive classification of gas origins for the analyzed CBM gases is difficult. The measured $\delta^{13}C$ and δD ratios of methane most likely do not represent the primary isotope composition of the generated methane. Based on the CD Diagram (Figure 7.2) certain gases would have to be interpreted as of abiogenic and mantle derived origin, whereas others are of geothermal and crystalline origin, which is unreasonable for gases known to be originated from coal. Interestingly,

none of the analyzed CBM samples plot in the defined regions for natural gases associated with coal (methyl–type fermentation and Kerogen Type III; Figure 7.2).

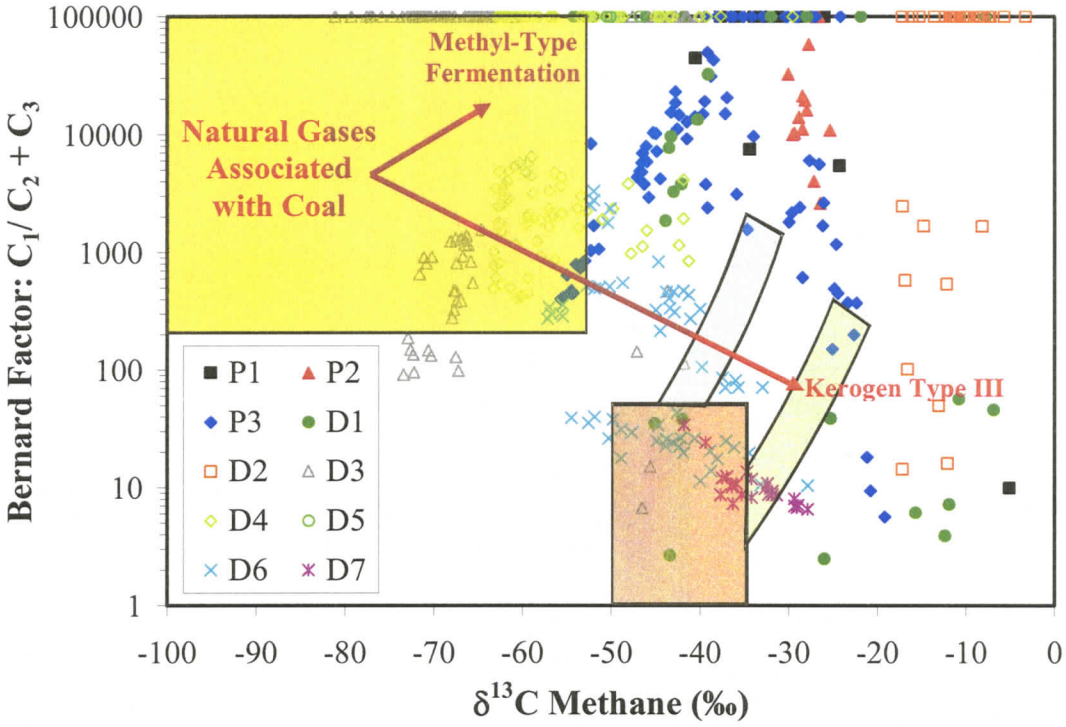


Figure 7.1: *Bernard Diagram showing samples from production sample sets P1, P2 and P3 and desorption experiment sample sets D1, D2, D3, D4, D5, D6 and D7. Diagram is modified from Whiticar (1999). For explanations of different areas see figure 6.16.*

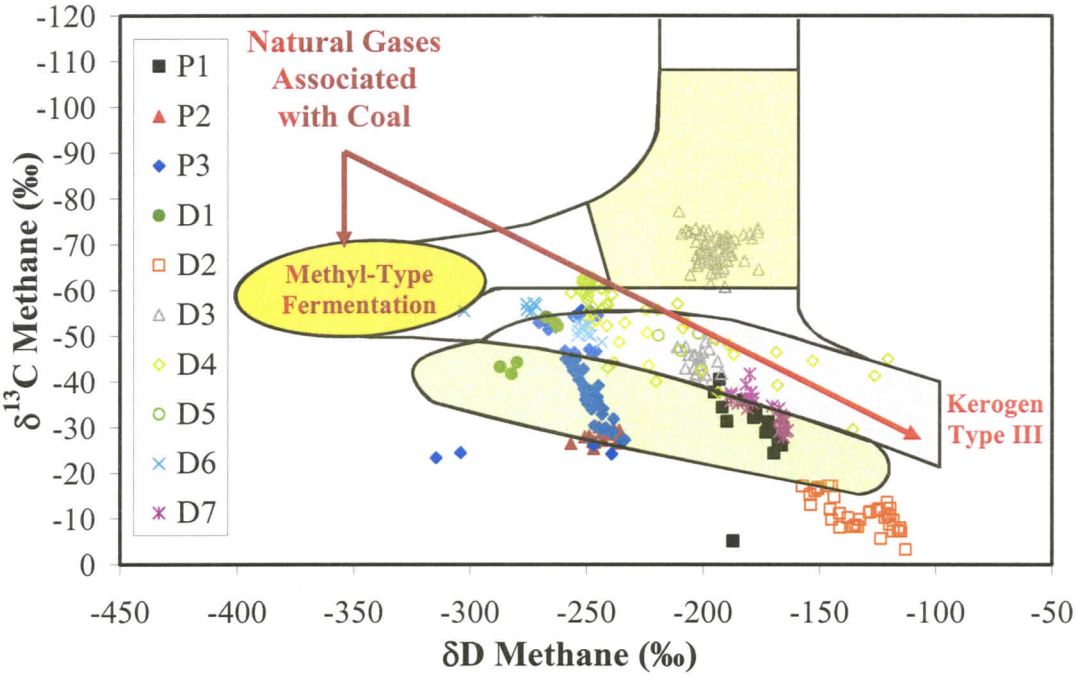


Figure 7.2: *$\delta^{13}C$–δD (methane) Diagram showing samples from production sample sets P1, P2 and P3 and from desorption experiment sample sets D1, D2, D3, D4, D5, D6 and D7. Diagram is modified from Whiticar (1999). For explanations of different areas see figure 6.19.*

The application of the CD Diagram for the differentiation of different gas generation pathways for CBM gases is questionable, and new approaches for gas classification will be necessary, incorporating the effect of secondary processes and attendant molecular and isotope effects.

7.3 Secondary Effects

Mixture of Coal Gas with Microbial Gas

The application of natural gas plots (Chung et al., 1988) and $\delta^{13}C$–$\%R_O$ relationships (Berner and Faber, 1996) for the determination of fractions of thermogenic and microbial gas in CBM gases is possible, but attention has to be paid to secondary processes and sample collection. The type of secondary process leading to relative ^{13}C depletion in methane would lead to an overestimation of microbial gas, whereas the type of secondary process leading to relative ^{13}C enrichment would overestimate the fraction

of thermogenic gas. Gas loss due to sample recovery with attendant relative ^{13}C enrichment in the residual methane would also lead to an overestimation of thermogenic gas.

Natural Gas Plots

Based on the natural gas plot approach by Chung et al. (1988) the analyzed CBM samples could be described as mixtures of thermogenic gas generated from a Kerogen Type III source rock and microbial gas, with proportions of microbial gas between 5% and 44%, and as pure thermogenic gases generated from a Kerogen Type III source rock.

$\delta^{13}C$–$\%R_O$ Relationships

Based on the approach using $\delta^{13}C$–$\%R_O$ relationships from Berner and Faber (1996) the analyzed CBM samples could be described as pure microbial gases and pure thermogenic gases generated from a Kerogen Type III source rock, as well as mixtures between these two gases with variable proportions.

Mixture of Coal Gas with Kerogen Type II Gas

Coal seams from sample sets D6 and D7 are thought to be underlain by thick successions of shale. Isotopic and molecular indications are found in CBM samples from these sample sets for a mixture of gases generated from a Kerogen Type II and a Kerogen Type III source rock. The calculated fractions for gas generated from a Kerogen Type II source rock varies between 0% and 100%, whereby overall Kerogen Type III derived gases are dominant.

Isotope Composition

Based on a comparison of measured $\delta^{13}C$ ratios of methane, ethane and propane with calculated $\delta^{13}C$ ratios for methane, ethane and propane generated from Kerogen Type II and Type III source rocks using $\delta^{13}C$–$\%R_O$ relationships by Berner and Faber (1996), measured $\delta^{13}C$ ratios for methane, ethane and propane show ^{13}C depletion relative to modeled $\delta^{13}C$ ratios for methane, ethane and propane. Relative to modeled $\delta^{13}C$ ratios

of methane, ethane and propane generated from a Kerogen Type II source rock, the analyzed $\delta^{13}C$ ratios show relative ^{13}C enrichment. Therefore, the measured $\delta^{13}C$ ratios of methane, ethane and propane could be the product of mixing of gases generated by Kerogen Type II and a Kerogen Type III source rocks.

Molecular Composition

The possibility of a mixture of gases generated from a Kerogen Type II and a Kerogen Type III source rocks in CBM sample sets D6 and D7 is supported by the proportion of higher hydrocarbons in the CBM samples relative to the abundances of liptinite in the corresponding coals. The proportion of higher hydrocarbons, especially in CBM gases from sample set D7, exceeds the proportion of higher hydrocarbons expected based on the relatively low amounts of liptinite in the corresponding coals.

Mixture of Coal Gas A with Coal Gas B

The identification of gases generated from two different Kerogen Type III source rocks in CBM gases is difficult, because of the similarities in gas composition and isotope ratios of the different chemical compounds. A differentiation between two different Kerogen Type III derived gases in the analyzed CBM samples is therefore not possible, but the possibility of such a mixture cannot be ruled out.

Microbial Oxidation of Methane

The presence of microbial methane oxidation in coal seams is likely, but it is difficult to detect evidences for this process from analyzes of gas composition and $\delta^{13}C$ ratios of methane from CBM samples. The consideration of $\delta^{13}C$ ratios of methane, as well as the proportions of carbon dioxide, over time, does not show any clear indications for the presence of microbial methane oxidation. No trend indicating microbial methane oxidation can be observed in the Bernard Diagram and in the $\delta^{13}C$– methane vs. $\delta^{13}C$–ethane cross plot. Trends indicating microbial methane oxidation may be masked by molecular and isotope effects due to other processes.

Adsorption and Desorption

CBM gases have to be influenced by adsorption and desorption and indications for desorption are found in the analyzed CBM samples. The observed isotope variations for methane cannot be attributed to gas generation itself. Secondary processes occurring during the geological history of the coal must have an impact on the molecular and isotope composition of CBM gases. These processes compound the processes of adsorption and desorption. Fractionation effects for these processes cannot be isolated and it is therefore not possible to delineate the impact of adsorption and desorption.

Repeated burial and uplift during the geological history of a coal seam, every time accompanied by adsorption and desorption, can result in continuous depletion of the gas pool in ^{13}C depleted methane. During the production and sampling of CBM gases not all gas adsorbed onto coal is removed and measured. Therefore, the recovered gas will not represent the mean composition, molecular and isotopic, of the total adsorbed gas. Coal has retentive capacity leading to the adsorption of gases generated at different stages of the coalification process, as well as to the adsorption of microbial gas and gases generated from other source rocks. Because of these complications and the lack of knowledge about the molecular and isotope effects due to adsorption and desorption the mean isotopic compositions of gases adsorbed onto coal cannot be determined.

Diffusion/Migration

CBM gases have to be subjected to molecular and isotope effects due to diffusion, but based on gas composition and the isotope ratios of methane from CBM samples no conclusive evidences for diffusion are observed in the data.

A diagram for the delineation of diffusion proposed by Colombo et al. (1970) and Prinzhofer and Pernaton (1997) is shown in Figure 7.3. Mixing Line 1 is based on endmembers with $\delta^{13}C$ ratios for methane of -80‰ and -35‰ and values for (concentration ethane/concentration methane) • 1000 of 0 and 300. Mixing Line 2 is based on endmembers with $\delta^{13}C$ ratios for methane of -60‰ for pure microbial methane (methyl–type fermentation), and -26‰ for methane generated from a Kerogen Type III

straight line. Therefore, based on the used approach, CBM sample sets D6 and D7 do not follow trends expected for the process of diffusion.

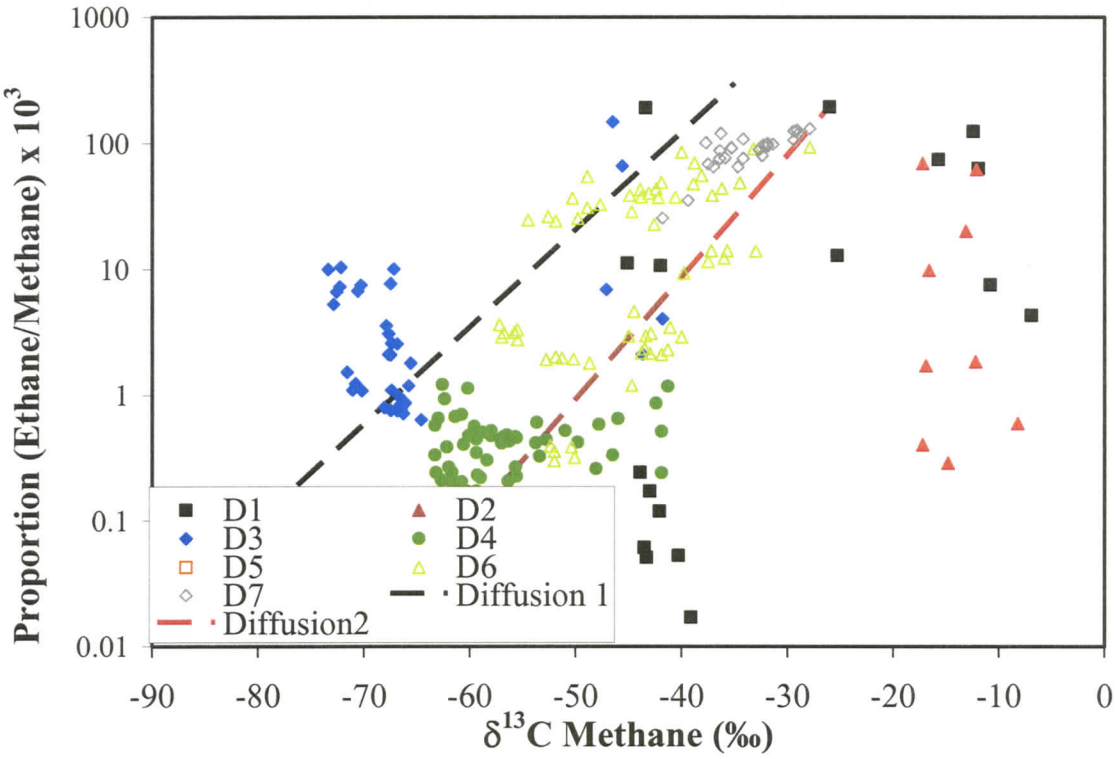


Figure 7.4: *Semi logarithmic diffusion plot showing $\delta^{13}C$ ratio for methane versus proportion ratio of methane over ethane for samples of desorption experiment sample sets D1, D2, D3, D4, D6 and D7. See text for details. No results are available for sample set D5. Diffusion lines are exemplary only and do not resemble measured values (diagram from Colombo et al., 1970 and Prinzhofer and Pernaton, 1997).*

Gases from sample sets D6 and D7 are thought to contain a mixture of gases generated from a Kerogen Type II and a Kerogen Type III source rock, and therefore, if the samples would resemble mixing in Figure 7.3, that mixing would have gases generated from the two different types of source rocks as endmembers, when a possible admixture of microbial gas would be neglected.

It is not likely that the observed variations are only an effect of diffusion, respectively mixing. Other processes, e.g., desorption, have similar effects on the molecular and isotope composition of CBM gases. Therefore, the approach for the delineation of diffusion by Colombo et al. (1970) and Prinzhofer and Pernaton (1997) is not useful for CBM samples and new approaches, which integrate the multitude of processes altering the molecular and isotope composition of CBM gases, have to be developed.

straight line. Therefore, based on the used approach, CBM sample sets D6 and D7 do not follow trends expected for the process of diffusion.

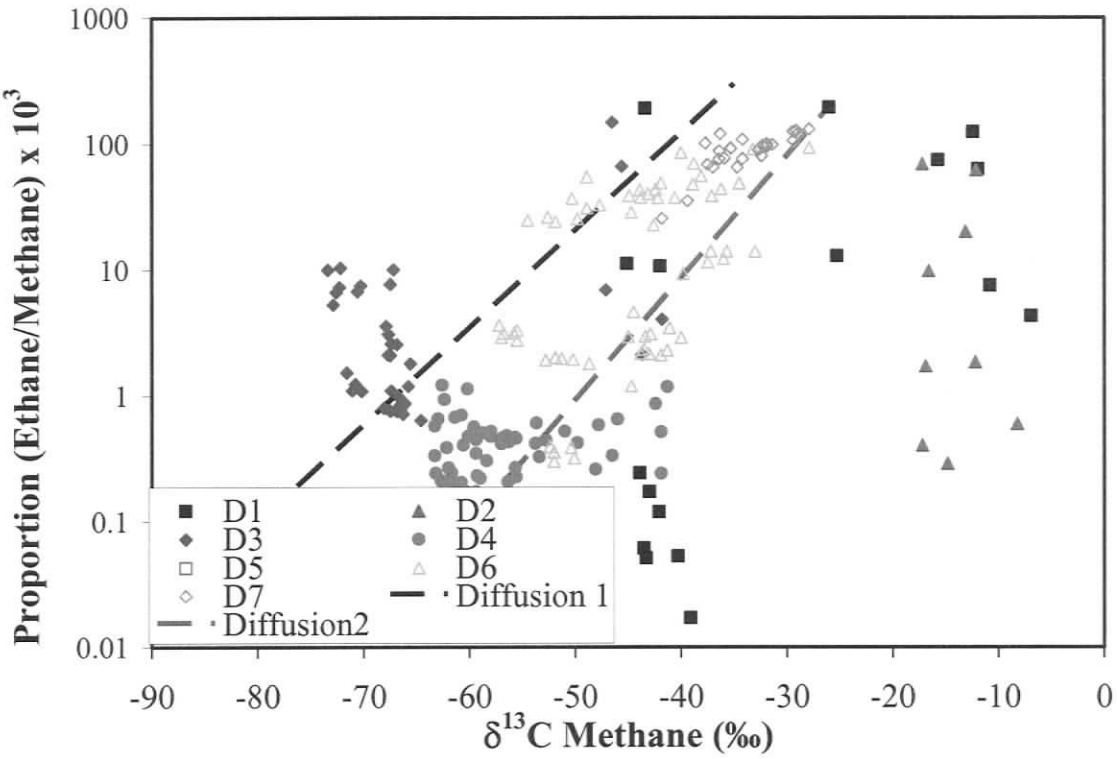


Figure 7.4: *Semi logarithmic diffusion plot showing $\delta^{13}C$ ratio for methane versus proportion ratio of methane over ethane for samples of desorption experiment sample sets D1, D2, D3, D4, D6 and D7. See text for details. No results are available for sample set D5. Diffusion lines are exemplary only and do not resemble measured values (diagram from Colombo et al., 1970 and Prinzhofer and Pernaton, 1997).*

Gases from sample sets D6 and D7 are thought to contain a mixture of gases generated from a Kerogen Type II and a Kerogen Type III source rock, and therefore, if the samples would resemble mixing in Figure 7.3, that mixing would have gases generated from the two different types of source rocks as endmembers, when a possible admixture of microbial gas would be neglected.

It is not likely that the observed variations are only an effect of diffusion, respectively mixing. Other processes, e.g., desorption, have similar effects on the molecular and isotope composition of CBM gases. Therefore, the approach for the delineation of diffusion by Colombo et al. (1970) and Prinzhofer and Pernaton (1997) is not useful for CBM samples and new approaches, which integrate the multitude of processes altering the molecular and isotope composition of CBM gases, have to be developed.

7.4 Production vs. Desorption Experiment

CBM Samples from Production Scenarios

Initial $\delta^{13}C$ ratios from production samples show relatively ^{13}C enriched methane and a progressive ^{13}C depletion with increasing production time. The corresponding proportions of methane show a correlation with the $\delta^{13}C$ ratios of methane (Figure 7.5).

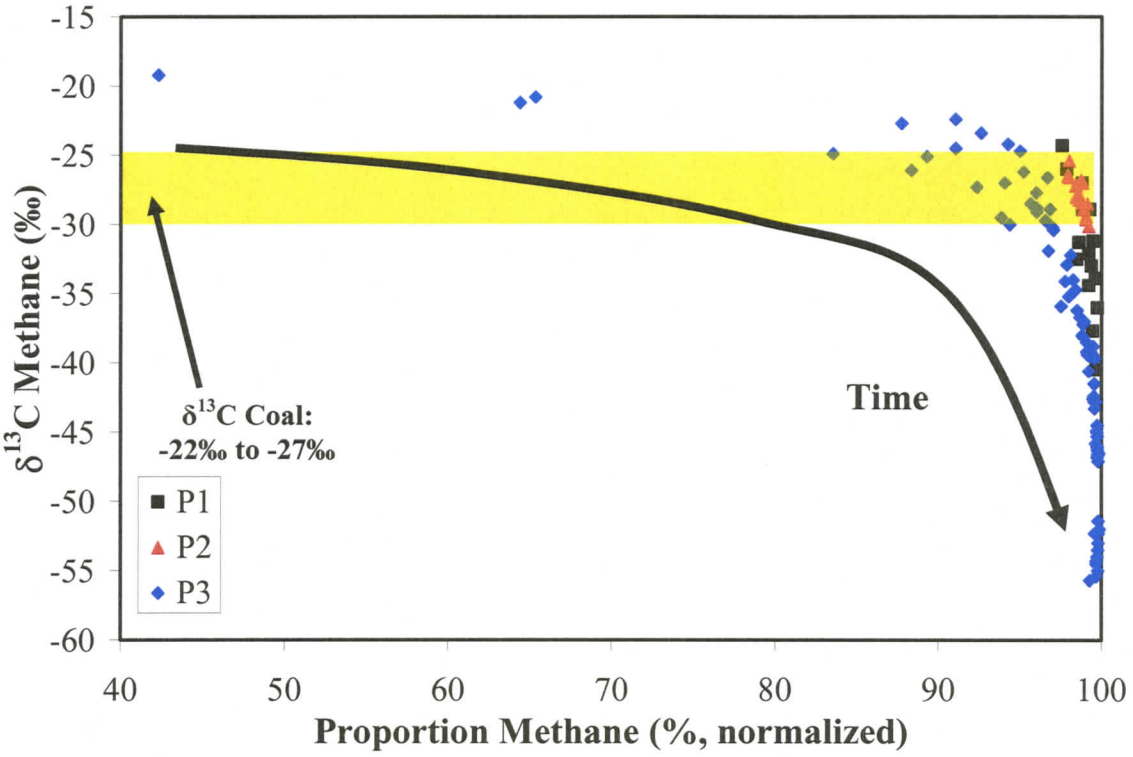


Figure 7.5: *Cross–plot of $\delta^{13}C$ methane versus proportion of methane for samples of production sample sets P1, P2 and P3. Concentrations are normalized on the basis of methane, ethane, propane, n–butane, i–butane and carbon dioxide concentrations. Isotope range for Kerogen Type III source rocks (coals) from Whiticar (1996a). See text for discussion.*

Relatively low proportions of methane correlate with relatively ^{13}C enriched methane. With increasing proportions of methane, the $\delta^{13}C$ ratio of methane changes only slightly towards relative ^{13}C depletion (Figure 7.5). At relatively high proportions of methane (> 90%) methane becomes strongly depleted in ^{13}C with small increases in the proportion of methane. At proportions of methane of over ca. 95% no relationship between proportion of methane and $\delta^{13}C$ ratio of methane is observed (Figure 7.5). Despite similar proportions, $\delta^{13}C$ ratios of methane cover a range of ca. 30‰. Initial $\delta^{13}C$ ratios of

methane are, close to -18‰, based on Figure 7.5. Compared with $\delta^{13}C$ ratios of coal (-22‰ to -27‰; Whiticar, 1996a), early methane is enriched in ^{13}C by 4‰ to 9‰, relative to organic matter. Berner and Faber (1996) reported a fractionation factor (αc; Equation 2.5) for the generation of methane from coal of α_c=1.003. Relative to generated methane, early CBM gases from production scenarios are therefore only affected by an isotope shift of 1‰ to 6‰. Therefore, fractionation factors for secondary effects are assumed to be relatively small (α_c 1.001 to α_c 1.006), or large fractions of the total adsorbed gas are released initially from the coal, resulting in no or only small isotope effects due to secondary processes. The attribution of the considered fractionation factor to a single process is not possible and therefore, does state the fractionation effect of several combined processes.

$\delta^{13}C$ ratios of carbon dioxide from production samples show no relationship with the proportion of carbon dioxide (Figure 7.6). $\delta^{13}C$ ratios of carbon dioxide from production samples cover a range between ca. -7‰ and ca. -14‰, but with increasing proportions of carbon dioxide, the $\delta^{13}C$ ratios of carbon dioxide merge on a $\delta^{13}C$ ratio of ca. -10‰ (Figures 7.6 and 7.7).

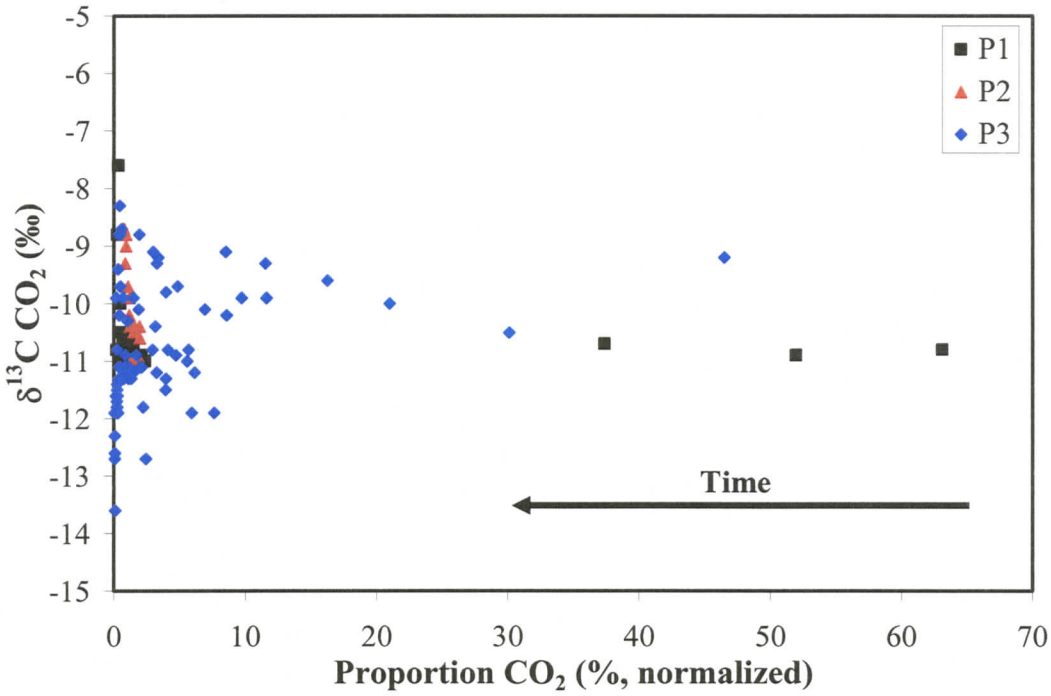


Figure 7.6: *Cross–plot of $\delta^{13}C$ carbon dioxide versus carbon dioxide proportions for samples of production sample sets P1, P2 and P3. Proportions are normalized on the basis of methane, ethane, propane, n–butane, i–butane and carbon dioxide proportions. See text for discussion.*

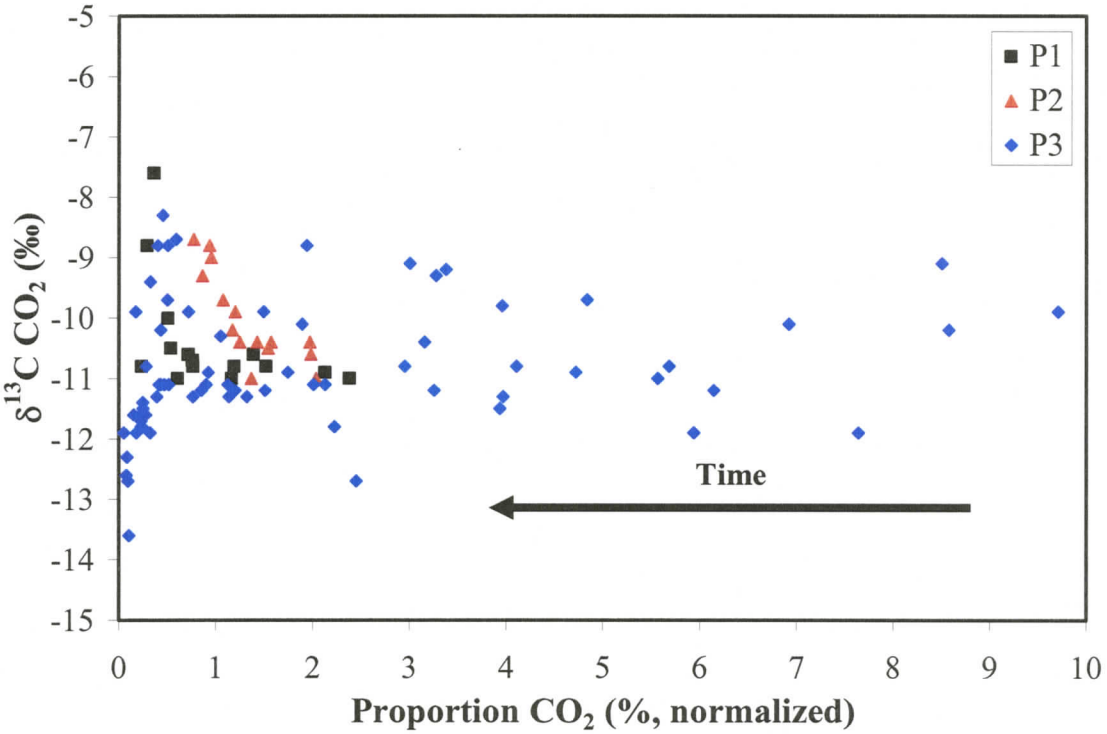


Figure 7.7: *Cross–plot of $\delta^{13}C$ carbon dioxide versus carbon dioxide proportions for samples of production sample sets P1, P2 and P3. Proportions are normalized on the basis of methane, ethane, propane, n–butane, i–butane and carbon dioxide proportions. Only proportions between 0% and 10% are shown. For the entire range see Figure 7.6. See text for discussion.*

CBM Samples from Desorption Experiment Scenarios

Initial $\delta^{13}C$ ratios from most desorption experiment samples show relatively ^{13}C depleted methane and a progressive ^{12}C depletion with increasing desorption time. With the exception of sample set D2 a correlation between $\delta^{13}C$ ratio of methane and the proportion of methane is observed (Figure 7.8). High proportions of methane correlate with relatively ^{13}C depleted methane, whereas relatively low proportions of methane correlate with relatively ^{13}C enriched methane (Figure 7.8). This trend is opposite to the observed trend for methane from production samples, and additionally greater variations are observed for samples from desorption experiments. Based on the isotopic composition of methane from sample set D2, these samples would fall into the described relationship, if the measured proportion of methane would be exaggerated, due to preferential enrichment of methane or preferential enrichment of the methane in ^{13}C during the geological history of the coal (Figure 7.8). Final $\delta^{13}C$ ratios of analyzed CBM samples from desorption experiments are between ca. -5‰ and ca. -45‰. A comparison with $\delta^{13}C$ ratios of coal (-22‰ to -27‰; Whiticar, 1996a) indicates that methane from final CBM gases are, relative to organic matter, ^{13}C depleted and ^{13}C enriched. Therefore, CBM gases likely are not primary gases and have to be altered by secondary processes.

$\delta^{13}C$ ratios of carbon dioxide from desorption experiment samples show no relationship with the proportion of carbon dioxide (Figure 7.9). $\delta^{13}C$ ratios of carbon dioxide from desorption experiment samples cover a range between ca. 25‰ and ca. -40‰, but with increasing proportions of carbon dioxide, the $\delta^{13}C$ ratios of carbon dioxide merge on a $\delta^{13}C$ ratio of ca. -10‰ (Figure 7.9). This is consistent with carbon dioxide from production samples (Figures 7.6 and 7.7). A mean $\delta^{13}C$ ratio for carbon dioxide of ca. -10‰ would translate, relative to organic matter (-22‰ to -27‰; Whiticar, 1996a), into a fractionation factor of ca. 14‰ (α_c 1.014). This isotope effect cannot be attributed to a single process, but has to be considered for a multitude of processes altering the isotopic composition of carbon dioxide, e.g., gas generation mixing with atmospheric carbon dioxide, adsorption, desorption and diffusion.

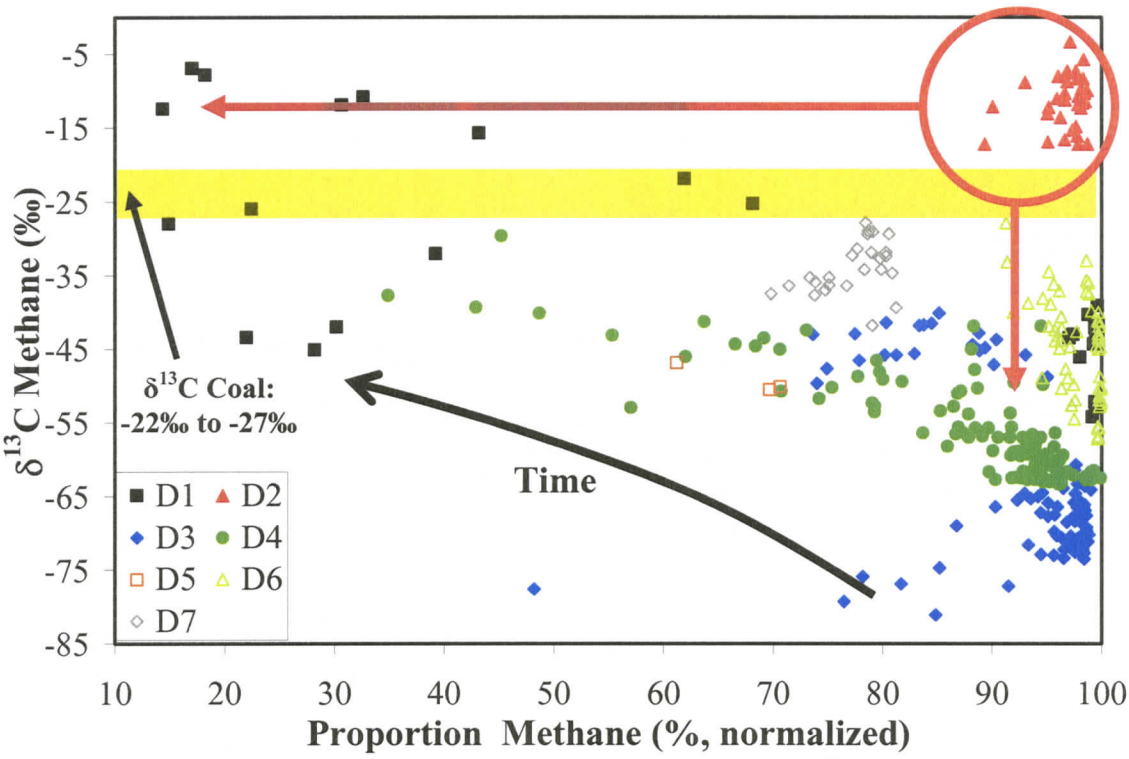


Figure 7.8: *Cross–plot of $\delta^{13}C$ methane versus methane proportions for samples of desorption experiment sample sets D1, D2, D3, D4, D5, D6 and D7. Proportions are normalized on the basis of methane, ethane, propane, n–butane, i–butane and carbon dioxide proportions. See text for discussion.*

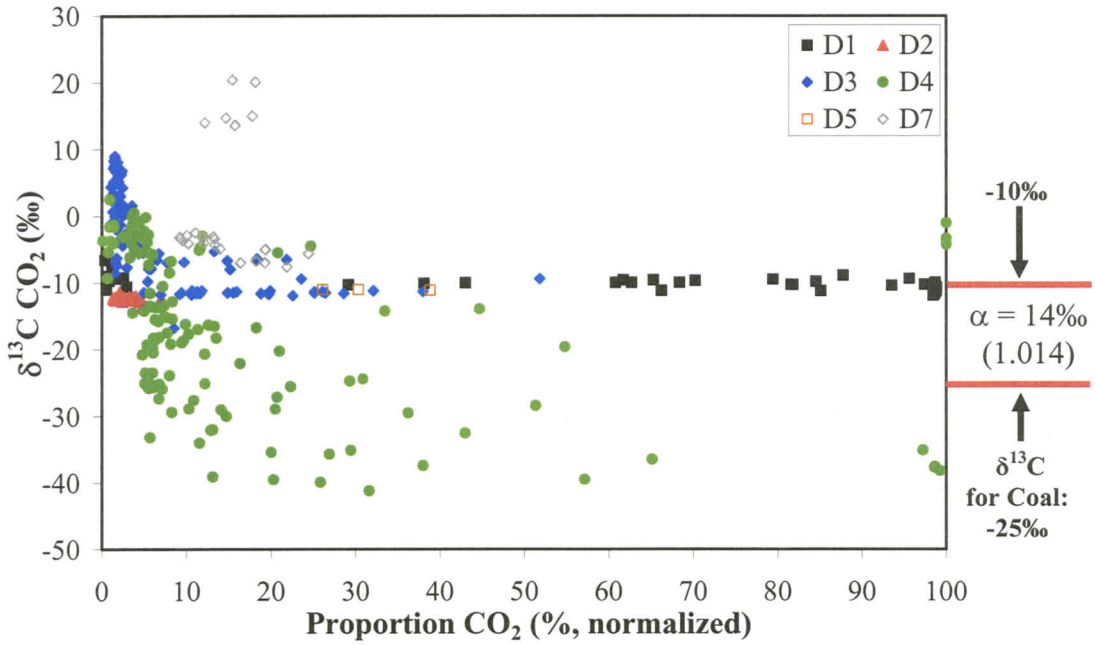


Figure 7.9: *$\delta^{13}C$–ratios of carbon dioxide versus carbon dioxide proportions for samples of desorption experiment sample sets D1, D2, D3, D4, D5 and D7. Proportions are normalized on the basis of methane, ethane, propane, n–butane, i–butane and carbon dioxide proportions. No results are available for sample set D6. Isotope ratio for coal is an average value. $\delta^{13}C$ ratios of coal range generally between -22‰ and -27‰ (Whiticar, 1996a). Isotope ratios of carbon dioxide approach a value of ca. -10‰ with increasing proportion of carbon dioxide. Based on the difference between -10‰ and the average isotope ratio of coal, the fractionation factor (α) is 14‰ or 1.014. See text for discussion.*

$\delta^{13}C$ ratios of ethane from desorption experiment samples show no relationship with the proportion of ethane (Figure 7.10). With relatively low proportions of ethane, the $\delta^{13}C$ ratios of ethane show variations between ca. -5‰ and ca. -30‰, but with increasing proportions of ethane the stable carbon isotope composition of ethane becomes similar for the different samples around a mean value of ca. -28‰ (Figure 7.10). Compared with the stable carbon isotope composition of coal (-22‰ to -27‰; Whiticar, 1996a), ethane is, relative to organic matter, enriched in ^{13}C. The corresponding fractionation is -3‰ (α_c 0.997). This fractionation factor cannot be attributed to a single process, but has to be considered for a multitude of processes altering the isotopic composition of ethane, e.g., gas generation, mixing with atmospheric carbon dioxide, adsorption, desorption and diffusion.

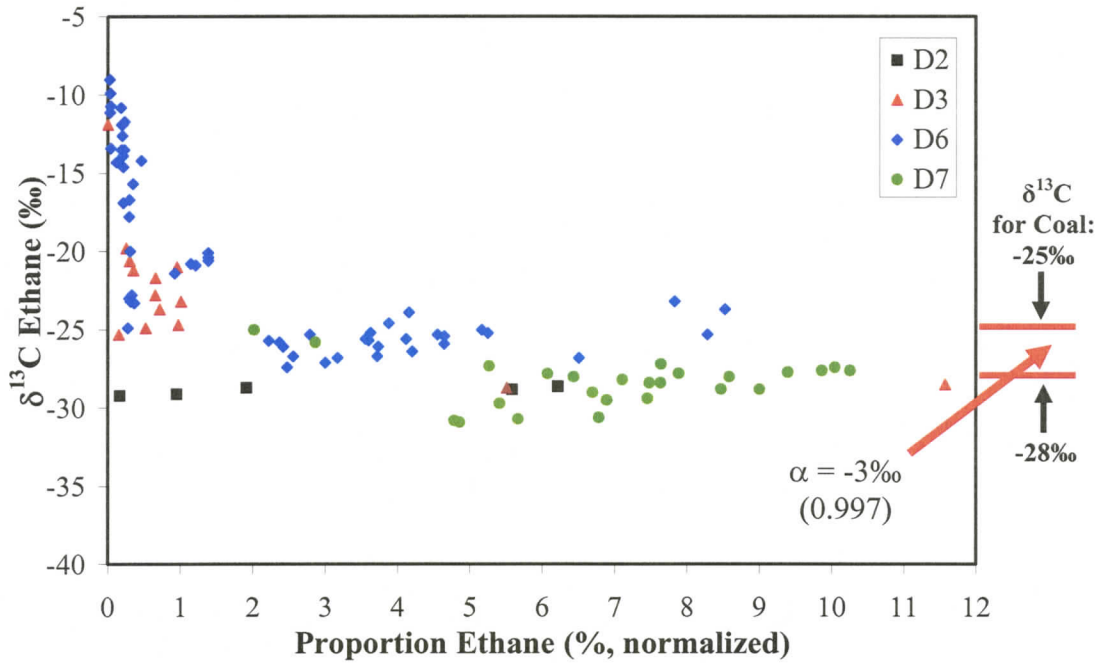


Figure 7.10: *Cross–plot of $\delta^{13}C$ ethane versus ethane proportions for samples of desorption experiment sample sets D2, D3, D6 and D7. Proportions are normalized on the basis of methane, ethane, propane, n–butane, i–butane and carbon dioxide proportions. No results are available for sample sets D1, D4 and D5. Isotope ratio for coal is an average value. $\delta^{13}C$ ratios of coal range generally between -22‰ and -27‰ (Whiticar, 1996a). Isotope ratios of ethane approach a value of ca. -28‰ with increasing proportion of ethane. Based on the difference between -28‰ and the average isotope ratio of coal, the fractionation factor (α) is -3‰ or 0.997.See text for discussion.*

Systematic of CBM Production from Producing Wells

Samples from production scenarios do not show the molecular and isotope trends expected based on the presence of the processes desorption and diffusion. Samples from production sample sets show initially relatively ^{13}C enriched methane correlating with relatively low proportions of methane and finally relatively ^{13}C depleted methane correlating with relatively high proportions of methane. Desorption and diffusion with the attendant molecular and isotope effects have to be present, so that the observed trends for samples from production sample sets have to be the result of a different process or different processes.

Due to a combined effect of hydraulic fracturing and pressure reduction in coal seams due to water removal, accelerated desorption and diffusion take place in coal located close to the well bore (Volume 1), allowing the liberation of early and late

methane at roughly the same time. These gases are the first samples produced from a CBM well and the gases should be relatively depleted in methane, due to higher proportions of higher hydrocarbons and carbon dioxide. The produced methane should be relatively enriched in ^{13}C. Later produced CBM gases should be a mixture of gases desorbing from coal relatively close to the well bore (Volume 1) and from coal further away (Volume 2). Due to less influence of hydraulic fracturing and elevated hydrostatic pressures, gas desorbing from coal in Volume 2 should be relatively enriched in methane and the methane should be relatively depleted in ^{13}C. Therefore, the later produced CBM gases, which are a mixture of gases desorbing from different locations within the coal seam (Volume 1 and Volume 2), should be, relative to the first produced CBM gases, relatively enriched in methane and the methane should be relatively depleted in ^{13}C. Gases, even later produced from a CBM well, should be a mixture of gases desorbing from Volumes 1 and 2 and of gases desorbing from coal even further away from the well bore (Volume 3). Due to relatively small influences of hydraulic pressure and even higher hydrostatic pressures, relative Volumes 1 and 2, this gas should be strongly enriched in methane and this methane should be strongly depleted in ^{13}C. Therefore, this late produced CBM gas should be relative to the early and later produced gases enriched in methane and methane should be depleted in ^{13}C, as it is observed in the analyzed samples from production scenarios.

7.5 Effect of CBM Production

CBM from sample set P3 shows trends described for CBM gases produced from production wells. After a production time of 95 days the proportion of methane decreased, accompanied by relative increases for the proportions of higher hydrocarbons and carbon dioxide. Additionally, methane became relatively enriched in ^{13}C and in ^{2}H, whereas carbon dioxide became relatively depleted in ^{13}C. The described molecular and isotopic changes occurred in a relatively short time frame. Following these changes, sample set P3 shows again the trends described for CBM gases from production scenarios.

The observed trend before the described molecular and isotopic changes represents production of CBM gases desorbing from different regions within a coal seam (cycle 1; see chapter 7.4). If the observed trend following the described molecular and isotopic changes (cycle 2) is also caused by mixing of gases originating from different coal volumes, then these gases have to come from a different location within the same coal seam, or from a different coal seam, both previously not or only slightly affected by the production of CBM. A continuous production from areas responsible for the observed trends of Cycle 1 would not result in the observed trends for Cycle 2, but CBM gases would still be relatively enriched in methane and the methane would still be relatively depleted in ^{13}C.

To access gas from different coal Volumes or different coal seams, new fractures or fracture systems have to be opened and previously open fractures have to become closed, or existing fracture systems have to become laterally and/or vertically extended. Due to gas desorption and gas release (production), shrinkage processes within the coal can be initiated (Harpalani & Schraufnagel, 1990; George & Barakat, 2001). These shrinkage processes might have been the initiation of the collapse of one fracture system and the opening of a new one. Reduced pressure might result in the extension of the fracture system, laterally and vertically, due to overpressure in adjacent coal volumes. The process of extension or collapse and opening of fracture systems have to happen on a short time scale and have to affect large regions, because the described molecular and isotopic changes occurred simultaneously in all three CBM wells of sample set P3 (all wells produce CBM gases from the same coal seams), which are located several hundred meters apart from each other.

8. Conclusions

1. Routine methods were developed to make isotope ratio and molecular measurements of CBM gases collected from production wells and desorption experiments.

2. The normalized molecular composition of analyzed CBM samples consists mostly of methane, with small concentrations of ethane and carbon dioxide and minor contributions of propane, *n*–butane and *i*–butane.

3. $\delta^{13}C$ values for methane of CBM gases do not represent primary gas generation, as it is more ^{12}C enriched than expected for primary methane generated from a coal or a Kerogen Type III source rock.

4. Maturity of coals appears to have no influence on the stable carbon and hydrogen isotope ratios of CBM gases, including methane, higher hydrocarbons and carbon dioxide.

5. The stable carbon and hydrogen isotope ratios of methane are not dependent on the relative abundance of vitrinite in coals.

6. The stable carbon and hydrogen ratios of methane, collected early during CBM production or during desorption experiments appear to be influenced by the amount of liptinite in coals.

7. The stable carbon and hydrogen isotope ratios of methane are independent on the amount of inertinite in coals.

8. Present day depth does not have an influence on the stable carbon and hydrogen isotope ratios of methane.

9. Repeated adsorption and desorption during the burial history of a coal seam leads to complications for the estimation of molecular and isotope composition of gases retained by coal.

10. Due to the inherent retentive capacity of coal, mixtures between gases of different origins (thermogenic, microbial) and mixtures of gases generated at different stages of the coalification process are possible, leading to interpretative challenges.

11. Isotope effects during desorption and diffusion of methane are observed.

12. Secondary processes, i.e., adsorption, desorption, mixing and diffusion can significantly alter the molecular and isotope composition of CBM gases.

13. A direct application of pyrolysis data to CBM situations would be inappropriate, due to substantial secondary processes.

14. The classical approaches for natural gas classification using Bernard Diagram and CD Diagram can not be directly applied to CBM. New approaches for gas classification are necessary, incorporating the effect of secondary processes and attendant molecular and isotope effects.

15. The presence of microbial methane oxidation in coal seams is likely, but it is difficult to detect evidence for this process from the analyses of gas composition and $\delta^{13}C$ ratios of methane from samples derived from desorption experiments or from producing wells.

16. Identification of microbially generated methane in CBM gases using the approaches by Chung et al. (1988) and Berner and Faber (1996) are possible, but the derived fractions have to be considered carefully. Both approaches are based on ^{12}C enrichment in methane of CBM samples relative to modeled $\delta^{13}C$ values,

but the ^{12}C enrichment for methane can also be the result of isotope fractionation due to other processes.

17. The combination of gas composition and stable carbon isotopes for methane, ethane and propane allows the identification of thermogenic gas, generated from a Kerogen Type II source rock in CBM samples.

18. Gases in CBM samples generated by different coals or Kerogen Type III source rocks can not be readily delineated.

19. CBM is most likely a mixture of gases generated from the coal at different times of the coalification process. This includes with possible admixtures of primary and secondary microbial gas and, sometimes, gases generated from other coals and/or gases generated from different source rocks.

20. Stable carbon isotope compositions of methane from desorption experiment samples and from production samples show opposite trends with increasing desorption/production time; methane from production samples shows ^{13}C depletion with increasing production time and methane from desorption experiment samples shows ^{13}C enrichment with increasing desorption time.

21. A schematic model is able to explain the observed isotope trend for CBM production samples of relative ^{13}C enrichment for methane with increasing production time, indicating mixing of CBM gases desorbing from different regions of an accessed coal seam during CBM production.

22. Indications were found for sudden closure and correlating opening of fractures and fracture–systems in coal seams leading to desorption and consequently production of CBM from different areas of the coal or even from different intersected coal seams.

23. With additional knowledge about the impact of secondary processes on the molecular and isotopical composition of CBM, the analyzes of stable carbon isotopes in CBM may provide further information about the total gas content of a given coal seam, including a more sophisticated estimation of lost and residual gas, and may be therefore competitive to the currently used desorption canister approach.

24. Further geochemical work is required for a better understanding and the establishment of the stable isotope systematics of CBM, including the individual and experimental consideration of adsorption, desorption and diffusion/migration of gases in coal.

9. References

Airey E.M. (1968): Gas emission from broken coal. An experimental and theoretical investigation; *International Journal of Rock Mechanics and Mining Science*, **v.5**, p.475-494.

Aravena R., Harrison S.M., Barker J.F., Abercombie H. and Rudolph D. (2003): Origin of methane in the Elk Valley coalfield, southeastern British Columbia, Canada; *Chemical Geology*, **v.195**, p.219-227.

Barker J.F. and Fritz P. (1981): Carbon isotope fractionation during microbial methane oxidation; *Nature*, **v.293**, p.289-291.

Beamish B.B. and Crosdale P.J. (1995): The influence of maceral content on the sorption of gases by coal and the association with outbursting; *in: Management and Control of High Gas Outbursts in Underground Coal Mines (Ed.: R.D. Lama)*, Westonprint, Kiama, NSW, Australia, p.353-362.

Bernard B.B., Brooks J.M. and Sackett W.M. (1976): Natural gas seepage in the Gulf of Mexico; *Earth and Planetary Science Letters*, **v.31**, p.48-54.

Bernard B.B., Brooks J.M. and Sackett W.M. (1978): Light hydrocarbons in recent Texas continental shelf and slope sediments; *Journal of Geophysical Research*, **v.83**, p.4053-4061.

Berner U. (1989): Entwicklung und Anwendung empirischer Modelle für die Kohlenstoffisotopenvariationen in Mischungen thermogener Erdgase; Ph.D. Thesis, University of Clausthal, Germany.

Berner U. and Faber E. (1988): Maturity related mixing model for methane, ethane and propane, based on carbon isotopes; *Organic Geochemistry*, **v.13**, no.1-3, p.67-72.

Berner U. and Faber E. (1996): Empirical carbon isotope/ maturity relationships for gases from algal kerogens and terrigenous organic matter, based on dry, open system pyrolysis; *Organic Geochemistry*, **v.24**, p.947-955.

Berner U., Faber E. and Stahl W. (1992): Mathematical simulation of the carbon isotopic fractionation between humunitic coals and related methane; *Chemical Geology*, **v.94**, p.315-319.

Berner U., Faber E., Scheeder G. and Panten D. (1995): Primary cracking of algal and landplant kerogens: kinetic models of isotope variations in methane, ethane and propane; *in: Processes of Natural Gas Formation (Eds.: D.D. Rice and M. Schoell), Chemical Geology*, **v.126**, p.233-245.

Bertard C., Bruyet B. and Gunther J. (1970): Determination of desorbable gas concentration of coal (direct method); *International Journal of Rock Mechanics and Mining Science*, **v.7**, p.43-65.

Beutl M. and Lesnik J. (2001): Adsorption dynamics of hydrogen and carbon monoxide on V/Pd(111) alloy surfaces; *Surface Science*, **v.482**, p.353-358.

Boigk H., Hagemann H.W., Stahl W. and Wollanke G (1976): Isotopenphysikalische Untersuchungen zur Herkunft und Migration des Stickstoffs Nord-Westdeutscher Erdgase aus dem Oberkarbon und dem Rotliegend; *Erdoel, Kohle, Erdgas Petrochemie*, **v.2**. p.103-112.

Bolt B.A. and Innes J.A. (1959): Diffusion of carbon dioxide from coal; *Fuel*, **v.38**, p.333-337.

Busch A., Gensterblum Y., Kroos B.M. and Littke R. (2004): Methane and carbon dioxide adsorption-diffusion experiments on coal: upscaling and modeling; *International Journal of Coal Geology*, **v.60**, p.151-168.

Bustin R.M., Clarkson C. and Levy J. (1995): Coalbed methane adsorption of coals of the Bulli and Wongawilli seams, southern Sydney basin: Effect of maceral composition; *Proceedings of the 29th Newcastle Symposium on Advances in the Study of the Sydney Basin*, p.22-28.

Chamberlin R.T. (1909): Notes on explosive mine gases and dusts, with special reference to the explosions in the Monongah, Darr and Naomi coal mines; *U.S. Geological Survey Bulletin*, **v.383.**

Chung H.M., Gromly J.R. and Squires R.M. (1988): Origin of gaseous hydrocarbons in subsurface environments: Theoretical considerations of carbon isotope distribution; *Chemical Geology*, **v.71**, p.97-103.

Clayton C. (1991): Carbon isotope fractionation during natural gas generation from kerogen; *Marine and Petroleum Geology*, **v.8**, p.232-240.

Colombo U., Gazzarrini F., Gonfiantini R., Kneuper G., Teichmüller M. and Teichmüller R. (1970): Carbon isotope study on methane from German coal deposits; *in: Advances in Organic Geochemistry 1966 (Eds.: G.D. Hobson and G.C. Speers)*, Pergamon Press, Oxford, p.1-26.

Cooper B.S. and Murchison D.G. (1969): Organic geochemistry of coal; *in: Organic Geochemistry (Eds.: G. Eglington and M.T.J. Murphy)*, Springer-Verlag, Berlin, p.699-726.

Cramer B. (2004): Methane generation from coal during open system pyrolysis investigated by isotope specific, Gaussian distributed reaction kinetics; *Organic Geochemistry*, **v.35**, p.379-392.

Creedy D.P. (1988): Geological controls on the formation and distribution of gas in British coal measure strata; *International Journal of Coal Geology*, **v.10**, p.1-31.

Criss R.E. (1999): Principles of stable isotope distribution; Oxford University Press, New York, 254 pp.

Crosdale P.J., Beamish B.B. and Valix M. (1998): Coalbed methane sorption related to coal composition; *in: Coalbed Methane: From Coal-Mine Outbursts to a Gas Resource (Ed.: R.M. Flores), International Journal of Coal Geology*, **v.35**, p.147-158.

Das B.M., Nikols D.J., Das Z.U. and Hucka V.J. (1991): Factors affecting rate and total volume of methane desorbed from coalbeds; in: Coalbed Methane of Western North America; Guidebook for the Rocky Mountain Association of Geologists Fall Conference and Field Trip (Eds.: S.D. Schwochow, D.K. Murray and M.F. Fahy), *Field ConferenceField - Rocky Mountain Association of Geologists*, p.69-76.

Diamond W.P. and Levine J.R. (1981): Direct method determination of the gas content of coal: procedures and results; *U.S. Bureau of Mines Report of Investigation*, no.8515, 35 pp.

Diamond W.P. and Schatzel S.J. (1998): Measuring the gas content of coal: a review; in: Coalbed Methane: from Coal-Mine Outbursts to a Gas Resource (Ed.: R.M. Flores), *International Journal of Coal Geology*, **v.35**, p.311-331.

Estep M.E. and Höring T.C. (1980): Biochemistry of the stable hydrogen isotopes; *Geochimica et Cosmochimica Acta*, **v.44**, p.1197-1206.

Ettinger I., Eremin I., Zimakov B. and Yanoskaya M. (1966): Natural factors influencing coal sorption properties. I. Petrography and sorption properties of coals; *Fuel*, **v.45**, p.267-275.

Faber E. (1987): Zur Isotopengeochemie gasförmiger Kohlenwasserstoffe; *Erdöl, Erdgas und Kohle*, **v.103**, p.210-218.

Faber E. and Stahl W.J. (1983): Analytical procedure and results of an isotope geochemical surface survey in area of the British North Sea; *in: Petroleum Geochemistry and Exploration of Europe (Ed.: J. Brooks)*, Blackwell Scientific Publications, p.51-63.

Faber E. and Stahl W.J. (1984): Geochemical surface exploration for hydrocarbons in North Sea; *American Association of Petroleum Geologists Bulletin*, **v.68**, no.3, p.363-386.

Faber E., Stahl W.J. and Whiticar M.J. (1992): Distinction of bacterial and thermogenic hydrocarbon gases; *in: Bacterial gas (Ed.: R. Vially)*, Editions Technip, Paris, p.63-74.

Flores R.M. (1998): Coalbed methane: from hazard to resource; in: Coalbed Methane: From Coal-Mine Outbursts to a Gas Resource (Ed.: R.M. Flores), *International Journal of Coal Geology*, **v.35**, p.3-26.

Friedrich H.U. and Jüntgen H. (1972): Some measurements of the 12C/13C ratio in methane or ethane desorbed from hard coal or released by pyrolysis*; in: Advances in Organic Geochemistry 1971 (Eds.: H.R. Gaertner and H. Wehner)*, Pergamon Press, Oxford, p.639-646.

Friedrich H.U. and Jüntgen H. (1973): Aussagen zum $^{13}C/^{12}C$-Verhältnis des bei der Inkohlung gebildeten Methans aufgrund von Pyrolyse-Versuchen; *Erdöl und Kohle, Erdgas, Petrochemie*, **v.26**, p.636-639.

Fuex A.N. (1980): Experimental evidence against an appreciable isotopic fractionation of methane during migration; *in: Advances in Organic Geochemistry 1979 (Eds.: A.G. Douglas and J.R. Maxwell)*, p.725-732.

Galimov E.M. (1975): Carbon isotopes in oil-gas geology*; NASA Technical Translation NASA TT F-682*, U.S. Government Printing Office.

Galimov E.M. (1988): Sources and mechanisms of formation of gaseous hydrocarbons in sedimentary rocks; in: Origins of Methane in the Earth (Ed.: M. Schoell), *Chemical Geology*, **v.71**, p.77-95.

Gaschnitz R., Kroos B.M., Gerling P., Faber E. and Littke R. (2001): On-line pyrolysis-GC-IRMS: isotope fractionation of thermally generated gases from coal; *Fuel*, **v.80**, p.2139-2153.

George J.D. St. and Barakat M.A. (2001): The change in effective stress associated with shrinkage from gas desorption in coal; *International Journal of Coal Geology*, **v.45**, p.105-113.

Gould K.W., Hargraves A.J. and Smith J.W. (1987): Variation in the composition of seam gases issuing from coal; *Bulletin of the Australian Institute for Mining and Metallurgy*, **v.292**, p.69-73.

Harpalani S. and Schraufnagel R.A. (1990): Measurement of parameters impacting methane recovery from coal seams; *International Journal of Mining and Geological Engineering*, **v.8**, p.369-384.

Hoefs J. (2004): Stable isotope geochemistry; Springer Verlag, Berlin, pp.244.

Hoefs J. and Frey M. (1976): The isotopic composition of carbonaceous matter in a metamorphic profile from the Swiss Alps; *Geochimica et Cosmochimica Acta*, **v.40**, p.945-951.

Hosgörmez H., Yalcin M.N., Cramer B., Gerling P., Faber E., Schäfer R.G. and Mann U. (2002): Isotopic and molecular composition of coal-bed gas in the Amasre region (Zonguldak basin – western Black Sea); *Organic Geochemistry*, **v.33**, p.1429-1439.

Hunt J.M. (1991): Generation of gas and oil from coal and other terrestrial organic matter; *Organic Geochemistry*, **v.17**, p.673-680.

Hunt J.M. (1995): Petroleum geochemistry and geology; Freeman and Company, 743 pp.

Joubert J.L., Grein C.T. and Bienstock D. (1973): Sorption of methane in moist coals, *Fuel*, **v.52**, p.181-185.

Joubert J.L., Grein C.T. and Bienstock D. (1974): Effect of moisture on the methane capacity of American coals; *Fuel*, **v.53, p.** 186-191.

Jüntgen H. and Karweil J. (1966a): Gasbildung und Gasspeicherung in Steinkohlenflözen. Part 1. Gasbildung; *Erdöl und Kohle, Erdgas, Petrochemie*, **v.19**, p.251-258.

Jüntgen H. and Karweil J. (1966b): Gasbildung und Gasspeicherung in Steinkohlenflözen. Part 2. Gasspeicherung; *Erdöl und Kohle, Erdgas, Petrochemie*, **v.19**, p.339-344.

Jüntgen H. and Klein J. (1975): Entstehung von Erdgas aus kohligen Sedimenten; *Erdöl und Kohle, Erdgas, Petrochemie*, **Ergänzungsband v.1**, p.52-68.

Kim A.G. (1977): Estimating methane content of bituminous coalbeds from adsorption data; *U.S. Bureau of Mines Report of Investigation*, no.8245, 22 pp.

King G.M.and Blackburn T.H. (1996): Controls of methane oxidation in sediments; *Mitteilungen der Internationalen Vereinigung von Limnologen*, **v.25**, p.25-38.

Kopp O.C., Bennett III M.E. and Clark C.E. (2000): Volatiles lost during coalification; *International Journal of Coal Geology*, **v.44**, p.69-84.

Kotarba M.J. and Lewan M.D. (2004): Characterizing thermogenic coalbed gas from Polish coals of different ranks by hydrous pyrolysis; *Organic Geochemistry*, **v.35**, p.615-646.

Kretschmar H.J., Czolbe P. and Bauer K. (1986): Diffusionsmessungen an Speichergesteinen mit unterschiedlichen Gasen und Messapparaturen; *Erdoel und Kohle, Erdgas Petrochemie*, **v.39**, p.135-138.

Kroos B.M. (1986): Diffusion of C1 to C5 hydrocarbons in water-saturated sedimentary rocks; *Erdoel und Kohle, Erdgas Petrochemie*, **v.39**, p.399-402.

Krooss B.M. and Leythäuser D. (1996): Molecular diffusion of light hydrocarbons in sedimentary rocks and its role in migration and dissipation of natural gas; in: hydrocarbon migration and its near-surface expression (Eds.: D. Schumacher and M.A. Abrams), *American Association of Petroleum Geologists Memoir* **66**, p.173-183.

Laubach S.E., Marrett R.A., Olson J.E. and Scott A.R. (1998): Characteristics and origins of coal cleat: a review; in: Coalbed Methane: From Coal-Mine Outbursts to a Gas Resource (Ed.: R.M. Flores), *International Journal of Coal Geology*, **v.35**, p.175-207.

Lebedev V.S. and Syngayevskiy E.D. (1971): Carbon isotope fractionation in sorption processes (translated title); *Geokhimiya*, **v.5**, p.615-619.

Levine J.R. (1993): Coalification: The evolution of coal as a source rock and reservoir rock for oil and gas; *in: Hydrocarbons from Coal, American Association of Petroleum Geologists Studies in Geology Series*, **v.38**, p39-77.

Leythäuser D., Schäfer R.G. and Yükler A. (1980): Diffusion of light hydrocarbons through near-surface rocks; *Nature*, **v.284**, p.522-525.

Lindemann F.A. (1919): Note on the vapour pressure and affinity of isotopes; *Philosophical Magazine*, **v.38**, p.173-181.

May F., Freund W., Műller E.P. and Dostal K.P. (1968): Modellversuche über Isotopenfraktionierung von Erdgaskomponenten während der Migration; *Zeitschrift für angewandte Geologie*, **v.14**, p.376-380.

McCulloch C.M. and Diamond W.P. (1976): Inexpensive method helps predict methane content of coalbeds; *Coal Age*, **v.81**, p.102-106.

McLennan J.D., Schafer P.S. and Pratt T.J. (1995): A guide to determining coalbed gas content; *Gas Research Institute file: reference No. GRI-94/0396.*

Meier-Augenstein W. (1999): Applied gas chromatography coupled to isotope ratio mass spectrometry; *Journal of Chromatography A*, **v.842**, p.351-371.

Meissner F.F. (1984): Cretaceous and Lower Tertiary coals as sources for gas accumulations in the Rocky Mountain area; *in: Hydrocarbon Source Rocks of the Greater Rocky Mountain region (Eds.: J. Woodward, F.F. Meissner and J.L. Clayton)*, Rocky Mountain Association of Geologists, Denver, p.401-431.

Niemann M., Clarke P.R., Cornelius C.T., Ryan B. and Whiticar M.J. (2005): Gas origin of the Blackhawk formation, Castlegate coalbed methane field, Utah; 2005 Rocky Mountain Section - AAPG Meeting, Jackson Hole, Wyoming, USA (http://www.searchanddiscovery.net/documents/2005/niemann/index.htm).

O'Neil J.R. (1986): Theoretical and experimental aspects of isotopic fractionation; in: Stable Isotopes in High Temperature Geologic Processes, (Eds.: J.W. Walley et al.), *Reviews in Mineralogy*, **v.16**, p.1-40.

Park R. and Epstein S. (1961): Metabolic fractionation of C^{13} and C^{12} in plants; *Plant Physiology*, **v.36**, p.133-138.

Pernaton E., Prinzhofer A. and Schneider F. (1996): Reconsideration of methane signature as a criterion for the genesis of natural gas: Influence of migration on isotopic signature; *Review IFP*, **v.51**, p.635-651.

Perrodon A. (1983): Primary migration and the source rock concept; in: Dynamics of oil and gas accumulations; *Bulletin des Centres de Recherches Exploration-Production Elf Aquitaine,* Memoir 5, p.79-89.

Prinzhofer A.A. and Huc A.Y. (1995): Genetic and post-genetic molecular and isotopic fractionations in natural gases; *Chemical Geology*, **v.126**, p.281-290.

Prinzhofer A.A. and Pernaton E. (1997): Isotopically light methane in natural gas: Bacterial imprint or diffusive fractionation?; *Chemical Geology*, **v.142**, p.193-200.

Rahn T. and Eiler J.M. (2001): Experimental constraints on the fractionation of $^{13}C/^{12}C$ and $^{18}O/^{16}O$ ratios due to adsorption of CO_2 on mineral substrates at conditions relevant to the surface of Mars; *Geochimica et Cosmochimica Acta*, **v.65**, p.839-846.

Rayleigh J.W.S. (1896): Theoretical considerations respecting the separation of gases by diffusion and similar processes; *Philosophical Magazine*, **v.42**, p.493-499.

Redding C.E., Schoell M., Monin J. and Durand B. (1980): Hydrogen and carbon isotopic composition of coals and kerogens; *in: Advances in Organic Geochemistry 1979 (Eds.: A.G. Douglas and J.R. Maxwell)*, p.711-723.

Rice D.D. (1992): Controls, habitat, resource potential of ancient bacterial gas; *in: Bacterial Gas (Ed.: R. Vially)*, Editions Technip, p.91-118.

Rice D.D. (1993): Compositions and origins of coalbed gas; in: Hydrocarbons from Coal (Eds.: B.E. Law and D.D. Rice), *American Association of Petroleum Geologists, Studies in Geology*, **v.34**, p.159-184.

Rice D.D. and Claypool G.E. (1981): Generation, accumulation, and resource potential of biogenic gas; *American Association of Petroleum Geologists Bulletin*, **v.65**, p.5-25.

Rigby D. and Smith J.W. (1981): An isotopic study of gases and hydrocarbons in the Cooper basin; *Australian Petroleum Exploration Association Journal*, **v.21**, p.222-229.

Rooney M.A., Claypool G.E. and Chung H.M. (1995): Modeling thermogenic gas generation using carbon isotope ratios of natural gas hydrocarbons; *Chemical Geology*, **v.126**, p.219-232.

Ryan B.D. and Dawson F.M. (1994): Coalbed methane canister desorption techniques; in: Geological Fieldwork 1993; a summary of field activities and current research (Eds.: B. Grant and J.M. Newell), *Paper-Ministry of Energy, Mines and Petroleum Resources*, p.245-256.

Schloemer S. and Kroos B.M. (2004): Molecular transport of methane, ethane and nitrogen and the influence of diffusion an the chemical and isotopic composition of natural gas accumulations; *Geofluids*, **v.4**, p.81-108.

Schoell M. (1980): The hydrogen and carbon isotopic composition of methane from natural gases of various origins; *Geochimica et Cosmochimica Acta*, **v.44**, p.649-661.

Schoell M. (1988): Multiple origins of methane in the Earth; *Chemical Geology*, **v.71**, p.1-10.

Schwartzkopf T. (1984): Kohlenstoff- und Wasserstoffisotope in Kohlen und ihren Nebengesteinen; Diplomarbeit, Ruhr University, Bochum, Germany, 39 pp.

Schwartzkopf T. and Schoell M. (1985): Die Variation der C- und H-Isotopenverhältnisse in Kohlen und Maceralzusammensetzungen und Inkohlungsgrad; *Fortschr. Geol. Rheinland Westfalen*, **v.33**, p.161-179.

Scott A.R. (1993): Composition and origin of coalbed gases from selected basins in the United States; *Proceedings of the 1993 International Methane Symposium, Birmingham, Alabama*, **v.1**, p.207-222.

Sevenster P.G. (1959): Diffusion of gases through coal; *Fuel*, **v.38**, p.403-418.

Sheppard S.M.F. (1986): Characterization and isotopic variations of natural waters; *Reviews in Mineralogy*, **v.16**, p.165-184.

Smith J.W., Rigby D., Gould K.W., Hart G. and Hargraves A.J. (1985): An isotopic study of hydrocarbon generation processes; *Organic Geochemistry*, **v.8**, p.341-347.

Stahl W. (1973): Carbon isotope ratios of German natural gases in comparison of gaseous hydrocarbons from other parts of the world; *in: Advances in Organic Geochemistry 1973 (Eds.: B. Tissot and F. Bienner)*, Pergamon Press, Oxford, p.453-462.

Stahl W. (1977): Carbon and nitrogen isotopes in hydrocarbon research and exploration; *Chemical Geology*, **v.20**, p.121-149.

Stahl W. and Koch J. (1974): $^{13}C/^{12}C$-Verhältnis norddeutscher Erdgase–Reifemerkmal ihrer Muttersubstanzen; *Erdöl, Kohle, Erdgas, Petrochemie*, **v.27**, p.1-36.

Stahl W. and Carey B.D. (1975): Source-rock identification by isotope analyses of natural gases from fields in the Val Verde and Delaware basins, west Texas; *Chemical Geology*, **v.16**, p.257-267.

Taylor G.H., Teichmüller M., Davis A., Diessel C.F.K., Littke R. and Robert P. (1998): Organic Petrology, Gebrüder Bornträger, Berlin,.704 pp.

Teichmüller M. and Teichmüller R. (1967): Diagenesis of coal (coalification); *in: Diagenesis of Sediments (Eds.: G. Larsen and G.V. Chiligail)*, Elsevier, Amsterdam, p.391-415.

Tissot B.P. and Welte D.H. (1978): Petroleum formation and occurrence: a new approach to oil and gas exploration; Springer Verlag, 538 pp.

Ulrich G., DeBruyn R., Finkelstein M. and Weber J. (2005): Active biogenesis of methane in Ft. Union coals of Wyoming's Powder River basin; 2005 Rocky Mountain Section - AAPG Meeting, Jackson Hole, Wyoming, USA.

van Heek K.H., Jüntgen H., Luft K.F. and Teichmüller M. (1971): Aussagen zur Gasbildung in frühen Inkohlungsstadien auf Grund von Pyrolyseversuchen; *Erdöl und Kohle, Erdgas, Petrochemie*, **v.24**, p.566-572.

van Krevelen D. (1963): Geochemistry of coal; *in: Organic Geochemistry (Ed.: I.A. Breger)*, Pergamon Press, Oxford, p.183-247.

Waldron S., Watson-Craik I.A., Hall A.J. and Fallick A.E. (1988): The carbon and hydrogen stable isotope composition of bacteriogenic methane: a laboratory study using a landfill inoculum; *Geomicrobiology*, **v.15**, p.157-169.

Waldron S., Lansdown J.M., Scott E.M., Fallick A.E. and Hall A.J. (1999): The global influence of the hydrogen composition of water of that of bacteriogenic methane from shallow freshwater environments; *Geochimica et Cosmochimica Acta*, **v.63**, p.2237-2245.

Welte D.H. and Yalçin M.N. (1988): Basin modeling-a new comprehensive method in petroleum geology; *in: Advances in Organic Geochemistry 1987, Organic Geochemistry*, **v.13**, p.141-151.

Whiticar M.J. (1990): A geochemical perspective of natural gas and atmospheric methane; *in: Advances in Organic Geochemistry 1989 (Eds.: B. Durand and F. Behar)*, Pergamon Press, Oxford, p.531-547.

Whiticar M.J. (1994): Correlation of natural gases with their sources; in: The petroleum system - from source to trap (Eds.: L.B. Magoon and W.G. Dow), *American Association of Petroleum Geologists Memoir* **60**, p.261-283.

Whiticar M.J. (1996a): Stable isotope geochemistry of coals, humic kerogens and related natural gases; *International Journal of Coal Geology*, **v.32**, p.191-215.

Whiticar M.J. (1996b): Isotope tracking of microbial methane formation and oxidation; *Mitteilungen der Internationalen Vereinigung von Limnologen*, **v.25**, p.39-54.

Whiticar M.J. (1999): Carbon and hydrogen isotope systematics of bacterial formation and oxidation of methane; *Chemical Geology*, **v.161**, p.291-314.

Whiticar M.J. and Faber E. (1986): Methane oxidation in sediment and water column environments – isotope evidence; *Organic Geochemistry*, **v.10**, p.759-768.

Whiticar M.J., Faber E. and Schoell M. (1986): Biogenic methane formation in marine and freshwater environments: CO_2 reduction vs. acetate fermentation – isotope evidence; *Geochimica et Cosmochimica Acta*, **v.50**, p.693-709.

Yee D., Seidle J.P. and Hanson W.B. (1993): Gas sorption on coal and measurement of gas content; in: Hydrocarbons from coal (Eds.: B.E. Law and D.D. Rice), *American Association of Petroleum Geologists Studies in Geology*, **v.38**, p.203-218.

Yeh H.W. and Epstein S. (1981): Hydrogen and carbon isotopes of petroleum and related organic matter; *Geochimica et Cosmochimica Acta*, **v.45**, p.753-762.

Zhang T. and Krooss B.M. (2001): Experimental investigation on the carbon isotope fractionation of methane during gas migration by diffusion through sedimentary rocks at elevated temperature and pressure; *Geochimica et Cosmochimica Acta*, **v.65**, p.2723-2742.

Appendix A: Datasheet Sample Set P1

Sample Set P1: Proportions

Sample	Proportion C_1 (%; norm.)	Proportion C_2 (%; norm.)	Proportion C_3 (%; norm.)	Proportion n-C_4 (%; norm.)	Proportion i-C_4 (%; norm.)	Proportion CO_2 (%; norm.)
Tr-1	56.9	5.7268				37.36
Tr-2	98.5					1.52
Tr-3	98.6					1.39
Tr-4	99.2	0.0060	0.0072			0.76
Tr-5	99.5					0.54
Tr-6	99.7	0.0022				0.29
Spi-1	48.1					51.93
Spi-2	97.6	0.0071	0.0108			2.38
Spi-3	98.8					1.16
Spi-4	99.2					0.77
Spi-5	99.4					0.61
Spi-6	99.8					0.24
Kv-1	36.9					63.11
Kv-2	97.9					2.13
Kv-3	98.8					1.19
Kv-4	99.3					0.72
Kv-5	99.5					0.51
Kv-6	99.6					0.36

Sample Set P1: Isotope ratios

Sample	$\delta^{13}C$ C_1 (‰)	δD C_1 (‰)	$\delta^{13}C$ C_2 (‰)	$\delta^{13}C$ C_3 (‰)	$\delta^{13}C$ n-C_4 (‰)	$\delta^{13}C$ i-C_4 (‰)	$\delta^{13}C$ CO_2 (‰)
Tr-1	-5.1	-187.1	-27.8				-10.7
Tr-2	-32.5	-177.4					-10.8
Tr-3	-31.3	-189.7					-10.6
Tr-4	-34.4	-191.7					-10.7
Tr-5	-37.7	-195.1					-10.5
Tr-6	-40.5	-192.9					-8.8
Spi-1							-10.9
Spi-2	-24.3	-169.6					-11.0
Spi-3	-28.9	-173.1					-11.0
Spi-4	-32.1	-178.3					-10.8
Spi-5	-33.0	-177.9					-11.0
Spi-6	-36.0	-182.9					-10.8
Kv-1							-10.8
Kv-2	-26.0	-166.2					-10.9
Kv-3	-27.0	-167.8					-10.8
Kv-4	-28.9	-171.2					-10.6
Kv-5	-31.2	-172.1					-10.0
Kv-6	-33.9	-177.3					-7.6

Appendix B: Datasheet Sample Set P2

Sample Set P2: Proportions

Sample	Proportions C_1 (%; norm.)	Proportions C_2 (%; norm.)	Proportions C_3 (%; norm.)	Proportions n-C_4 (%; norm.)	Proportions i-C_4 (%; norm.)	Proportions CO_2 (%; norm.)
100/07-1	97.9	0.0197	0.0180			2.04
100/07-2	98.5	0.0061				1.54
100/07-3	98.6	0.0050				1.37
102/02-1	98.4	0.0128	0.0117			1.57
102/02-2	98.9	0.0044	0.0027			1.07
102/02-3	99.2	0.0031				0.77
102/07-1	98.6	0.0017				1.43
102/07-2	99.0	0.0076	0.0023			0.95
102/07-3	99.1	0.0074	0.0023			0.93
103/02-1	98.0					1.98
103/02-2	98.8	0.0047				1.20
103/02-3	99.1	0.0068	0.0021			0.86
104/02-1	98.0	0.0041	0.0050			1.97
104/02-2	98.8					1.25
104/02-3	98.8					1.17

Sample Set P2: Isotope ratios

Sample	$\delta^{13}C$ C_1 (‰)	δD C_1 (‰)	$\delta^{13}C$ C_2 (‰)	$\delta^{13}C$ C_3 (‰)	$\delta^{13}C$ n-C_4 (‰)	$\delta^{13}C$ i-C_4 (‰)	$\delta^{13}C$ CO_2 (‰)
100/07-1	-26.5	-256.7					-11.0
100/07-2	-28.0	-250.7					-10.5
100/07-3	-28.2	-248.7					-11.0
102/02-1	-27.2	-242.8					-10.4
102/02-2	-28.9	-243.4					-9.7
102/02-3	-30.1	-244.5					-8.7
102/07-1	-27.8	-235.6					-10.4
102/07-2	-29.6	-238.3					-9.0
102/07-3	-29.4	-235.9					-8.8
103/02-1	-26.6	-237.1					-10.6
103/02-2	-28.5	-240.0					-9.9
103/02-3	-28.5	-241.0					-9.3
104/02-1	-25.4	-246.8					-10.4
104/02-2	-26.8	-246.5					-10.4
104/02-3	-27.0	-247.2					-10.2

Appendix C: Datasheet Sample Set P3

Sample Set P3: Proportions

Sample	Proportions C_1 (%; norm.)	Proportions C_2 (%; norm.)	Proportions C_3 (%; norm.)	Proportions n-C_4 (%; norm.)	Proportions i-C_4 (%; norm.)	Proportions CO_2 (%; norm.)
2,1	65.4	3.1573	3.7885	6.7257		20.98
2,2	91.1	0.0902	0.1118	0.1676		8.58
2,3	92.6	0.1186	0.1287	0.2066		6.92
2,4	96.0	0.0052	0.0108	0.0246		3.96
2,5	96.7	0.0076	0.0097	0.0194		3.27
2,6	98.1					1.94
2,7	98.1					1.89
2,8	99.3	0.0052				0.72
2,9	99.6	0.0044	0.0023	0.0043		0.39
2,10	99.7	0.0184	0.0053	0.0077		0.23
2,11	99.6	0.0340				0.32
2,12	99.7	0.2090	0.0105	0.0007	0.0024	0.10
2,13	99.3	0.2323	0.0140	0.0004	0.0036	0.47
2,14	95.2	0.0257	0.0310			4.72
2,15	94.3			0.0538		5.68
2,16	97.1					2.95
2,17	97.9					2.13
2,18	98.2	0.0048	0.0054			1.74
2,19	99.1	0.0020		0.0039		0.90
2,20	98.7					1.32
2,21	99.1	0.0023				0.92
2,22	99.5	0.0080	0.0010			0.52
2,23	99.6	0.0065				0.41
2,24	99.7	0.0138				0.28
2,25	99.8	0.0143				0.15
2,26	99.8	0.0173				0.23
2,27	99.8	0.0917	0.0039			0.09
2,28	99.7	0.1201	0.0051	0.0650		0.07

Sample Set P3: Proportions (continued)

Sample	Proportions C_1 (%; norm.)	Proportions C_2 (%; norm.)	Proportions C_3 (%; norm.)	Proportions n-C_4 (%; norm.)	Proportions i-C_4 (%; norm.)	Proportions CO_2 (%; norm.)
5,1	42.3	3.8047	3.6606	3.7594		46.46
5,2	89.3	0.2839	0.3064	0.3998		9.71
5,3	83.5	0.1041	0.0651	0.0689		16.22
5,4	95.7	0.0768	0.0791	0.0805		4.11
5,5	96.8					3.16
5,6	97.0					3.00
5,7	98.9	0.0048				1.05
5,8	99.5	0.0032				0.50
5,9	99.6	0.0077				0.43
5,10	99.6	0.0119				0.40
5,11	99.7	0.0250	0.0012	0.0037		0.22
5,12	99.7	0.2083	0.0013	0.0026	0.0017	0.11
5,13	99.8	0.1538	0.0011	0.0015	0.0015	0.07
5,14	94.1					5.94
5,15	92.4					7.64
5,16	96.0	0.0163	0.0236			3.94
5,17	96.7					3.25
5,18	97.8					2.22
5,19	98.8					1.20
5,20	98.9	0.0032	0.0034			1.12
5,21	99.2					0.85
5,22	99.6	0.0054				0.43
5,23	99.5	0.0068				0.47
5,24	99.7	0.0098				0.27
5,25	99.7	0.0202				0.24
5,26	99.8	0.0229				0.18
5,27	99.9	0.0589				0.05
5,28	99.8	0.1345	0.0007			0.09

Sample Set P3: Proportions (continued)

Sample	Proportions C_1 (%; norm.)	Proportions C_2 (%; norm.)	Proportions C_3 (%; norm.)	Proportions n-C_4 (%; norm.)	Proportions i-C_4 (%; norm.)	Proportions CO_2 (%; norm.)
13,1	64.4	1.7969	1.7391	1.9488		30.11
13,2	87.7	0.2188	0.2189	0.3068		11.51
13,3	91.1	0.1147	0.1297	0.1938		8.50
13,4	88.3	0.0198	0.0138	0.0143		11.61
13,5	96.6	0.0234	0.0211	0.0242		3.38
13,6	95.0	0.0380	0.0431	0.0744		4.84
13,7	98.4	0.0328	0.0300	0.0366		1.49
13,8	99.3	0.0212	0.0203	0.0355		0.59
13,9	99.4	0.0143	0.0120	0.0196		0.50
13,10	99.5	0.0108				0.45
13,11	99.8	0.0193	0.0014	0.0041		0.17
13,12	99.7	0.2121	0.0110	0.0004	0.0028	0.09
13,13	99.7	0.2241	0.0144	0.0003	0.0040	0.08
13,14	96.0					3.97
13,15	93.9					6.14
13,16	94.4	0.0523				5.57
13,17	97.5	0.0312				2.45
13,18	98.0					2.01
13,19	98.9					1.13
13,20	98.5					1.51
13,21	99.2	0.0070				0.76
13,22						
13,23	99.7	0.0043				0.32
13,24	99.7	0.0125				0.25
13,25	99.7	0.0096				0.25
13,26	99.8	0.0169				0.23
13,27	99.8	0.0892	0.0040			0.10
13,28	99.8	0.1114	0.0055			0.08

Sample Set P3: Isotope ratios

Sample	$\delta^{13}C$ C_1 (‰)	δD C_1 (‰)	$\delta^{13}C$ C_2 (‰)	$\delta^{13}C$ C_3 (‰)	$\delta^{13}C$ n-C_4 (‰)	$\delta^{13}C$ i-C_4 (‰)	$\delta^{13}C$ CO_2 (‰)
2,1	-20.8			-33.2	-29.5		-10.0
2,2	-24.5	-304.0					-10.2
2,3	-23.4	-314.5					-10.1
2,4	-27.7						-9.8
2,5	-26.6						-9.3
2,6	-35.1						-8.8
2,7	-32.2						-10.1
2,8	-39.5						-9.9
2,9	-39.7						-11.3
2,10	-44.5						-11.7
2,11	-45.8						-9.4
2,12	-54.3	-255.4					
2,13	-55.7	-252.1	-33.8				
2,14	-26.2	-246.9					-10.9
2,15	-24.2	-239.2					-10.8
2,16	-30.4	-246.6					-10.8
2,17	-32.9	-243.3					-11.1
2,18	-34.0	-247.7					-10.9
2,19	-39.2	-244.8			-30.2		-11.1
2,20	-36.7	-245.4					-11.3
2,21	-38.5	-251.1					-10.9
2,22	-42.6	-254.1					-11.1
2,23	-43.3	-256.1					-11.1
2,24	-44.9	-254.7	-19.6				-10.8
2,25	-46.5	-255.3					-11.6
2,26	-46.6	-245.9					-11.8
2,27	-52.3	-265.6	-30.0				-12.3
2,28	-54.0	-265.9	-32.5		-28.7		

Sample Set P3: Isotope ratios (continued)

Sample	$\delta^{13}C$ C_1 (‰)	δD C_1 (‰)	$\delta^{13}C$ C_2 (‰)	$\delta^{13}C$ C_3 (‰)	$\delta^{13}C$ n-C_4 (‰)	$\delta^{13}C$ i-C_4 (‰)	$\delta^{13}C$ CO_2 (‰)
5,1	-19.2						-9.2
5,2	-25.1						-9.9
5,3	-24.9						-9.6
5,4	-28.5						-10.8
5,5	-28.9						-10.4
5,6	-30.2						-9.1
5,7	-37.0						-10.3
5,8	-38.8						-9.7
5,9	-41.5						-10.2
5,10	-52.3						-8.8
5,11	-46.3						-11.6
5,12	-54.5	-252.6	-33.2				
5,13	-55.0	-252.6	-33.2				
5,14	-27.0	-234.8					-11.9
5,15	-27.3	-233.6					-11.9
5,16	-28.8	-239.1					-11.5
5,17	-31.9	-238.4					-11.2
5,18	-34.1	-242.9					-11.8
5,19	-38.0	-250.3					-11.2
5,20	-37.2	-250.2					-11.1
5,21	-39.4	-251.4					-11.2
5,22	-42.8	-254.0					-11.1
5,23	-42.4	-255.6					-11.1
5,24	-45.0	-258.9					-11.6
5,25	-46.8	-259.2	-23.1				-11.8
5,26	-47.1	-248.8	-23.8				-11.9
5,27	-52.0	-263.3	-30.2				-11.9
5,28	-53.5	-268.9	-32.4				-12.7

Sample Set P3: Isotope ratios (continued)

Sample	$\delta^{13}C$ C_1 (‰)	δD C_1 (‰)	$\delta^{13}C$ C_2 (‰)	$\delta^{13}C$ C_3 (‰)	$\delta^{13}C$ n-C_4 (‰)	$\delta^{13}C$ i-C_4 (‰)	$\delta^{13}C$ CO_2 (‰)
13,1	-21.2						-10.5
13,2	-22.7						-9.3
13,3	-22.4						-9.1
13,4	-26.1						-9.9
13,5	-29.7						-9.2
13,6	-24.7						-9.7
13,7	-34.7						-9.9
13,8	-39.2						-8.7
13,9	-39.4						-8.8
13,10	-41.5						-8.3
13,11	-46.6						-9.9
13,12	-54.5	-245.2	-34.2				
13,13	-55.4	-248.3	-33.8				
13,14	-29.1	-238.8					-11.3
13,15	-29.5	-243.4					-11.2
13,16	-30.0	-241.7					-11.0
13,17	-35.9	-245.6					-12.7
13,18	-35.2	-249.4					-11.1
13,19	-38.1	-248.5					-11.3
13,20	-36.2	-250.5					-11.2
13,21	-40.6	-253.3					-11.3
13,22		-240.1					
13,23	-42.8	-251.3					-11.9
13,24	-46.1	-254.8					-11.5
13,25	-45.3	-255.0					-11.4
13,26	-46.0	-247.3					-11.7
13,27	-51.4	-266.3	-29.8				-13.6
13,28	-53.0	-270.3	-31.5				-12.6

Appendix D: Datasheet Sample Set D1

Sample Set D1: Proportions

Sample	Proportions C_1 (%; norm.)	Proportions C_2 (%; norm.)	Proportions C_3 (%; norm.)	Proportions n-C_4 (%; norm.)	Proportions i-C_4 (%; norm.)	Proportions CO_2 (%; norm.)
1,1	22.0	4.2108	4.0194	4.5155		65.27
1,2	6.1	2.1992	2.6941	4.4993		84.51
1,3	1.3					98.69
3,1	1.1	0.0861	0.0698	0.0893		98.67
3,2	1.0	0.0593	0.0361	0.0692		98.83
3,3	1.2					98.81
4,1	1.1	0.1070	0.0651	0.0832		98.62
4,2	1.2					98.82
4,3	1.3					98.66
6,1	1.5					98.47
6,2	6.4	0.0283	0.0344	0.0550		93.51
6,3	14.9					85.09
6,4	12.3					87.75
6,5	32.6	0.2453	0.3281	0.5627		66.25
6,6	61.9					38.09
6,7	98.0					1.97
6,8	99.5					0.54
6,9	99.4					0.60
6,10	99.2					0.83
7,1	2.6					97.44
7,2	4.4					95.63
7,3	22.4	4.3734	4.6562	5.8449		62.71
7,4	18.2					81.79
7,5	30.6	1.9313	2.3117	3.4130		61.72
7,6	14.3	1.7736	1.9033	2.5404		79.44
7,7	99.7					0.27
7,8	99.7	0.0051	0.0053	0.0065		0.31
7,9	99.4	0.0119	0.0142	0.0190		0.54
7,10	99.3					0.72
8,1	28.2	0.3164	0.4838	0.8099		70.20
8,2	30.2	0.3245	0.4631	0.6903		68.35
8,3	39.2					60.78
8,4	17.0	0.0733	0.2976	1.0409		81.57
8,5	68.1	0.8804	0.8726	0.9658		29.14
8,6	43.2	3.2117	3.8435	6.7643		43.00
8,7	99.5	0.0242	0.0295	0.0507		0.39
8,8	99.6	0.0017	0.0014	0.0025		0.37
8,9	98.8	0.0052	0.0021	0.0042		1.20
8,10	97.4	0.0168	0.0131	0.0142		2.53
8,11	97.1	0.0059	0.0066	0.0159		2.90

Sample Set D1: Isotope ratios

Sample	$\delta^{13}C$ C_1 (‰)	δD C_1 (‰)	$\delta^{13}C$ C_2 (‰)	$\delta^{13}C$ C_3 (‰)	$\delta^{13}C$ n-C_4 (‰)	$\delta^{13}C$ i-C_4 (‰)	$\delta^{13}C$ CO_2 (‰)
1,1	-43.4		-28.0				-9.6
1,2					-29.1		-9.8
1,3							-10.0
3,1							-10.2
3,2							-10.8
3,3							-11.3
4,1							-11.7
4,2							-10.7
4,3							-10.4
6,1							-11.9
6,2							-10.4
6,3	-28.0						-11.2
6,4							-8.9
6,5	-10.8						-11.2
6,6	-21.9						-10.1
6,7	-46.1						-9.4
6,8	-52.9	-263.3					-11.0
6,9	-52.2	-262.4					-9.0
6,10	-54.2	-267.2					-9.7
7,1							-10.3
7,2							-9.4
7,3	-26.0			-33.2	-29.8		-10.0
7,4	-7.8						-10.3
7,5	-11.9				-28.7		-9.6
7,6	-12.4						-9.5
7,7	-41.8	-282.2					
7,8	-43.3	-287.1					
7,9	-42.1						
7,10	-44.3	-279.8					-9.5
8,1	-45.1						-9.7
8,2	-42.0						-10.0
8,3	-32.0						-10.0
8,4	-6.9						-10.3
8,5	-25.3						-10.3
8,6	-15.7				-29.3		-10.0
8,7	-43.9						
8,8	-39.1						-6.6
8,9	-40.3						-7.5
8,10	-43.0						-9.2
8,11	-43.5						-10.6

Appendix E: Datasheet Sample Set D2

Sample Set D2: Proportions

Sample	Proportions C_1 (%; norm.)	Proportions C_2 (%; norm.)	Proportions C_3 (%; norm.)	Proportions n-C_4 (%; norm.)	Proportions i-C_4 (%; norm.)	Proportions CO_2 (%; norm.)
R.6.1	89.3	6.2165				4.48
R.6.2	95.0	1.9125				3.06
R.6.3	97.3					2.67
R.6.4	97.8					2.24
R.6.5	98.7					1.29
R.6.6	97.8	0.0587				2.12
R7.1	95.1	0.1638				4.74
R7.2	90.1	5.5837				4.36
R7.3	96.6	0.9498				2.43
R7.4	97.9	0.0397				2.09
R7.5	97.7	0.0283	0.0299			2.27
R7.6	98.2					1.78
R17.1	95.2	0.1763				4.65
R17.2	97.9					2.14
R17.3	98.3					1.72
R18.1	96.2					3.76
R18.2	98.1					1.90
R18.3	96.9					3.12
R19.1	96.6					3.36
R19.2	96.8					3.23
R19.3	97.9					2.12
R19.4	98.1					1.86
R20.1	93.0					7.01
R20.2	95.9					4.06
R20.3	96.0					3.96
R20.4	98.5					1.49
R20.5	97.6					2.36
R20.6	97.1					2.87
R20.7	98.3					1.65
H3.1	96.6					3.36
H3.2	96.9					3.14
H3.3	98.4					1.57
H3.4	97.8					2.22
H3.5	98.3					1.69
H3.6	98.7					1.33

Sample Set D2: Isotope ratios

Sample	$\delta^{13}C$ C_1 (‰)	δD C_1 (‰)	$\delta^{13}C$ C_2 (‰)	$\delta^{13}C$ C_3 (‰)	$\delta^{13}C$ n-C_4 (‰)	$\delta^{13}C$ i-C_4 (‰)	$\delta^{13}C$ CO_2 (‰)
R.6.1	-17.2	-157.3	-28.6				-12.8
R.6.2	-13.1	-153.8	-28.7				-12.5
R.6.3	-15.3	-154.0					-12.1
R.6.4	-16.1	-151.8					-12.4
R.6.5	-17.2	-144.8					-12.2
R.6.6	-8.2	-141.3					-12.0
R7.1	-16.9	-150.7	-29.2				-12.6
R7.2	-12.1	-145.4	-28.8				-12.4
R7.3	-16.6	-150.7	-29.1				-12.8
R7.4	-17.2	-146.2					-11.3
R7.5	-14.8	-143.7					-12.0
R7.6	-9.9	-144.7					-12.2
R17.1	-12.2	-124.5					-13.8
R17.2	-11.8	-125.1					-12.5
R17.3	-11.6	-128.2					-12.4
R18.1	-13.6	-120.9					-12.1
R18.2	-12.3	-119.5					-12.3
R18.3	-7.3	-114.9					-12.2
R19.1	-10.3	-121.8					-12.2
R19.2	-7.5	-116.0					-12.0
R19.3	-10.7	-119.6					-12.2
R19.4	-9.7	-118.2					-12.5
R20.1	-8.8	-119.7					-12.3
R20.2	-11.0	-120.6					-12.3
R20.3	-8.0	-115.3					-11.9
R20.4	-11.4	-128.5					-12.2
R20.5	-7.3	-118.2					-11.9
R20.6	-3.3	-112.9					-12.6
R20.7	-5.7	-123.6					-12.1
H3.1	-11.2	-141.4					-12.3
H3.2	-8.7	-134.5					-12.6
H3.3	-10.3	-137.6					-12.6
H3.4	-8.3	-133.4					-12.2
H3.5	-8.3	-135.5					-12.4
H3.6	-9.9	-132.5					-12.4

Appendix F: Datasheet Sample Set D3

Sample Set D3: Proportions

Sample	Prportions C_1 (%; norm.)	Prportions C_2 (%; norm.)	Prportions C_3 (%; norm.)	Prportions n-C_4 (%; norm.)	Prportions i-C_4 (%; norm.)	Prportions CO_2 (%; norm.)
1,1						100.00
1,2						100.00
1,3						
1,4						100.00
1,5						
1,6						100.00
1,7						
1,8						
1,9	23.7					76.33
2,1						100.00
2,2						100.00
2,3						
2,4						100.00
2,5						
2,6						100.00
2,7						
2,8						
2,9						100.00
3,1						100.00
3,2						100.00
3,3						
3,4						100.00
3,5						
3,6						100.00
3,7						
3,8						
3,9						100.00
4,1	29.8					70.20
4,2						100.00
4,3						
4,4						100.00
4,5						
4,6	25.3					74.74
4,7						
4,8						
4,9	31.1					68.91

Sample Set D3: Proportions (continued)

Sample	Proportions C_1 (%; norm.)	Proportions C_2 (%; norm.)	Proportions C_3 (%; norm.)	Proportions n-C_4 (%; norm.)	Proportions i-C_4 (%; norm.)	Proportions CO_2 (%; norm.)
5,1	78.2					21.83
5,2	95.6					4.37
5,3	94.4	0.9539				4.63
5,4	95.7	0.7427				3.55
5,5	95.9	0.7254				3.39
5,6	97.2	0.6603				2.18
5,7	97.6	0.6518				1.77
5,8	97.4	0.7158				1.85
5,9	96.6	1.0098				2.41
5,10	96.5	0.9720	0.0895			2.40
5,11	98.2	0.5220				1.32
5,12	77.8	11.5718				10.60
5,13	82.9	5.5119				11.59
5,14	83.7					16.27
6,1	84.8					15.16
6,2	91.5					8.53
6,3	97.8					2.25
6,4	99.0					1.00
6,5	98.4					1.55
6,6	98.6					1.38
6,7	98.5					1.51
6,8	98.5	0.1223				1.37
6,9	98.8	0.1080				1.09
6,10	98.7	0.1088				1.16
6,11	98.3	0.1512				1.51
6,12	83.3	0.3377	0.3978			15.93
6,13	88.2					11.80
6,14	90.1	0.6288				9.23
6,15	95.0					4.96
7,1	93.5					6.51
7,2	97.5					2.50
7,3	97.6					2.35
7,4	97.8					2.20
7,5	98.0	0.1774				1.86
7,6	97.9	0.2069				1.89
7,7	98.2	0.2083				1.61
7,8	97.9	0.2561				1.84
7,9	98.1	0.2521				1.68
7,10	97.7	0.3031				1.98
7,11	97.4	0.3500				2.29
7,12	85.2					14.85
7,13	88.8					11.23
7,14	90.4	0.1924				9.41

Sample Set D3: Proportions (continued)

Sample	Proportions C_1 (%; norm.)	Proportions C_2 (%; norm.)	Proportions C_3 (%; norm.)	Proportions n-C_4 (%; norm.)	Proportions i-C_4 (%; norm.)	Proportions CO_2 (%; norm.)
8,1	85.2					14.82
8,2	95.1					4.91
8,3	96.5					3.50
8,4	97.8					2.24
8,5	98.0					2.01
8,6	98.2					1.81
8,7	98.6					1.41
8,8	98.4	0.0749				1.55
8,9	98.5	0.0776				1.45
8,10	98.2	0.0790				1.70
8,11	97.5	0.1169				2.41
8,12	77.4					22.56
8,13	80.3					19.70
8,14	93.0					6.97
9,1	76.4					23.56
9,2	95.1					4.88
9,3	96.0					4.04
9,4	97.6	0.0627				2.35
9,5	97.8	0.0702				2.16
9,6	98.0	0.0773				1.97
9,7	98.4	0.0743				1.51
9,8	98.3	0.0844				1.59
9,9	98.4	0.0856				1.48
9,10	98.3	0.0963	0.0103			1.64
9,11	97.9	0.1081	0.0130			1.97
9,12	84.5					15.54
9,13	88.8					11.16
9,14	89.4					10.64
10,1	86.7					13.27
10,2	92.3					7.73
10,3	94.2					5.81
10,4	96.8					3.19
10,5	97.6					2.44
10,6	98.3					1.73
10,7	98.5					1.51
10,8	98.6					1.38
10,9	98.5					1.53
10,10	98.5					1.54
10,11	98.3					1.75
10,12	73.6					26.41
10,13	80.1					19.86
10,14	81.2					18.79

Sample Set D3: Proportions (continued)

Sample	Proportions C_1 (%; norm.)	Proportions C_2 (%; norm.)	Proportions C_3 (%; norm.)	Proportions n-C_4 (%; norm.)	Proportions i-C_4 (%; norm.)	Proportions CO_2 (%; norm.)
11,1	48.2					51.82
11,2	81.7					18.33
11,3	94.4					5.55
11,4	93.3					6.71
11,5	95.7					4.34
11,6	97.2					2.84
11,7	97.8					2.18
11,8	98.2					1.82
11,9	97.2					2.82
11,10	96.3					3.65
11,11	62.0					37.98
11,12	74.9					25.14
11,13	74.9					25.14
12,1	90.3					9.71
12,2	94.6					5.40
12,3	92.9					7.06
12,4	97.0					2.97
12,5	98.2					1.75
12,6	98.3					1.75
12,7	98.4					1.61
12,8	98.4					1.60
12,9	74.0					26.04
12,10	71.4					28.59
12,11	67.9					32.12

Sample Set D3: Isotope ratios

Sample	$\delta^{13}C$ C_1 (‰)	δD C_1 (‰)	$\delta^{13}C$ C_2 (‰)	$\delta^{13}C$ C_3 (‰)	$\delta^{13}C$ n-C_4 (‰)	$\delta^{13}C$ i-C_4 (‰)	$\delta^{13}C$ CO_2 (‰)
1,1							-8.8
1,2							-8.5
1,3							
1,4							-10.3
1,5							
1,6							-10.1
1,7							
1,8							
1,9							-8.0
2,1							-10.3
2,2							-8.8
2,3							
2,4							-11.1
2,5							
2,6							-7.7
2,7							
2,8							
2,9							-11.4
3,1							-9.6
3,2							-7.9
3,3							
3,4							-8.5
3,5							
3,6							-8.4
3,7							
3,8							
3,9							-8.4
4,1							-9.4
4,2							-12.5
4,3							
4,4							-7.6
4,5							
4,6	-73.8						-8.9
4,7							
4,8							
4,9	-74.3						-9.3

Sample Set D3: Isotope ratios (continued)

Sample	$\delta^{13}C$ C_1 (‰)	δD C_1 (‰)	$\delta^{13}C$ C_2 (‰)	$\delta^{13}C$ C_3 (‰)	$\delta^{13}C$ n-C_4 (‰)	$\delta^{13}C$ i-C_4 (‰)	$\delta^{13}C$ CO_2 (‰)
5,1	-75.9						-6.5
5,2	-73.0	-207.2					-4.7
5,3	-67.2	-199.0	-21.0				-1.8
5,4	-67.5	-202.7					1.6
5,5	-70.3	-199.3					1.0
5,6	-70.6	-203.0	-21.7				3.1
5,7	-72.6	-205.7	-22.8				5.5
5,8	-72.3	-209.2	-23.7				4.9
5,9	-72.2	-201.0	-23.2				4.3
5,10	-73.4	-203.1	-24.7	-26.8			1.8
5,11	-72.9	-199.9	-24.9				0.7
5,12	-46.5	-200.2	-28.5				-11.8
5,13	-45.6	-201.3	-28.7				-11.6
5,14	-41.7	-203.0	-11.9				
6,1	-81.1						-8.0
6,2	-77.2	-210.3					-16.8
6,3	-68.2	-195.7					-3.4
6,4	-64.1	-192.4					-1.2
6,5	-63.6	-196.5					0.0
6,6	-69.7	-189.2					3.4
6,7	-70.7	-192.9					4.9
6,8	-70.8	-190.2					5.1
6,9	-70.2	-187.8					4.4
6,10	-71.1	-186.6					2.4
6,11	-71.6	-189.3	-25.3				2.4
6,12	-41.8	-192.0					-11.3
6,13	-44.4	-193.7					-11.2
6,14	-47.1	-197.4					-11.7
6,15	-48.8	-198.9					-11.5
7,1	-65.3	-202.4					-6.6
7,2	-61.4	-196.9					0.1
7,3	-60.7	-190.6					0.7
7,4	-63.3	-205.6					1.7
7,5	-65.6	-195.3					6.5
7,6	-67.5	-195.9					5.8
7,7	-67.7	-197.6					7.1
7,8	-67.4	-198.5					8.1
7,9	-66.9	-194.6	-19.8				7.1
7,10	-67.7	-198.5	-20.6				7.3
7,11	-67.9	-199.6	-21.2				6.3
7,12	-40.1	-199.9					-11.5
7,13	-42.8	-201.2					-11.3
7,14	-43.7	-200.4					-11.5

Sample Set D3: Isotope ratios (continued)

Sample	$\delta^{13}C$ C_1 (‰)	δD C_1 (‰)	$\delta^{13}C$ C_2 (‰)	$\delta^{13}C$ C_3 (‰)	$\delta^{13}C$ n-C_4 (‰)	$\delta^{13}C$ i-C_4 (‰)	$\delta^{13}C$ CO_2 (‰)
8,1	-74.7						-6.7
8,2	-67.7	-191.6					-5.1
8,3	-63.9	-194.5					-0.1
8,4	-66.5	-191.7					1.9
8,5	-66.1	-193.8					3.1
8,6	-67.6	-188.4					6.5
8,7	-67.6	-187.6					7.2
8,8	-67.5	-195.8					9.0
8,9	-66.9	-192.2					8.3
8,10	-68.1	-196.1					7.1
8,11	-65.8	-194.0					6.8
8,12	-42.9	-207.6					-11.9
8,13	-41.4	-203.4					-11.7
8,14	-45.8	-205.9					-11.8
9,1	-79.3						-9.4
9,2	-65.9	-202.0					-5.5
9,3	-66.4	-189.6					-3.5
9,4	-64.6	-191.2					1.6
9,5	-66.3	-198.0					3.0
9,6	-66.5	-195.6					5.2
9,7	-66.9	-196.2					7.1
9,8	-66.5	-198.8					8.7
9,9	-66.1	-199.7					7.5
9,10	-66.7	-201.7					6.7
9,11	-67.4	-200.2					6.1
9,12	-41.5	-198.9					-11.5
9,13	-45.2	-201.7					-11.6
9,14	-44.8	-201.2					-11.2
10,1	-69.0						-5.3
10,2	-65.5						-7.0
10,3	-65.0	-193.7					-7.9
10,4	-68.5	-197.8					-3.8
10,5	-68.4	-189.3					-4.4
10,6	-68.8	-201.0					-1.9
10,7	-69.8	-196.5					-1.5
10,8	-69.2	-188.9					-1.5
10,9	-70.3	-192.6					0.8
10,10	-71.1	-192.7					-1.0
10,11	-70.9	-192.2					-2.0
10,12	-43.0	-203.7					-11.5
10,13	-45.8	-203.4					-11.2
10,14	-45.8	-204.1					-11.6

Sample Set D3: Isotope ratios (continued)

Sample	$\delta^{13}C$ C_1 (‰)	δD C_1 (‰)	$\delta^{13}C$ C_2 (‰)	$\delta^{13}C$ C_3 (‰)	$\delta^{13}C$ n-C_4 (‰)	$\delta^{13}C$ i-C_4 (‰)	$\delta^{13}C$ CO_2 (‰)
11,1	-77.6						-9.4
11,2	-76.9						-6.4
11,3	-72.9	-197.7					-7.9
11,4	-71.6	-194.0					-5.6
11,5	-69.8	-199.0					-5.6
11,6	-70.4	-197.0					-2.6
11,7	-70.7	-190.9					-1.3
11,8	-70.5	-189.9					-1.2
11,9	-71.8	-190.1					0.7
11,10	-70.6	-190.1					-1.1
11,11		-208.0					-11.3
11,12	-47.6	-211.0					-11.5
11,13	-47.6	-207.4					-11.3
12,1	-66.4	-182.2					-6.9
12,2	-64.5	-176.2					-9.8
12,3	-64.6						-10.6
12,4	-71.3	-178.8					-7.7
12,5	-72.1	-182.6					-6.3
12,6	-72.3	-179.9					-7.4
12,7	-73.5	-176.5					-6.9
12,8	-72.7	-176.7					-8.6
12,9	-49.6	-195.8					-11.3
12,10		-195.4					-11.6
12,11		-203.0					-11.2

Appendix G: Datasheet Sample Set D4

Sample Set D4: Proportions

Sample	Proportions C_1 (% ; norm.)	Proportions C_2 (% ; norm.)	Proportions C_3 (% ; norm.)	Proportions n-C_4 (% ; norm.)	Proportions i-C_4 (% ; norm.)	Proportions CO_2 (% ; norm.)
1,1	99.9					0.09
1,2	94.6	0.0401				5.33
1,3	94.5	0.0229				5.51
1,4	92.8					7.19
1,5	93.7				0.0339	6.29
1,6	93.9	0.0208				6.09
1,7	85.9					14.09
1,8	88.5	0.0239				11.52
1,9	86.9	0.0198				13.08
1,10	79.7	0.0208				20.27
1,12	80.0					19.99
1,14	74.2					25.83
1,16	48.7					51.32
2,1	93.2					6.79
2,2	88.1					11.90
2,3	96.4	0.0481				3.54
2,4	94.7	0.0538			0.0256	5.23
2,5	93.9	0.0494				6.00
2,6	91.6	0.0558				8.30
2,7	90.1	0.0459				9.87
2,8	89.7	0.0421				10.30
2,9	86.8	0.0454				13.12
2,10	73.0	0.0632				26.90
2,12	62.0	0.0404				37.98
2,14	42.9					57.13
2,16	34.9					65.12
3,1	98.6					1.36
3,2	95.8	0.0199				4.22
3,3	95.1	0.1086	0.1161	0.2373	0.0099	4.45
3,4						100.00
3,5	96.1					3.86
3,6	95.0					5.00
3,7	94.8					5.18
3,8	95.2	0.0165				4.78
3,9	91.7	0.0159				8.28
3,10	92.8	0.0190				7.14
3,12	79.3					20.72
3,14	70.7					29.28
3,16	69.1					30.86

Sample Set D4: Proportions (continued)

Sample	Proportions C_1 (%; norm.)	Proportions C_2 (%; norm.)	Proportions C_3 (%; norm.)	Proportions n-C_4 (%; norm.)	Proportions i-C_4 (%; norm.)	Proportions CO_2 (%; norm.)
4,1	99.3					0.66
4,2						100.00
4,3	95.9	0.0650	0.1224	0.0292	0.0996	3.83
4,4	95.3	0.0674	0.0148	0.0469		4.57
4,5	95.6					4.35
4,6	94.3		0.0196			5.68
4,7	94.9		0.0515			5.04
4,8	93.3	0.0217	0.0222			6.69
4,9	93.7	0.0286	0.0459			6.20
4,10	93.1	0.0444	0.0546			6.76
4,12	87.3	0.0377	0.0616			12.63
4,14	83.7					16.33
4,16	79.0					20.96
5,1	98.6					1.40
5,2	96.5	0.0375				3.47
5,3	95.9	0.0905	0.0875			3.87
5,4	94.5					5.50
5,5	96.9	0.0238		0.0159		3.07
5,6	93.6					6.39
5,7	93.1					6.90
5,8	94.0					6.00
5,9	94.3	0.0176				5.66
5,10	94.3	0.0254				5.68
5,12	87.8					12.16
5,14	70.6					29.41
5,16	68.4					31.61
6,1	99.3					0.73
6,2						100.00
6,3	75.3					24.67
6,4	88.4	0.0520	0.0381			11.50
6,5	79.2					20.77
6,6	86.5	0.0385				13.49
6,7	91.6		0.0274			8.33
6,8	85.3	0.0280				14.70
6,9	81.7					18.25
6,10	77.7					22.29
6,12	66.5					33.47
6,14	55.3					44.66
6,16	45.2					54.79

Sample Set D4: Proportions (continued)

Sample	Proportions C_1 (%; norm.)	Proportions C_2 (%; norm.)	Proportions C_3 (%; norm.)	Proportions n-C_4 (%; norm.)	Proportions i-C_4 (%; norm.)	Proportions CO_2 (%; norm.)
7,1	99.0					0.96
7,2	96.1	0.0323	0.0620			3.80
7,3	95.3	0.0629	0.0913	0.1059		4.46
7,4	95.6					4.44
7,5	96.7					3.31
7,6	94.1		0.0191			5.87
7,7	92.6					7.38
7,8	94.6		0.0269			5.32
7,9	92.0		0.0141			8.00
7,10	93.2	0.0197	0.0315			6.74
7,12	90.3		0.0362			9.66
7,14	89.7		0.0314			10.25
7,16	94.4	0.0201	0.0118			5.54
8,1	99.1					0.91
8,2	95.9	0.0461	0.1736	0.0168	0.0998	3.73
8,3	95.1	0.0427	0.1669		0.0800	4.66
8,4	95.2	0.0388	0.1903		0.0484	4.56
8,5	96.5	0.0338	0.1236	0.0164		3.34
8,6	92.6					7.41
8,7	92.4					7.63
8,8	93.9		0.0295			6.09
8,9	87.1					12.88
8,10	79.4	0.0267	0.0438			20.48
8,12	2.7		0.0705			97.24
8,14	1.4					98.60
8,16	0.7					99.26
9,1	98.6					1.44
9,2	96.3	0.0235	0.1001	0.0154		3.55
9,3	96.1	0.0554	0.1395			3.74
9,4	95.7	0.1171			0.0350	4.12
9,5	97.5			0.0102		2.54
9,6	96.4		0.0282			3.61
9,7	94.4					5.63
9,8	93.9		0.0564			6.06
9,9	94.9					5.11
9,10	94.9		0.0383			5.06
9,12	91.8		0.0521			8.14
9,14	92.2		0.0602			7.74
9,16	93.9	0.0194	0.0609			6.01

Sample Set D4: Proportions (continued)

Sample	Proportions C_1 (%; norm.)	Proportions C_2 (%; norm.)	Proportions C_3 (%; norm.)	Proportions n-C_4 (%; norm.)	Proportions i-C_4 (%; norm.)	Proportions CO_2 (%; norm.)
10,1	99.1					0.94
10,2	88.3	0.0457				11.66
10,3	88.6					11.36
10,4	94.4	0.0394	0.0167			5.52
10,5	92.0					8.00
10,6	91.8	0.0423				8.21
10,7	86.7	0.0418				13.29
10,8	90.5	0.0382				9.43
10,9	87.8	0.0368				12.14
10,10	89.1	0.0418				10.84
10,12	63.7	0.0753				36.21
10,14	57.0					42.98
10,16	1.4					98.64

Sample Set D4: Isotope ratios

Sample	$\delta^{13}C$ C_1 (‰)	δD C_1 (‰)	$\delta^{13}C$ C_2 (‰)	$\delta^{13}C$ C_3 (‰)	$\delta^{13}C$ n-C_4 (‰)	$\delta^{13}C$ i-C_4 (‰)	$\delta^{13}C$ CO_2 (‰)
1,1	-62.5						-3.7
1,2	-49.8						-3.9
1,3	-41.9						-5.5
1,4	-57.0						-10.5
1,5	-56.6						-15.5
1,6	-59.0	-239.1					-25.7
1,7	-58.2						-29.0
1,8	-55.7	-224.5					-34.0
1,9	-55.6						-39.1
1,10	-48.1	-189.1					-39.5
1,12	-49.1	-194.5					-35.4
1,14	-51.7	-208.7					-39.9
1,16	-40.1	-220.2					-28.4
2,1	-61.8						-25.2
2,2	-45.0						-3.0
2,3	-59.5						-4.1
2,4	-59.6						-5.3
2,5	-58.0						-5.8
2,6	-53.7	-248.8					-15.4
2,7	-58.8						-16.2
2,8	-55.7	-219.4					-28.9
2,9	-51.0						-32.0
2,10	-42.4	-200.7					-35.7
2,12	-46.0	-186.9			-25.0		-37.4
2,14	-39.3	-168.2					-39.5
2,16	-37.7	-193.5					-36.5
3,1	-62.4						-4.1
3,2	-56.4						-2.3
3,3	-60.2						-2.9
3,4							-3.4
3,5	-60.1						-5.0
3,6	-60.7	-247.6					-14.2
3,7	-60.0						-0.2
3,8	-60.3	-243.4					-20.8
3,9	-59.4						-29.4
3,10	-61.6	-245.2					-25.9
3,12	-52.7	-206.9					-27.1
3,14	-50.7	-224.0					-24.7
3,16	-43.5	-223.3					-24.4

Sample Set D4: Isotope ratios (continued)

Sample	$\delta^{13}C$ C_1 (‰)	δD C_1 (‰)	$\delta^{13}C$ C_2 (‰)	$\delta^{13}C$ C_3 (‰)	$\delta^{13}C$ n-C_4 (‰)	$\delta^{13}C$ i-C_4 (‰)	$\delta^{13}C$ CO_2 (‰)
4,1	-61.9						-9.3
4,2							-1.1
4,3	-61.4			-24.0			-1.0
4,4	-60.8						-3.0
4,5	-58.3						-5.5
4,6	-59.6	-252.1					-11.6
4,7	-59.3						-2.3
4,8	-59.3	-250.8					-15.8
4,9	-58.4						-18.7
4,10	-58.0	-249.6					-18.2
4,12	-56.3	-242.5					-16.3
4,14	-56.4	-247.4					-22.1
4,16	-52.3	-241.2					-20.2
5,1	-62.3						-1.3
5,2	-62.2						-1.7
5,3	-62.4						-2.1
5,4	-62.2						-2.8
5,5	-61.7						-2.9
5,6	-62.2	-249.1					-13.7
5,7	-61.8						-13.7
5,8	-60.9	-241.7					-19.8
5,9	-60.9						-25.1
5,10	-62.0	-247.7					-33.2
5,12	-57.0	-211.0					-25.1
5,14	-45.0	-120.6					-35.1
5,16	-44.6	-152.9					-41.2
6,1	-61.5						-5.4
6,2							-4.3
6,3	-50.2						-4.5
6,4	-47.8						-5.1
6,5	-53.5						-5.5
6,6	-52.8	-248.5					-18.3
6,7	-57.0						-12.8
6,8	-53.4	-246.0					-30.0
6,9	-49.4						-16.7
6,10	-48.7	-236.0					-25.5
6,12	-44.3	-238.3					-14.2
6,14	-43.1	-240.9					-13.9
6,16	-29.6	-135.6					-19.6

Sample Set D4: Isotope ratios (continued)

Sample	$\delta^{13}C$ C_1 (‰)	δD C_1 (‰)	$\delta^{13}C$ C_2 (‰)	$\delta^{13}C$ C_3 (‰)	$\delta^{13}C$ n-C_4 (‰)	$\delta^{13}C$ i-C_4 (‰)	$\delta^{13}C$ CO_2 (‰)
7,1	-62.7						-3.7
7,2	-63.3						0.5
7,3	-63.0						-0.8
7,4	-62.7						-2.4
7,5	-61.8						-6.2
7,6	-62.6	-251.6					-13.6
7,7	-62.5						-13.4
7,8	-63.0	-250.2					-19.3
7,9	-59.0						-23.9
7,10	-62.7	-249.2					-27.4
7,12	-62.7	-247.2					-18.7
7,14	-61.7	-251.7					-17.7
7,16	-62.1	-251.3					-25.8
8,1	-62.0						-1.6
8,2	-60.1						-1.1
8,3	-59.4						-2.1
8,4	-60.6						-1.9
8,5	-59.4						-3.4
8,6	-59.5	-256.7					-15.1
8,7	-58.9						-15.2
8,8	-58.9	-249.4					-18.3
8,9	-50.7						-32.1
8,10	-46.5	-168.6					-28.9
8,12							-35.1
8,14							-37.7
8,16							-38.2
9,1	-62.7						-1.6
9,2	-63.2			-24.6			-0.1
9,3	-63.3						0.4
9,4	-62.6						-2.1
9,5	-62.1						-3.1
9,6	-62.4	-250.8					-14.5
9,7	-62.6						-13.5
9,8	-62.7	-250.2					-20.5
9,9	-62.8						-23.5
9,10	-62.8	-248.7					-25.1
9,12	-62.5	-249.4					-19.2
9,14	-62.4	-250.1					-17.5
9,16	-60.8	-248.8					-23.5

Sample Set D4: Isotope ratios (continued)

Sample	$\delta^{13}C$ C_1 (‰)	δD C_1 (‰)	$\delta^{13}C$ C_2 (‰)	$\delta^{13}C$ C_3 (‰)	$\delta^{13}C$ n-C_4 (‰)	$\delta^{13}C$ i-C_4 (‰)	$\delta^{13}C$ CO_2 (‰)
10,1	-61.7						2.5
10,2	-41.9						-4.7
10,3	-50.3						-17.0
10,4	-57.0						-7.3
10,5	-49.5						-8.5
10,6	-55.6	-249.1					-6.8
10,7	-56.5						-16.5
10,8	-57.0	-241.4					-19.0
10,9	-53.8						-20.7
10,10	-56.8	-240.9					-27.6
10,12	-41.3	-126.3					-29.5
10,14	-52.9	-233.5					-32.5
10,16							-37.6

Appendix H: Datasheet Sample Set D5

Sample Set D5: Proportions

Sample	Proportions C_1 (%; norm.)	Proportions C_2 (%; norm.)	Proportions C_3 (%; norm.)	Proportions n-C_4 (%; norm.)	Proportions i-C_4 (%; norm.)	Proportions CO_2 (%; norm.)
A1	70.6			3.2771		26.10
C1	61.2					38.80
C2	69.7					30.34

Sample Set D5: Isotope ratios

Sample	$\delta^{13}C$ C_1 (‰)	δD C_1 (‰)	$\delta^{13}C$ C_2 (‰)	$\delta^{13}C$ C_3 (‰)	$\delta^{13}C$ n-C_4 (‰)	$\delta^{13}C$ i-C_4 (‰)	$\delta^{13}C$ CO_2 (‰)
A1	-50.1	-219.1			-11.0		-28.2
C1	-46.8	-209.7			-11.1		
C2	-50.5	-202.0			-11.0		

Appendix I: Datasheet Sample Set D6

Sample Set D6: Proportions

Sample	Proportions C_1 (%; norm.)	Proportions C_2 (%; norm.)	Proportions C_3 (%; norm.)	Proportions n-C_4 (%; norm.)	Proportions i-C_4 (%; norm.)	Proportions CO_2 (%; norm.)
77-1	99.7	0.2754				
77-2	99.6	0.3639				
77-3	99.7	0.2908				
77-4	99.7	0.3142		0.0146		
77-5	99.7	0.3164		0.0123		
77-6	99.6	0.3314	1.8920	0.0142		0.01
88-1	99.8	0.1927		0.0000		
88-2	99.8	0.2023		0.0000		0.01
88-3	99.8	0.1975		0.0000		
88-4	99.8	0.1942		0.0000		0.01
88-5	99.8	0.1803	0.9669	0.0000		0.01
90-1	99.9	0.0395		0.0000		0.01
90-2	100.0	0.0301		0.0000		
90-3	100.0	0.0359		0.0000		
90-4	99.9	0.0388		0.0172	0.0274	
90-5	100.0	0.0321	0.1764	0.0102		
105-1	93.3	6.5067		0.2166		
105-2	96.1	3.7180		0.1322		
105-3	95.6	4.2012		0.1605		
105-4	95.2	4.6456		0.1831		
105-5	91.4	8.2842	27.3557	0.3444		
111-1	99.8	0.2161				
111-2	99.7	0.2948		0.0110		
111-3	99.7	0.2958				
111-4	99.7	0.2894		0.0114		
111-5	99.8	0.2330		0.0108		
111-6	99.7	0.3086		0.0108		
111-7	99.6	0.3451	1.6935	0.0198		
136-1	97.5	2.4172		0.0592	0.0219	
136-2	97.3	2.5571		0.1773		
136-3	97.6	2.3633		0.0687		
136-4	96.3	3.5513		0.1066		
136-5	94.6	5.1636		0.1585	0.1230	
136-6	91.9	7.8307	23.8831	0.2469		
153-1	99.1	0.9225		0.0113		
153-2	98.9	1.1448				
153-3	98.6	1.3852				
153-4	98.8	1.2099				
153-5	98.6	1.3845				

Sample Set D6: Proportions (continued)

Sample	Proportions C_1 (%; norm.)	Proportions C_2 (%; norm.)	Proportions C_3 (%; norm.)	Proportions n-C_4 (%; norm.)	Proportions i-C_4 (%; norm.)	Proportions CO_2 (%; norm.)
161-1	99.9	0.1197				
161-2	99.5	0.4611				
161-3	99.8	0.2146				
161-4	99.8	0.2105				
161-5	99.8	0.2291	1.2352			
188-1	97.4	2.4746		0.0778		
188-2	96.9	2.9977		0.0995		
188-3	96.7	3.1692		0.1088		
188-4	96.1	3.7315		0.1264		
188-5	95.7	4.1151		0.1420		
188-6	95.2	4.6467	21.1349	0.1716		
192-1	97.7	2.2181		0.0461		
192-2	96.3	3.5646		0.0854		
192-3	96.3	3.5994		0.0848		
192-4	94.6	5.2459		0.1299		
192-5	95.3	4.5511		0.1105		
192-6	91.3	8.5271	27.7063	0.2160		
201-1	97.1	2.7880		0.0775		
201-2	96.3	3.6262		0.1126		
201-3	96.0	3.8781		0.1245		
201-4	95.7	4.1580	14.4504	0.1360		

Sample Set D6: Isotope ratios

Sample	$\delta^{13}C$ C_1 (‰)	δD C_1 (‰)	$\delta^{13}C$ C_2 (‰)	$\delta^{13}C$ C_3 (‰)	$\delta^{13}C$ n-C_4 (‰)	$\delta^{13}C$ i-C_4 (‰)	$\delta^{13}C$ CO_2 (‰)
77-1	-55.5	-302.5	-24.9				-29.0
77-2	-57.2	-272.6	-23.3				-20.9
77-3	-57.0	-275.7	-23.0				-15.8
77-4	-56.8	-271.8	-23.2				-16.9
77-5	-55.8	-275.5	-23.1				-13.8
77-6	-55.5	-273.4	-22.8				-16.3
88-1	-52.8	-253.6	-13.5				-14.8
88-2	-51.9	-251.8	-11.9				-8.7
88-3	-51.3	-253.5	-12.6				-5.6
88-4	-50.2	-253.7	-11.9				-6.3
88-5	-48.7	-243.4	-10.8				-7.3
90-1	-52.4	-249.0	-10.7				-5.2
90-2	-52.0	-250.9	-9.0				-4.0
90-3	-52.0	-251.6	-9.9				-1.3
90-4	-50.4	-249.5	-13.4				1.5
90-5	-50.1	-248.3	-11.1	-31.7			-0.4
105-1	-38.8		-26.8	-22.4			
105-2	-37.1		-26.7	-22.7			-9.8
105-3	-36.2		-26.4	-22.4			
105-4	-34.5		-25.9	-21.9			-11.7
105-5	-33.2		-25.3	-21.8			
111-1	-43.8		-16.9				10.6
111-2	-45.0		-17.8				7.5
111-3	-43.4		-16.7				9.5
111-4	-40.0			-18.0			0.3
111-5	-43.5		-11.7	-18.2			
111-6	-42.9		-20.0				
111-7	-41.1		-15.7	-12.8			
136-1	-54.5		-26.1	-22.0			-3.2
136-2	-52.6		-26.7	-31.3			
136-3	-51.9		-25.8	-22.2			
136-4	-50.3		-25.6	-20.9			
136-5	-48.9		-25.0				
136-6	-40.0		-23.2				
153-1	-39.8		-21.4				
153-2	-37.5		-20.8				
153-3	-37.2		-20.6				
153-4	-36.0		-20.9				
153-5	-35.7		-20.4				
153-6	-33.0		-20.1				
161-1	-44.7		-14.3				
161-2	-44.5		-14.2				
161-3	-43.0		-14.6				
161-4	-41.9		-13.9				
161-5	-41.3		-13.5				

Sample Set D6: Isotope ratios (continued)

Sample	$\delta^{13}C$ C_1 (‰)	δD C_1 (‰)	$\delta^{13}C$ C_2 (‰)	$\delta^{13}C$ C_3 (‰)	$\delta^{13}C$ n-C_4 (‰)	$\delta^{13}C$ i-C_4 (‰)	$\delta^{13}C$ CO_2 (‰)
188-1	-49.8		-27.4	-21.6			
188-2	-48.9		-27.1				
188-3	-47.7		-26.8	-21.2			
188-4	-44.9		-26.1	-21.3			
188-5	-43.9		-25.6	-20.9			
188-6	-41.9		-25.4	-20.9			
192-1	-42.6		-25.7				
192-2	-42.2		-25.6	-20.2			
192-3	-40.6		-25.7	-19.8			
192-4	-38.1		-25.2	-19.7			
192-5	-38.9		-25.3	-19.4			
192-6	-27.9		-23.7	-19.3			
201-1	-44.7		-25.3	-20.3			
201-2	-43.8		-25.2				
201-3	-43.1		-24.6	-20.4			
201-4	-42.4		-23.9	-19.5			

Appendix J: Datasheet Sample Set D7

Sample Set D7: Proportions

Sample	Proportions C_1 (%; norm.)	Proportions C_2 (%; norm.)	Proportions C_3 (%; norm.)	Proportions n-C_4 (%; norm.)	Proportions i-C_4 (%; norm.)	Proportions CO_2 (%; norm.)
03-c	79.1	2.0141	0.3033	0.4870		18.13
03-d	81.2	2.8621	0.4905			15.43
04-c	73.8	7.4525	0.9941			17.77
04-d	75.1	8.9990	1.2533			14.67
05-c	76.7	6.6940	0.8464			15.73
05-d	78.3	8.4689	1.0347			12.16
06-c	69.8	4.7839	0.9882			24.44
06-d	73.8	5.6624	1.1816			19.32
08-c	74.7	4.8564	1.1465			19.26
08-d	73.4	6.7820	1.6309			18.23
09-c	71.4	5.4070	1.2879			21.86
09-d	75.1	6.8920	1.6161			16.37
10-c	77.2	7.4767	1.3387			13.96
10-d	78.7	9.3927	1.6856			10.22
11-c	77.7	7.6333	1.3510			13.35
11-d	78.5	10.2518	1.6978			9.60
13-c	80.3	6.4315	0.9604	0.2768		12.04
13-d	80.6	8.5817	1.4077	0.0736		9.36
15-c	79.0	7.8834	1.1761	0.0862		11.90
15-d	79.1	10.0419	1.6045	0.0538		9.18
16-c	79.8	7.1044	1.0357	0.0907		12.01
16-d	78.6	9.8630	1.4103	0.0571		10.04
17-c	79.9	6.0732	0.6937	0.0529		13.32
18-c	80.9	5.2651	0.6546	0.0480		13.16
18-d	80.3	7.6399	0.9627	0.0401		11.06

Sample Set D7: Isotope ratios

Sample	$\delta^{13}C$ C_1 (‰)	δD C_1 (‰)	$\delta^{13}C$ C_2 (‰)	$\delta^{13}C$ C_3 (‰)	$\delta^{13}C$ n-C_4 (‰)	$\delta^{13}C$ i-C_4 (‰)	$\delta^{13}C$ CO_2 (‰)
03-c	-41.8	-180.0	-25.0	-26.9	-27.8		20.1
03-d	-39.4	-181.6	-25.8	-27.2			20.4
04-c	-37.7	-179.4	-29.4	-27.9			15.0
04-d	-36.3	-179.7	-28.8	-28.0			14.7
05-c	-36.4	-181.3	-29.0	-28.0			13.6
05-d	-34.2	-181.0	-28.8	-27.9			14.0
06-c	-37.5	-187.9	-30.8	-29.6			-5.6
06-d	-35.9	-187.9	-30.7	-29.6			-5.0
08-c	-37.0	-187.9	-30.9	-29.8			-7.0
08-d	-35.3	-185.0	-30.6	-29.9			-6.7
09-c	-36.4	-178.6	-29.7	-29.5			-7.6
09-d	-35.3	-178.8	-29.5	-29.6			-7.0
10-c	-32.3	-165.6	-28.4	-27.2			-4.9
10-d	-29.0	-167.1	-27.7	-26.8			-4.1
11-c	-31.4	-165.1	-28.4	-27.1			-4.3
11-d	-27.9	-165.5	-27.6	-26.6			-3.7
13-c	-32.4	-167.0	-28.0	-26.9	-28.7		-4.0
13-d	-29.4	-163.7	-28.0	-26.9			-3.4
15-c	-31.9	-165.3	-27.8	-26.9			-3.3
15-d	-29.1	-164.7	-27.4	-26.8			-3.2
16-c	-32.7	-166.6	-28.2	-26.8			-3.2
16-d	-29.4	-167.0	-27.6	-26.8			-2.9
17-c	-34.2	-167.4	-27.8	-27.1			-3.4
18-c	-34.7	-170.3	-27.3	-26.3			-3.1
18-d	-31.9	-166.9	-27.2	-25.9			-2.5

Appendix K:

Estimated $\delta^{13}C$ values for methane, ethane and propane, based on maturities of coals considered for all ten sample sets. Calculations are performed by using maturity–$\delta^{13}C$ relationships by Berner and Faber (1996). Values are represented per well, respectively canister, but only for wells, respectively canisters where the considered hydrocarbon species was actually measured.

Sample Set	Well Canister	Maturity (%R_O)	$\delta^{13}C$ Methane (‰)	$\delta^{13}C$ Ethane (‰)	$\delta^{13}C$ Propane (‰)
P1	TR	n/a	n/a	n/a	n/a
	SPI	n/a	n/a	n/a	n/a
	KV	n/a	n/a	n/a	n/a
P2	100/07	1.20	-26.9	n/a	n/a
	102/02	1.20	-26.9	n/a	n/a
	102/07	1.20	-26.9	n/a	n/a
	103/02	1.20	-26.9	n/a	n/a
	104/02	1.20	-26.9	n/a	n/a
P3	2	0.57	n/a	n/a	n/a
	5	0.57	n/a	n/a	n/a
	13	0.57	n/a	n/a	n/a
D1	6	n/a	n/a	n/a	n/a
	7	n/a	n/a	n/a	n/a
	8	n/a	n/a	n/a	n/a
D2	R6	4.41	n/a	n/a	n/a
	R7	4.27	n/a	n/a	n/a
	R17	4.00	n/a	n/a	n/a
	R18	4.55	n/a	n/a	n/a
	R19	4.41	n/a	n/a	n/a
	R20	4.41	n/a	n/a	n/a
	H3	4.41	n/a	n/a	n/a
D3	5	0.67	-28.8	-24.8	n/a
	6	0.67	-28.8	n/a	n/a
	7	0.67	-28.8	-24.8	n/a
	8	0.67	-28.8	n/a	n/a
	9	0.67	-28.8	n/a	n/a
	10	0.67	-28.8	n/a	n/a
	11	0.67	-28.8	n/a	n/a
	12	0.67	-28.8	n/a	n/a
D4	1	0.67	-28.8	n/a	n/a
	2	0.67	-28.8	n/a	n/a
	3	0.67	-28.8	n/a	n/a
	4	0.67	-28.8	n/a	n/a
	5	0.67	-28.8	n/a	n/a
	6	0.67	-28.8	n/a	n/a
	7	0.67	-28.8	n/a	n/a
	8	0.67	-28.8	n/a	n/a
	9	0.67	-28.8	n/a	n/a
	10	0.67	-28.8	n/a	n/a
D5	A	0.67	-28.8	n/a	n/a

Sample Set	Well Canister	Maturity (%R_O)	$\delta^{13}C$ Methane (‰)	$\delta^{13}C$ Ethane (‰)	$\delta^{13}C$ Propane (‰)
D5	C	0.67	-28.8	n/a	n/a
D6	77	1.55	-25.6	-21.9	n/a
	88	1.55	-25.6	-21.9	n/a
	90	1.55	-25.6	-21.9	n/a
	105	1.23	-26.8	-23.0	-21.4
	111	1.77	-24.8	-21.2	-21.0
	136	1.23	-26.8	-23.0	-21.4
	153	1.77	-24.8	-21.2	n/a
	161	1.77	-24.8	-21.2	n/a
	188	1.23	-26.8	-23.0	-21.4
	192	1.23	-26.8	-23.0	-21.4
	201	1.23	-26.8	-23.0	-21.4
D7	03	0.69	-28.8	-24.7	-23.6
	04	0.69	-28.8	-24.7	-23.6
	05	0.69	-28.8	-24.7	-23.6
	06	0.69	-28.8	-24.7	-23.6
	08	0.69	-28.8	-24.7	-23.6
	09	0.69	-28.8	-24.7	-23.6
	10	0.63	-29.0	-24.9	-24.1
	11	0.63	-29.0	-24.9	-24.1
	13	0.63	-29.0	-25.0	-24.1
	15	0.61	-29.0	-25.0	-24.3
	16	0.61	-29.0	-25.0	-24.3
	17	0.71	-28.6	-24.6	-23.4
	18	0.71	-28.6	-24.6	-23.4

Appendix L:

Calculated differences between measured and estimated $\delta^{13}C$ ratios for methane. Estimated $\delta^{13}C$ values for methane are based on maturities of coals considered for all ten sample sets. Calculations are performed by using maturity–$\delta^{13}C$ relationships by Berner and Faber (1996). t_{START} represents the earliest value obtained from well, respectively canister, t_{END} represents the last value obtained from well, respectively canister and t_{WGH} is a value calculated by relating absolute concentration per sample to correlating $\delta^{13}C$ ratio (Equation 2.16). Positive values indicate relative ^{13}C enrichment in the measured methane and negative values represent relative ^{12}C enrichment in the measured methane. Calculations are only shown for wells, respectively canisters, where coal maturities and $\delta^{13}C$ ratios are available.

Sample Set	Well Canister	$\Delta\delta^{13}C$ t_{START} (‰)	$\Delta\delta^{13}C$ t_{END} (‰)	$\Delta\delta^{13}C$ $t_{WEIGHTED}$ (‰)
P2	100/07	+0.4	-1.3	-0.7
	102/02	-.03	-3.2	-1.8
	102/07	-0.9	-2.5	-2.0
	103/02	+0.3	-1.6	+1.0
	104/02	+1.5	-0.1	+0.5
D3	5	-47.1	-12.9	-37.6
	6	-52.3	-20.0	-35.5
	7	-36.5	-14.9	-32.2
	8	-45.9	-17.0	-34.0
	9	-50.5	-16.0	-33.8
	10	-40.2	-17.0	-35.7
	11	-48.8	-18.8	-39.6
	12	-37.6	-20.8	-39.2
D4	1	-33.7	-11.3	-13.2
	2	-33.0	-8.9	-12.4
	3	-33.6	-14.7	-16.5
	4	-33.1	-23.5	-17.3
	5	-33.5	-15.8	-18.6
	6	-32.7	-0.8	-9.5
	7	-33.9	-33.3	-21.2
	8	-33.2	-17.7	-29.1
	9	-33.9	-32.0	-21.5
	10	-32.9	-24.1	-15.8
D5	A	-21.3	n/a	-21.3
	C	-18.0	-21.7	-20.0
D6	77	-29.9	-29.9	-30.7
	88	-27.2	-23.1	-25.4
	90	-26.5	-24.5	-25.8
	105	-12.0	-6.4	-9.2
	111	-19.0	-16.3	-18.0
	136	-27.7	-13.2	-23.0
	153	-15.0	-8.2	-11.7
	161	-19.9	-16.5	-18.3
	188	-23.0	-15.1	-19.4

Sample Set	Well Canister	$\Delta\delta^{13}C$ t_{START} (‰)	$\Delta\delta^{13}C$ t_{END} (‰)	$\Delta\delta^{13}C$ $t_{WEIGHTED}$ (‰)
D6				
	192	-15.8	-1.1	-11.7
	201	-17.9	-15.6	-16.7
D7	03	-13.0	-10.6	-11.8
	04	-8.9	-7.5	-8.2
	05	-7.6	-5.4	-6.5
	06	-8.7	-7.1	-7.9
	08	-8.2	-6.5	-7.4
	09	-7.6	-6.5	-7.0
	10	-3.3	±0.0	-1.6
	11	-2.4	+1.1	-0.6
	13	-3.4	-0.4	-1.9
	15	-2.9	-0.1	-1.5
	16	-3.7	-0.4	-2.1
	17	-5.5	n/a	-5.5
	18	-6.0	-3.2	-4.6

Appendix M:

Calculated differences between measured and estimated $\delta^{13}C$ ratios for ethane. Estimated $\delta^{13}C$ values for ethane are based on maturities of coals considered for all ten sample sets. Calculations are performed by using maturity–$\delta^{13}C$ relationships by Berner and Faber (1996). t_{START} represents the earliest value obtained from well, respectively canister, t_{END} represents the last value obtained from well, respectively canister and t_{WGH} is a value calculated by relating absolute concentration per sample to correlating $\delta^{13}C$ ratio (Equation 2.17). Positive values indicate relative ^{13}C enrichment in the measured ethane and negative values represent relative ^{12}C enrichment in the measured ethane. Calculations are only shown for wells, respectively canisters, where coal maturities and $\delta^{13}C$ ratios are available.

Sample Set	Well Canister	$\Delta\delta^{13}C$ t_{START} (‰)	$\Delta\delta^{13}C$ t_{END} (‰)	$\Delta\delta^{13}C$ $t_{WEIGHTED}$ (‰)
D3	5	+3.8	+12.9	-0.8
	6	n/a	n/a	n/a
	7	+5.0	+3.6	+4.2
	8	n/a	n/a	n/a
	9	n/a	n/a	n/a
	10	n/a	n/a	n/a
	11	n/a	n/a	n/a
	12	n/a	n/a	n/a
D6	77	-3.0	-0.9	-1.4
	88	+8.4	+11.1	+9.7
	90	+11.2	+10.8	+11.0
	105	-3.8	-2.3	-3.1
	111	+4.3	+5.5	+4.6
	136	-3.1	-0.2	-1.9
	153	+0.2	+1.1	+0.6
	161	+6.9	+7.7	+7.1
	188	-4.4	-2.4	-3.2
	192	-2.7	-0.7	-1.9
	201	-2.3	-0.9	-1.7
D7	03	-0.3	-1.1	-0.8
	04	-4.7	-4.1	-4.4
	05	-4.3	-4.1	-4.2
	06	-6.1	-6.0	-6.0
	08	-6.2	-5.9	-6.0
	09	-5.0	-4.8	-4.9
	10	-3.5	-2.8	-3.1
	11	-3.5	-2.7	-3.0
	13	-3.1	-3.1	-3.1
	15	-2.9	-2.5	-2.7
	16	-3.3	-2.7	-3.0
	17	-3.2	n/a	-3.2
	18	-2.7	-2.6	-2.6

Appendix N:

Calculated differences between measured and estimated $\delta^{13}C$ ratios for propane. Estimated $\delta^{13}C$ values for propane are based on maturities of coals considered for all ten sample sets. Calculations are performed by using maturity–$\delta^{13}C$ relationships by Berner and Faber (1996). t_{START} represents the earliest value obtained from well, respectively canister, t_{END} represents the last value obtained from well, respectively canister and t_{WGH} is a value calculated by relating absolute concentration per sample to correlating $\delta^{13}C$ ratio (Equation 2.18). Positive values indicate relative ^{13}C enrichment in the measured propane and negative values represent relative ^{12}C enrichment in the measured propane. Calculations are only shown for wells, respectively canisters, where coal maturities and $\delta^{13}C$ ratios are available.

Sample Set	Well Canister	$\Delta\delta^{13}C$ t_{START} (‰)	$\Delta\delta^{13}C$ t_{END} (‰)	$\Delta\delta^{13}C$ $t_{WEIGHTED}$ (‰)
D6	77	n/a	n/a	n/a
	88	n/a	n/a	n/a
	90	n/a	n/a	n/a
	105	-1.0	-0.4	-0.8
	111	+3.0	+2.8	+5.4
	136	-0.6	+0.5	-4.4
	153	n/a	n/a	n/a
	161	n/a	n/a	n/a
	188	-0.2	+0.5	+0.2
	192	+1.2	+2.1	+1.8
	201	+1.1	+1.9	+1.4
D7	03	-3.3	-3.6	-3.5
	04	-4.3	-4.4	-4.4
	05	-4.4	-4.3	-4.3
	06	-6.0	-6.0	-6.0
	08	-6.2	-6.3	-6.3
	09	-5.9	-6.0	-6.0
	10	-3.1	-2.7	-2.9
	11	-3.0	-2.5	-2.7
	13	-2.8	-2.8	-2.8
	15	-2.6	-2.5	-2.6
	16	-2.5	-2.5	-2.5
	17	-3.7	n/a	-3.7
	18	-2.9	-2.5	-2.7

Appendix O:

Extrapolated $\delta^{13}C$ values for methane and calculated proportions of thermogenic and microbial gas in samples from sample sets D6 and D7. Extrapolations are based on natural gas plots and are performed following description by Chung et al. (1988). Calculations of proportions of thermogenic and microbial gas are performed by applying a mass–balance equation (Equation 6.3). Measured $\delta^{13}C$ ratio for methane (C_1) is considered isotope ratio of gas mix (thermogenic and microbial gas), extrapolated $\delta^{13}C$ ratio for methane is considered of pure thermogenic origin and $\delta^{13}C$ ratio for pure microbial methane is considered to be -60‰ (Whiticar, 1999). Measured $\delta^{13}C$ ratios are t_{WGH} values for methane.

Sample Set	Canister	$\delta^{13}C$ C_1 Measured (‰)	$\delta^{13}C$ C_1 Extrapolated (‰)	Fraction Thermogenic (%)	Fraction Microbial (%)
D6	105	-36.0	n/a	n/a	n/a
	111	-42.8	-19.5	43	57
	136	-49.8	n/a	n/a	n/a
	188	-16.2	-41.0	100	0
	192	-38.5	n/a	100	0
	201	-43.5	-38.9	78	22
D7	03	-40.6	n/a	n/a	n/a
	04	-37.0	-32.1	82	18
	05	-35.3	-31.8	88	12
	06	-36.7	-34.0	90	10
	08	-36.2	-28.6	76	24
	09	-35.8	-30.8	83	17
	10	-30.6	n/a	100	0
	11	-29.6	n/a	100	0
	13	-30.9	n/a	100	0
	15	-30.5	n/a	100	0
	16	-31.1	-29.8	95	5
	18	-33.3	-30.5	91	9

Appendix P:

Calculated $\delta^{13}C$ values for methane and calculated proportions of thermogenic and microbial gas in samples from sample sets D6 and D7. Calculations are based on maturity–$\delta^{13}C$ relationship by Berner and Faber (1996). Calculations of proportions of thermogenic and microbial gas are performed by applying a mass–balance equation (Equation 6.3). $\delta^{13}C$ ratios for methane (t_{WGH}; C_1) are considered isotope ratio of gas mix (thermogenic and microbial gas), calculated $\delta^{13}C$ ratio for methane is considered of pure thermogenic origin and $\delta^{13}C$ ratio for pure microbial methane is considered to be -60‰ (Whiticar, 1999).

Sample Set	Well Canister	$\delta^{13}C$ Calculated (‰)	$\delta^{13}C$ $t_{WEIGHTED}$ (‰)	Fraction Thermogenic (%)	Fraction Microbial (%)
P2	100/07	-26.9	-27.6	98	2
	102/02	-26.9	-28.7	95	5
	102/07	-26.9	-28.9	94	6
	103/02	-26.9	-27.9	97	3
	104/02	-26.9	-26.4	100	0
D3	5	-28.8	-66.4	0	100
	6	-28.8	-64.3	0	100
	7	-28.8	-61.0	0	100
	8	-28.8	-62.8	0	100
	9	-28.8	-62.6	0	100
	10	-28.8	-64.5	0	100
	11	-28.8	-68.4	0	100
	12	-28.8	-68.0	0	100
D4	1	-28.8	-42.0	58	42
	2	-28.8	-41.2	60	40
	3	-28.8	-45.3	47	53
	4	-28.8	-46.1	45	55
	5	-28.8	-47.4	40	60
	6	-28.8	-38.3	70	30
	7	-28.8	-50.0	32	68
	8	-28.8	-57.9	1	99
	9	-28.8	-50.3	31	69
	10	-28.8	-44.6	49	51
D5	A	-28.8	-50.1	32	68
	C	-28.8	-48.8	36	64
D6	77	-25.6	-56.3	11	89
	88	-25.6	-51.0	26	74
	90	-25.6	-51.4	25	75
	105	-26.8	-36.0	72	28
	111	-24.8	-42.8	49	51
	136	-26.8	-49.8	31	69
	153	-24.8	-36.5	67	33
	161	-24.8	-43.1	48	52
	188	-26.8	-46.2	42	58
	192	-26.8	-28.5	95	5
	201	-26.8	-43.5	50	50
D7	03	-28.8	-40.6	62	38

Sample Set	Well Canister	$\delta^{13}C$ Calculated (‰)	$\delta^{13}C$ $t_{WEIGHTED}$ (‰)	Fraction Thermogenic (%)	Fraction Microbial (%)
D7	04	-28.8	-37.0	74	26
	05	-28.8	-25.3	100	0
	06	-28.8	-36.7	75	25
	08	-28.8	-36.2	76	24
	09	-28.8	-35.8	78	22
	10	-29.0	-30.6	95	5
	11	-29.0	-29.6	98	2
	13	-29.0	-30.9	94	6
	15	-29.0	-30.5	95	5
	16	-29.0	-31.1	93	7
	17	-28.6	-34.2	82	18
	18	-28.6	-33.3	85	15

Appendix Q:

Comparison of calculated fractions for thermogenic gas generated from a Kerogen type III source rock and microbial based on the approaches by Chung et al. (1988) and Berner and Faber (1996) for sample sets D6 and D7. See text for description of both approaches

Sample Set	Canister	Chung et al., 1988		Berner & Faber, 1996	
		Thermogenic (%)	Microbial (%)	Thermogenic (%)	Microbial (%)
D6	105	n/a	n/a	11	89
	111	43	57	26	74
	136	n/a	n/a	25	75
	188	100	0	72	28
	192	100	0	49	51
	201	78	22	31	69
	Ø	80	20	36	64
D7	03	n/a	n/a	62	38
	04	82	18	74	26
	05	88	12	100	0
	06	90	10	75	25
	08	76	24	76	24
	09	83	17	78	22
	10	100	0	95	5
	11	100	0	98	2
	13	100	0	94	6
	15	100	0	95	5
	16	95	5	93	7
	18	91	9	85	15
	Ø	91	9	67	33

Appendix R:

Calculated differences for the estimated $\delta^{13}C$ ratios for methane based on the approaches by Chung et al. (1988) and Berner and Faber (1996) for sample sets D6 and D7. See text for description of both approaches Negative values represent relative ^{12}C enriched values for methane and positive values represent relative ^{13}C enriched values for methane calculated by applying the approach by Berner and Faber (1996).

Sample Set	Canister	$\delta^{13}C$ Methane (estimated) (‰)		Difference (‰)
		Chung et al., 1988	Berner & Faber, 1996	
D6	105	n/a	-26.8	n/a
	111	-19.5	-24.8	-5.3
	136	n/a	-26.8	n/a
	188	-41.0	-26.8	+14.2
	192	n/a	-26.8	n/a
	201	-38.9	-26.8	+12.1
D7	03	n/a	-28.8	n/a
	04	-32.1	-28.8	+3.3
	05	-31.8	-28.8	+3.0
	06	-34.0	-28.8	+5.2
	08	-28.6	-28.8	-0.2
	09	-30.8	-28.8	+2.0
	10	-30.6	-29.0	+1.6
	11	-29.6	-29.0	+0.6
	13	-30.9	-29.0	+1.9
	15	-30.5	-29.0	+1.5
	16	-31.1	-28.6	+2.5
	18	-33.3	-28.6	+4.7

Appendix S:

Comparison between calculated and measured $\delta^{13}C$ values for ethane and propane from sample set D7. Calculations are based on maturity–$\delta^{13}C$ relationships by Berner and Faber (1996). See text for description of used approach. Measured values represent t_{WGH} values. Negative differences represent relative ^{12}C enrichment for measured ethane and propane.

Can.	Ethane			Propane		
	$\delta^{13}C$ Calculated (‰)	$\delta^{13}C$ Measured (‰)	$\Delta\delta^{13}C$ (‰)	$\delta^{13}C$ Calculated (‰)	$\delta^{13}C$ Measured (‰)	$\Delta\delta^{13}C$ (‰)
03	-24.7	-25.5	-0.8	-23.6	-27.1	-3.5
04	-24.7	-29.1	-4.4	-23.6	-28.0	-4.4
05	-24.7	-28.9	-4.2	-23.6	-27.9	-4.3
06	-24.7	-30.7	-6.0	-23.6	-29.6	-6.0
08	-24.7	-30.7	-6.0	-23.6	-29.9	-6.3
09	-24.7	-29.6	-4.9	-23.6	-29.6	-6.0
10	-24.9	-28.0	-3.1	-24.1	-27.0	-2.7
11	-24.9	-27.9	-3.0	-24.1	-26.8	-2.7
13	-24.9	-28.0	-3.1	-24.1	-26.9	-2.8
15	-24.9	-27.6	-2.7	-24.3	-26.8	-2.5
16	-24.9	-27.9	-3.0	-24.3	-26.8	-2.5
18	-24.6	-27.2	-2.6	-23.4	-26.1	-2.7

Appendix T:

Comparison between measured $\delta^{13}C$ ratios for methane (C_1) with calculated $\delta^{13}C$ ratios for methane expected to be generated from a Kerogen Type II and Kerogen Type III source rock at a given maturity. Maturity of Kerogen Type III source rock (coal) is known and maturity of Kerogen Type II source rock is equal or higher. For the conducted calculations the same maturities derived from the maturity of the considered coal is used for both types of source rocks. Calculations are conducted by applying maturity–$\delta^{13}C$ relationships by Berner and Faber (1996) for both types of source rocks (see text for details about used approach). Proportions for Kerogen Type II and Type III derived methane are calculated by using a mass–balance equation with the calculated $\delta^{13}C$ ratios as end–members and the measured $\delta^{13}C$ ratios as values for the gas mixture (see text for details). Meas. = measured; calc. = calculated.

Sample Set	Canister	$\delta^{13}C_1$ meas. (‰)	$\delta^{13}C_1$ calc. Type II (‰)	$\delta^{13}C_1$ calc. Type III (‰)	Fraction Type II (%)	Fraction Type III (%)
D6	77	-56.3	-38.2	-25.6	100	0
	88	-51.0	-38.2	-25.6	100	0
	90	-51.4	-38.2	-25.6	100	0
	105	-36.0	-41.0	-26.8	65	35
	111	-42.8	-36.6	-24.8	100	0
	136	-49.8	-41.0	-26.8	100	0
	153	-36.5	-36.6	-24.8	99	1
	161	-43.1	-36.6	-24.8	100	0
	188	-16.2	-41.0	-26.8	0	100
	192	-28.5	-41.0	-26.8	12	88
	201	-43.5	-41.0	-26.8	100	0
	Ø	-	-	-	80	20
D7	03	-40.6	-46.2	-28.8	68	32
	04	-37.0	-46.2	-28.8	47	53
	05	-25.3	-46.2	-28.8	0	100
	06	-36.7	-46.2	-28.8	45	55
	08	-36.2	-46.2	-28.8	43	57
	09	-35.8	-46.2	-28.8	40	60
	10	-30.6	-46.4	-29.0	9	91
	11	-29.6	-46.4	-29.0	4	96
	13	-30.9	-46.4	-29.0	11	89
	15	-30.5	-46.4	-29.0	9	91
	16	-31.1	-46.4	-29.0	12	88
	18	-33.3	-46.1	-28.6	27	73
	Ø	-	-	-	26	74

Appendix U:

Comparison between measured $\delta^{13}C$ ratios for ethane (C_2) with calculated $\delta^{13}C$ ratios for ethane expected to be generated from a Kerogen Type II and Kerogen Type III source rock at a given maturity. Maturity of Kerogen Type III source rock (coal) is known and maturity of Kerogen Type II source rock is equal or higher. For the conducted calculations the same maturities derived from the maturity of the considered coal is used for both types of source rocks. Calculations are conducted by applying maturity–$\delta^{13}C$ relationships by Berner and Faber (1996) for both types of source rocks (see text for details about used approach). Proportions for Kerogen Type II and Type III derived ethane are calculated by using a mass–balance equation with the calculated $\delta^{13}C$ ratios as end–members and the measured $\delta^{13}C$ ratios as values for the gas mixture (see text for details). Meas. = measured; calc. = calculated.

Sample Set	Canister	$\delta^{13}C_2$ meas. (‰)	$\delta^{13}C_2$ calc. Type II (‰)	$\delta^{13}C_2$ calc. Type III (‰)	Fraction Type II (%)	Fraction Type III (%)
D6	77	-23.3	-29.1	-21.9	19	81
	88	-12.2	-29.1	-21.9	0	100
	90	-10.9	-29.1	-21.9	0	100
	105	-26.1	-30.7	-23.0	40	60
	111	-16.6	-28.1	-21.4	0	100
	136	-24.9	-30.7	-23.0	25	75
	153	-20.6	-28.1	-21.4	0	100
	161	-14.1	-28.1	-21.4	0	100
	188	-26.2	-30.7	-23.0	42	58
	192	-24.9	-30.7	-23.0	25	75
	201	-24.7	-30.7	-23.0	22	78
	Ø	-	-	-	16	84
D7	03	-25.5	-38.8	-24.7	0	100
	04	-29.1	-38.8	-24.7	31	69
	05	-28.9	-38.8	-24.7	30	70
	06	-30.7	-38.8	-24.7	43	57
	08	-30.7	-38.8	-24.7	43	57
	09	-29.6	-38.8	-24.7	35	65
	10	-28.0	-39.2	-24.9	22	78
	11	-27.9	-39.2	-24.9	21	79
	13	-28.0	-39.2	-24.9	22	78
	15	-27.6	-39.2	-25.0	18	82
	16	-27.9	-39.2	-25.0	20	80
	18	-27.2	-38.6	-24.6	19	81
	Ø				25	75

Appendix V:

Comparison between measured $\delta^{13}C$ ratios for propane (C_2) with calculated $\delta^{13}C$ ratios for propane expected to be generated from a Kerogen Type II and Kerogen Type III source rock at a given maturity. Maturity of Kerogen Type III source rock (coal) is known and maturity of Kerogen Type II source rock is equal or higher. For the conducted calculations the same maturities derived from the maturity of the considered coal is used for both types of source rocks. Calculations are conducted by applying maturity–$\delta^{13}C$ relationships by Berner and Faber (1996) for both types of source rocks (see text for details about used approach). Proportions for Kerogen Type II and Type III derived propane are calculated by using a mass–balance equation with the calculated $\delta^{13}C$ ratios as end–members and the measured $\delta^{13}C$ ratios as values for the gas mixture (see text for details). Meas. = measured; calc. = calculated.

Sample Set	Canister	$\delta^{13}C_3$ meas. (‰)	$\delta^{13}C_3$ calc. Type II (‰)	$\delta^{13}C_3$ calc. Type III (‰)	Fraction Type II (%)	Fraction Type III (%)
D6	77	n/a	-26.0	-21.3	n/a	n/a
	88	n/a	-26.0	-21.3	n/a	n/a
	90	n/a	-26.0	-21.3	n/a	n/a
	105	-22.2	-28.0	-21.4	12	88
	111	-25.6	-25.5	-21.0	100	0
	136	-25.8	-28.0	-21.4	67	33
	153	n/a	-25.5	-21.0	n/a	n/a
	161	n/a	-25.5	-21.0	n/a	n/a
	188	-21.1	-28.0	-21.4	0	100
	192	-19.6	-28.0	-21.4	0	100
	201	-20.0	-28.0	-21.4	0	100
	Ø				30	70
D7	03	-27.1	-38.8	-24.7	17	83
	04	-28.0	-38.8	-24.7	23	77
	05	-27.9	-38.8	-24.7	23	77
	06	-29.6	-38.8	-24.7	35	65
	08	-29.6	-38.8	-24.7	35	65
	09	-29.6	-38.8	-24.7	35	65
	10	-27.0	-39.2	-24.9	15	85
	11	-26.8	-39.2	-24.9	13	87
	13	-26.9	-39.2	-24.9	14	86
	15	-26.8	-39.2	-25.0	13	87
	16	-26.8	-39.2	-25.0	13	87
	18	-26.1	-38.6	-24.6	11	89
	Ø				21	79

Appendix W:

Comparison of proportions of Kerogen Type II derived gas (methane, ethane and propane) for sample sets D6 and D7. Fractions are calculated by applying maturity–$\delta^{13}C$ relationships by Berner and Faber (1996) with a consequent comparison with measured $\delta^{13}C$ ratios for methane, ethane and propane (see text for details).

Sample Set	Canister	Fraction Type II (Methane) (%)	Fraction Type II (Ethane) (%)	Fraction Type II (Propane) (%)
D6	77	100	19	n/a
	88	100	0	n/a
	90	100	0	n/a
	105	65	40	12
	111	100	0	100
	136	100	25	67
	153	99	0	n/a
	161	100	0	n/a
	188	0	42	0
	192	12	25	0
	201	100	22	0
	Ø	80	16	30
D7	03	68	0	17
	04	47	31	23
	05	0	30	23
	06	45	43	35
	08	43	43	35
	09	40	35	35
	10	9	22	15
	11	4	21	13
	13	11	22	14
	15	9	18	13
	16	12	20	13
	18	27	19	11
	Ø	26	25	21

Appendix X:

Maturities, liptinite amounts and average proportions for higher gaseous hydrocarbon gases (ethane, propane, *n*-butane and *i*-butane) for samples from sample sets D6 and D7.

Sample Set	Canister	Maturity (%R_O)	Amount Liptinite (%)	Average Proportion C_{2+} (%, normalized)
D6	77	1.55	0.0	0.32
	88	1.55	0.0	0.20
	90	1.55	0.0	0.05
	105	1.23	0.3	5.68
	111	1.77	0.0	0.29
	136	1.23	0.3	4.14
	153	1.77	0.0	1.24
	161	1.77	0.0	0.25
	188	1.23	0.3	3.64
	192	1.23	0.3	4.73
	201	1.23	0.3	3.73
	Ø	1.46	0.14	2.21
D7	03	0.69	5	3.08
	04	0.69	5	9.35
	05	0.69	5	8.52
	06	0.69	5	6.31
	08	0.69	5	7.21
	09	0.69	5	7.60
	10	0.63	3	9.95
	11	0.63	3	10.47
	13	0.63	3	8.87
	15	0.61	3	10.42
	16	0.61	3	9.78
	18	0.71	5	7.31
	Ø	0.66	4.17	8.24

Appendix Y:

Weighted $\delta^{13}C$ values for methane, ethane and propane. See text for details about calculation of t_{WGH} values

Sample Set	Well Canister	$t_{WEIGHTED}$ Methane (‰)	$t_{WEIGHTED}$ Ethane (‰)	$t_{WEIGHTED}$ Propane (‰)
P1	TR	-32.2	n/a	n/a
	SPI	-30.9	n/a	n/a
	KV	-29.4	n/a	n/a
P2	100/07	-27.6	n/a	n/a
	102/02	-28.7	n/a	n/a
	102/07	-28.9	n/a	n/a
	103/02	-27.9	n/a	n/a
	104/02	-26.4	n/a	n/a
P3	2	-38.3	-32.3	n/a
	5	-39.1	-32.0	n/a
	13	-40.5	-33.0	n/a
D1	6	-42.1	n/a	n/a
	7	-37.9	n/a	n/a
	8	-37.5	n/a	n/a
D2	R6	-14.5	-28.6	n/a
	R7	-14.6	-28.9	n/a
	R17	-11.9	n/a	n/a
	R18	-11.1	n/a	n/a
	R19	-9.6	n/a	n/a
	R20	-7.9	n/a	n/a
	H3	-9.4	n/a	n/a
D3	5	-66.4	-25.6	n/a
	6	-64.3	n/a	n/a
	7	-61.0	-20.6	n/a
	8	-62.8	n/a	n/a
	9	-62.6	n/a	n/a
	10	-64.5	n/a	n/a
	11	-68.4	n/a	n/a
	12	-68.0	n/a	n/a
D4	1	-42.0	n/a	n/a
	2	-41.2	n/a	n/a
	3	-45.3	n/a	n/a
	4	-46.1	n/a	n/a
	5	-47.4	n/a	n/a
	6	-38.3	n/a	n/a
	7	-50.0	n/a	n/a
	8	-57.9	n/a	n/a
	9	-50.3	n/a	n/a
	10	-44.6	n/a	n/a
D5	A	-50.1	n/a	n/a
	C	-48.8	n/a	n/a
D6	77	-56.3	-23.3	n/a
	88	-51.0	-12.2	n/a

Sample Set	Well Canister	$t_{WEIGHTED}$ Methane (‰)	$t_{WEIGHTED}$ Ethane (‰)	$t_{WEIGHTED}$ Propane (‰)
D6	90	-51.4	-10.9	n/a
	105	-36.0	-26.1	-22.2
	111	-42.8	-16.6	-15.6
	136	-49.8	-24.9	-25.8
	153	-36.5	-20.6	n/a
	161	-43.1	-14.1	n/a
	188	-46.2	-26.2	-21.1
	192	-38.5	-24.9	-19.6
	201	-43.5	-24.7	-20.0
D7	03	-40.6	-25.5	-27.1
	04	-37.0	-29.1	-28.0
	05	-35.3	-28.9	-27.9
	06	-36.7	-30.7	-29.6
	08	-36.2	-30.7	-29.9
	09	-35.8	-29.6	-29.6
	10	-30.6	-28.0	-27.0
	11	-29.6	-27.9	-26.8
	13	-30.9	-28.0	-26.9
	15	-30.5	-27.6	-26.8
	16	-31.1	-27.9	-26.8
	17	-34.2	-27.8	-27.1
	18	-33.3	-27.2	-26.1